AD_____

Award Number: W81XWH-08-1-0455

TITLE: Isolation and Characterization of Prostate Cancer Stem Cells

PRINCIPAL INVESTIGATOR: Isla Garraway, M.D., Ph.D.

CONTRACTING ORGANIZATION: The University of California
Los Angeles, CA 90024

REPORT DATE: October 2013

TYPE OF REPORT: Annual Summary

PREPARED FOR: U.S. Army Medical Research and Materiel Command
Fort Detrick, Maryland 21702-5012

REPORT DOCUMENTATION PAGE

Form Approved
OMB No. 0704-0188

1. REPORT DATE *(DD-MM-YYYY)*	2. REPORT TYPE	3. DATES COVERED *(From - To)*
October 2013	Annual Summary	1 August 2008 - 31 July 2013

4. TITLE AND SUBTITLE

Isolation and Characterization of Prostate Cancer Stem Cells

5a. CONTRACT NUMBER

5b. GRANT NUMBER

W81XWH-08-1-0455

5c. PROGRAM ELEMENT NUMBER

6. AUTHOR(S)

Isla Garraway, M.D., Ph.D.

E-Mail: igarraway@mednet.ucla.edu

5d. PROJECT NUMBER

5e. TASK NUMBER

5f. WORK UNIT NUMBER

7. PERFORMING ORGANIZATION NAME(S) AND ADDRESS(ES)

The University of California
Los Angeles, CA 90024

8. PERFORMING ORGANIZATION REPORT NUMBER

9. SPONSORING / MONITORING AGENCY NAME(S) AND ADDRESS(ES)

U.S. Army Medical Research and Materiel Command
Fort Detrick, Maryland 21702-5012

10. SPONSOR/MONITOR'S ACRONYM(S)

11. SPONSOR/MONITOR'S REPORT NUMBER(S)

12. DISTRIBUTION / AVAILABILITY STATEMENT

Approved for Public Release; Distribution Unlimited

13. SUPPLEMENTARY NOTES

14. ABSTRACT

Human prostate epithelial cells that form "prostaspheres" in vitro, display characteristics of stem/progenitor cells, including self-renewal and ability to induce prostate tubule formation in vivo. Prostaspheres derived from patient specimens containing the TMPRSS-ERG translocation, however, fail to demonstrate this translocation/deletion resulting in TMPRSS-ERG fusion. This finding suggests that TMPRSS-ERG+ cancer cells do not efficiently expand in vitro, compared to the basal-like cells from benign glands that appear to populate in vitro cultures. In order to optimize retrieval of tumor cells and support tumor regeneration in vivo, we implemented multiple strategies, including optimization of tissue processing to single cells, cell fractionation, and refinement of the microenvironment to support xenograft growth in vivo. These modifications have improved retrieval of cancer cells, however, only a small minority expand transiently in vitro, or engraft in vivo. Characterization of benign prostate cells with stem-like characteristics has demonstrated that cells with the ability to initiate branching morphogenesis express several genes that are found in prostate tumors associated with bone metastases, findings which have many translational and therapeutic possibilities.

15. SUBJECT TERMS

Prostate Cancer, prostate stem cells, TMPRSS-ERG, prostate tissue regeneration

16. SECURITY CLASSIFICATION OF:			17. LIMITATION OF ABSTRACT	18. NUMBER OF PAGES	19a. NAME OF RESPONSIBLE PERSON
a. REPORT	b. ABSTRACT	c. THIS PAGE			USAMRMC
U	U	U	UU	138	19b. TELEPHONE NUMBER *(include area code)*

Table of Contents

I - INTRODUCTION:

The aims of this proposal are based on the observations from our initial studies with human prostate cancer surgical specimens. We discovered that prostate stem/early progenitor cells recovered from tumor specimens lack the TMPRSS-ERG translocation found in the original tumor, when examined by fluorescence in situ hybridization (FISH). Our findings suggest either ETS rearrangements are not present at the stem/progenitor cell level, or that genetically deranged prostate stem/progenitor cells are particularly vulnerable to apoptosis or senescence in vitro, resulting in selective advantage of benign cells. We have evaluated the growth requirements that enable survival and expansion of prostate stem/progenitor cells from benign and malignant human tissue specimens. As such, we have generated an extensive biorepository of human prostate tissue and/or primary cell lines from more than 500 prostate cancer cases that may serve as provide valuable biological tools for understanding the mechanisms of tumorigenesis and identifying new therapeutic targets in future studies. Factors that have affected the ability to isolate and expand primary tumors include low tumor grade/volume present in surgical samples, increased sensitivity of tumor cells to apoptosis after tissue dissociation, semi-competent immune systems in many SCID mouse strains that inhibit tumor take, and a microenvironment that lacks critical growth factors and cellular interactions.

Our laboratory has made significant progress towards tackling this problem, as evident in the published and unpublished data presented over the course of this grant. By incorporating NOD-SCID^{IL2grNULL} (NSG) mice, we have greatly increased the efficiency of human cell engraftment. We have isolated primary stromal cells from 15 human fetal prostate specimens, in an effort to improve the microenvironment in support of tumorigenesis. These fetal cells support normal prostate tubule formation, induced by benign (adult) human prostate epithelial cells, and eliminate the need for murine additives (i.e., urogenital sinus mesenchyme). More importantly, early data demonstrates, for the first time, prostate tumor regeneration may be optimized using these support cells. We have obtained tumor grafts that recapitulate the patient's original cancer specimen, without any genetic manipulation of the patient's tumor cells.

II - BODY:

Background and Specific Aims:

Expansion of Prostate Stem/Progenitor Cells: The study of prostate stem/progenitor cells (SCs) is facilitated by culturing dissociated primary cells as spheres[1, 2]. Spheres are multicellular globes that form in anchorage-independent conditions, and these cultures have been commonly used to study mammary and nervous system development[3, 4]. In our human prostate studies, spheres can be dissociated and passaged for multiple generations (self-renew), as well as induce branching morphogenesis and form fully differentiated glands in vivo[5].

The TMPRSS-ERG Fusion is Not Identified in Prostaspheres: Since prostaspheres were generated from primary tumors, we presumed that in vitro cultures would include clonally derived benign and cancerous prostaspheres, reflective of the heterogeneity of glands found in tissue specimens. We were not able, however, to distinguish prostaspheres based on phenotype, marker expression, or growth rate. With the discovery of prevalent gene rearrangements involving ETS family members in prostate cancer, we anticipated that cytogenetic tools may enable identification of cancerous prostaspheres[6]. Gene fusions involving ERG, ETV1, and ETV4 involve a variety of 5' partners that direct aberrant expression of these transcription factors and possibly initiate a cascade of events leading to tumorigenesis [6]. The most common rearrangement involves juxtaposition of the androgen-regulated TMPRSS2 gene with ERG. TMPRSS-ERG gene fusions have been detected in primary prostate tumor specimens, metastases, and xenografts by fluorescence in situ hybridization (FISH)[6]. Analysis of prostate tumor surgical cohorts have found 36-78% of prostate cancers possess the TMPRSS-ERG fusion[6]. We wondered whether we could use TMPRSS-ERG to distinguish normal and malignant prostaspheres. The presence of this fusion in individual prostaspheres may suggest that cancer stem/early progenitor cells can be expanded in our cultures.

To test the feasibility of this approach, FISH analysis was performed on select prostate tissue specimens and coordinating prostaspheres. The TMPRSS-ERG fusion was found in approximately 60% of cancer cases tested. Surprisingly, the fusion was conspicuously absent from prostasphere cultures derived from TMPRSS-ERG+ tissues, even when the specimens contained >90% tumor. Analysis of monolayer cultures concomitantly derived from prostate tumor specimens also failed to demonstrate the presence of the gene fusion, indicating that both spheroid and adherent cultures select for fusion-negative cells[5].

Review of ETS Rearrangements in Cultured Prostate Epithelial Cells: The TMPRSS-ERG fusion has previously been identified in only one prostate cancer cell line, NCI-H660, derived from an androgen-independent small cell carcinoma of the prostate[7, 8]. None of the common prostate cancer cell lines including LnCaP, DU-145, PC-3, and CWR22 contain this fusion[6]. LnCaP and MDA-PCa2b were recently reported to contain rearrangement of the ETV1 gene to a prostate specific region resulting in aberrant expression with increased invasive activity[6]. The general inability to culture primary prostate cells that contain TMRPSS-ERG, and the under-representation of ETS rearrangements in prostate cancer cell lines is intriguing and suggests critical elements are absent in vitro, preventing the growth of these cells.

We have formulated three distinct possibilities why TMPRSS-ERG is not preserved in human prostate cells in vitro 1) prostate cancer stem cells responsible for propagating primary cells do not contain the TMPRSS-ERG fusion, rather it is a genetic event that occurs later in tumorigenesis as a result of genomic instability 2) Fusion-positive prostate cells undergo anoikis, apoptosis, or senescence unless additional growth/survival factors or stromal interaction is provided, or 3) genetically normal cells have a dramatic growth advantage over TMPRSS-ERG cancer cells, resulting in their rapid overgrowth.

Since the TMPRSS-ERG fusion is so prevalent in prostate cancer regardless of grade or stage, analyses of the genetic impact of these rearrangements is critical. Deciphering the fundamental survival factors necessary for culturing these cells will yield biological tools for the study of ETS rearrangements in addition to valuable insight into the vulnerabilities of these cells. Consequently, we proposed to define what factors are critical for survival and expansion of TMPRSS-ERG fusion-positive prostate cancer cells via the following aims:

Aim 1: Generate a collection of tumor specimens that contain the TMPRSS-ERG translocation, as demonstrated by FISH of the primary tumor.

a. Generate xenografts from TMPRSS-ERG tissue specimens
b. Generate prostasphere and monolayer (adherent) cultures from TMPRSS-ERG specimens in a variety of culture conditions, including altering media and additives (i.e., androgen, stroma)
c. Generate a biorepository of TMPRSS-ERG+/- cancer tissue and primary cells

Aim 2: Assess for the retention of the TMPRSS-ERG mutation in xenografts, expanded in vitro monolayer (adherent) cultures, and prostasphere cultures.

Aim 3: Assess the effect of inhibiting anoikis and/or apoptosis pathways in dissociated prostate epithelial cells derived from TMPRSS-ERG+ tissues on prostasphere formation via viral mediated gene transfer of genes that are known to disrupt these processes (i.e., Bcl-2, Ras, dominant negative p53).

III -KEY RESEARCH ACCOMPLISHMENTS:

The tasks of the training program include:

1) Regularly meet with mentor to discuss career goals and progress
2) Attend group meetings, journal clubs, and seminars related to research topics
3) Direct research project outlined in the proposal according to the specific aims:
    a. Develop a collection of TMPRSS-ERG fusion positive human prostate cancers
    b. Evaluate the ability to preserve the TMPRSS-ERG fusion in prostaspheres by varying culture conditions.
    c. Evaluate the ability to propagate TMPRSS-ERG+ cells in prostate epithelial monolayer cultures and in xenografts
    d. Perform viral mediated gene transfer of genes that block anoikis and apoptosis pathways in dissociated human prostate cells and evaluate the ability to maintain TMPRSS-ERG+ cells as prostaspheres.

Mentoring (Tasks 1 and 2): As transitioned to developing my own independent research focus in human prostate stem cells and their role in tumor-initiation/progression, my interactions with Dr. Witte were essential and assisted me in developing new collaborations. The interactions with members of his research team were also highly valuable in developing my critical thinking skills.

Accomplishments Related to Specific Aims:

Generating a prostate tissue biorepository inclusive of TMPRSS-ERG+ samples: We generated a large, diverse collection of fresh, frozen, and and formalin-fixed, paraffin-embedded (FFPE) specimens over the past 5 years of this DOD award for experimental studies (see sample annotated population in appendix). We worked with the Tissue Procurement Core Laboratory (TPCL) at UCLA and at the Greater Los Angeles VA Medical Center to obtain tissue samples. The expert pathologists and technical staff facilitated specimen macrodissection and benign/tumor nodule separation and isolation from surgical samples. Generally, after the prostate surgical specimens were removed en bloc, an experienced technician from TPCL prepared 5 or 6 prostatic sections ranging in thickness from 3-4mm. A sleeve of fresh tissue was obtained from the posterior (peripheral zone) of selected sections. Frozen slides were prepared and stained by H&E staining. GU pathologists examined the slides and cancerous areas are marked and mapped to the remaining fresh tissue (see appendix Table 1). Tumor nodules were then dissected and isolated from benign tissue and processed via enzymatic and mechanical digestion into single cells for additional in vitro and in vivo analysis.

Epcam/CD44 fractionation enables enrichment of TMPRSS-ERG+ cells: In an effort to improve retrieval of TMPRSS-ERG+ prostate cancer cells required for our studies, we utilized Epcam/CD44 fractionation to enrich for luminal cells from macrodissected tumor nodules. In initial experiments with tumor tissues, we found a minor population of $Epcam^{+}CD44^{-}$ luminal cells after standard 12-hour digestion with Collagenase (Figure 1A). This result was surprising, since immunohistochemical (IHC) analysis demonstrated that the majority of cells present in tumor nodules display $Epcam^{+}CD44^{-}$ (luminal) profiles (data not shown). In order to evaluate whether or not standard enzymatic digestion procedures resulted in over digestion and loss of tumor cells, a series of experiments evaluating a variety of digestion times and collagenase concentrations was performed. When digestion time was reduced to 4 hours in 0.25% collagenase, a marked shift in $Epcam^{+}CD44^{-}$ cells was noted, enabling optimization of luminal cells recovery (Figure 1B). FACS and RT-PCR of fractionated cells confirmed enrichment of basal $Epcam^{+}CD44^{-}$ and luminal $Epcam^{+}CD44^{+}$ fractions (Figure 1C). In order to confirm enrichment of tumor cells, PCR for TMPRSS-ERG fusion was performed on RNA isolated from cell fractions. Significant TMPRSS-ERG message was detected exclusively in the $Epcam^{+}CD44^{-}$ cell fraction (Figure 1D). This confirms that the luminal cell optimization procedure for enzymatic digestion of prostate tumor specimens enables robust recovery of tumor cells containing TMPRSS-ERG. This significant improvement in TMPRSS-ERG+ recovery may translate into an improved ability to expand primary prostate cancer cells in vitro and in vivo.

Recreating the tumor microenvironment to preserve tumor cells: In addition to enrichment of the TMPRSS-ERG+ cells, we focused on recreating the microenvironment conducive to prostate tumor growth in vivo. One factor that may enable cancer cell growth is the incorporation of support cells that recreate the tumor microenvironment. Although we have traditionally utilized rodent urogenital sinus mesenchyme to support human tissue regeneration in immunocompromised mice, murine growth factors secreted by these cells may not be optimal stimulants of tumor growth. As a result, we isolated stromal cells from fetal tissue, which demonstrate abundant growth potential and support benign human prostate tissue regeneration when combined with adult prostate cells or prostaspheres [9]. The use of fetal prostate stroma for tissue regeneration assays of primary prostate tumor cells enabled retrieval of tumor grafts. Tumor nodules were dissected from high-grade surgical specimens and combined with human fetal prostate stroma and Matrigel prior to subcutaneous injection into NSG mice. Approximately 12-weeks following implantation, grafts were harvested and evaluated by immunohistochemistry (Figure 2). High-grade tumor foci were observed as well as areas of benign growth. Tumor foci demonstrated similar expression pattern of prostate markers as the original tumor (data not shown). The ability to regenerate primary tumors is a leap forward in our ability to identify and characterize human prostate stem cells. We are aggressively pursing tissue regeneration of more high-grade tumors with passaging in order to determine reproducibility of this technique. We also hope to begin to interrogate fractionated cells from tumors for their ability to function as cancer stem cells and trace the TMRPSS-ERG population throughout tumor development.

Niche Interactions of benign SC fraction may be exploited in tumors: The use of our human prostate tissue regeneration system and methods for separating prostate cells isolated from dissociated surgical specimens is a valuable tool for characterizing genetic events and cells of origin in prostate tumorigenesis. The ability to functionally distinguish cell populations that can interact with the niche to form benign or malignant-appearing tubular outgrowths is a huge step. We have characterized epithelial subpopulations isolated from benign human prostate tissue based upon surface marker expression and demonstrated specific functional capabilities of each subpopulation in vitro and in vivo (Figure 3). We confirmed that functionally and

genetically distinct prostate subpopulations were consistently obtained via fractionation using Epcam, CD44, and CD49f antigenic combinations[9]. This approach led to the enrichment of putative stem cells (SCs), progenitor cells (PCs), and terminally differentiated luminal cells (LCs). Putative Epcam+CD44-CD49f^{Hi} human SCs were found to be highly efficient at inducing new tubule formation, in vivo, relative to PCs and LCs. Subsequent studies of these subpopulations have provided additional insight into the relationship between SCs and aggressive tumor cells (TCs) that may lead to valuable prognostic tools and therapeutic approaches.

What can benign prostate stem cells tell us about metastatic tumor cells? Published reports and our preliminary data suggest that human prostate SCs and aggressive tumor cells (TCs) display many similarities, including androgen responsiveness but not dependence, radiation-resistance, and microenvironment interactions capable of driving angiogenesis, tubule initiation, and branching morphogenesis[9, 10]. SCs are often isolated based upon self-renewal (in vitro sphere-formation) and tubule-initiating (in vivo tissue regeneration) capabilities[5, 11]. We hypothesized that markers unique to the SC subpopulation may be expressed by specific PCa variants with aggressive clinical features (high pathological grade, advanced clinical stage, and/or metastases). In order to evaluate this prospect, comparative DNA microarray studies were performed in an effort to identify potential biomarkers of SCs isolated form benign surgical specimens. Among the most differentially expressed genes identified in SCs compared to PCs and LCs was cytokeratin that had yet to be described in the prostate, keratin 13 (K13). K13 is a type 1 cytokeratin typically found in intermediate filaments within suprabasal layers of non-cornified stratified epithelia. Cytokeratins classically designate basal (K5/6) and luminal (K8/18) compartments within adult prostate glands [12]. K13 represented a new cytokeratin biomarker with potential to designate the location of SC niches in human prostate tissues. Consistent with the notion that K13 may identify sites of stem/progenitor activity, clusters of K13+ cells were found sporadically throughout the basal compartment of benign adult prostate glands. K13+ cells comprised the majority of Epcam+CD44- epithelial cords identified in fetal prostate tissues during the androgen-low phase of development (14-18 weeks) (Figure 4). Additional evidence in support of K13 marking resilient prostate SCs was the observation that K13+ glands were prevalent in post-mortem prostate tissue collected from a patient who underwent radiation and androgen deprivation treatment (including abiraterone) (Figure 4). These cumulative results indicate that adult and fetal K13+ SCs are castration-resistant, yet poised to respond to androgen and populate mature ducts/acini. Aggressive TCs share similar traits to SCs (castration-resistance, microenvironment interactions, anti-apoptotic mechanisms). Therefore, the stem-like state, designated by markers of benign adult and fetal SCs (i.e., K13), may also identify prostate tumor variants with the potential for aggressive behavior.

K13 expression in prostate tumor foci is significantly associated with poor clinical outcome. To investigate the prevalence of K13 expression in prostate tumors from patients who underwent radical prostatectomy for PCa and determine correlation of K13 expression with clinical outcome, we evaluated the Greater Los Angeles (GLA) Veterans Affairs Tissue Microarray (VA-TMA). This TMA contains prostate tissue samples from 338 cases that have at least 12 years of clinical follow-up. After optimizing K13 immunostaining, the array was scored for K13 expression (both in benign and cancer cores). The prevalence of K13 expression in benign tissue samples and prostate intraepithelial neoplasia (PIN) did not correlate with clinical progression. However, intratumoral expression of K13 was identified in 30 cases (9.0%) and statistical analysis revealed that men who recurred, progressed to CRPC, and/or developed metastasis disproportionately exhibited K13+ tumors (Figure 5). Evaluation of an independent cohort of prostate biopsy cores from patients with diffuse metastasis at diagnosis demonstrated K13 tumor foci in more than 70% of the cases examined (Figure 6A and data not shown). Immunofluorescent staining of circulating tumor cells (CTCs), captured from a patient with diffusely metastatic PCa, demonstrated co-expression of K13 and Epcam (epithelial cell marker) (Figure 6B). These combined findings suggest the intriguing possibility K13 is a putative SC marker that emerges in primary tumors with significant potential to disseminate and metastasize. Hence, K13 may represent an important staging and/or prognostic biomarker for PCa. These findings has led to the filing of a patent for use of K13 as a metastatic marker for prostate cancer (see Appendix).

IV - REPORTABLE OUTCOMES:

Throughout the course of this grant, our laboratory has generated 10 publications (copied in appendix below) and 3 additional publications that are currently being prepared for submission. Additionally, we have generated 1 patent application. We have presented our work at numerous national conferences, including DOD Impact, Prostate Cancer Foundation Annual Retreat, and Invited Lectures at Ohio State University, Cedars Sinai Medical Center, UCLA, and University of South Carolina.

V - CONCLUSIONS:

Our laboratory has generated new techniques for isolating prostate cancer cells and performed extensive characterization of benign prostate stem cells over the course of this grant that has led to the identification of markers that may be important for staging and prognosis of prostate cancer. Because of the abundant data that we have generated, we have applied for numerous grants for continued support of this work. Pending grant applications include DOD Idea, Biomarker, and Health Disparity Award, P01 in prostate cancer bone metastasis (Co-Investigator), Stein Oppenheimer Foundation, and SPORE Developmental grant. We are also in the process of preparing and R01 application for submission in February 2014.

VI - REFERENCES:

1. Al-Hajj, M. and M.F. Clarke, *Self-renewal and solid tumor stem cells.* Oncogene, 2004. **23**(43): p. 7274-82.
2. Singh, S.K., et al., *Cancer stem cells in nervous system tumors.* Oncogene, 2004. **23**(43): p. 7267-73.
3. Dontu, G., et al., *In vitro propagation and transcriptional profiling of human mammary stem/progenitor cells.* Genes Dev, 2003. **17**(10): p. 1253-70.
4. Bez, A., et al., *Neurosphere and neurosphere-forming cells: morphological and ultrastructural characterization.* Brain Res, 2003. **993**(1-2): p. 18-29.
5. Garraway, I.P., et al., *Human prostate sphere-forming cells represent a subset of basal epithelial cells capable of glandular regeneration in vivo.* Prostate, 2010. **70**(5): p. 491-501.
6. Tomlins, S.A., et al., *Recurrent fusion of TMPRSS2 and ETS transcription factor genes in prostate cancer.* Science, 2005. **310**(5748): p. 644-8.
7. van Bokhoven, A., et al., *Widely used prostate carcinoma cell lines share common origins.* Prostate, 2001. **47**(1): p. 36-51.
8. Mertz, K.D., et al., *Molecular characterization of TMPRSS2-ERG gene fusion in the NCI-H660 prostate cancer cell line: a new perspective for an old model.* Neoplasia, 2007. **9**(3): p. 200-6.
9. Guo, C., et al., *Epcam, CD44, and CD49f distinguish sphere-forming human prostate basal cells from a subpopulation with predominant tubule initiation capability.* PLoS One, 2012. **7**(4): p. e34219.
10. Shen, M.M., et al., *Progenitor cells for the prostate epithelium: roles in development, regeneration, and cancer.* Cold Spring Harb Symp Quant Biol, 2008. **73**: p. 529-38.
11. Goldstein, A.S., et al., *Trop2 identifies a subpopulation of murine and human prostate basal cells with stem cell characteristics.* Proc Natl Acad Sci U S A, 2008. **105**(52): p. 20882-7.
12. van Leenders, G.J., et al., *Expression of basal cell keratins in human prostate cancer metastases and cell lines.* J Pathol, 2001. **195**(5): p. 563-70.

APPENDIX: ATTACHED

ATTACHED FIGURES WITH LEGENDS:

Figure 1
Figure 2
Figure 3
Figure 4
Figure 5
Figure 6

Publications:

1. **Garraway, IP***, Sun, W, Tran, CP, Perner, S, Zhang, B, Goldstein, A, Hahm, S, Haider, M, Head, C, Reiter, R, Rubin, M, and Witte, O. Human prostate sphere-forming cells represent a subset of basal epithelial cells capable of glandular regeneration in vivo. Prostate, April 1, 2010 70(5):491-501. PMID: 19938015; PMC2885946

2. Klatte, T, Seligson, DB, Rao, JY, Yu, H, de Martino, M, **Garraway, IP**, Wong, SG, Belldegrun, As, and Pantuck AJ. Absence of CD44v6 expression is an independent predictor of poor outcome for patients with urothelial bladder cancer. Journal of Urology, April 17, 2010. PMID: 20403620

3. Goldstein, AS, Huang, J, **Garraway, IP**, and Witte, ON. Identification of a cell-of-origin for human prostate cancer. Science, July 30, 2010; 329(5991): 568-71. PMID: 20671189; PMC2917982

4. Mulholland, DJ, Tran, LM, Li, Y, Cai, H, Morim, A, Wang, S, Plaisier, S, **Garraway, IP**, Huang, J, Greaber, T, Wu, H. Cell Autonomous Role of PTEN regulating castrate-resistant prostate cancer growth. Cancer Cell, May 25, 2011. PMID: 21620777; PMC3157296

5. Guo, C, Liu, H., Zhang, B, Cadaneanu, RM, Mayle, AM, and **Garraway, IP***. Epcam, CD44, and CD49f Distinguish Sphere-Forming Human Prostate Basal Cells From a Subpopulation With Increased Tubule Initiation Capability. PLOS One, April 13, 2012. PMID: 22514625; PMC3326009

6. **Garraway, IP***. Will identification of a prostate cancer stem cell lead to its cure? Urologic Oncology: Seminars and Investigations, 2012.

7. Jing, J, Hindoyan, A, Goldstein, A, Lawson, D, Chen, D, Li, Y, Wang, S, Guo, C, Zhang, B, Gleave, M, Witte, O, **Garraway, IP**, and Wu, H. Identification of CD166 as a marker for enriching prostate tumor initiating cells. PLOS One, August 3, 2012. PMID: 22880034; PMCID: PMC3411798

8. Hance, MW, Dole, K, Fopal, U, Bohonowych, JE, Jerzierska-Drutel, A, Neumann, CA, Liu, H, **Garraway, IP**, and Isaacs, JS. Secreted Hsp90 is a novel regulator of the epithelial to mesenchymal transition (EMT) in prostate cancer. Journal of Biological Chemistry, September 18, 2012. PMID: 22989880

9. Peek, EM, Li, DR, Zhang, H, Kim, HP, Zhang, B, **Garraway, IP**, and Chin, AI. Stromal modulation of bladder cancer-initiating cells in a subcutaneous tumor model. American Journal of Cancer Research, November 20, 2012. PMID 23226620; PMCID: PMC3512189

10. **Garraway, IP**. Targeting the RANKL Pathway: Putting the Brakes on Prostate Cancer Progression in Bone. Journal of Clinical Oncology, September 16, 2013. PMID: 24043735

***Denotes Corresponding Author**

Research Papers in Preparation

1. Liu, H, Cadaneanu, RM, Lai, K, Zhang, B, An, DS, Li, X, and **Garraway, IP.** Differential Gene Expression Profiling of Functionally and Developmentally Distinct Human Prostate Epithelial Populations, 2013. In Preparation.

2. Liu, H., Lai, K., Cadaneanu, R., Mayle, AM, **Garraway, IP*.** Keratin 13 is a marker of human prostate stem/progenitor cells and is expressed on a rare subpopulation in benign prostate tissue. In Preparation

3. Mayle, AM., Chamie, K., Litwin, M., and **Garraway, IP*.** Prevalence of health disparity in prostate cancer disease presentation in Southern California veterans. In Preparation.

Patent Application – Attached in Appendix

TABLE 1: Sample Set From Prostate Tissue Biorepository

CODE ID	Eth	Age	Size	PSA	Biopsy Gleason	Biopsy Gleason #	Clinical	Risk	Path	Final Gleason	Treatment
00001	h	71	35g	6.09	4+5	9	T2b	**3**	T3a, N1, 4+5	9	RRP
00002	aa	62	40g	7.70	4+3	7	T1c	**2**	n/a	7	XRT
00003	aa	63	30g	5.85	4+5	9	T2b	**3**	T3b, N0, 4+5	9	RRP
00004	h	63	31.5g	1.57	4+5	9	T2b	**3**	n/a	9	XRT/ADT
00005	w	66	73g	3.27	B	0	n/a	**0**	n/a	0	n/a
00006	w	67	34g	9.80	4+4	8	T2b	**3**	T2c, N0, 4+4	8	RRP
00007	w	84	large	90.00	3+4	7	T2a	**3**	n/a	7	ADT
00008	w	61	65g	10.16	4+4	8	T1c	**3**	T3b, N0, 4+3	7	RRP
00009	w	65	40 - 60g	7.85	3+3	6	T2b	**2**	T2c, N0, 3+3	6	RRP
00010	w	69	26g	6.71	4+5	9	T1c	**3**	n/a	9	XRT
00011	aa	68	17g	7.37	3+4	7	T1c	**2**		7	SEEDS
00012	h	87	n/a	7.40	4+5	9	T2c	**3**	n/a	9	XRT/ADT
00014	aa	63	57g	8.83	B	0	n/a	**0**	n/a	0	n/a
00015	aa	67	85g	5.67	B	0	n/a	**0**	n/a	0	n/a
00016	w	72	n/a	2.68	B	0	n/a	**0**	n/a	0	n/a
00017	aa	71	large	4.32	B	0	n/a	**0**	n/a	0	n/a
00018	aa	61	68g	8.07	3+3	6	T2	**1**		6	AS
00019	w	78	n/a	n/a	B	0	n/a	**0**	n/a	0	n/a
00021	w	62	40g	7.82	3+3	6	T1c	**1**	n/a	6	PnBx
00022	aa	56	20g	27.25	4+4	8	T2a	**3**	T3a, N0, 4+4	8	PnBx
00023	aa	70	68g	5.78	B	0	n/a	**0**	n/a	0	n/a
00024	h	66	67g	7.53	B	0	n/a	**0**	n/a	0	n/a
00025	aa	62	37g	14.93	3+4	7	T2a	**2**		7	XRT
00026	w	68	n/a	1.26	B	0	n/a	**0**	n/a	0	n/a
00027	h	62	88g	4.27	B	0	n/a	**0**	n/a	0.00	n/a
00028	w	69	80g	5.49	3+3	6	T1c	**1**	n/a	6	AS
00029	w	65	47g	6.7	B	0	n/a	**0**	n/a	0	n/a
00030	w	61	50g	4.85	3+4	7	T2b	**2**	T2c, N0, 3+4	7	RRP
00031	aa	62	55g	7.37	B	0	n/a	**0**	n/a	0	n/a
00032	w	63	19g	5.7	4+5	9	T1c	**3**	n/a	9	XRT
00033	aa	63	51g	8.35	3+4	7	T1c	**2**		7	SEEDS
00034	h	66	32g	5.02	3+4	7	T1c	**2**	T2c, N0, 4+3	7	RRP
00036	w	66	29.1g	27.5	3+4	7	T1c	**2**	n/a	7	AS
00038	w	65	20g	4.4	3+5	8	T2c	**3**	T2c, N0, 3+4	7	RRP

00039	h	63	101g	1.96	B	0	n/a	**0**	n/a	0.00	n/a
00040	aa	64	n/a	11	3+3	6	T1c	**2**	T2c, N0, 3+4	7	RRP
00041	w	70	46g	5.69	3+4	7	T1c	**2**	T2c, N0, 3+4	7	RRP
00042	aa	65	31g	19.8	4+4	8	T2c	**3**	T3, N0, 4+3	7	RRP
00043	aa	64	n/a	1.8	B	0	n/a	**0**	n/a	0	n/a
00044	w	63	53g	9.74	3+3	6	T2a	**1**	T2b,N0, 3+4	7	RRP
00045	w	61	n/a	0.63	B	0	n/a	**0**	n/a	0	n/a
00046	w	58	20g	4.34	3+5	8	T2c	**3**	T3a, N0, 4+4	8	RRP
00047	w	67	27g	4.57	4+3	7	T1c	**2**	T2c, N0, 4+5	9	RRP
00048	aa	61	18g	4.8	3+3	6	T1c	**1**	T2c, N0, 3+4	7	RRP
00049	aa	63	15g	8.42	4+3	7	T1c	**2**	T3b, N0, 4+3	7	RRP
00050	aa	62	40g	8.5	4+3	7	T1c	**2**	T3a, N0, 4+4	8	RRP
00051	w	62	18g	7.22	3+4	7	T2b	**2**	T3a, N0, 3+4	7	RRP
00052	h	66	50g	11.53	3+5	8	T1c	**3**	T3a, N1, 4+4	8	RRP
00053	w	62	69g	6.8	3+3	6	T2a	**1**	T2a, N0, 3+3	6	RRP
00054	w	77	33g	7.71	3+5	8	T3a	**3**	T3b, N0, 4+5	9	RRP
00055	aa	69	122g	19.4	4+3	7	T1c	**2**	T2a, N0, 4+3	7	RRP
00056	w	78	134g	3.05	B	0	n/a	**0**	n/a	0	n/a
00057	w	60	24g	9.44	3+4	7	T2b	**2**	T2c, N0, 4+4	8	RRP
00058	w	64	55g	25	4+5	9	T2b	**3**	n/a	9	ChTurp
00059	w	61	28g	4.92	4+5	9	T1c	**3**	T3b, N1, 4+5	9	RRP
00061	aa	65	28g	10.17	3+3	6	T1c	**2**		6	SEEDS
00062	aa	76	63g	5.22	4+5	9	T2b	**3**	T3b, N0, 3+4	7	RRP
00063	w	69	58g	4.77	3+3	6	T2c	**3**	n/a	6	AS
00064	w	72	35.5g	3.19	3+4	7	T2	**2**	n/a	7	WW
00065	aa	52	22g	31.52	5+5	10	T2c	**3**	n/a	10	ADT/XRT
00066	aa	70	84g	11.86	3+4	7	T1c	**2**	Refused	7	RRP
00067	aa	64	30g	16.26	4+4	8	T2b	**3**	n/a	8	XRT
00068	w	61	40g	4.51	3+4	7	T2a	**2**	T2b, N0, 4+5	9	RRP
00069	h	70	35g	250.38	4+5	9	T3	**3**	n/a	9	ADT
00070	aa	58	33g	152.11	5+5	10	T3	**3**	n/a	10	ADT
00071	aa	56	15g	2.25	3+4	7	T1c	**2**	T2c, N0, 4+3	7	RRP
00072	w	76	61g	6.18	4+4	8	T2b	**3**	T3a, N0, 4+4	8	RRP
00073	w	76	95g	33.42	3+3	6	T1c	**3**	n/a	6	WW
00074	w	60	n/a	7	4+5	9	T3	**3**	T3, N1, 4+5	9	RRP
00075	aa	64	39g	15.47	3+4	7	T1c	**2**		7	XRT
00076	w	68	35g	8.5	4+5	9	T2a	**3**	T3, N1, 4+5	9	RRP
00077	aa	68	40 -50g	8.86	4+5	9	T2a	**3**	n/a	9	Acupuncture

00078	aa	71	70g	8.34	3+3	6	T2a	**1**		6	AS
00079	aa	59	30g	40.33	3+4	7	T1c	**3**	n/a	7	XRT
00080	aa	56	32g	4.82	4+3	7	T1c	**2**	n/a	7	RRP
00081	aa	67	52g	5.3	3+4	7	T2a	**2**		7	Brach T
00082	aa	83	62g	296.78	4+3	7	T3	**3**	n/a	7	ADT
00083	aa	69	57g	17.51	3+4	7	T1c	**2**		7	XRT/HT
00084	aa	79	27.8g	110.13	4+5	9	T3	**3**	n/a	9	ADT
00085	aa	62	38.1g	4.34	4+4	8	T2b	**3**	n/a	8	WW
00086	w	59	23g	7.16	4+5	9	T1c	**3**		9	HT
00087	aa	63	19g	18.06	3+4	7	T1c	**2**	T3b, N0, 3+4	7	RRP
00088	w	79	28g	0.64	3+3	6	T1c	**1**	T1a, N0, 3+3	6	RRP
00089	aa	69	50g	7.24 > 1.01	4+4	8	T1c	**3**	n/a	8	ADT
00090	aa	55	37g	9.48	3+4	7	T1c	**2**		7	XRT
00091	h	65	40g	4.64 > 1.27	4+4	8	T1c	**3**	n/a	8	XRT/ADT
00092	aa	57	22.4g	7.9	4+4	8	T2b	**3**	n/a	8	XRT/ADT
00093	aa	61	36g	9.09	3+4	7	T1c	**2**		7	HT
00094	w	58	36g	9.04	4+5	9	T2b	**3**	T3, N0, 4+5	9	RRP
00095	aa	62	40g	14.4	4+3	7	T1c	**2**	n/a	7	XRT
00096	aa	65	50g	4.56	4+5	9	T1c	**3**	T3a, N0, 4+5	9	RRP
00097	aa	65	21g	5.76	B	0	n/a	**0**	n/a	0	n/a
00098	w	68	62g	2.16	B	0	n/a	**0**	n/a	0	n/a
00099	w	63	82g	6.87	B	0	n/a	**0**	n/a	0	n/a
00100	w	65	22g	5.98	3+4	7	T1c	**2**	n/a	7	AS
00101	aa	62	U	19.58	3+3	6	T2a	**2**	T2c, N0, 3+4	7	RRP
00102	aa	69	100g	4.27	B	0	n/a	**0**	n/a	0	n/a
00103	w	68	40g	9.11	3+3	6	T2a	**1**	n/a	6	AS
00104	w	67	34g	8.58	3+3	6	T1c	**1**	n/a	6	AS
00105	aa	62	44g	6.54	B	0	n/a	**0**	n/a	0	n/a
00106	aa	66	17g	8.34	3+3	6	T1c	**1**	n/a	6	AS
00107	aa	55	47.6g	5.17	4+4	8	T1C	**3**	n/a	8	XRT/ADT
00108	w	63	54g	5.58	3+3	6	T1c	**1**	n/a	6	AS
00110	aa	70	16g	0.87	3+3	6	T1c	**1**	n/a	6	AS
00111	h	64	40g	10.27	3+4	7	T1c	**2**	T2c, N0, 3+4	7	RRP
00112	aa	67	30g	5.06	4+4	8	T1c	**3**	n/a	8	RRP
00113	w	64	40g	4.5	3+4	7	T2c	**3**	n/a	7	XRT
00114	aa	63	17g	6.14	4+3	7	T1C	**2**	n/a	7	AS
00116	w	79	n/a	1.74	B	0	n/a	**0**	n/a	0	TURP
00117	w	62	38.3g	5.04	B	0	n/a	**0**	n/a	0	n/a

00119	w	65	50g	4.12	B	0	n/a	**0**	n/a	0	n/a
00122	w	55	60g	0.28	B	0	n/a	**0**	n/a	0	n/a
00123	w	63	22.2g	2.24	3+3	6	T1c	**1**	n/a	6	RRP
00125	w	63	40g	14.15	4+4	8	T2b	**3**	n/a	n/a	RRP
00126	w	69	30g	1.13	B	0	n/a	**0**	n/a	0	n/a
00133	aa	64	34.3g	0.76	3+3	6	T2a	**1**	n/a	n/a	n/a
00134	aa	69	n/a	1.73	B	0	n/a	**0**	n/a	0	TURP
00136	w	65	36g	9.78	B	0	n/a	**0**	n/a	0	n/a

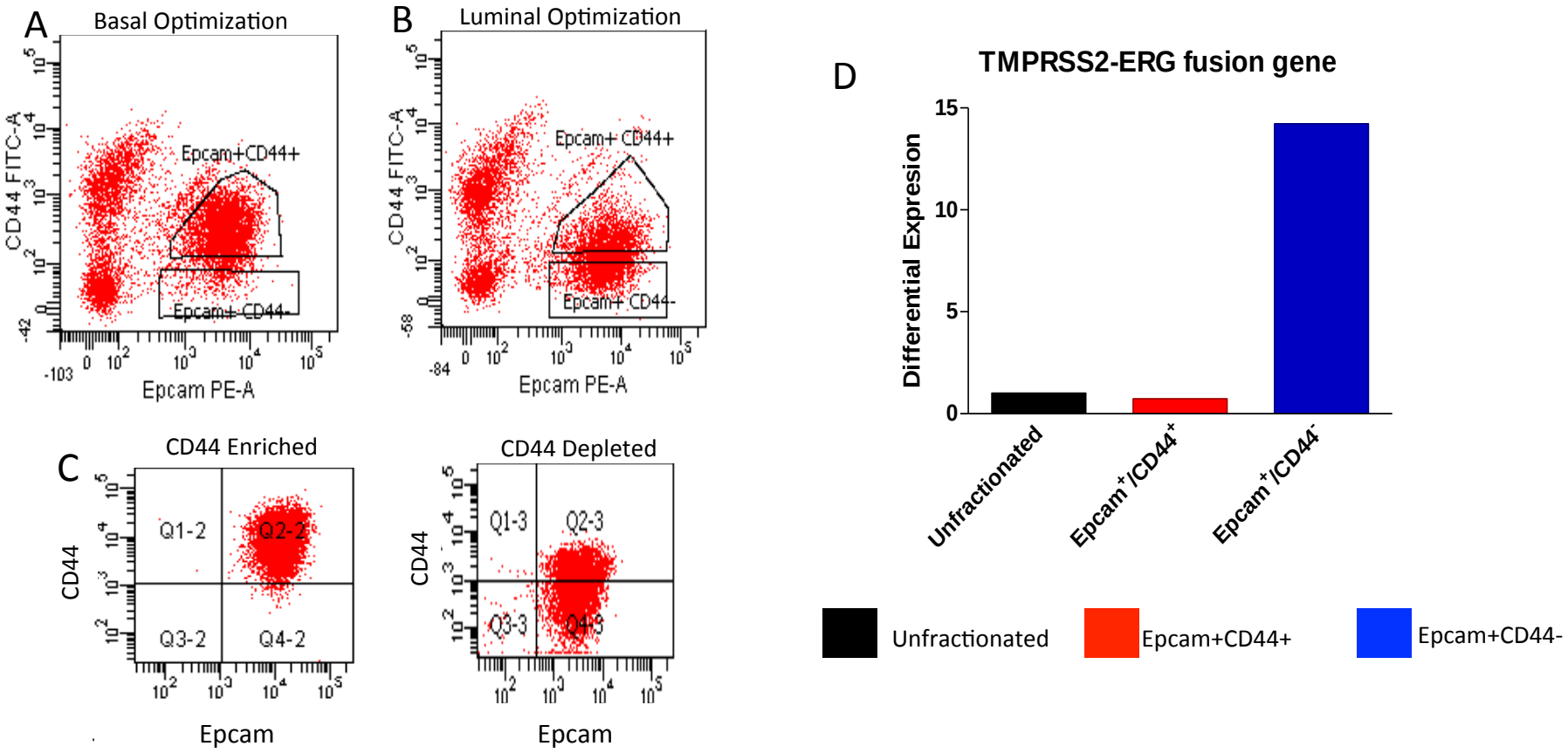

Figure 1. TMPRSS-ERG fusion expression in fractionated prostate epithelial cells. The combination of Epcam and CD44 was used to isolate Epcam+CD44+ basal-enriched (A) and Epcam+CD44- luminal-enriched cell fractions (B) for quantitative RT-PCR. Fractionated cells were compared to total (unfractionated) cells. Relative increased expression of luminal markers (AR, PSA, CK8) in Epcam+CD44^{-} fractions confirms enrichment in this population (D). Expression of TMPRRS-ERG is detected exclusively in the Epcam+CD44- fraction (E).

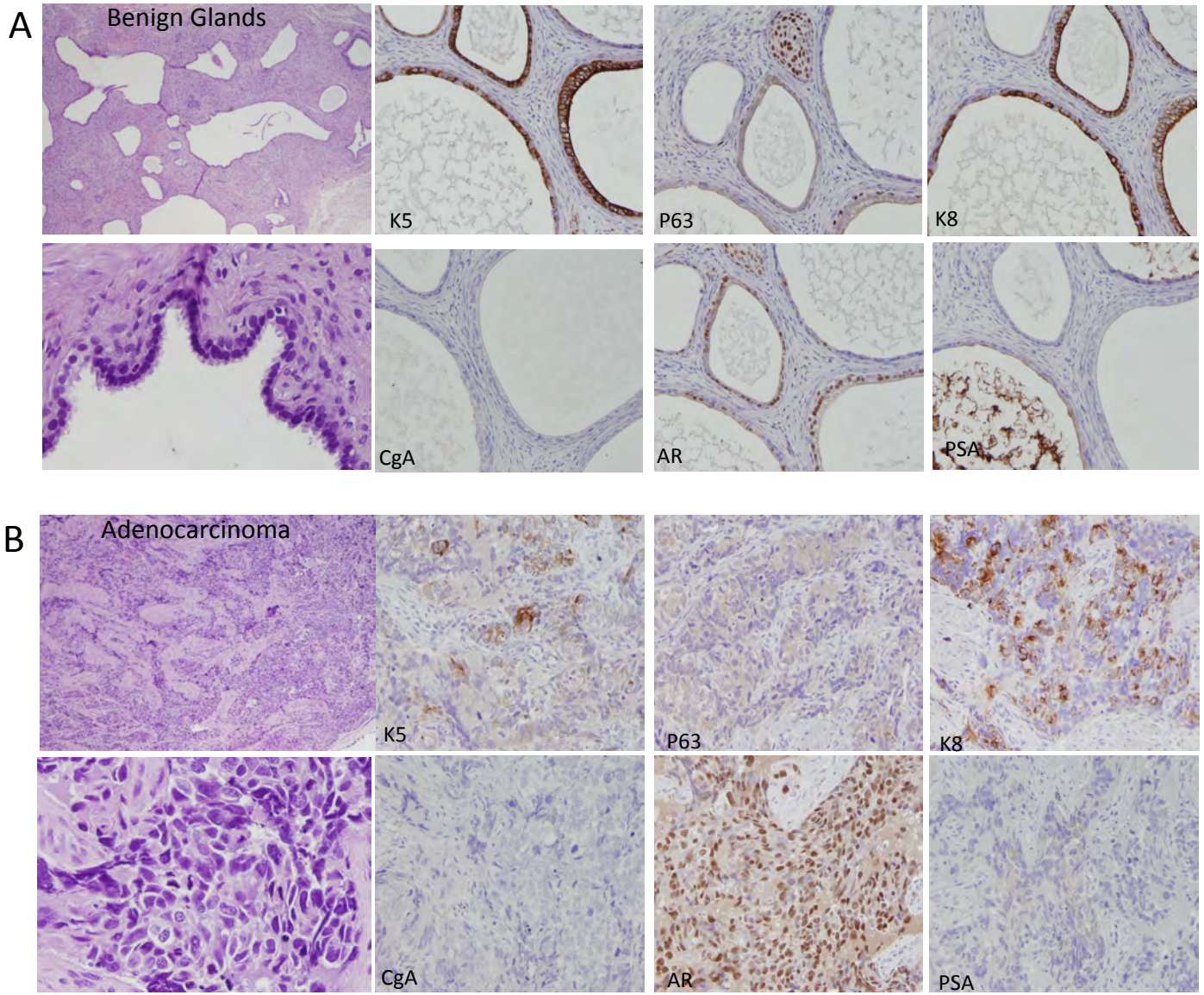

Figure 2. Prostate Cancer Regeneration. A slice of tissue from a radical prostatectomy specimen from a patient with high-grade (Gleason 5+4, pStage T3bN1M0) prostate cancer was procured with preparation of an adjacent frozen section. Tumor and benign tissue were separated and tissues were dissociated into single cells. $5x10^4$ epithelial cells were combined with $1x10^6$ fetal prostate stroma and injected subQ into NOD-SCID mice. After 5 months, grafts were harvested for histological analysis. Marker staining of xenografts matched that found in original surgical specimens (data not shown).

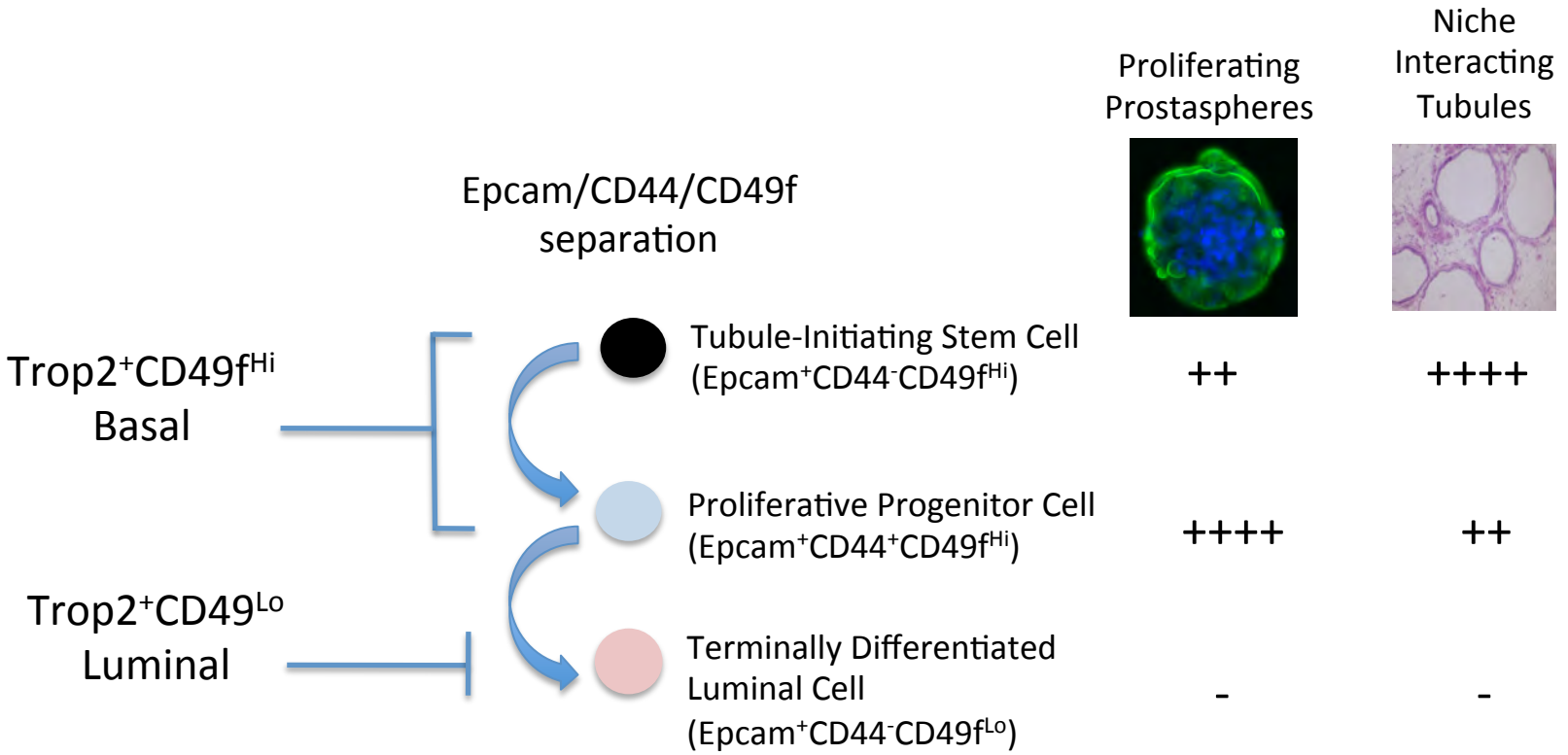

Figure 3. Fractionation of benign prostate epithelial cells enables functional characterization in vitro and in vivo. Trop2+CD49f^{Hi} basal cells contain Epcam+CD44-CD49f^{Hi} putative stem cell (SC) and Epcam+CD44+CD49f^{Hi} putative progenitor cell (PC) subpopulations. Luminal cells (LCs) are isolated based on Trop2+CD49f^{Lo} or Epcam+CD44-CD49f^{Lo} antigenic profile. The functional capability of each prostate epithelial subpopulation to form prostaspheres in vitro or induce new prostate tubules in vivo is summarized.

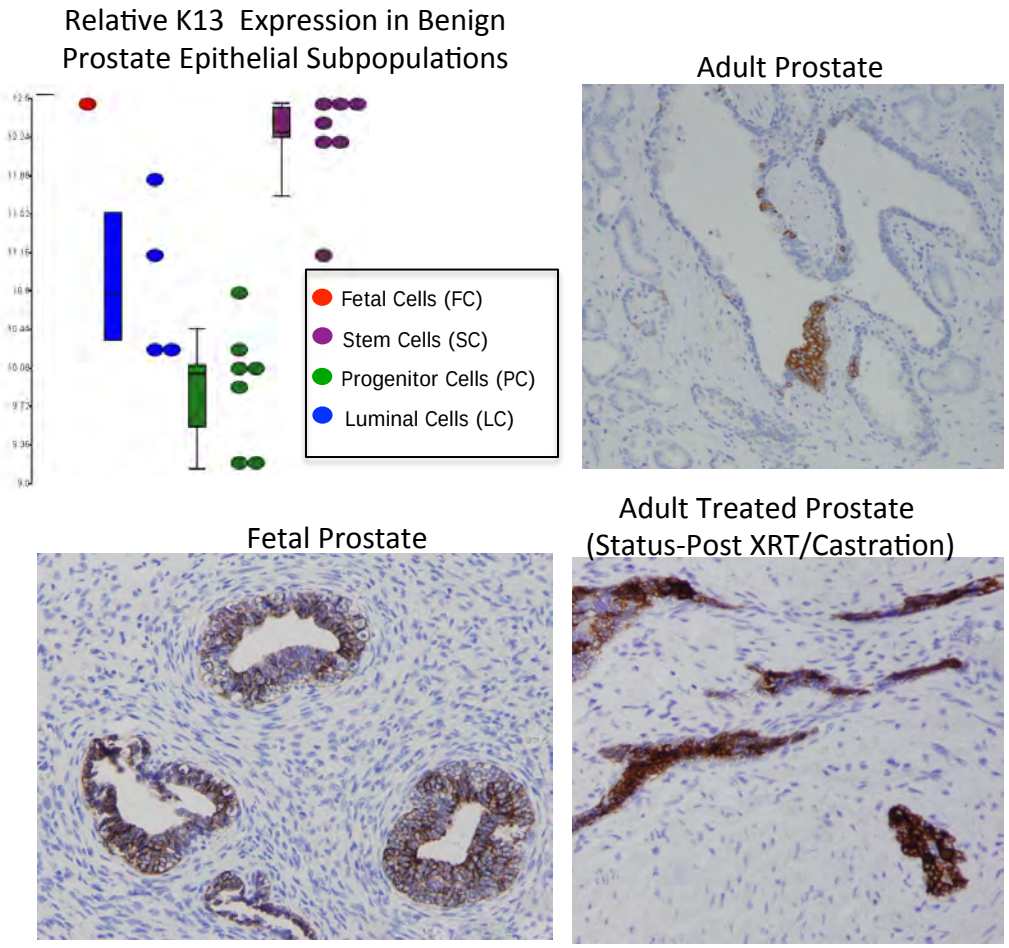

Figure 4. K13 expression may indicate a stem-like cell in benign and cancer tissue. Sorting of adult and fetal prostate epithelial cells based upon Epcam/CD44/CD49f expression yielded functionally and genetically distinct populations. K13 was highly expressed in fetal prostate cells (FCs) and putative adult stem cells (SCs) in DNA microarray analysis (upper left panel). Immunohistochemical staining of fetal and adult prostate tissue for K13 demonstrated focal K13+ cells within the basal compartment of benign adult prostate glands (upper right panel). In androgen-low settings such as in the fetal prostate and castrate adult prostate, predominant K13 expression was observed in cord-like structures, ducts, and acini (lower panels).

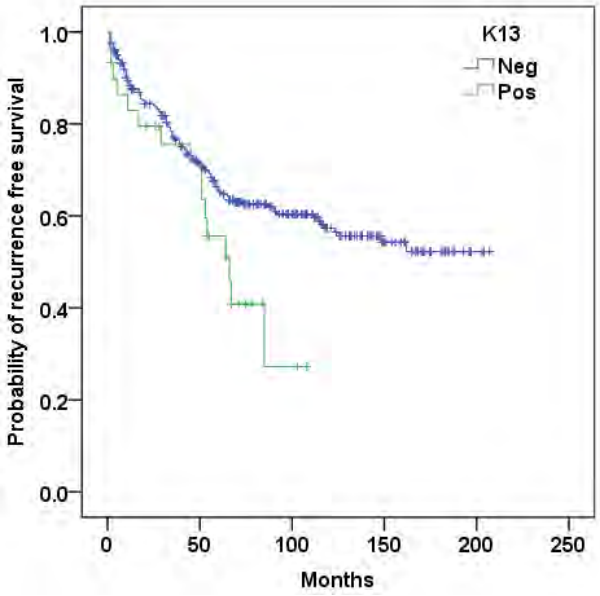

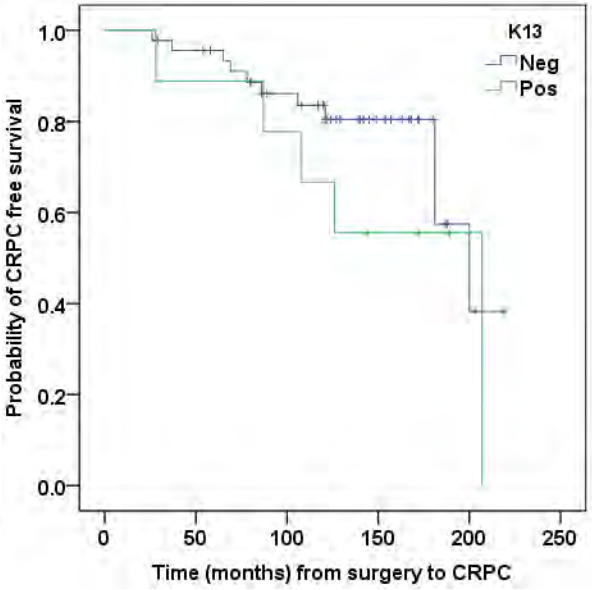

mets * K13 Crosstabulation

			K13		
			Neg	Pos	Total
mets	0	Count	292	26	318
		% within mets	91.8%	8.2%	100.0%
	1	Count	10	4	14
		% within mets	71.4%	28.6%	100.0%
Total		Count	302	30	332
		% within mets	91.0%	9.0%	100.0%

K13+ patients are more likely to develop metastases (p-value = 0.009)

Figure 5. K13 expression in primary tumors is significantly associated with recurrence, CRPC, and metastases. Kaplan-Meier curves demonstrate this phenomenon after analysis of the GLA-VA TMA that contains prostatectomy specimens from 338 patients.

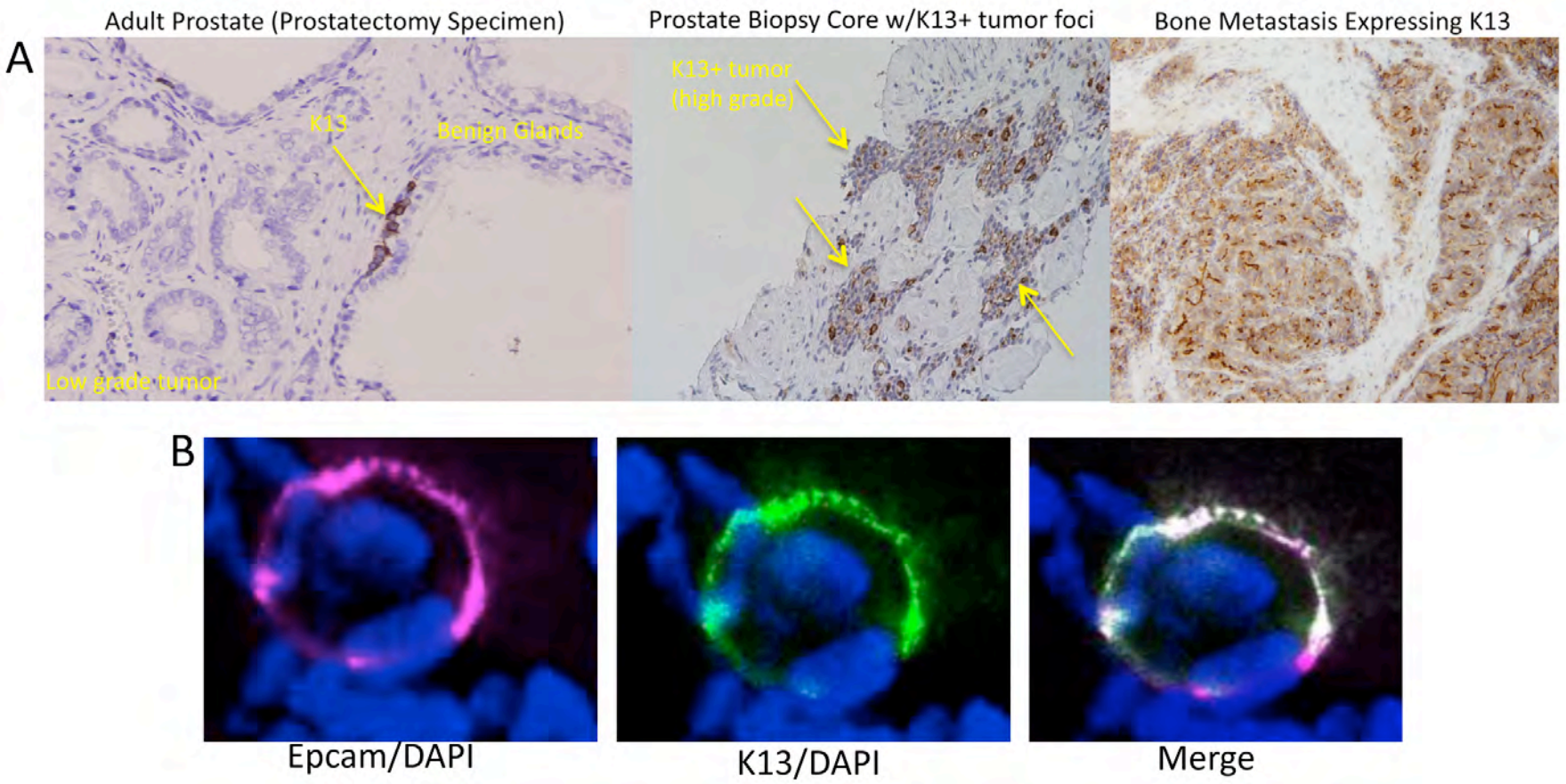

Figure 6. K13 expression is identified in benign glands adjacent to K13-negative, low-grade prostate cancer (left panel), and a prostate biopsy core from a patient with bone metastases at diagnosis (middle panel), and a bone metastasis to the spine (right panel). Ciculating tumor cells from a patient with widespread bone metastasis also display Epcam and K13 co-expression (lower panel).

Published in final edited form as:
Prostate. 2010 April 1; 70(5): 491–501. doi:10.1002/pros.21083.

Human Prostate Sphere-Forming Cells Represent A Subset of Basal Epithelial Cells Capable of Glandular Regeneration In Vivo

Isla P. Garraway[1,2,*], **Wenyi Sun**[1,2], **Chau P. Tran**[1,2], **Sven Perner**[3], **Bao Zhang**[1,2], **Andrew S. Goldstein**[4], **Scott A. Hahm**[1], **Maahum Haider**[1], **Christian S. Head**[2,5], **Robert E. Reiter**[1,2], **Mark A. Rubin**[3], and **Owen N. Witte**[2,4,6]

[1]Department of Urology, David Geffen School of Medicine at UCLA

[2]Jonsson Comprehensive Cancer Center

[3]Department of Pathology, Room C-440, Weill Medical Center of Cornell University

[4]Department of Microbiology, Immunology, and Molecular Genetics, UCLA

[5]Division of Head and Neck Surgery, David Geffen School of Medicine at UCLA

[6]Department of Pathology and Clinical Medicine, David Geffen School of Medicine at UCLA

[7]Investigator of the Howard Hughes Medical Institute, Broad ISCBM

Abstract

Background—Prostate stem/progenitor cells function in glandular development and maintenance. They may be targets for tumor initiation, so characterization of these cells may have therapeutic implications. Cells from dissociated tissues that form spheres in vitro often represent stem/progenitor cells. A subset of human prostate cells that form prostaspheres were evaluated for self-renewal and tissue regeneration capability in the present study.

Methods—Prostaspheres were generated from 59 prostatectomy specimens. Lineage marker expression and TMPRSS-ERG status was determined via immunohistochemistry and fluorescence in situ hybridization (FISH). Subpopulations of prostate epithelial cells were isolated by cell sorting and interrogated for sphere-forming activity. Tissue regeneration potential was assessed by combining sphere-forming cells with rat urogenital sinus mesenchyme (rUGSM) subcutaneously in immunocompromised mice.

Results—Prostate tissue specimens were heterogeneous, containing both benign and malignant (Gleason 3–5) glands. TMPRSS-ERG fusion was found in approximately 70% of cancers examined. Prostaspheres developed from single cells at a variable rate (0.5–4%) and could be serially passaged. A basal phenotype (CD44+CD49f+CK5+p63+CK8−AR−PSA−) was observed among sphere-forming cells. Subpopulations of prostate cells expressing tumor-associated calcium signal transducer 2 (Trop2), CD44, and CD49f preferentially formed spheres. In vivo implantation of sphere-forming cells and rUGSM regenerated tubular structures containing discreet basal and luminal layers. The TMPRSS-ERG fusion was absent in prostaspheres derived from fusion-positive tumor tissue, suggesting a survival/growth advantage of benign prostate epithelial cells.

Conclusion—Human prostate sphere-forming cells self-renew, have tissue regeneration capability, and represent a subpopulation of basal cells.

[*]To Whom Correspondence Should Be Addressed: Box 951738 CHS, 10833 LeConte Avenue, LA, CA 90095-1738, 310-206-4890, igarraway@mednet.ucla.edu.

Introduction

Adult multipotential stem cells (SCs) are responsible for the development, maintenance, and regeneration of the range of specialized cell types comprising mammalian tissues(1,2). Self-renewal is a fundamental characteristic of SCs and refers to asymmetric divisions that give rise to genetically identical daughter cells in addition to more differentiated progenitors. Substantial evidence suggests that this process may be deregulated in cancer, as transformed SCs or early progenitors demonstrate uncontrolled self-renewal that results in phenotypically diverse tumors(3–5). Isolation of these cells may allow antigenic/molecular profiling and the delineation of mechanisms that regulate self-renewal and differentiation(5,6).

Several studies have attempted to identify human prostate SCs (7–12). Richardson et al found that the $\alpha_2\beta_1^{hi}$-integrin cells co-expressing CD133 had increased proliferative activity, in vitro and limited tissue regeneration capacity, in vivo(10). The CD133+/$\alpha_2\beta_1^{hi}$ cells represent a small fraction (<1%) of prostate epithelial cells in benign and cancer tissues(8,10,12,13). In a study of non-immortalized and immortalized human prostate cell lines, prostate stem cells were suggested to be CD133+/ABCG2+/$\alpha_2\beta_1^{hi}$/P63−/PSCA−/AR −/PSA− based on the low frequency of these cells in primary prostate epithelial (PrEC) cultures in relation to neuroendocrine and transient amplifying cells(12). Additionally, sorted CD133+ cells yielded cultures containing a mix of CD133+ and CD133− prostate cells, representing the lineage cell types (11,12).

In order to adequately analyze prostate SCs and hierarchical order of prostate lineage cells derived from human tissue, methods that enable the efficient isolation and expansion of these rare cells is critical. Culture conditions that support proliferation of prostate cells that form spheres may represent a strategy for SC isolation(8,14–16). Spheres are multicellular globes that develop from cells that survive anchorage-independent conditions in vitro, such as growth in ultra-low attachment (ULA) plates or 3D Matrigel cultures(17). Spheres include SCs and early progenitors in studies of breast, brain, and skin and are frequently used to study the processes of self-renewal and differentiation in these systems(14,18–20). Lang et al observed human sphere formation from dissociated prostate tissue(21). Spheroid formation and branching morphogenesis with expression of luminal markers in response to androgen and stromal growth factors was noted when primary human prostate cells were grown in 3D Matrigel cultures(21). Other human studies have suggested that prostasphere formation is a functional validation of prostate SC activity in fractionated cell lines or xenografts(9,22,23). In order to further characterize the relationship between stem/progenitor cells and sphere-formation, self-renewal and tissue regeneration properties of prostaspheres should be addressed.

In the present study, a diverse collection of human prostate surgical specimens was accrued and prostaspheres were generated reproducibly and robustly from all prostate tissue types when cells were cultured in low calcium, serum free, defined medium(12). Clonally derived prostaspheres could be dissociated and passaged for multiple generations and induced the formation of ductal/acinar-like structures *in vivo*. Trop2, alpha 6-integrin (CD49f), and CD44 mark cells with enriched sphere-forming capability. The self-renewing and differentiation features of prostaspheres support preservation of SC activity in these cultures. As previously suggested, low calcium, serum free culture conditions that support human prostate stem/progenitor growth appears to select exclusively for normal cells, since the *TMPRSS-ERG* fusion was never observed in the prostaspheres derived from fusion positive tissue specimens(11,12,24).

Materials and Methods

Tissue acquisition, isolation and culture of prostate epithelial cells

Human prostate tissue was obtained from 59 patients (ages 41–76), undergoing prostate surgery (radical prostatectomy or cystoprostatectomy). All subjects were consented for tissue collection in accordance with an approved protocol through the Office for the Protection of Research Subjects at UCLA. For a list of patient characteristics, see supplemental Table 1. Adjacent tissue specimens were fixed in formalin and paraffin-embedded to determine the presence of benign or malignant glands. The remainder of the tissue specimens were mechanically and enzymatically digested as previously described(25). Dissociated prostate cell suspensions were sequentially filtered through 100-micron and 40-micron filters, and then passed through a 23-gauge needle. Cells were counted with a hemocytometer and resuspended in PREGM (Clonetics) supplemented with FGF2 (Invitrogen), EGF (Sigma), B27 (Invitrogen), and heparin (Sigma). The cells were then cultured (as described below), or subjected to cell separation using MACS beads columns (Miltenyi Biotec LTD, Surrey, UK) or a cell sorter, as described below.

Antigenic cell separation

Cells were mixed with MACS microbeads linked to a cocktail of lineage antibodies (Lineage Depletion Kit, Miltenyi Biotec Ltd, Surrey, UK). After selection through the magnetic column, lineage negative cells were incubated with Trop-2 (R&D Systems), anti-CD44 (Abcam), anti-CD49f (Biolegend), or anti-CD133 (Miltenyi) antibodies, followed by incubation with MACS goat anti-mouse IgG microbeads (Miltenyi) and application to a MACS column. Alternatively, Lin− cells stained with fluorescent-linked primary antibody were subjected to sorting. Sorted cells were counted and plated in 3D Matrigel cultures.

In vitro prostasphere culture

Epithelial cells were counted and re-suspended in 50:50 matrigel:PREGM a concentration of 1×10^3–6×10^4 cells/80microliters. This matrigel/cellular suspension was plated at the edge of the well on 12-well plates and allowed to set by incubation at 37°C for 30 minutes. One milliliter of defined media was then added to each well and plates were replaced in 37°C incubator. For dissociation and passage of prostaspheres, 1-hour incubation in 1mg/ml Dispase (Invitrogen) was performed. Spheres were collected, washed in RPMI, and trypsinized (TripLE 100microliters/12-well plate). Cells were washed, counted, and replated as described above.

Lentiviral infection of prostate epithelial cells

Prostate epithelial cells were cultured in PREGM for 48–72 hours. Viral supernatant containing lentivirus (CCR-dsRed, a gift from the laboratory of Dr. Irvin Chen at UCLA) and polybrene was added for 3 hours at 37°C. Red fluorescence was detected 48–72 hours post-infection. Monolayer cells were detached with TripLE and plated in Matrigel for sphere formation.

Immunohistochemistry of tissue/prostasphere sections

Prostate tissue was paraffin embedded as previously described(26). For paraffin embedding of prostaspheres, matrigel cultures were subjected to Dispase (1mg/ml, Invitrogen) and whole prostaspheres were collected and fixed in 10% buffered formalin at 4°C for twelve hours. After fixation, prostaspheres were washed in PBS and 50% ethanol, pelleted by centrifugation, and resuspended in 10–20microliters of Histogel (Richard-Allen Scientific). Four-micron thick sections of frozen or paraffin embedded tissue were deparaffinized with xylene and rehydrated through a descending series of ethanol washes as described. Antigen

retrieval and standard immunoperoxidase procedures were used in combination with primary antibodies. For Immunofluorescence assays, permeablization of tissue was performed using cold methanol:acetone, followed by staining with antibodies.

Fluorescence-activated cell sorting and analysis

Prostate cells were suspended in PBS/10% FCS and stained with antibody for 30 minutes at 4°C. Fluorescence-activated cell sorting and analysis are performed on a BD Special Order FACSAria II system and Diva v6.1.1. Live single cells are gated based on scatter properties and analyzed for their surface marker expression. Cells are sorted and collected at 40C using 100um nozzle and 23psi.

Subcutaneous Injections in Immunocompromised mice

Male SCID mice age 8–24 weeks was subjected to subcutaneous injections of prostaspheres +/− 2×10^5 rat urogenital sinus mesenchyme (rUGSM) suspended in 100 microliters 50:50 matrigel:PREGM. Subcutaneous implantation of time-release testosterone pellets was performed. Subcutaneous nodules at the site of injection were removed and frozen/paraffin-embedded sections were generated for immunohistochemical analysis. Rat UGSM was prepared as previously described (27). Fresh UGSM cells were cultured in DMEM +10%FBS and passaged twice prior to use in tissue regeneration assays.

Fluorescence Activated In Situ Hybridization

Paraffin-embedded human prostate tumor specimens were subjected to FISH as previously described(28). Briefly, the break-apart assay is utilized with probes that recognize the centromeric and telomeric portions of the ERG gene. If there is a break in the gene, distinct red and green signals are detected. If the gene is intact, the red and green probes remain adjacent and sometimes overlap, resulting in a yellow signal (See Figure 4).

Results

A small fraction human prostate cells obtained from a diverse collection of human prostate tumor specimens form prostaspheres

To investigate whether sphere-forming cells may be derived from all types of human prostate tissue, specimens were obtained from 59 patients undergoing radical prostatectomy or cystoprostatectomy. Pathological examination of collected specimens confirmed inclusion of either benign (normal and BPH) or a mixture of benign and malignant glands with Gleason grades ranging from 3–5 (Supplemental Table 1). Fresh tissues were mechanically and enzymatically dissociated and single cells were seeded in ULA plates or Matrigel at densities ranging from 10^2 to 10^5 cells/well (Figure 1, Supplemental Figure 1). Prostaspheres formed from 21/24 specimens cultured in ULA plates and 35/35 specimens cultured in Matrigel within 3 days of plating, with continued growth over 2 weeks to diameters of 100–400 microns (Figure 1). There were only three patient specimens that failed to for prostaspheres, which may be attributed to variations in tissue processing as conditions were worked out. We observed that Matrigel cultures facilitated enumeration of prostaspheres by preventing the aggregation of cells that occurs in floating culture (14, 29). Sphere architecture and marker expression was similar in both growth conditions (Supplemental Figure 1).

Although significant variability in the number of prostaspheres that developed from individual patient specimens was observed, consistent variation in the number or appearance of prostaspheres according to specific clinical or pathological parameters was not apparent (Figure 1A–B). Further prospective analysis with dissection/isolation of tumor nodules may allow more definitive conclusions on the relationship of sphere-formation and Gleason

grade. Tallies of prostaspheres were obtained from a sample of 10 individual patients with varying pathologies (benign to malignant) after replicate plating in 6-well culture dishes. The average number of prostaspheres obtained with similar seeding densities per patient was plotted (Figure 1B). The frequency of sphere-forming cells derived from all 59 patients was found to range from approximately 0.5%–4% (data not shown).

Human prostaspheres are clonally derived and self-renew

To confirm the clonal origin of prostaspheres, 10^5 freshly isolated prostate epithelial cells were grown as a monolayer for 48 hours and then labeled with red fluorescent protein via lentiviral-mediated gene transfer of the dsRed gene. Approximately 90% of prostate cells appeared to be expressing dsRed within seventy-two hours after exposure to virus (data not shown). Infected (red) prostate epithelial cells were detached and mixed with wild-type (colorless) cells at a ratio of 1:5. The mixed cell populations were plated in Matrigel in triplicate. Approximately 7 days following plating, robust prostasphere formation was observed and only monochromatic (all red or all colorless) prostaspheres were identified, consistent with the concept of clonality (Figure 1C). Microscopic examination of frozen sections of DSRED and clear prostaspheres demonstrated that all cells within a single sphere were monochromatic (Figure 1C–E).

All of the prostasphere specimens cultured in Matrigel could be passaged for multiple generations. Repetitive passaging was specifically assessed in 4 individual prostasphere cultures and more than 20 generations were obtained without any sign of growth decline after dissociation and passage (data not shown). DsRed-infected prostaspheres could also be dissociated, mixed, and passaged repeatedly (>3 generations) with formation of new monochromatic prostaspheres. Single red fluorescent prostaspheres were isolated by serial dilution in 96-well plates, followed by dissociation and incubation of single cells in Matrigel. Secondary red prostaspheres were noted to develop, supporting the self-renewal potential of individual prostaspheres (Figure 1C–F).

Prostate cells obtained from dissociated prostaspheres also remained viable after freeze/thaw, with formation of new spheres in Matrigel that could be serially passaged. Dissociated prostaspheres (passage 2–10) were cryopreserved for 1 month followed by thaw and seeding in Matrigel. New prostaspheres developed 7–10 days after plating that could be passaged >3 generations (data not shown). Taken together, these findings highlight the versatility of prostaspheres, in that they can be genetically manipulated, expanded continuously in vitro, and cryopreserved.

Prostaspheres express predominately basal markers

The prostate epithelium is composed of basal cells, including stem cells and transient amplifying cells, terminally differentiated luminal cells, and neuroendocrine cells(30). Prostate epithelial cells can be differentiated based on expression of a variety of markers(31). The majority of basal cells express the high molecular weight cytokeratins (CK5 and CK14), p63, CD44, alpha integrin, and do not express significant low molecular weight cytokeratins (CK8/18), AR or PSA(12,25). Luminal cells, in contrast, do not express p63, but exhibit relatively high levels of AR, PSA, CK8/18(31). Transient amplifying (intermediate) cells express basal marker, CK5 and often co-express the luminal marker, CK8 and prostate stem cell antigen (PSCA)(25). Neuroendocrine cells are express neuropeptides, including chromogranin A and synaptophysin(31).

In order to determine the expression profile of prostate epithelial cells within prostaspheres, immunostaining was performed using antibodies against several basal and luminal markers (Figure 2A). The basal markers CK5, alpha 6 integrin (CD49f), CD44, and p63 were

strongly expressed by the majority of sphere-forming cells. Greater than 95% of the sphere-forming cells/20× objective high-powered field (hpf) appeared to express CK5 and p63. Between 50–80% of cells/hpf expressed CD44 and CD49f. Luminal markers, including AR (androgen receptor) and PSA (prostate-specific antigen) were not observed in prostaspheres (data not shown). CK8 expression was noted in approximately 1% of sphere-forming cells/hpf. Co-expression with CK5 was seen in these cells (Figure 2A). We did not observe cells expressing the neuroendocrine markers, synaptophysin or Chromogranin A (data not shown).

In addition to prostatic markers, the spheres were assessed for cell proliferation and apoptosis via Ki-67 and TUNEL staining (Supplemental Figure 2). Approximately 2% of the sphere cells/hpf were observed to have Ki-67 activity, with the outermost layer of the sphere demonstrating the most activity. TUNEL staining was not clearly detected in prostaspheres (Supplemental Figure 2).

Antigenic profile of human prostasphere-forming cells

To determine the surface markers that identify cells capable of prostasphere formation, we fractionated subpopulations of prostate cells via microbeads or automatic cell sorter separation (Figure 2B–D). Cell fractionation resulted in a variable decrease (2–10 fold) in the overall number of prostaspheres formed following manipulation secondary to decreased cell viability following these manipulations (data not shown). However, comparison of fractionated cell populations within individual specimens allowed relative sphere-forming activity to be assessed.

In order to eliminate the possibility that cells of the hematopoeitic lineage retained in the prostate tissue contributed to the sphere-forming population, we performed depletions with blood lineage antibodies. FACS analysis with representative lineage antibodies CD31 and CD45 confirmed removal of hematopoeitic/endothelial cells (Supplemental 3B). Lin− and Lin+ cells were plated in Matrigel cultures in several replicates of 1×10^4 cells/well to assess sphere-forming activity. Prostaspheres formed exclusively in the Lin− cell fraction (Figure 2B).

Previous investigations of human and murine prostate SCs have suggested that CD44 may be an important marker(10). In order to investigate whether CD44+ prostate epithelial cells were enriched for sphere-forming capability, we used microbeads or automatic cell sorting to isolate cells expressing this antigen. FACS analysis confirmed enrichment of CD44+ cells (Supplemental Figure 3B). Plating of CD44+ cells in Matrigel demonstrated enriched sphere-forming capability (>2.5-fold) with 1/15 Lin−CD44+ cells forming spheres (Figure 2B). Although the presence of CD44 greatly enriched for sphere-forming capability, some spheres were noted in the Lin−CD44− fraction. This likely represents incomplete separation of CD44+ and CD44− cells, but the possible that a fraction of Lin−CD44− cells have sphere-forming capability cannot be excluded.

We used a similar approach to examine whether CD49f or the putative human prostate stem cell marker, CD133, marked the sphere-forming population. FACS analysis demonstrated CD49f+ (8–20%) and CD133+ cells (2–7%) after lineage depletion (data not shown). Fractionated prostate cells were evaluated by FACS prior to seeding in Matrigel (Supplemental Figure 3B). A marked increase in sphere formation was observed with Lin−CD49f+ cells compared to Lin−CD49f− cells (Figure 2B). On the other hand, multiple attempts to separate CD133+ and CD133− cells resulted in highly variable results in sphere-forming capability. For most of the patient samples, more spheres appeared to form in the CD133− fraction, however, a smaller number of spheres consistently formed within the CD133+ fraction as well (Figure 2B). Our difficulties in obtaining consistent results with

CD133 cell separation could be due to the fact that the CD133+ cells are so rare, usually composing 0.25–2% of unfractionated prostate cells. This made isolation and plating in sphere cultures difficult. We typically isolated $<2\times10^3$ CD133+ cells via this approach. Alternatively, CD133 as a solitary marker may subdivide, but not distinguish the sphere-forming population.

Our previous studies have demonstrated that human prostate sphere-forming cells are similar to murine prostate sphere-forming cells in regard to antigenic profile. The epithelial marker, Trop-2 in combination with the high expression of the integrin, CD49f (a marker of human basal cells), enables sphere-forming cells to be isolated. Trop-2 expression appears confined to epithelial cells in the human prostate and may be used in combination with other markers to evaluate subpopulations of prostate epithelial cells for sphere-forming capability. We performed cell sorting based on Trop2/CD49f and Trop2/CD44 expression and found that the double positive fractions (Trop2+CD49fHI and Trop2+CD44+) demonstrate the highest sphere-forming capability in multiple patients (Figure 2C–D).

Prostaspheres do not contain the *TMPRSS-ERG* gene rearrangement

Since the human prostaspheres were generated from primary tumors that contain a heterogeneous mix of benign and malignant glands, evaluation to distinguish benign and cancerous spheres, was warranted. However, qualitative and quantitative differences were not observed among prostaspheres derived from different pathological specimens (Figure 1). With the discovery of prevalent gene rearrangements involving ETS family members in prostate cancer, we predicted that cytogenetic tools may enable identification of cancerous prostaspheres(28). Gene fusions involving *ERG*, *ETV1*, and *ETV4* involve a variety of 5' partners that direct aberrant expression of these transcription factors and may initiate a cascade of events leading to tumorigenesis(28). The most common rearrangement involves juxtaposition of the androgen-regulated *TMPRSS2* gene with *ERG*. *TMPRSS-ERG* gene fusions have been detected in primary prostate tumor specimens, metastases, and xenografts by fluorescence in situ hybridization (FISH)(28). Analysis of prostate tumor surgical cohorts have found 36–78% of prostate cancers possess the *TMPRSS-ERG* fusion(28). The presence of this fusion in individual prostaspheres may suggest that cancer stem/early progenitor cells are expanded in our cultures.

To test the feasibility of this approach, FISH analysis was performed on select prostate tissue specimens and coordinating prostaspheres (Figure 3). The *TMPRSS-ERG* fusion was found in approximately 7/10 (70%) cancer cases tested (Figure 3A). The fusion, however, was consistently absent in prostasphere cultures derived from *TMPRSS-ERG*+ tissues, even when the specimens obtained contained >80% tumor (Figure 3B–E). Analysis of monolayer cultures concomitantly derived from prostate tumor specimens also failed to demonstrate the presence of the gene fusion, indicating that both spheroid and adherent cultures select for fusion-negative, genetically normal cells (data not shown).

Sphere-mediated prostate tissue regeneration

To evaluate whether human prostaspheres can form ductal/acini structures in vivo, whole prostaspheres from eight patients were injected subcutaneously into NOD-SCID/IL2rγNull mice with or without 2×10^5 rUGSM cells. The number of sphere forming cells injected ranged from 5×10^4 to 1×10^6. All experiments were performed in duplicate. In the mice injected with whole prostaspheres combined with Matrigel, 10/16 grafts were obtained 6–12 weeks post injection (Figure 4A). The grafts ranged in weight between approximately 25 mg and 250 mg. Control mice injected with rat UGSM without prostaspheres, were included for comparison (Figure 4A). Grafts were fixed in formalin and embedded in paraffin to prepare tissue sections. H&E staining revealed the prostaspheres induced formation of acinar-like

structures. No acini were observed in the rUGSM only grafts. In the absence of rUGSM, prostaspheres induced the development of rudimentary appearing acini/epithelial cords with multiple layers of epithelial cells and rare lumen formation (Figure 4A). On the other hand, when human prostaspheres were combined with rat rUGSM and Matrigel, acini contained well-defined lumens with secretions (Figure 4A). IHC analysis showed that these acinar structures were reminiscent of normal adult human adult prostate glands with CK8 and AR positive luminal cells as well as CK5 and p63 positive basal cells (Figure 4B). Human prostate-specific markers, prostate stem cell antigen (PSCA), prostate membrane antigen (PSMA), and prostate specific antigen (PSA) were also observed (Figure 4B). Immunostaining for the neuroendocrine markers synaptophysin and chromogranin A did not demonstrate neuroendocrine cells (data not shown). Although prostaspheres regenerated xenografts resembling normal human prostate, the efficiency of glandular structure formation was relatively low with 1–12 tubules ranging per 20×/hpf. Our results indicate that prostaspheres are capable of glandular regeneration with basal and luminal compartments comparable to normal human prostate tissue.

Discussion

Sphere-formation in anchorage-independent conditions is a characteristic of SCs initially described in neural and mammary systems(16,18). Studies of murine prostate have demonstrated that a small fraction of prostate epithelial cells expressing Sca-1 and alpha-6 integrin (CD49f), and Trop2 formed spheres in 3D-Matrigel cultures that possessed self-renewal and differentiation characteristics(14,17,21,32). Additionally, only the sphere-forming fraction of murine prostate epithelial cells can induce gland formation via in vivo tissue regeneration(17,33). In human studies, in vitro prostate spheroid formation with branching morphogenesis has been observed, but self-renewal, tissue regeneration capability, and antigenic profiling to delineate the sphere-forming population was not addressed(32,34). Here, we show that 0.5%–4% of epithelial cells obtained from a wide variety of dissociated human prostate specimens form prostaspheres that possess features of self-renewal, as demonstrated by serial passage. Human prostaspheres can also be dissociated and cryopreserved with the retention of sphere-forming ability following thaw (data not shown). These practical traits of human prostaspheres enable viable repositories of prostate stem/progenitor cells to be generated that could facilitate high throughput studies of large collections of patient specimens in the future.

In prior human prostate stem cell studies, epithelial cells expressing $\alpha_2\beta_1^{hi}$ integrin, CD44, and CD133 have displayed stem-like qualities of increased proliferative potential in vitro and regeneration of acinar-like structures in vivo(7,10,13). Consistent with previous reports characterizing prostate SCs, the putative SC markers, CD44 and α_6 integrin (CD49f) appeared to greatly enhance for the sphere-forming population in this study, in addition to the epithelial marker, Trop2. The CD133+ population was technically difficult to evaluate, given the small fraction of these cells present in human prostate tissue specimens. Furthermore, recent studies suggest that CD133 antibody binding may inhibit survival of these cells in vitro(11). It was observed that expression of CD133 did not segregate basal epithelial cells based on sphere-forming capability, since both CD133+ and CD133− fractions formed spheres. In contrast to CD44 and CD49f, immunostaining and FACS of prostaspheres failed to detect CD133, indicating that this marker is not preserved in prostasphere cultures (data not shown). The significance of CD133 expression should be evaluated in future studies examining characteristics of prostaspheres capable of tubule formation in vivo (see below).

The marker profile of sphere-forming cells with abundant expression of CK5 and p63 suggest that normal basal cells were selected in our prostasphere cultures. Basal markers are

frequently lost in cancer and malignant glands display a luminal phenotype that includes abundant CK8/18 and AR expression, with loss of CK5 and p63(35). Until the discovery of ETS translocations, antigenic or genetic marker that clearly delineated normal and cancerous prostate cells were not available. With ETS family fusions now detectable via FISH, genetic events associated with malignancy can be evaluated in prostaspheres(28,36). Consistent with the benign basal marker profile of prostaspheres and regenerated tubules, the *TMPRSS-ERG* fusion was not identified in sphere-forming cells from fusion+ tissue specimens. Although some of the collected tissue specimens contained large tumor volumes (>80% tumor glands), all of the prostaspheres demonstrated a predominance of benign basal cells. Although it is possible that prostate cancer stem/progenitor cells do not contain gene rearrangements, a more likely scenario is that the culture conditions that support human prostate SC isolation and expansion inhibit cancer cell outgrowth. This observation is consistent with previous studies suggesting that cancer cells do not proliferate in the defined medium typically used to expand prostate epithelial cells(12,24). Dissection of tumor nodules and outgrowth in more permissive media conditions may enable selection of prostate CSCs and will have to be addressed in future studies (24).

The acinar structures observed in vivo also appeared to resemble normal human prostate tissue, with preservation of discreet basal and luminal layers. In vivo tissue regeneration occurred at low efficiency with approximately 1×10^6 sphere forming cells yielding scant tubules in regenerated grafts. One possibility for the limited differentiation potential of prostaspheres is that a significant proportion of develop from progenitor cells, not bona fide SCs, and are not capable of tubule formation/maturation. To distinguish between human prostate SCs and progenitors, it will be necessary to further subdivide sphere-forming cells and evaluate tissue regeneration capacity of fractionated sphere-forming cells. It is possible that bona fide SCs will have the exclusive ability to recapitulate prostate glands in vivo, while progenitors will demonstrate restricted differentiation.

Conclusions

Prostate sphere-forming cells include stem/progenitor cells that are capable of self-renewal and tissue regeneration. Sphere forming cells exhibit a basal profile that resembles benign prostate epithelial cells and induce the formation of ductal/acinar structures *in vivo*.

Supplementary Material

Refer to Web version on PubMed Central for supplementary material.

Acknowledgments

The authors thank Donghui Cheng in the laboratory of Dr. Owen Witte for providing technical expertise in the area of cell sorting. Additional flow cytometry was performed in the UCLA Jonsson Comprehensive Cancer Center (JCCC) and Center for AIDS Research Flow Cytometry Core Facility that is supported by National Institutes of Health awards CA-16042 and AI-28697, and by the JCCC, the UCLA AIDS Institute, and the David Geffen School of Medicine at UCLA. These studies were supported by the Prostate Cancer Foundation, the Jean Perkins Foundation, and the Department of Defense (PC061068 and PC07373).

REFERENCES

1. Majka M, Kucia M, Ratajczak MZ. Stem cell biology - a never ending quest for understanding. Acta Biochim Pol. 2005; 52:353–358. [PubMed: 15990920]
2. Moore KA, Lemischka IR. Stem cells and their niches. Science. 2006; 311:1880–1885. [PubMed: 16574858]
3. Polyak K, Hahn WC. Roots and stems: stem cells in cancer. Nat Med. 2006; 12:296–300. [PubMed: 16520777]

4. Cozzio A, Passegue E, Ayton PM, Karsunky H, Cleary ML, Weissman IL. Similar MLL-associated leukemias arising from self-renewing stem cells and short-lived myeloid progenitors. Genes Dev. 2003; Vol. 17:3029–3035. [PubMed: 14701873]
5. Al-Hajj M, Clarke MF. Self-renewal and solid tumor stem cells. Oncogene. 2004; 23:7274–7282. [PubMed: 15378087]
6. Jordan CT, Guzman ML, Noble M. Cancer stem cells. N Engl J Med. 2006; 355:1253–1261. [PubMed: 16990388]
7. Collins AT, Habib FK, Maitland NJ, Neal DE. Identification and isolation of human prostate epithelial stem cells based on alpha(2)beta(1)-integrin expression. J Cell Sci. 2001; 114:3865–3872. [PubMed: 11719553]
8. Brown MD, Gilmore PE, Hart CA, Samuel JD, Ramani VA, George NJ, Clarke NW. Characterization of benign and malignant prostate epithelial Hoechst 33342 side populations. Prostate. 2007; 67:1384–1396. [PubMed: 17639507]
9. Gu G, Yuan J, Wills M, Kasper S. Prostate cancer cells with stem cell characteristics reconstitute the original human tumor in vivo. Cancer Res. 2007; 67:4807–4815. [PubMed: 17510410]
10. Richardson GD, Robson CN, Lang SH, Neal DE, Maitland NJ, Collins AT. CD133, a novel marker for human prostatic epithelial stem cells. J Cell Sci. 2004; 117:3539–3545. [PubMed: 15226377]
11. Vander Griend DJ, Karthaus WL, Dalrymple S, Meeker A, DeMarzo AM, Isaacs JT. The role of CD133 in normal human prostate stem cells and malignant cancer-initiating cells. Cancer Res. 2008; 68:9703–9711. [PubMed: 19047148]
12. Litvinov IV, Vander Griend DJ, Xu Y, Antony L, Dalrymple SL, Isaacs JT. Low-calcium serum-free defined medium selects for growth of normal prostatic epithelial stem cells. Cancer Res. 2006; 66:8598–8607. [PubMed: 16951173]
13. Collins AT, Berry PA, Hyde C, Stower MJ, Maitland NJ. Prospective identification of tumorigenic prostate cancer stem cells. Cancer Res. 2005; 65:10946–10951. [PubMed: 16322242]
14. Lawson DA, Xin L, Lukacs RU, Cheng D, Witte ON. Isolation and functional characterization of murine prostate stem cells. Proc Natl Acad Sci U S A. 2007; 104:181–186. [PubMed: 17185413]
15. Wang TY, Sen A, Behie LA, Kallos MS. Dynamic behavior of cells within neurospheres in expanding populations of neural precursors. Brain Res. 2006; 1107:82–96. [PubMed: 16859652]
16. Ishibashi S, Sakaguchi M, Kuroiwa T, Yamasaki M, Kanemura Y, Shizuko I, Shimazaki T, Onodera M, Okano H, Mizusawa H. Human neural stem/progenitor cells, expanded in long-term neurosphere culture, promote functional recovery after focal ischemia in Mongolian gerbils. J Neurosci Res. 2004; 78:215–223. [PubMed: 15378509]
17. Goldstein AS, Lawson DA, Cheng D, Sun W, Garraway IP, Witte ON. Trop2 identifies a subpopulation of murine and human prostate basal cells with stem cell characteristics. Proc Natl Acad Sci U S A. 2008; 105:20882–20887. [PubMed: 19088204]
18. Dontu G, Abdallah WM, Foley JM, Jackson KW, Clarke MF, Kawamura MJ, Wicha MS. In vitro propagation and transcriptional profiling of human mammary stem/progenitor cells. Genes Dev. 2003; 17:1253–1270. [PubMed: 12756227]
19. Bez A, Corsini E, Curti D, Biggiogera M, Colombo A, Nicosia RF, Pagano SF, Parati EA. Neurosphere and neurosphere-forming cells: morphological and ultrastructural characterization. Brain Res. 2003; 993:18–29. [PubMed: 14642827]
20. Blatchford DR, Quarrie LH, Tonner E, McCarthy C, Flint DJ, Wilde CJ. Influence of microenvironment on mammary epithelial cell survival in primary culture. J Cell Physiol. 1999; 181:304–311. [PubMed: 10497309]
21. Lang SH, Sharrard RM, Stark M, Villette JM, Maitland NJ. Prostate epithelial cell lines form spheroids with evidence of glandular differentiation in three-dimensional Matrigel cultures. Br J Cancer. 2001; 85:590–599. [PubMed: 11506501]
22. Snoek R, Rennie PS, Kasper S, Matusik RJ, Bruchovsky N. Induction of cell-free, in vitro transcription by recombinant androgen receptor peptides. J Steroid Biochem Mol Biol. 1996; 59:243–250. [PubMed: 9010316]
23. Tang DG, Patrawala L, Calhoun T, Bhatia B, Choy G, Schneider-Broussard R, Jeter C. Prostate cancer stem/progenitor cells: identification, characterization, and implications. Mol Carcinog. 2007; 46:1–14. [PubMed: 16921491]

24. Dalrymple S, Antony L, Xu Y, Uzgare AR, Arnold JT, Savaugeot J, Sokoll LJ, De Marzo AM, Isaacs JT. Role of notch-1 and E-cadherin in the differential response to calcium in culturing normal versus malignant prostate cells. Cancer Res. 2005; 65:9269–9279. [PubMed: 16230388]
25. Tran CP, Lin C, Yamashiro J, Reiter RE. Prostate stem cell antigen is a marker of late intermediate prostate epithelial cells. Mol Cancer Res. 2002; 1:113–121. [PubMed: 12496358]
26. Garraway IP, Seligson D, Said J, Horvath S, Reiter RE. Trefoil factor 3 is overexpressed in human prostate cancer. Prostate. 2004; 61:209–214. [PubMed: 15368472]
27. Hayward SW, Haughney PC, Rosen MA, Greulich KM, Weier HU, Dahiya R, Cunha GR. Interactions between adult human prostatic epithelium and rat urogenital sinus mesenchyme in a tissue recombination model. Differentiation. 1998; 63:131–140. [PubMed: 9697307]
28. Tomlins SA, Rhodes DR, Perner S, Dhanasekaran SM, Mehra R, Sun XW, Varambally S, Cao X, Tchinda J, Kuefer R, Lee C, Montie JE, Shah RB, Pienta KJ, Rubin MA, Chinnaiyan AM. Recurrent fusion of TMPRSS2 and ETS transcription factor genes in prostate cancer. Science. 2005; 310:644–648. [PubMed: 16254181]
29. Singec I, Knoth R, Meyer RP, Maciaczyk J, Volk B, Nikkhah G, Frotscher M, Snyder EY. Defining the actual sensitivity and specificity of the neurosphere assay in stem cell biology. Nat Methods. 2006; 3:801–806. [PubMed: 16990812]
30. Collins AT, Maitland NJ. Prostate cancer stem cells. Eur J Cancer. 2006; 42:1213–1218. [PubMed: 16632344]
31. van Leenders GJ, Aalders TW, Hulsbergen-van de Kaa CA, Ruiter DJ, Schalken JA. Expression of basal cell keratins in human prostate cancer metastases and cell lines. J Pathol. 2001; 195:563–570. [PubMed: 11745692]
32. Bello-DeOcampo D, Kleinman HK, Deocampo ND, Webber MM. Laminin-1 and alpha6beta1 integrin regulate acinar morphogenesis of normal and malignant human prostate epithelial cells. Prostate. 2001; 46:142–153. [PubMed: 11170142]
33. Shi X, Gipp J, Bushman W. Anchorage-independent culture maintains prostate stem cells. Dev Biol. 2007; 312:396–406. [PubMed: 17976567]
34. Lang SH, Stower M, Maitland NJ. In vitro modelling of epithelial and stromal interactions in non-malignant and malignant prostates. Br J Cancer. 2000; 82:990–997. [PubMed: 10732776]
35. Gil-Diez de Medina S, Salomon L, Colombel M, Abbou CC, Bellot J, Thiery JP, Radvanyi F, Van der Kwast TH, Chopin DK. Modulation of cytokeratin subtype, EGF receptor, and androgen receptor expression during progression of prostate cancer. Hum Pathol. 1998; 29:1005–1012. [PubMed: 9744319]
36. Lei Q, Jiao J, Xin L, Chang CJ, Wang S, Gao J, Gleave ME, Witte ON, Liu X, Wu H. NKX3.1 stabilizes p53, inhibits AKT activation, and blocks prostate cancer initiation caused by PTEN loss. Cancer Cell. 2006; 9:367–378. [PubMed: 16697957]

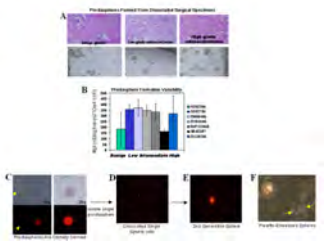

Figure 1.

Formation of Prostaspheres from Dissociated Human Prostate Tissue. Prostate tissue obtained from patients undergoing cancer surgery was mechanically and enzymatically digested. Single cells were and plated in Matrigel seeded at a density 2×10^4/well in 6-well culture dishes. Adjacent tissue samples were paraffin-embedded and stained with H&E for histological evaluation. Human prostaspheres developed robustly from all prostate specimens (A), including benign prostate tissue, low-grade (Gleason 3+3) adenocarcinoma, and high-grade (Gleason 4+5) adenocarcinoma. Prostaspheres derived from these tissues formed prostaspheres in Matrigel (A, lower panel). B. Prostaspheres were plated in triplicate in 6-well plates at a seeding density of 1x10e4 cells/well. After approximately 14 days, prostaspheres were counted and the average number of spheres from 7 individual patients with pathological diagnosis of benign prostate, low- grade, and high-grade adenocarcinoma is depicted in the graph. Freshly dissociated prostate cells were grown as a monolayer for 48 hours followed by incubation with lentivirus carrying the gene for red fluorescent protein (RFP). Red cells were mixed with uninfected (colorless) cells at a ratio of 1:5 and plated in Matrigel culture (1×10^4 cells/well). Only monochromatic spheres were observed in (C) as seen in light and fluorescent views. Monochromatic spheres were isolated and plated by serial dilution into ULA 96-well plates so that 1-sphere/well was obtained. Single spheres were subjected to digest with TrypLE and single cells were then re-incubated in PREGM media (D). New monochromatic spheres were noted to form from single cells after 2-weeks of incubation (E). Frozen sections of RFP/clear spheres demonstrate that all cells within the sphere are red or clear and confirm clonogenicity (F).

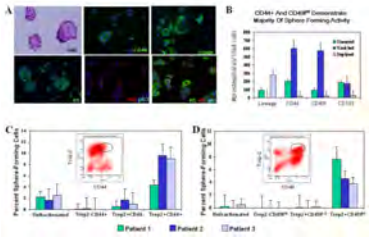

Figure 2.

Human prostaspheres exhibit a predominately basal expression profile. Paraffin-embedded human prostaspheres were stained for prostate epithelial markers (A). H&E staining, CD44 (green), CK5 (green), CK8 (red), and p63 (blue) are shown individually as well as co-staining. B. Fractionation of dissociated prostate cells subjected via enrichment/depletion of lineage, CD44, CD49f, or CD133 antigens demonstrate sphere-forming capability of these cell populations. At least 3 different patient samples were tested per antigen. Lineage, CD44, and CD49f isolates were plated at a rate of 1×10^4 cells per well. CD133 isolates were plated at 1×10^3 cells/well. C, D. Percentage of spheres formed from prostate epithelial cells sorted based on Trop2/CD44 and Trop2/CD49f expression.

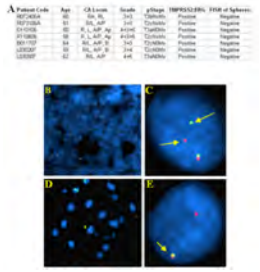

Figure 3.

Patients undergoing radical prostatectomy for prostate cancer were consented for tissue donation according to an approved protocol through the Office for the Protection of Research Subjects at UCLA. Patient information including age, pre-operative prostate specific antigen (PSA), tumor location on final pathology (R, Right, L, Left, A, Anterior, P, Posterior, Ap, Apex, B, Base), and pathological stage (T2, tumor confined within the prostatic capsule, T3, tumor extends beyond the prostate capsule) is presented in the panel A. Tissue specimens from these patients were mechanically and enzymatically dissociated and cultured in 50:50 Matrigel:PREGM (supplemented with EGF, FGF, and B27) to allow prostasphere formation. Paraffin-embedded tumor specimens and prostaspheres were subjected to FISH for *TMPRSS-ERG* gene rearrangement. Human prostate cancer FISH is shown in panels B (40×) and C (100×) in a case that displays the ERG break-apart genetic variation. In contrast, FISH of the prostaspheres shown in panels D and E show an intact *ERG* gene with overlap of the probes. None of the prostaspheres derived from patients with *TMPRSS-ERG* fusion in their cancer specimens displayed a similar genetic abnormality.

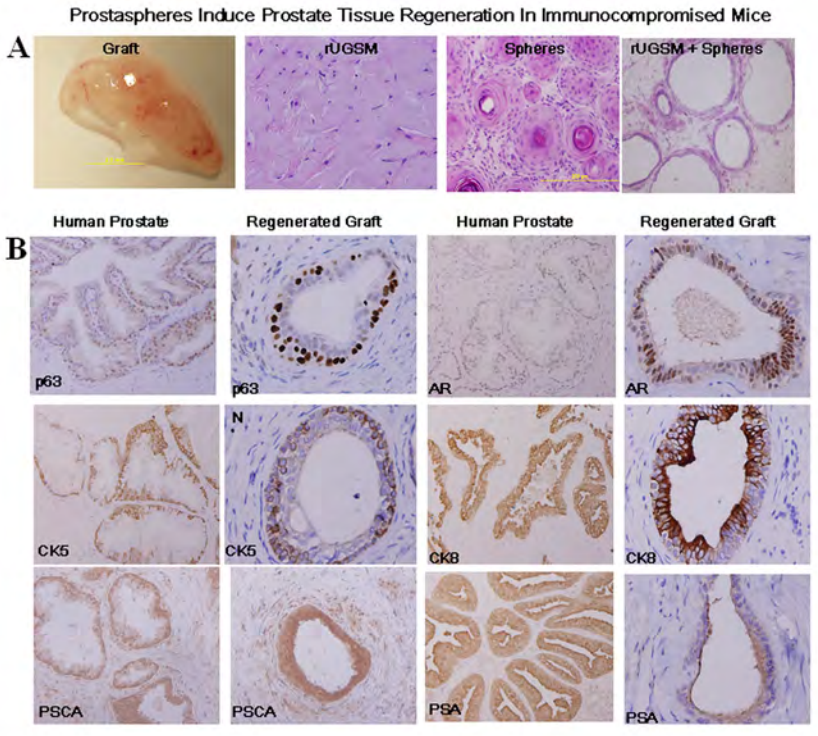

Figure 4.

Prostaspheres form acinar structures in immunocompromised mice. Whole prostaspheres were isolated, mixed with Matrigel and injected subcutaneously into mice either with or without rUGSM. Glandular structures could be palpated 6–12 weeks post-injection. Glandular-like structures recovered 8 weeks after subcutaneous implantation of whole prostaspheres (containing from 5×10^4 to 1×10^6 cells) suspended in Matrigel. A. H&E staining of graft containing 2×10^5 rat UGSM only, graft containing regenerated prostate tissue induced by prostaspheres without UGSM, showing tightly packed acinar structures separated by mouse infiltrating stroma, and grafts of regenerated prostate tissue formed by combining whole prostaspheres with 2×10^5 rat UGSM. B. IHC analysis of the expression of CK5, p63, PSCA, AR, CK8, and PSA in normal human prostate tissue sections and acini derived induced by prostaspheres (regenerated graft).

Published in final edited form as:
Science. 2010 July 30; 329(5991): 568–571. doi:10.1126/science.1189992.

Identification of a cell-of-origin for human prostate cancer

Andrew S. Goldstein[1], **Jiaoti Huang**[2,3,8], **Changyong Guo**[2,4], **Isla P. Garraway**[2,4], and **Owen N. Witte**[1,5,6,7,8]

[1]Molecular Biology Institute, University of California, Los Angeles, CA 90095

[2]Jonsson Comprehensive Cancer Center, University of California, Los Angeles, CA 90095

[3]Department of Pathology and Laboratory Medicine, University of California, Los Angeles, CA 90095

[4]Department of Urology, University of California, Los Angeles, CA 90095

[5]Department of Microbiology, Immunology and Molecular Genetics, University of California, Los Angeles, CA 90095

[6]Department of Molecular and Medical Pharmacology, University of California, Los Angeles, CA 90095

[7]Howard Hughes Medical Institute, David Geffen School of Medicine, University of California, Los Angeles, CA 90095

[8]Eli and Edythe Broad Center of Regenerative Medicine and Stem Cell Research, University of California, Los Angeles, CA 90095

Abstract

Prostate cancer induced in primary human prostate basal cells recapitulates disease initiation and progression in immunodeficient mice.

Luminal cells are believed to be the cells-of-origin for human prostate cancer because the disease is characterized by luminal cell expansion and absence of basal cells. Yet functional studies addressing the origin of human prostate cancer have not previously been reported due to a lack of relevant in vivo human models. Here we show that basal cells, from primary benign human prostate tissue, can initiate prostate cancer in immunodeficient mice. The cooperative effects of AKT, ERG, and androgen receptor (AR) in basal cells recapitulated the histological and molecular features of human prostate cancer with loss of basal cells and expansion of luminal cells expressing prostate-specific antigen (PSA) and alpha-methylacyl-CoA racemase (AMACR). Our results demonstrate that histological characterization of cancers does not necessarily correlate with the cellular origins of the disease.

Prostate cancer research has been hindered by an absence of model systems in which the disease is initiated from primary human prostate epithelial cells, precluding investigation of transforming alterations and cells-of-origin. Commonly used human prostate cancer cell lines and xenografts were derived from metastatic lesions. Murine prostate cancer models prohibit testing of species-specific therapies such as monoclonal antibodies against human proteins (1). An ideal model system would be human cell-derived and present as a multi-focal disease to accurately represent the heterogeneity of prostate malignancy (2). The

Corresponding Author: Owen N. Witte, M.D., Howard Hughes Medical Institute, University of California, Los Angeles, 675 Charles E. Young Dr. South, 5-748 MRL, Los Angeles, CA 90095-1662, Phone: 310-206-0386, FAX: 310-206-8822, owenwitte@mednet.ucla.edu.

system should allow one to investigate the role that specific genetic alterations and paracrine signals play in disease initiation and progression. Finally, the model system should be highly malleable, allowing for comparisons of lesions derived from different cell populations or driven by different genetic alterations. We create such a system by directly transforming naïve adult human prostate epithelium with genetic alterations that are commonly found in human prostate cancer. Activation of the PI3K pathway, typically via loss of PTEN (3), and increased expression of the ETS family transcription factor ERG through chromosomal translocation (4) occur frequently together in human prostate cancer and cooperate to promote disease progression in mice (5–7). AR is commonly upregulated in human prostate cancer and the androgen signaling axis is implicated in late stage disease (8).

Luminal cells are generally accepted as the cells-of-origin for human prostate cancer (9,10) because pathologists diagnose the disease based on the absence of basal cell markers (11). Evidence from the mouse implicates both luminal cells (12–14) and basal cells (15–17) in prostate cancer initiation. While murine cancer cell-of-origin studies typically involve transgenic mice with oncogene expression or Cre-mediated deletion of tumor suppressors driven by cell-type specific promoters (18), parallel studies in the human system require both a method to reliably separate sub-populations of primary cells and an in vivo transformation model.

In addition to rare neuroendocrine cells and reported intermediate phenotypes, the three main epithelial cell populations described in the human prostate are K5 (Keratin 5)+ K14+ $K8/18^{lo}$ basal cells, K5+ K14− $K8/18^{lo}$ basal cells, and K5− K14− $K8/18^{hi}$ luminal cells (19). No commonly accepted strategy exists to isolate such populations from dissociated human prostate tissue. We have previously demonstrated expression of CD49f (integrin alpha 6) and Trop2 (TACSTD2) in human prostate tissue by immunohistochemical staining and flow cytometry, where these two antigens distinguish four separate populations (20,21). To determine the cellular identities of each population, we performed intracellular flow cytometry for basal (K14) and luminal (K18) keratins on primary human prostate cells in addition to western blot and quantitative PCR (qRT-PCR) analyses on fractions isolated by fluorescence-activated cell sorting (FACS). The $CD49f^{lo}Trop2^{hi}$ fraction expresses high levels of the luminal keratins K8 and K18, low or negative levels of basal keratins K5 and K14, and high expression of AR and several androgen-regulated genes such as PSA, Nkx3-1 and TMPRSS2 (Fig. 1A–C,fig S1). The $CD49f^{hi}Trop2^{hi}$ fraction expresses high levels of K5 and the basal transcription factor p63, and two discrete peaks for K14 by intracellular flow cytometry, presumably containing both K14+ and K14− basal cells (Fig. 1A–C,fig S1). $CD49f^{hi}Trop2^{hi}$ cells express intermediate levels of the luminal-type keratins (Fig. 1A), confirming previous reports that basal cells express low but detectable levels of K8/18 (19). CD117 (kit) expression is not enriched in either epithelial fraction (fig S1). The results from three different approaches confirm that we can reproducibly enrich for the isolation of basal and luminal epithelial cells from primary human prostate tissue. The remaining cells are negative for both epithelial keratins and gene expression analysis indicates enrichment for CD31+ von Willebrand factor (VWF)+ endothelial cells ($CD49f^{hi}Trop2^{-}$) and CD90+ Vimentin+ stromal cells ($CD49f^{lo}Trop2^{-}$) (Fig. 1A–C, fig S1).

Classic human epithelial transformation studies involve an initial selection process via immortalization through manipulation with genetic influences like the SV40 T-antigen and/or the catalytic subunit of telomerase in addition to the selected oncogenes (22). We wanted to avoid culture selection by directly transforming primary cells prior to transplantation, so we looked to a recent report by Morrison and colleagues to gain insight into in vivo conditions. Quintana *et al*. reported that the number of primary human melanoma cells capable of tumor formation could be vastly improved by transplanting primary cells subcutaneously with Matrigel into NOD-SCID-IL2Rγ^{null} (NSG) mice (23). Adapting this

strategy, we transduced primary human prostate cells with lentivirus, combined these cells with murine Urogenital Sinus Mesenchyme (UGSM) cells in Matrigel and injected subcutaneously into NSG mice. Starting materials were obtained from patients undergoing radical prostatectomy surgeries and benign tissues were carefully separated from cancer by an experienced Urologic Pathologist. Benign starting materials were negative for expression of human prostate malignancy markers and displayed no features of histologic transformation (fig. S2). Transplantation of cells without genetic modification never resulted in PIN or cancer, demonstrating an absence of malignant cells in starting materials.

We transduced 10^5 primary human prostate basal or luminal cells with a control lentivirus carrying the fluorescent marker RFP and found that both cell types were capable of lentiviral transduction (fig. S3). We next combined freshly-sorted cells with UGSM in Matrigel and transplanted into NSG mice. Although we were concerned that one cell type might preferentially undergo apoptosis in response to sorting, injection or residence in the subcutaneous space, we found that both cell types survived at relatively equal rates (fig. S4). When grafts were harvested after 8–16 weeks in vivo, outgrowths were only observed from basal cells (Fig. 1D). Luminal-derived grafts lacked epithelial structures and mimicked transplantation of UGSM cells alone (Fig. 1D). Basal-derived prostatic tubules exhibited a remarkable similarity to the native architecture of the gland, demonstrated by an outer K5+ p63+ basal cell layer and one or multiple K8+ AR+ luminal layers (Fig. 1E). As few as 5,000 basal cells were sufficient to generate ducts with distinct basal and luminal layers (table S1). Dissociated cells from grafts recapitulated the original four populations by flow cytometry discerned by expression of Trop2 and CD49f (Fig. 1F). Staining for a human-specific Trop2 antibody confirmed the development of human prostatic tissue (fig. S5). Results were reproducible for four independent patient samples and showed little variation between replicate grafts.

We next introduced a lentivirus carrying both activated (myristoylated) AKT and ERG (7) into primary basal and luminal cells (Fig. 2A). After 8–16 weeks in vivo, we observed the development of abnormal structures expressing AKT, nuclear ERG and the fluorescently linked marker RFP (Fig. 2B, 2D) from primary basal cells but not luminal cells (Fig. 2B). Structures lacking RFP expression, indicating an absence of lentiviral infection, were benign, demonstrating the requirement for expression of oncogenes to initiate a malignant phenotype. We observed an expansion of AR+ luminal-like cells with retention of the p63+ basal layer in basal cell-derived lesions (Fig. 2C). In many areas, cells were positive for both PSA and AMACR (Fig. 2C), a marker of both high grade PIN and prostate cancer (24). Based on the presence of morphologically malignant AR^+/PSA^+ luminal cells surrounded by $p63^+$ basal cells, basal cell-derived lesions fulfill the histological criteria for the diagnosis of high grade PIN, the precursor lesion to invasive prostate cancer (25).

We evaluated if additional genetic alterations could be used to recapitulate human prostate cancer. Primary cells were transduced with the RFP-marked lentivirus carrying AKT and ERG and a GFP-marked lentivirus carrying AR (26) (Fig. 3A). Combination of AKT, ERG and AR resulted in the development of adenocarcinoma from basal cells (Fig. 3B) but not luminal cells. While some basal cell-derived structures retained expression of p63 and resembled PIN (fig. S6), many glands had lost the basal layer (Fig. 3B,fig. S6), a defining histological feature used by pathologists for the diagnosis of human prostate cancer (11). Cancerous glands expressed PSA (Fig. 3B,fig S7), AR and AMACR (Fig. 3B) in patterns indistinguishable from patient samples of clinical prostate cancer (Fig. 3C). At high power, cells from cancer lesions exhibited hyperchromatic nuclei with visible nucleoli (Fig. 3B–C, H&E insets). Clinical prostate cancer presents as a multifocal disease with considerable heterogeneity of disease grade (2). Within the same grafts, we observed lesions that correspond to benign structures (AR+/PSA+/p63+/AMACR−), PIN (AR+/PSA+/p63+/

AMACR+) and cancer (AR+/PSA+/p63−/AMACR+), recapitulating the mixed histology found in cancer patients (fig. S6).

Cells within the basal fraction can regenerate benign prostate tissue in immunodeficient mice. Introduction of oncogenic alterations in the target cells can induce a disease that mimics human prostate cancer, establishing basal cells as one cell-of-origin for prostate cancer. Our results support studies in the mouse demonstrating that histological characterization of cancers in the absence of functional studies can be misleading for determining cells-of-origin (27–30). As the human prostate epithelial hierarchy is further delineated, additional cell-types may be identified with cancer-initiating properties.

Even though basal cells express low levels of AR, they share the property of androgen-independence (31) with late stage castration-resistant prostate cancer cells (8), suggesting that pathways involved in basal cell function and self-renewal may play a role in tumor cell survival and disease recurrence after androgen withdrawal. Therefore, further interrogation of target cells may provide insight into treatments for castration-resistant prostate cancer.

Supplementary Material

Refer to Web version on PubMed Central for supplementary material.

References

1. Pienta KJ, et al. Prostate 2008 May 1;68:629. [PubMed: 18213636]
2. Ruijter ET, van de Kaa CA, Schalken JA, Debruyne FM, Ruiter DJ. J Pathol 1996 Nov;180:295. [PubMed: 8958808]
3. Yoshimoto M, et al. Cancer Genet Cytogenet 2006 Sep;169:128. [PubMed: 16938570]
4. Tomlins SA, et al. Science 2005 Oct 28;310:644. [PubMed: 16254181]
5. Carver BS, et al. Nat Genet 2009 May;41:619. [PubMed: 19396168]
6. King JC, et al. Nat Genet 2009 May;41:524. [PubMed: 19396167]
7. Zong Y, et al. Proc Natl Acad Sci U S A 2009 Jul 28;106:12465. [PubMed: 19592505]
8. Chen CD, et al. Nat Med 2004 Jan;10:33. [PubMed: 14702632]
9. Okada H, et al. Virchows Arch A Pathol Anat Histopathol 1992;421:157. [PubMed: 1381129]
10. Parsons JK, Gage WR, Nelson WG, De Marzo AM. Urology 2001 Oct;58:619. [PubMed: 11597556]
11. Wojno KJ, Epstein JI. Am J Surg Pathol 1995 Mar;19:251. [PubMed: 7532918]
12. Ma X, et al. Cancer Res 2005 Jul 1;65:5730. [PubMed: 15994948]
13. Wang X, et al. Nature 2009 Sep 24;461:495. [PubMed: 19741607]
14. Iwata T, et al. PLoS One 5:e9427. [PubMed: 20195545]
15. Lawson DA, et al. Proc Natl Acad Sci U S A Feb 9;107:2610. [PubMed: 20133806]
16. Mulholland DJ, et al. Cancer Res 2009 Nov 15;69:8555. [PubMed: 19887604]
17. Wang S, et al. Proc Natl Acad Sci U S A 2006 Jan 31;103:1480. [PubMed: 16432235]
18. Barker N, et al. Nature 2009 Jan 29;457:608. [PubMed: 19092804]
19. Verhagen AP, et al. Cancer Res 1992 Nov 15;52:6182. [PubMed: 1384957]
20. Goldstein AS, et al. Proc Natl Acad Sci U S A 2008 Dec 30;105:20882. [PubMed: 19088204]
21. Garraway IP, et al. Prostate Apr 1;70:491. [PubMed: 19938015]
22. Hahn WC, et al. Nature 1999 Jul 29;400:464. [PubMed: 10440377]
23. Quintana E, et al. Nature 2008 Dec 4;456:593. [PubMed: 19052619]
24. Wu CL, et al. Hum Pathol 2004 Aug;35:1008. [PubMed: 15297968]
25. McNeal JE, Bostwick DG. Hum Pathol 1986 Jan;17:64. [PubMed: 3943853]
26. Xin L, et al. Proc Natl Acad Sci U S A 2006 May 16;103:7789. [PubMed: 16682621]

27. Youssef KK, et al. Nat Cell Biol. Feb 14;
28. Passegue E, Wagner EF, Weissman IL. Cell 2004 Oct 29;119:431. [PubMed: 15507213]
29. So CW, et al. Cancer Cell 2003 Feb;3:161. [PubMed: 12620410]
30. Cozzio A, et al. Genes Dev 2003 Dec 15;17:3029. [PubMed: 14701873]
31. English HF, Santen RJ, Isaacs JT. Prostate 1987;11:229. [PubMed: 3684783]
32. We thank Barbara Anderson for manuscript preparation, Donghui Cheng for cell sorting, Yang Zong for vectors, Hong Zhang for tissue preparation, and Akanksha Chhabra, Ben Van Handel, David Mulholland, Camille Soroudi and Tanya Stoyanova for discussion and technical help. A.S.G. is supported by an institutional Ruth L. Kirschstein National Research Service Award GM07185. J.H. is supported by the American Cancer Society, the DOD Prostate Cancer Research Program, and the UCLA SPORE in Prostate Cancer (Principal Investigator: Rob Reiter). I.P.G is supported by the DOD and the Jean Perkins Foundation. O.N.W. is an Investigator of the Howard Hughes Medical Institute. J.H., I.P.G. and O.N.W. are supported by a Challenge Award from the Prostate Cancer Foundation.

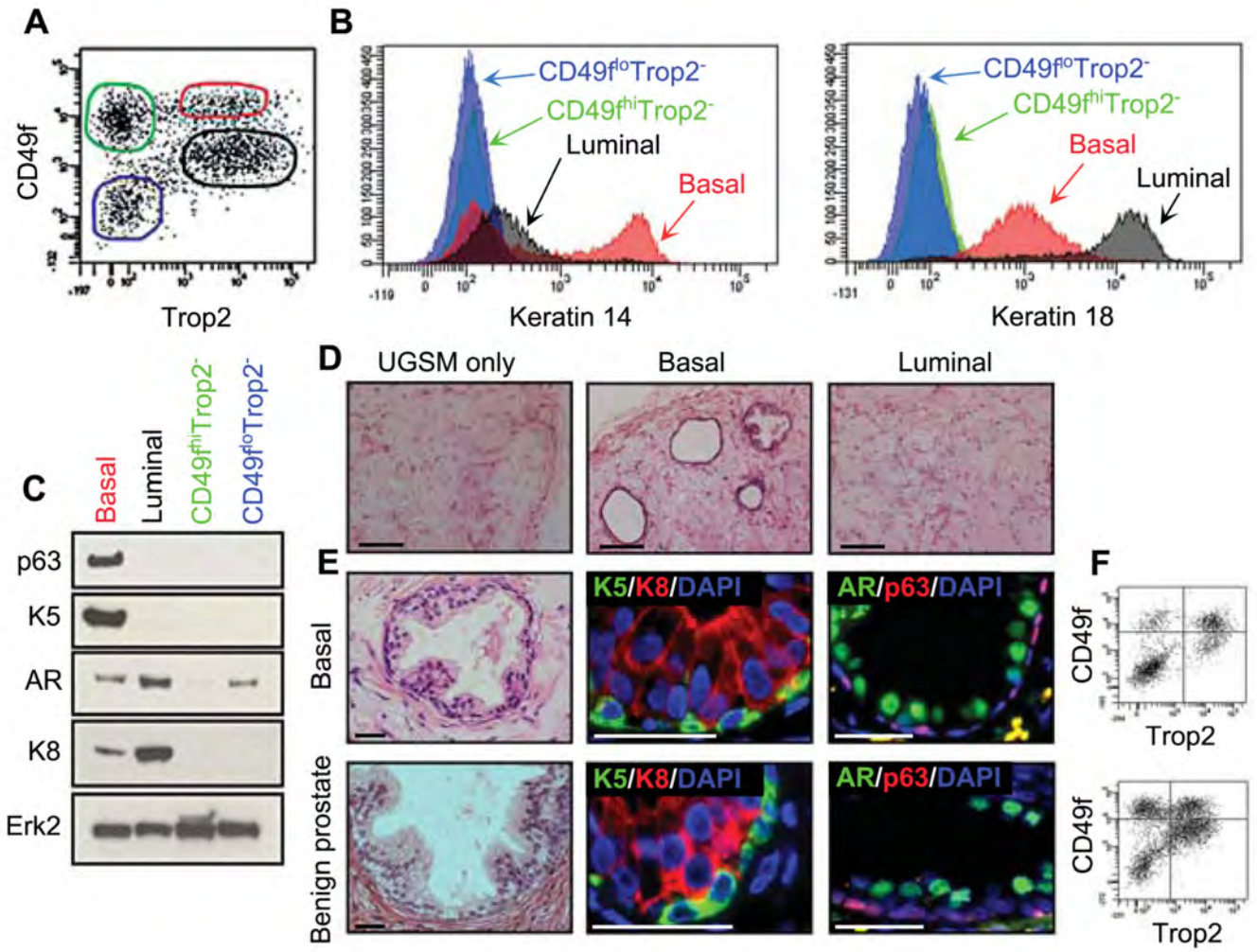

Fig. 1.

Purification of epithelial cell fractions from primary prostate tissue. (A) FACS plots show the distribution of dissociated primary prostate cells based on expression of CD49f and Trop2 and gates drawn to distinguish four populations. (B) Expression of Keratin 14 (K14) and Keratin 18 (K18) for each of the four populations indicated in A. (C) Immunoblots of lysates from each subpopulation analyzed for expression of basal proteins Keratin 5 (K5) and p63, and luminal proteins Keratin 8 (K8) and androgen receptor (AR). Erk2 is included as a loading control. (D) Haematoxylin and eosin (H&E) stained sections of outgrowths generated from dissociated cells transplanted subcutaneously into NSG mice. Scale bars, 200 μm. (E) Tissue generated from human prostate basal cells (top row) resembles benign human prostate tissue (bottom row). H&E shows tubule structure. High power images of immunostained prostatic tubules demonstrate presence of distinct basal and luminal layers. Yellow spots are negative for DAPI and indicate auto-fluorescent spots rather then nuclei. Scale bars, 40 μm. (F) FACS plots show presence of four populations with regards to CD49f and Trop2 staining on dissociated cells from basal-derived outgrowths or benign human prostate tissue.

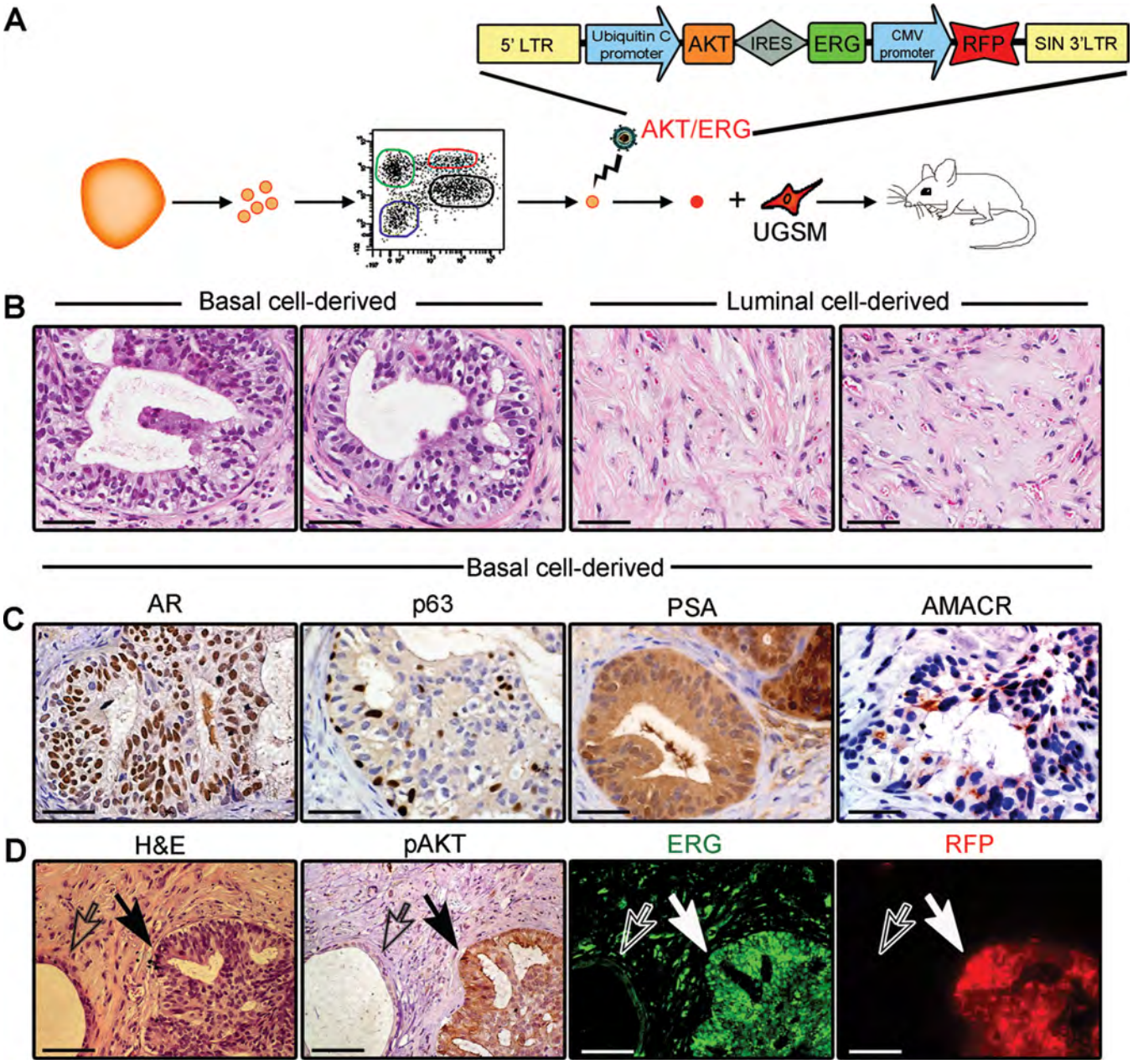

Fig. 2.

A model of PIN initiated in primary basal cells. (A) Schematic of cell sorting, lentiviral infection (with bicistronic vector encoding activated/myristoylated AKT, ERG and the fluorescent marker RFP) and transplantation to induce initiation of PIN. (B) Images of H&E stained sections of grafts derived from transduced basal and luminal cells. Scale bars, 50 μm. (C) Immunohistochemistry of basal cell-derived lesions demonstrates prominent nuclear expression of AR with retention of p63+ cells, and cytoplasmic staining for PSA and AMACR within PIN lesions. Scale bars, 50 μm. (D) Serial sections of basal cell-derived PIN (closed arrow) next to a benign tubule (open arrow) that was not infected with lentivirus. High levels of expression of RFP (red), membrane-bound phospho-AKT (brown), and nuclear ERG (green) in PIN (closed arrow) but not in the neighboring un-infected benign tubule (open arrow). Scale bars, 100 μm.

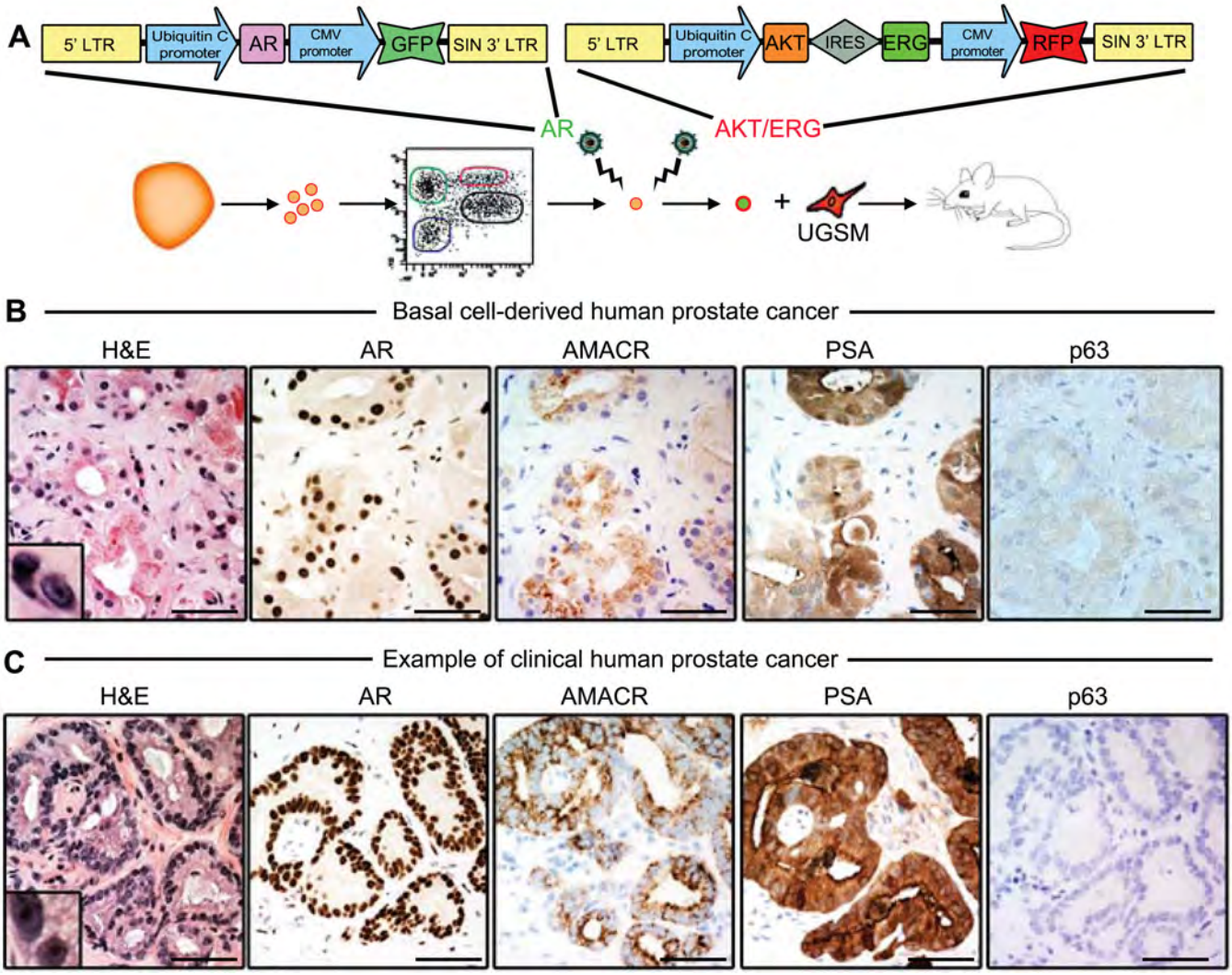

Fig. 3.

A model of prostate cancer initiated in primary basal cells. (A) Schematic of cell sorting, double lentiviral infection (with GFP-encoding AR vector and bicistronic AKT/ERG vector) and transplantation to induce initiation of prostate cancer. (B–C) High-power images show similar staining patterns between basal cell-derived human prostate cancer (B) and clinical human prostate cancer (C). H&E insets demonstrate hyperchromatic nuclei with visible nucleoli at high magnification. Cancer lesions are positive for AR, AMACR and PSA and do not express the basal cell marker p63. Scale bars, 50 μm. Low power images provided in fig. S6 demonstrate heterogeneity of disease grade in both clinical human prostate cancer and basal cell-derived human prostate cancer with co-existence of benign, PIN and cancer structures.

Absent CD44v6 Expression is an Independent Predictor of Poor Urothelial Bladder Cancer Outcome

Tobias Klatte, David B. Seligson, Jian Yu Rao, Hong Yu, Michela de Martino, Isla Garraway, Steven G. Wong, Arie S. Belldegrun and Allan J. Pantuck*

From the Departments of Urology (TK, MdM, IG, ASB, AJP), Pathology and Laboratory Medicine (DBS, JYR, HY) and Medicine (SGW), University of California-Los Angeles, Los Angeles, California

Purpose: CD44v6 is a cell surface protein involved in cell migration, cell adhesion, tumor progression and metastatic spread. We evaluated its role as a molecular marker for urothelial bladder cancer.

Materials and Methods: A tissue microarray was constructed containing 410 primary urothelial bladder cancers, each in triplicate. Immunohistochemical staining was done with a commercially available antibody. The percent of tumor cells staining positive for CD44v6 was evaluated and we assessed associations with stage, grade and survival.

Results: CD44v6 expression was higher in noninvasive (Ta, Tis) vs invasive (T1–T4) tumors ($p < 0.001$). It decreased with increasing grade ($p < 0.001$). In patients who underwent transurethral bladder resection absent CD44v6 expression was associated with a 2.3-fold increased risk of recurrence (95% CI 1.28 to 4.08). Median time to recurrence for tumors with vs without CD44v6 expression was 23 vs 9 months ($p = 0.003$). In a multivariate Cox model absent CD44 expression was an independent adverse prognostic factor for tumor recurrence (HR 2.33, $p = 0.006$). In cystectomy cases median overall survival for CD44v6 nonexpression vs expression was 30 vs 75 months ($p = 0.0027$) and CD44v6 expression was retained as an independent prognostic factor for overall survival (HR 1.54, $p = 0.042$).

Conclusions: Absent CD44v6 expression is an independent adverse predictor of urothelial bladder cancer recurrence and overall survival. Routine evaluation of CD44v6 expression may allow the identification of high risk patients who require more intensive surveillance or aggressive therapy. Targeting of CD44v6 with monoclonal antibodies may provide new avenues for urothelial bladder cancer imaging and treatment.

Key Words: urinary bladder neoplasms; urothelium; risk; mortality; antigens, CD44

Abbreviations and Acronyms

BC = urothelial bladder cancer

CD44v = CD44 variant

CIS = carcinoma in situ

TUR = transurethral resection

Submitted for publication August 26, 2009.

Study received institutional review board approval.

* Correspondence: Department of Urology, David Geffen School of Medicine at University of California-Los Angeles, 10833 Le Conte Ave., Room B7-298A CHS, Los Angeles, California 90095-1738 (telephone: 310-206-2436; FAX: 310-794-3513; e-mail: apantuck@mednet.ucla.edu).

UROTHELIAL bladder cancer is the most common urinary tract tumor with approximately 70,000 new cases in the United States each year.[1] Generally a newly diagnosed tumor is first removed by TUR, revealing nonmuscle invasive BC (stage Ta, CIS, T1) in 75% to 85% of cases.[2] These patients may also receive intravesical therapy such as mitomycin or bacillus Calmette-Guerin and then surveillance.[2] Despite aggressive treatment with surgery and adjuvant therapy tumor recurs in about 50% of patients but the rate may be as high as 78% in the high risk group.[3] In addition to a 15% to 25% a priori risk, there is a 10% risk of progression from noninvasive

0022-5347/10/1836-2403/0
THE JOURNAL OF UROLOGY®

Vol. 183, 2403-2408, June 2010
Printed in U.S.A.
DOI:10.1016/j.juro.2010.01.064

to muscle invasive BC, ultimately requiring radical cystectomy. Conventional pathological factors predicting recurrence and progression are the number of tumors, tumor diameter, stage, concomitant CIS and grade.[3] However, predicting recurrence and progression remains difficult and integrating immunohistochemical markers may be beneficial,[4] although currently studies remain inconclusive.[5,6]

CD44 forms a family of cell surface proteins involved in cell migration, cell adhesion, tumor progression and metastatic spread.[7] The CD44 gene, located on chromosome 11p13, contains at least 20 exons.[8] Exons 1 to 16 encode the extracellular domain involved in ligand binding and interaction with other membrane proteins, exon 17 encodes the transmembrane domain and the remaining exons encode the cytoplasmic domain. The 10 exons 5a to 14 are known as variant exons v1–v10 because they can be spliced alternatively, resulting in more than 700 possible variations of the extracellular domain. The smallest CD44 transcript, CD44s, does not contain any variant exons and is expressed in various tissues and cell types.[9,10] The larger CD44v transcripts encode proteins similar to CD44s but have additional sequences selected from exons v1–v10, such as v6 from exon 10. In contrast to CD44s, variant CD44 forms such as CD44v6 are restricted to a limited number of tissues and differentially expressed in various carcinomas.[9,10] In colorectal and breast cancer cases CD44v6 expression was identified as a prognostic factor.[11–14] In BC cases CD44v6 is highly expressed in low grade tumors but progressively lost in high grade neoplasms, indicating stem cell properties,[15–17] and a role as a prognostic marker for recurrence and progression. However, there are few reports of the prognostic value of CD44v6 for BC, of which all were limited in sample size or followup and have yielded inconclusive results.[16,18–20]

Thus, we evaluated the role of CD44v6 in the biology of BC and explored its usefulness as a prognostic molecular marker for this disease. For this aim we studied samples from 410 patients derived from a large cohort with long-term followup treated at a single institution.

PATIENTS AND METHODS

Patient Selection

Our study cohort consisted of 410 randomly selected BCs derived from TUR or cystectomy done at UCLA Medical Center between 1985 and 1995 in a total of 340 men (83%) and 70 women (17%) a median of 70 years old (range 33 to 96). Serial analysis was performed in 73 patients who had tissue analyzed from more than 1 bladder TUR. Clinical, pathological and followup data were gathered on each patient. Hematoxylin and eosin slides were reviewed by 2 anatomical pathologists (DBS and JYR). Pathological staging was done according to the 2002 TNM classification and grading was done according to 1973 WHO criteria. The study received institutional review board approval.

Tissue Microarray Construction

Formalin fixed, paraffin embedded archival tissue specimens were obtained from the UCLA Medical Center department of pathology. Three core tissue biopsies, each 0.6 mm in diameter, were taken from morphologically representative tumor regions and precisely arrayed using a custom-built instrument, as described previously.[21] When possible, additional core tissue biopsies were taken from morphologically benign-appearing urothelial tissue of the same specimen. Four μm sections of the resulting tissue microarray block were transferred to glass slides using the paraffin sectioning aid system comprising adhesive coated PSA-CS4x slides, adhesive tape and an ultraviolet lamp (Instrumedics, Hackensack, New Jersey) to support the cohesion of 0.6 mm array elements.

Immunohistochemical Staining and Evaluation

TMA sections were assayed using anti-CD44v6 monoclonal mouse IgG1 antibody (BMS116, clone VFF-7, Bender MedSystems®). After dewaxing in xylene and standard rehydration in graded alcohol tissue antigens were retrieved by immersing slides in sodium citrate buffer, pH 6.0, in a pressure cooker for 15 minutes. Endogenous peroxidase was quenched using 3% hydrogen peroxide in methanol and protein blocking followed using 5% horse normal serum. Endogenous biotin was capped using avidin/biotin blocking steps. Primary antibody was applied at 1:200 (5 μg/ml) and incubated for 2 hours at room temperature. Antibody binding was visualized using the Vector® Elite Mouse Kit containing a diaminobenzidine based peroxidase substrate. IgG1 mouse nonimmune antibody was assayed under identical conditions and concentration as a negative control and no staining was seen.

Two anatomical pathologists (HY and DBS) blinded to pathological variables and survival semiquantitatively assessed CD44v6 staining. Expression was evaluated as the percent of the entire tumor sample that stained positive for CD44v6. After individual assessment of each spot a consensus was reached. The overall score used in subsequent analysis was the pooled mean from all spots of the same tumor.

Statistical Methods

CD44v6 expression data were tested for normal distribution using the Kolmogorov-Smirnow-Lilliefors test and found to be not normally distributed ($p < 0.001$). Thus, associations between pathological parameters and CD44v6 expression were assessed with the nonparametric Kruskal-Wallis test.

Different stage appropriate survival end points were assessed in patients treated with TUR and cystectomy. The primary end point of interest for TUR was time to recurrence, calculated from the date of TUR to the date of recurrence or last followup. For cystectomy the primary end point of interest was overall survival, defined as the interval from the date of cystectomy to death or last followup. Time to event curves were estimated with the Kaplan-Meier method and compared with the log rank

Table 1. *Patient and tumor characteristics*

Variable	No. Pts (%)
T stage:	
Ta	124 (30)
T1	77 (19)
T2	99 (24)
T3	60 (15)
T4	18 (4)
Tis	32 (8)
N stage N1 or greater	35 (9)
Grade:	
G1	43 (10)
G2	124 (30)
G3	211 (51)
CIS	32 (8)
Recurrence after TUR*	71 (61)
Death after cystectomy*	140 (68)

* In 117 patients after TUR and 205 after cystectomy with available follow-up data.

test. We dichotomized CD44v6 expression based on staining to allow easier application to clinical practice. For this purpose an expression cutoff was determined by recursive partitioning based survival tree analysis, which identified a simple 0% cutoff (no CD44v6 expression vs CD44v6 expression). Multivariate Cox proportional hazards models were fit to identify covariates independently associated with survival. Analysis was done with R, version 2.8 with significance considered at 0.05.

RESULTS

Table 1 lists patient and tumor characteristics. In normal urothelial tissue CD44v6 was expressed on the basal and lower intermediate cell layers but immunoreactivity was increasingly lost toward the luminal cell layer. CD44v6 expression was also observed predominantly in the luminal layer for grade 1 BC. The staining pattern was homogeneous for grade 1 cancer while a more heterogeneous pattern was observed in some grade 3 tumors (fig. 1). Overall CD44v6 was expressed in 332 of the 410 BCs (81%). There was a significant association of expression with T stage and grade (fig. 2, *A*). Papillary tumors confined to the urothelium (Ta) showed significantly higher expression than invasive tumors (T1 to T4) ($p = 0.001$). Flat (CIS) and noninvasive papillary (Ta) lesions expressed CD44v6 to a similar degree ($p = 0.336$). No difference was found between invasive stages ($p = 0.336$ and 0.713, respectively). CD44v6 expression gradually decreased with increasing grade (fig. 2, *B*).

A total of 117 patients underwent bladder TUR and had followup data available at a median of 56 months (range 2 to 218). In this group absent CD44v6 expression was associated with a 2.29-fold increased risk of recurrence (95% CI 1.28 to 4.08). Median time to recurrence for tumors with vs without CD44v6 expression was 23 vs 9 months ($p = 0.0032$, fig. 3, *A*). In a multivariate Cox model absent CD44v6 expression (HR 2.33, 95% CI 1.28 to 4.25, $p = 0.006$) and increasing T stage (HR 1.32, 95% CI 1.003 to 1.73, $p = 0.047$) but not tumor grade ($p = 0.820$) were independent prognostic factors for tumor recurrence. In tumors with CD44v6 expression the absolute amount of CD44v6 expression was not associated with survival (HR 1.001, $p = 0.912$). There was also no association of CD44v6 with response to adjuvant therapy.

In the 205 patients with cystectomy median followup in survivors was 102 months (range 1 to 215). Showing the same trend as in patients with TUR, overall survival in CD44v6 nonexpressors vs expressors was 30 vs 75 months ($p = 0.003$), corresponding to a 1.73-fold increased risk of death (95% CI 1.21 to 2.58) when CD44v6 expression was absent (fig. 3, *B*).

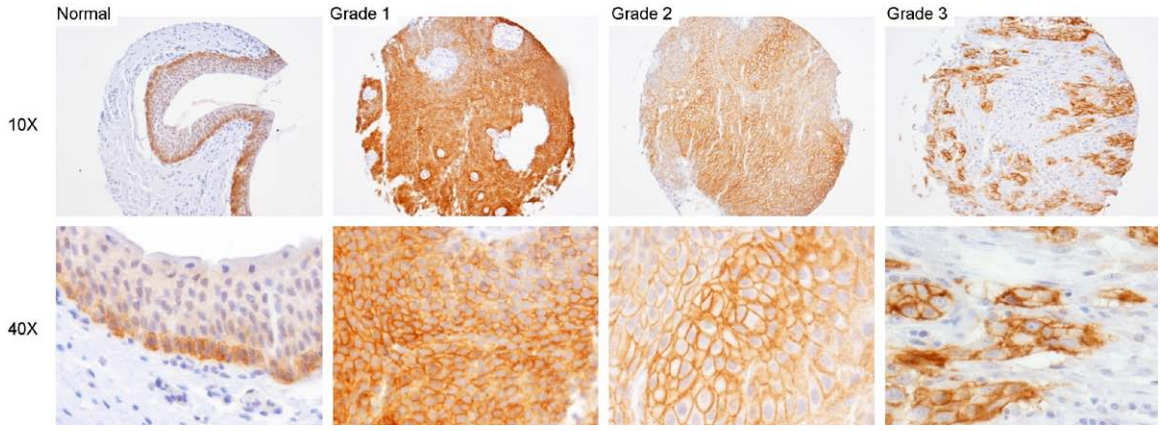

Figure 1. In normal urothelial tissue CD44v6 was expressed in basal and lower intermediate cell layers but immunoreactivity was lost in upper intermediate or superficial cell layers. Expression was also observed in superficial layer for grade 1 BC. Staining pattern was homogeneous for grade 1, and decreased and heterogeneous for grade 3. H & E and CD44v6 staining.

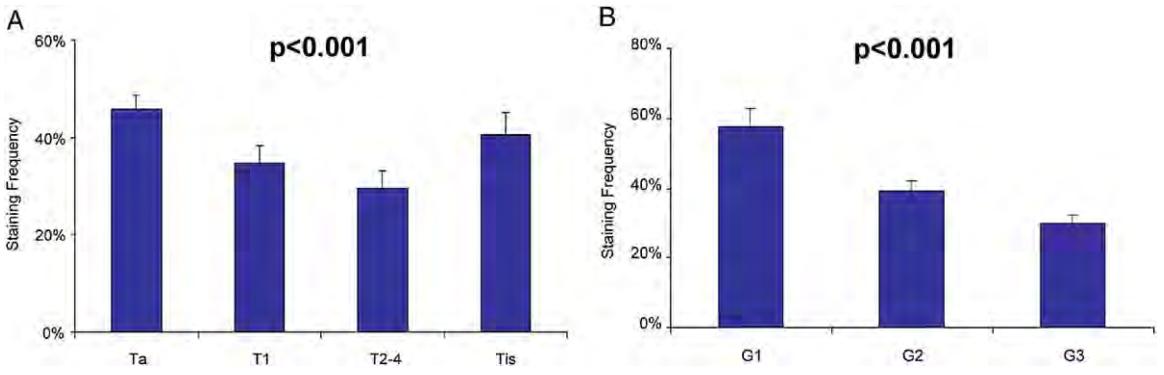

Figure 2. CD44v6 staining by T classification (*A*) and grade (*B*). CD44v6 was differentially expressed in noninvasive (Ta, Tis) vs invasive (T1–T4) BC and decreased with increasing grade.

Absent CD44v6 expression was retained as an independent, adverse prognostic factor for survival (HR 1.54, p = 0.042, table 2). Further stratification of the amount of CD44v6 expression did not provide further prognostic information (HR 1.003, p = 0.259).

DISCUSSION

We evaluated CD44v6 expression in 410 BCs surgically removed by TUR or cystectomy and found that CD44v6 is differentially expressed in noninvasive vs invasive and low grade vs high grade lesions. Absent CD44v6 expression was identified as an independent adverse predictor of recurrence and overall survival. Thus, routine evaluation of CD44v6 expression may allow the identification of patients at high risk who require more intensive surveillance or aggressive therapy. Also, targeting CD44v6 with monoclonal antibody preparations may provide new avenues for BC imaging and treatment.

In several small studies CD44v6 expression decreased with increasing BC grade,[19] paralleling the loss of other cell adhesion molecules such as E-cadherin.[18] Thus, CD44v6 may be a prognostic factor for BC.[15–17] Lipponen et al studied 173 patients and found that those with negative CD44v6 immunoreactivity had worse prognosis.[19] In 84 T2–T4 tumors they identified CD44v6 as an independent prognostic factor. However, no significant association was observed in patients treated for nonmuscle invasive disease. Hong et al evaluated CD44v6 in 115 BCs by immunohistochemistry using a self-developed antibody.[20] Mirroring our results, they found lower expression in poorly differentiated carcinomas, although no significant association with survival was observed. However, median followup was only 14 months. More recently Chuang and Liao did not detect a significant association of CD44v6 expression with grade, stage or recurrence in a series of 55

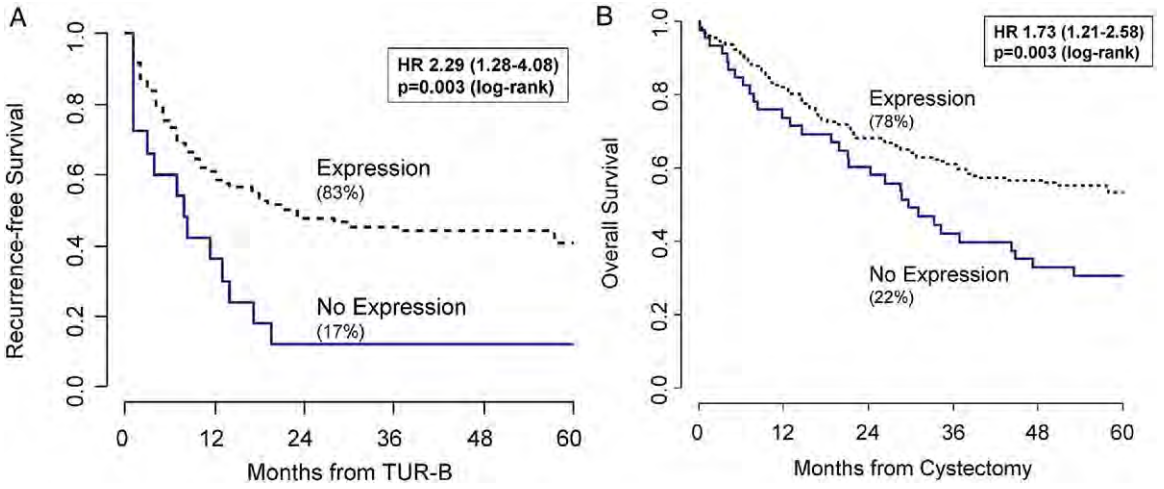

Figure 3. Kaplan-Meier survival estimates in patients with TUR (*A*) and cystectomy (*B*). Absent CD44v6 expression, observed in 17% and 22% of BC tumors removed by TUR and cystectomy, respectively, was associated with poorer prognosis in terms of recurrence-free and overall survival.

Table 2. *Multivariate Cox proportional hazards regression model predicting overall survival in patients with radical cystectomy*

Covariate	HR (95% CI)	p Value
Age greater than 60	1.20 (0.74–1.93)	0.463
T stage T3 or greater	1.71 (1.03–2.84)	0.036
N stage N1 or greater	1.15 (0.73–1.81)	0.558
Grade 3	1.19 (0.75–1.89)	0.461
Lymphovascular invasion	1.28 (0.79–2.08)	0.308
Concomitant CIS	0.96 (0.64–1.44)	0.833
Absent CD44v6	1.54 (1.02–2.35)	0.042

BC specimens.[16] To our knowledge our series is the largest to date confirming that CD44v6 expression is lost with BC progression. Also, our study shows that this protein marker has prognostic value. Thus, patients with absent tumor CD44v6 expression should be considered at higher risk for recurrence and death.

In our analysis tumor grade was not retained as an independent prognostic factor, which may be explained by the close significant correlation of CD44v6 with grade. CD44v6 may be a more powerful predictor of recurrence than conventional grade and may represent a molecular grade. It may be also possible to integrate CD44v6 expression for risk assessment after TUR, thereby replacing grade. Tumors with absent CD44v6 expression may be considered high risk and may undergo first surveillance cystoscopy after 3 months or possibly repeat resection. However, to date BC recurrence has only been predicted based on clinical and pathological factors.[3] Integrating molecular markers such as p53 or carbonic anhydrase IX may be beneficial but has not yet become routine.[4,5,22]

In normal urothelial tissue CD44v6 is not expressed in the superficial urothelial layer, as in BC.[15,23,24] Thus, CD44v6 positive cells may have properties of cancer stem cells, eg higher proliferative activity and the ability to change into more differentiated superficial layer cells.[17] Recently Yang and Chang confirmed that bladder cancer stem cells are among those that are CD44v6 positive, and have the ability to form colonies, self-renew and proliferate.[25]

With this in mind CD44v6 may also represent a diagnostic and therapeutic target. Blocking v6 epitope by systemic application of antibodies retards tumor growth and blocks metastatic spread in vivo.[26] Thus, an antibody targeting CD44v6 may be applied alone as intravesical treatment. The stem cell may then be targeted directly. However, this therapy may be restricted to low risk tumors with CD44v6 expression. As another possibility, several CD44v6 antibody preparations are available.[27]

The fact that CD44v6 is expressed in the luminal layer of low grade BC but rarely observed in the superficial urothelial layer led to the hypothesis that urinary CD44v6 levels may serve as a urinary based proteomic marker for BC detection and followup. To address this Woodman et al developed a sandwich enzyme-linked immunosorbent assay that detects protein concentrations in voided urine samples.[28] However, in a confirmative study of this test Sun et al noted an AUC of only 66.4%, which is insufficient for clinical practice.[29]

Our study has several limitations inherent to its retrospective nature. All findings should be confirmed and validated, preferably in a large prospective data set, before CD44v6 staining can be integrated into clinical routine. Tumors were collected in a 10-year period and were somewhat heterogeneous. Thus, further significant associations may exist but were not observed, such as the CD44v6 and response to adjuvant therapy. Finally, we suggest testing the generated hypotheses, namely the potential role of CD44v6 as a diagnostic and therapeutic target.

CONCLUSIONS

CD44v6 is differentially expressed in noninvasive vs invasive and in low grade vs high grade BC. Absent CD44v6 expression is an independent adverse predictor of recurrence and overall survival. Routine evaluation of CD44v6 expression may allow the identification of patients at high risk who require more intensive surveillance or aggressive therapy. Targeting CD44v6 with monoclonal antibodies may provide new avenues for BC imaging and treatment.

REFERENCES

1. Jemal A, Siegel R, Ward E et al: Cancer statistics, 2009. CA Cancer J Clin 2009; **59:** 225.
2. Babjuk M, Oosterlinck W, Sylvester R et al: EAU guidelines on non-muscle-invasive urothelial carcinoma of the bladder. Eur Urol 2008; **54:** 303.
3. Sylvester RJ, van der Meijden AP, Oosterlinck W et al: Predicting recurrence and progression in individual patients with stage Ta T1 bladder cancer using EORTC risk tables: a combined analysis of 2596 patients from seven EORTC trials. Eur Urol 2006; **49:** 466.
4. Klatte T, Seligson DB, Rao JY et al: Carbonic anhydrase IX in bladder cancer: a diagnostic, prognostic, and therapeutic molecular marker. Cancer 2009; **115:** 1448.
5. Malats N, Bustos A, Nascimento CM et al: P53 as a prognostic marker for bladder cancer: a meta-analysis and review. Lancet Oncol 2005; **6:** 678.
6. van Rhijn BW, Burger M, Lotan Y et al: Recurrence and progression of disease in non-muscle-invasive bladder cancer: from epidemiology to treatment strategy. Eur Urol 2009; **56:** 430.
7. Martin TA, Harrison G, Mansel RE et al: The role of the CD44/ezrin complex in cancer metastasis. Crit Rev Oncol Hematol 2003; **46:** 165.

8. Ponta H, Wainwright D and Herrlich P: The CD44 protein family. Int J Biochem Cell Biol 1998; **30:** 299.

9. Mackay CR, Terpe HJ, Stauder R et al: Expression and modulation of CD44 variant isoforms in humans. J Cell Biol 1994; **124:** 71.

10. Sherman L, Wainwright D, Ponta H et al: A splice variant of CD44 expressed in the apical ectodermal ridge presents fibroblast growth factors to limb mesenchyme and is required for limb outgrowth. Genes Dev 1998; **12:** 1058.

11. Ropponen KM, Eskelinen MJ, Lipponen PK et al: Expression of CD44 and variant proteins in human colorectal cancer and its relevance for prognosis. Scand J Gastroenterol 1998; **33:** 301.

12. Mulder JW, Kruyt PM, Sewnath M et al: Colorectal cancer prognosis and expression of exon-v6-containing CD44 proteins. Lancet 1994; **344:** 1470.

13. Wielenga VJ, Heider KH, Offerhaus GJ et al: Expression of CD44 variant proteins in human colorectal cancer is related to tumor progression. Cancer Res 1993; **53:** 4754.

14. Kaufmann M, Heider KH, Sinn HP et al: CD44 variant exon epitopes in primary breast cancer and length of survival. Lancet 1995; **345:** 615.

15. Southgate J, Trejdosiewicz LK, Smith B et al: Patterns of splice variant CD44 expression by normal human urothelium in situ and in vitro and by bladder-carcinoma cell lines. Int J Cancer 1995; **62:** 449.

16. Chuang CK and Liao SK: Differential expression of CD44 variant isoforms by cell lines and tissue specimens of transitional cell carcinomas. Anticancer Res 2003; **23:** 4635.

17. Kuncová J, Kostrouch Z, Viale M et al: Expression of CD44v6 correlates with cell proliferation and cellular atypia in urothelial carcinoma cell lines 5637 and HT1197. Folia Biol (Praha) 2005; **51:** 3.

18. Ross JS, del Rosario AD, Bui HX et al: Expression of the CD44 cell adhesion molecule in urinary bladder transitional cell carcinoma. Mod Pathol 1996; **9:** 854.

19. Lipponen P, Aaltoma S, Kosma VM et al: Expression of CD44 standard and variant-v6 proteins in transitional cell bladder tumours and their relation to prognosis during a long-term follow-up. J Pathol 1998; **186:** 157.

20. Hong RL, Pu YS, Hsieh TS et al: Expressions of E-cadherin and exon v6-containing isoforms of CD44 and their prognostic values in human transitional cell carcinoma. J Urol 1995; **153:** 2025.

21. Kononen J, Bubendorf L, Kallioniemi A et al: Tissue microarrays for high-throughput molecular profiling of tumor specimens. Nat Med 1998; **4:** 844.

22. Klatte T, Belldegrun AS and Pantuck AJ: The role of carbonic anhydrase IX as a molecular marker for transitional cell carcinoma of the bladder. BJU Int, suppl., 2008; **101:** 45.

23. Sugino T, Gorham H, Yoshida K et al: Progressive loss of CD44 gene expression in invasive bladder cancer. Am J Pathol 1996; **149:** 873.

24. Kuncová J, Urban M and Mandys V: Expression of CD44s and CD44v6 in transitional cell carcinomas of the urinary bladder: comparison with tumour grade, proliferative activity and p53 immunoreactivity of tumour cells. APMIS 2007; **115:** 1194.

25. Yang YM and Chang JW: Bladder cancer initiating cells (BCICs) are among EMA-CD44v6+ subset: novel methods for isolating undetermined cancer stem (initiating) cells. Cancer Invest 2008; **26:** 725.

26. Naor D, Sionov RV and Ish-Shalom D: CD44: structure, function, and association with the malignant process. Adv Cancer Res 1997; **71:** 241.

27. Heider KH, Kuthan H, Stehle G et al: CD44v6: a target for antibody-based cancer therapy. Cancer Immunol Immunother 2004; **53:** 567.

28. Woodman AC, Goodison S, Drake M et al: Noninvasive diagnosis of bladder carcinoma by enzyme-linked immunosorbent assay detection of CD44 isoforms in exfoliated urothelia. Clin Cancer Res 2000; **6:** 2381.

29. Sun Y, He DL, Ma Q et al: Comparison of seven screening methods in the diagnosis of bladder cancer. Chin Med J (Engl) 2006; **119:** 1763.

ELSEVIER

Urologic Oncology: Seminars and Original Investigations xx (2011) xxx

UROLOGIC ONCOLOGY

News and topics

Will identification of a prostate cancer stem cell lead to its cure?

There is abundant evidence in mouse and man that the prostate contains normal tissue stem cells within the epithelium that are capable of self-renewal and inducing benign tubule formation [1–5]. The premise that prostate tumors contain cancer stem cells (CSCs) that ultimately lead to development of castration-resistant prostate cancer remains to be determined. The basic theory of CSCs is that they represent a small fraction of tumor cells possessing biological characteristics that render an exceptional propensity for tumor initiation and resilience to traditional therapy [6–9]. CSCs self-renew, but also generate more differentiated progeny that comprise the bulk and heterogeneity of tumors. CSCs may be transformed normal tissue stem cells with inherent self-renewal capability or deranged progenitor cells with reactivated stem cell pathways, resulting in limitless self-renewal potential. In the case of prostate cancer, it is postulated that CSCs are relatively androgen insensitive. Similar to normal prostate tissue stem cells, CSCs may respond to androgen, but not require it for survival. CSCs may be the seeds for local recurrence and metastasis, by spreading from niche to niche. Hence, if CSCs are not eliminated, the cancer cannot be cured. But do prostate CSCs really exist?

Evidence supporting CSC populations is based on functional evaluation of fractionated tumor cells. In order to be characterized as a CSC, self-renewal must be demonstrated. Putative CSCs, isolated according to a particular antigenic profile, must also be capable of seeding and propagating heterogeneous tumors. CSCs reside in niches and have biologic regulatory mechanisms that induce chemo- and radioresistance. Abundant evidence for CSCs exist for hematologic malignancies, (acute myeloblastic leukemia) as well as, glioblastoma, breast cancer, and colon cancer [10–16].

Evidence for the existence of prostate CSCs has lagged because of technical hurdles associated with human prostate tumor modeling [17]. Primary prostate cancer cells obtained from human prostatectomy specimens are extremely difficult to culture in vitro, even for brief periods [18,19]. Cells with luminal profiles (including tumor cells) are difficult to recover following tissue dissociation, with the majority of the cells retrieved being of basal, stromal, and blood lineage [3,20]. Metastatic tumors are rarely available for live cell investigations. Without isolation of viable prostate cancer cells, fractionation and engraftment studies that evaluate tumor regeneration capability cannot be done. Even if viable tumor cells can be successfully isolated, xenograft formation in immunocompromised mice remains a challenge. Highly immunodeficient mouse models are required, and it is likely that species-specific prostatic growth factors and support cells may also be essential for recreation of the niche and efficient tumorigenesis [17,21].

Studies that have advocated for the existence of human prostate CSCs are limited in number and scope. The first reports of prostate CSCs indicated that CD133+ cells isolated from tumors were more proliferative and could produce heterogeneous progeny [22]. These studies, however, did not demonstrate tumor regeneration in vivo, an important component supporting CSC function. Evaluation of prostate cancer xenografts and cell lines indicate that CD44 may be a marker of prostate cancer CSCs [23,24]. Serially passaged xenografts and cell lines, however, may not accurately reflect primary tumor cell biology. Without confirmatory studies with primary prostate tumors or metastases, the relevance of these observations comes into question.

Recent reports have identified a human cancer cell of origin from benign prostate tissue [20]. Prostate cells from dissociated tissues were fractionated based on surface marker expression and genetically manipulated to overexpress AR, in combination with the oncogenes, AKT and ERG. Only prostate cellular fractions containing $Trop2^{+}Cd49f^{Hi}$ basal cells were able to induce tumors in immunocompromised mice. Whether or not the cell of origin for prostate cancer and CSCs (the cancer cells that propagate tumor and metastasize) share a common antigenic profile remains to be determined.

If there are CSCs in human prostate cancer, would their targeting and elimination lead to cure of castration resistant disease? If the hypothesized CSC in prostate cancer is indeed androgen insensitive and equipped with anti-apoptotic mechanisms, specific targeting may achieve clinical benefit in patients with metastatic disease. CSCs may be targeted by interference of self-renewal and other pathways involved in CSC maintenance, aptamer, or antibody-mediated toxin-linked agents, or by disrupting the niche [25–27].

An alternative approach to curing prostate cancer is to inhibit its initiation. Targeting the cells of origin for prostate cancer (normal prostate stem cells) before cancer develops or spreads should be considered. As prostate imaging mo-

1078-1439/$ – see front matter
doi:10.1016/j.urolonc.2011.01.015

dalities improve, it is conceivable that small lesions could be susceptible to treatment with agents targeting stem cells.

In order to make progress in the isolation and characterization of prostate cancer stem cells, improved methodologies are needed to retrieve viable cells from primary prostate tumors and metastases for evaluation of CSC activity. In the meantime, further characterization of the role of normal stem cells in tumorigenesis is warranted, in order to determine if genetic profiling or targeting of these cells will make a diagnostic and/or prognostic impact.

Isla P. Garraway, M.D., Ph.D.
Department of Urology
Jonsson Comprehensive Cancer Center
Broad Center of Regenerative Medicine and Stem Cell Research
David Geffen School of Medicine at UCLA
Los Angeles, CA, USA

References

[1] Isaacs JT, Coffey DS. Etiology and disease process of benign prostatic hyperplasia. Prostate 1989;2(Suppl):33–50.
[2] Xin L, Ide H, Kim Y, et al. In vivo regeneration of murine prostate from dissociated cell populations of postnatal epithelia and urogenital sinus mesenchyme. Proc Natl Acad Sci U S A 2003;100(Suppl 1):11896–903.
[3] Garraway IP, Sun W, Tran CP, et al. Human prostate sphere-forming cells represent a subset of basal epithelial cells capable of glandular regeneration in vivo. Prostate 2010;70:491–501.
[4] Burger PE, Xiong X, Coetzee S, et al. Sca-1 expression identifies stem cells in the proximal region of prostatic ducts with high capacity to reconstitute prostatic tissue. Proc Natl Acad Sci U S A 2005;102:7180–5.
[5] Hayward SW, Haughney PC, Rosen MA, et al. Interactions between adult human prostatic epithelium and rat urogenital sinus mesenchyme in a tissue recombination model. Differentiation 1998;63:131–40.
[6] Reya T, Morrison SJ, Clarke MF, et al. Stem cells, cancer, and cancer stem cells. Nature 2001;414:105–11.
[7] Al-Hajj M, Clarke MF. Self-renewal and solid tumor stem cells. Oncogene 2004;23:7274–82.
[8] Jordan CT, Guzman ML, Noble M. Cancer stem cells. N Engl J Med 2006;355:1253–61.
[9] Polyak K, Hahn WC. Roots and stems: Stem cells in cancer. Nat Med 2006;12:296–300.
[10] Dontu G, Abdallah WM, Foley JM, et al. In vitro propagation and transcriptional profiling of human mammary stem/progenitor cells. Genes Dev 2003;17:1253–70.
[11] Dontu G, Al-Hajj M, Abdallah WM, et al. Stem cells in normal breast development and breast cancer. Cell Prolif 2003;36(Suppl 1):59–72.
[12] Dontu G, El-Ashry D, Wicha MS. Breast cancer, stem/progenitor cells and the estrogen receptor. Trends Endocrinol Metab 2004;15:193–7.
[13] O'Brien CA, Pollett A, Gallinger S, et al. A human colon cancer cell capable of initiating tumour growth in immunodeficient mice. Nature 2007;445:106–10.
[14] Singh SK, Clarke ID, Terasaki M, et al. Identification of a cancer stem cell in human brain tumors. Cancer Res 2003;63:5821–8.
[15] Singh SK, Hawkins C, Clarke ID, et al. Identification of human brain tumour initiating cells. Nature 2004;432:396–401.
[16] Lapidot T, Sirard C, Vormoor J, et al. A cell initiating human acute myeloid leukaemia after transplantation into SCID mice. Nature 1994;367:645–8.
[17] Li H, Jiang M, Honorio S, et al. Methodologies in assaying prostate cancer stem cells. Methods Mol Biol 2009;568:85–138.
[18] Peehl DM. Are primary cultures realistic models of prostate cancer? J Cell Biochem 2004;91:185–95.
[19] Peehl DM. Primary cell cultures as models of prostate cancer development. Endocr Relat Cancer 2005;12:19–47.
[20] Goldstein AS, Huang J, Guo C, et al. Identification of a cell of origin for human prostate cancer. Science 2010;329:568–71.
[21] Ito M, Kobayashi K, Nakahata T. NOD/Shi-scid IL2rgamma(null) (NOG) mice more appropriate for humanized mouse models. Curr Top Microbiol Immunol 2008;324:53–76.
[22] Collins AT, Berry PA, Hyde C, et al. Prospective identification of tumorigenic prostate cancer stem cells. Cancer Res 2005;65:10946–51.
[23] Patrawala L, Calhoun T, Schneider-Broussard R, et al. Highly purified CD44+ prostate cancer cells from xenograft human tumors are enriched in tumorigenic and metastatic progenitor cells. Oncogene 2006;25:1696–708.
[24] Li H, Chen X, Calhoun-Davis T, et al. PC3 human prostate carcinoma cell holoclones contain self-renewing tumor-initiating cells. Cancer Res 2008;68:1820–5.
[25] Takebe N, Harris PJ, Warren RQ, et al. Targeting cancer stem cells by inhibiting Wnt, Notch, and Hedgehog pathways. Nat Rev Clin Oncol 2011;8:97–106.
[26] Guise T. Examining the metastatic niche: Targeting the microenvironment. Semin Oncol 2010;37(Suppl 2):S2–14.
[27] Min K, Jo H, Song K, et al. Dual-aptamer-based delivery vehicle of doxorubicin to both PSMA (+) and PSMA (−) prostate cancers. Biomaterials 2011;32:2124–32.

OPEN ACCESS Freely available online

PLoS one

Epcam, CD44, and CD49f Distinguish Sphere-Forming Human Prostate Basal Cells from a Subpopulation with Predominant Tubule Initiation Capability

Changyong Guo[1,2], Haibo Liu[1,2], Bao-Hui Zhang[1,2], Radu M. Cadaneanu[1,2], Aqila M. Mayle[1,2,3], Isla P. Garraway[1,2,3]*

1 Department of Urology, David Geffen School of Medicine at University of California Los Angeles, Los Angeles, California, United States of America, **2** Jonsson Comprehensive Cancer Center, David Geffen School of Medicine at University of California Los Angeles, Los Angeles, California, United States of America, **3** Greater Los Angeles Veterans Affairs Medical Center, Los Angeles, California, United States of America

Abstract

Background: Human prostate basal cells expressing alpha-6 integrin ($CD49f^{Hi}$) and/or CD44 form prostaspheres in vitro. This functional trait is often correlated with stem/progenitor (S/P) activity, including the ability to self-renew and induce differentiated tubules in vivo. Antigenic profiles that distinguish tubule-initiating prostate stem cells (SCs) from progenitor cells (PCs) and mature luminal cells (LCs) with less regenerative potential are unknown.

Methodology/Principle Findings: Prostasphere assays and RT-PCR analysis was performed following FACS separation of total benign prostate cells based upon combinations of Epcam, CD44, and/or CD49f expression. Epithelial cell fractions were isolated, including $Epcam^{+}CD44^{+}$ and Epcam+CD44+$CD49f^{Hi}$ basal cells that formed abundant spheres. When non-sphere-forming $Epcam^{+}CD44^{-}$ cells were fractionated based upon CD49f expression, a distinct subpopulation ($Epcam^{+}CD44^{-}CD49f^{Hi}$) was identified that possessed a basal profile similar to $Epcam^{+}CD44^{+}CD49f^{Hi}$ sphere-forming cells ($p63^{+}AR^{Lo}PSA^{-}$). Evaluation of tubule induction capability of fractionated cells was performed, in vivo, via a fully humanized prostate tissue regeneration assay. Non-sphere-forming $Epcam^{+}CD44^{-}$ cells induced significantly more prostate tubular structures than $Epcam^{+}CD44^{+}$ sphere-forming cells. Further fractionation based upon CD49f co-expression identified $Epcam^{+}CD44^{-}CD49f^{Hi}$ (non-sphere-forming) basal cells with significantly increased tubule induction activity compared to $Epcam^{+}CD44^{-}CD49f^{Lo}$ (true) luminal cells.

Conclusions/Significance: Our data delineates antigenic profiles that functionally distinguish human prostate epithelial subpopulations, including putative SCs that display superior tubule initiation capability and induce differentiated ductal/acini structures, sphere-forming PCs with relatively decreased tubule initiation activity, and terminally differentiated LCs that lack both sphere–forming and tubule-initiation activity. The results clearly demonstrate that sphere-forming ability is not predictive of tubule-initiation activity. The subpopulations identified are of interest because they may play distinct roles as cells of origin in the development of prostatic diseases, including cancer.

Citation: Guo C, Liu H, Zhang B-H, Cadaneanu RM, Mayle AM, et al. (2012) Epcam, CD44, and CD49f Distinguish Sphere-Forming Human Prostate Basal Cells from a Subpopulation with Predominant Tubule Initiation Capability. PLoS ONE 7(4): e34219. doi:10.1371/journal.pone.0034219

Editor: Andreas Androutsellis-Theotokis, Universitätsklinikum Carl Gustav Carus an der Technischen Universität Dresden, Germany

Received November 17, 2011; **Accepted** February 27, 2012; **Published** April 13, 2012

Funding: Support for these studies was provided by the Prostate Cancer Foundation (Challenge Award, PI: Dr. Owen Witte), the Jean Perkins Foundation, the Department of Defense (PC061068 and PC07373), and the National Institutes of Health CA-16042 and AI-28697. The funders had no role in study design, data collection and analysis, decision to publish, or preparation of the manuscript.

Competing Interests: The authors have declared that no competing interests exist.

* E-mail: igarraway@mednet.ucla.edu

Introduction

Human adult prostate S/Ps are characterized by surface marker expression, as well as functional traits, including the ability to self-renewal and differentiate into multiple lineages [1,2,3,4,5]. Markers that have been utilized to isolate human prostate S/Ps include Trop2, CD44, $alpha_2beta_1$-$integrin^{Hi}$, $alpha_6$-$integrin^{Hi}$ (CD49f), and CD133 [1,2,4,6]. However, a consensus does not exist regarding the antigenic profile of a functionally pure human prostate SC population and how to distinguish multipotent tubule-initiating SCs from progenitors with more limited potential. Making such a distinction may have important implications in understanding the etiology of prostatic disease, including benign prostatic hypertrophy and cancer.

Sphere-forming cells isolated from dissociated primary tissues are enriched in S/P cells in multiple organ systems [7,8,9,10]. In the human prostate, sphere-forming capability enables the selection of a subpopulation of epithelial cells with SC-like traits, including self-renewal and the ability to differentiate into tubular structures when implanted into immunocompromised mice [1,4]. Previous studies evaluating the antigenic profile of cells capable of forming prostaspheres indicate that they reside within the basal layer of normal prostatic ducts [1,4,11,12]. onsequently, the combination of Trop2 and $CD49f^{Hi}$ expression enables isolation of the basal cell fraction ($Trop2^{+}CD49f^{Hi}$), which exclusively forms

spheres, regenerates benign tubules, and demonstrates malignant transformation after genetic manipulations [1,4,6]. Sphere-forming cells are rare in prostate subpopulations that display luminal profiles ($Trop2^{+}CD49f^{Lo}$ or $Trop2^{+}CD44^{-}$)[1,4].

Subdivision of the basal population and enrichment of a sphere-forming and/or tubule-regenerating SC population has yet to be accomplished. However, a functional delineation of the human prostate cellular hierarchy, in addition to basal/luminal profile, could provide more specific insight about the cells of origin for prostate cancer and the pathways utilized by normal SCs that may become corrupted in prostate disease. The aim of this work is to employ in vitro sphere culture and in vivo tissue regeneration assays to interrogate combinations of surface antigens that may further subdivide human prostate epithelial cells and enable functional separation of tubule-initiating SCs from progenitors with more limited capabilities. In this report, we accomplish these goals by incorporating a refined tissue regeneration assay, in which human fetal prostate stroma (hFPS) is utilized to induce tubule formation/differentiation in a fully humanized system. Our results demonstrate that the combination of Epithelial Cell Adhesion Molecule (Epcam), CD44, and CD49f can be used to isolate three distinct populations: (i) a putative prostate SC population that does not form spheres, but induces relatively robust tubule regeneration, (ii) PCs possessing maximal sphere-forming ability, but decreased tubule-initiation capability, and (iii) terminally differentiated LCs that lack both sphere-forming and tissue regenerating potential. The uncoupling of sphere-forming and tubule-initiating functions indicates that human prostate cells with the most potential for niche interaction and tubule development appear to be quiescent in sphere-forming culture conditions.

Results

Epcam and CD44 enable separation of prostate cell lineages.

Epcam/Trop1 is a pan-epithelial antigen that is also expressed on most carcinomas, including prostate cancer [13]. In benign human prostate, immunohistochemical (IHC) staining demonstrates confinement of Epcam expression to epithelial cells that compose prostate ducts and acini (Figure 1A). CD44 is a single pass transmembrane glycoprotein involved in cell-cell matrix adhesion, cell signaling, inflammation, and cell migration ([14]). In the benign human prostate, CD44 marks basal cells and rare neuroendocrine cells [15]. Based on the expression pattern of Epcam and CD44 observed in IHC analysis of benign prostate tubules, it appears that $Epcam^{+}CD44^{+}$ cells compose the basal layer, while $Epcam^{+}CD44^{-}$ cells appear predominantly luminal (Figure 1A). We hypothesized that fractionating total prostate cells based upon the combination of Epcam and CD44 expression profiles could be a first step in determining antigenic profiles that delineate human prostate cellular hierarchy, by enabling basal and luminal separation. An advantage of both Epcam and CD44 is that conjugated magnetic beads are readily available that enable rapid fractionation of prostate cells without the need for a cell sorter. This may increase the accessibility and feasibility of fractionating surgical specimens. FACS analysis of total prostate epithelial cells using fluorescent antibodies to detect Epcam and CD44 expression demonstrate clear separation of ($Epcam^{+}$) epithelial cells from ($Epcam^{-}$) stromal/blood cells (Figure 1B). Although FACS analysis demonstrates that separation based on CD44 expression is not as distinct as Epcam, both $CD44^{+}$ and $CD44^{-}$ fractions were obtained via cell sorting or magnetic beads separation (Figure 1B).

Expression of basal- and luminal-specific genes correlates with Epcam/CD44 status.

Prostate basal and luminal cells can be distinguished based on marker profile, in addition to architectural organization. The tumor protein p63 is a hallmark indicator of basal cells, which also express relatively low levels of AR and PSA [16,17]. On the other hand, luminal cells lack p63, but express strong levels of AR, PSA, and cytokeratin 8 (CK8) [18,19]. In order to confirm enrichment of basal and luminal cells after fractionation based on Epcam/CD44 expression, quantitative RT-PCR analysis was performed on total RNA isolated from fractionated cells with primers targeting basal-specific and luminal-specific genes (Figure 1C). Compared to unfractionated cells and the $Epcam^{+}CD44^{+}$ fraction, $Epcam^{+}CD44^{-}$ cells demonstrated significantly increased expression of AR, PSA, and CK8 with low relatively low expression of the basal marker, p63. On the other hand, $Epcam^{+}CD44^{+}$ cells demonstrated virtually undetectable AR, PSA, and CK8 and enhanced expression of p63. These results are compatible with the known expression profiles of basal and luminal cells and indicate that the combination of Epcam and CD44 can effectively enrich for these lineages [19,20].

We have previously shown that prostate S/P cells are capable of prostasphere formation in vitro [4]. Additionally, we have found that basal cells are exclusively capable of forming spheres [1]. Therefore sphere-forming capability of $Epcam^{+}CD44^{+}$ and $Epcam^{+}CD44^{-}$ cell fractions was evaluated in comparison to unfractionated (U) cells. Consistent with previous studies, virtually all of the sphere-forming cells were confined to the basal-enriched $Epcam^{+}CD44^{+}$ cell fraction (Figure 1D), and this fraction demonstrated a 3-fold increase in sphere-forming cells compared to unfractionated total prostate cells. This data suggests that Epcam/CD44 fractionation enables a functional segregation of epithelial cell populations, in addition to basal and luminal separation.

HFPS Supports Prostate Tissue Regeneration Induced by Adult Human Prostate Cells In Vivo.

We have previously described regeneration of human prostate tissue following implantation of adult prostate cells (or prostaspheres) combined with rat urogenital sinus mesenchyme (rUGSM) and Matrigel® into Non-Obese Diabetic Severely Combined Immunodeficient mice that are Interluekin-2 Receptor Null (SCID-$NOD^{IL2grNULL}$) [4,6]. In an effort to employ a fully humanized prostate tissue regeneration system, rUGSM was replaced with human prostate stromal cells cultured from dissociated fetal prostate tissue (Figure 2). Histological evaluation of fetal prostate specimens demonstrates abundant stroma surrounding the prostatic urethra with developing epithelial buds/tubules (Figure 2A). FBS-supplemented culture media supported the outgrowth of a nearly pure (Epcam-negative) human fetal stromal cell population (hFPS) that could be passaged continuously for more than 10 generations (Figure 2B and data not shown). Cryopreservation of hFPS, followed by thaw and re-culture enabled further expansion of these cells prior to use in vivo. When hFPS was combined with freshly isolated adult prostate epithelial cells (Figure 2C) or sphere-forming cells (data not shown) and Matrigel®, followed by subcutaneous implantation into SCID-$NOD^{IL2grNULL}$ mice, epithelial cord-like structures formed as early as 6 weeks (data not shown). Fully differentiated ductal/acinar structures with PSA-expressing luminal cells were prominent by 6 months (Figure 2C). Epithelial cords and/or tubular structures failed to form if Matrigel® and hFPS were recombined in the absence of prostate epithelial cells (Figure S1). No differences in tubule development were noted in grafts induced by rUGSM or hFPS (Figure S1). All structures typically identified in benign

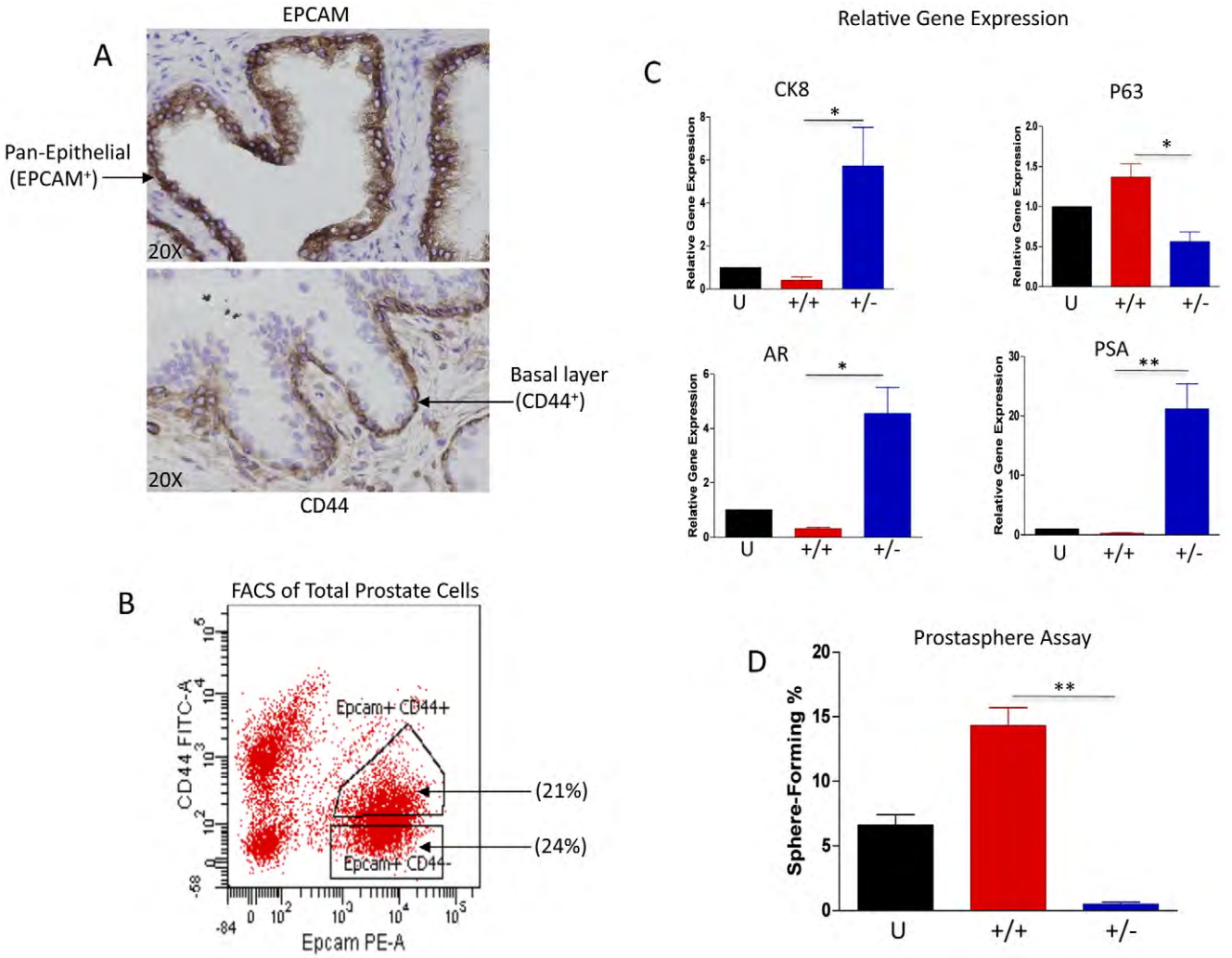

Figure 1. Variation in expression of Epcam and CD44 enables separation of distinct populations of prostate cells from dissociated surgical specimens. A. Immunohistochemical analysis of Epcam and CD44 expression in benign human prostate tissue specimens (20× magnification). B. FACS analysis of Epcam and CD44 expression in total prostate cells isolated from dissociated benign human prostate tissue. Total prostate cells stained with Epcam-PE and CD44-FITC conjugated antibodies prior to FACS analysis. C. Epcam^{+}CD44^{+} and Epcam^{+}CD44^{-} fractions display basal (P63+) and luminal (CK8+, AR+, PSA+) profiles, respectively. Quantitative RT-PCR reactions were performed in triplicate with a minimum of 3 individual patient specimens. Black columns represent Unfractionated (U) cells, red columns represent Epcam^{+}CD44^{+} cells (+/+), and blue columns represent Epcam^{+}CD44^{-} cells (+/−). D. Unfractionated prostate epithelial cells isolated from benign prostate tissue specimens or cells fractionated based on Epcam/CD44 expression were evaluated for sphere-forming capability in vitro. 1×10^{4} cells were plated in semi-solid (Matrigel®) cultures. Approximately 14 days after seeding, prostaspheres were quantitated in all wells and the percentage of sphere-forming cells was calculated in each fraction. All experiments were performed in triplicate, using a minimum of three individual patient samples. Statistical analysis was performed using standard one-way ANOVA analysis; $P<0.05$(*), $P<0.01$(**).
doi:10.1371/journal.pone.0034219.g001

prostate surgical specimens were present in hFPS regenerated grafts, including epithelial cords, corporal amylacea, and secretion-filled ducts/acini. Layers of epithelial cells expressing basal markers (K5, P63), luminal markers (K8, AR, PSA), or a combination of both were also identified (Figure 2C). HFPS was generated from 6 different fetal specimens and all demonstrated similar growth in culture, FACS profile, and ability to support tubular outgrowth when combined with adult prostate epithelial cells (data not shown).

Tubule initiating capability is prevalent in the non-sphere-forming Epcam^{+}CD44^{-} luminal-enriched cell fraction.

Although sphere formation is a common feature of S/Ps, one critical characteristic that prostate SCs must demonstrate is the ability to induce new tubule formation inclusive of ducts/acini composed of both basal and luminal cells. Prostate tissue regeneration assays have been utilized to interrogate the tubule initiation capability of putative S/P populations in mouse and human [4,21,22]. In these assays, total or fractionated cells obtained from fetal or adult prostate tissues are combined with supportive stroma (i.e., UGSM) followed by sub-renal implantation as a collagen graft or subcutaneous implantation with Matrigel® into immunocompromised mice. Cell fractions that possess S/P activity induce multi-layered tubular outgrowths with secretions surrounded by stroma. We have previously shown that sphere-forming cells as well as basal cells isolated based on co-expression of Trop2 and high levels of CD49f have an increased

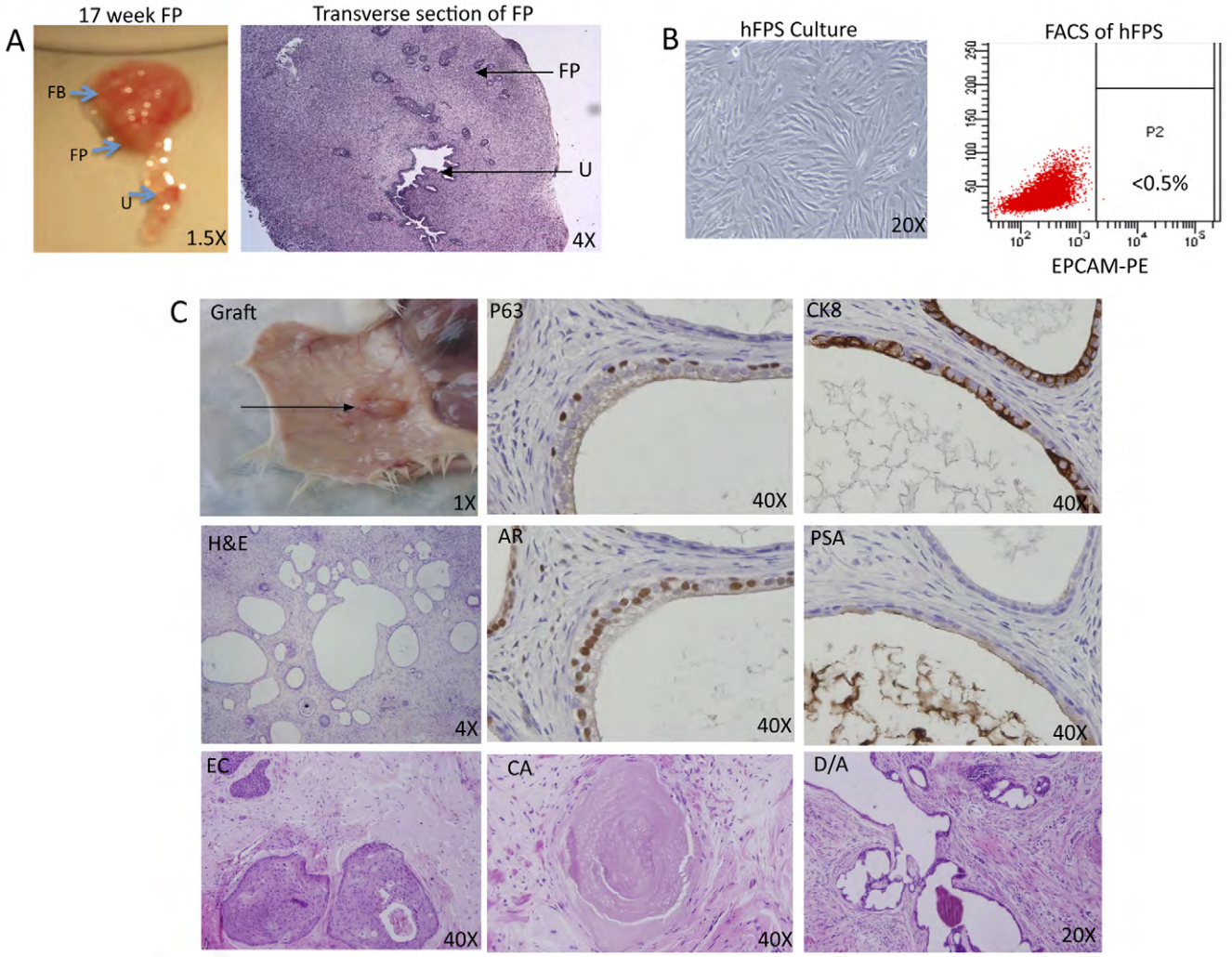

Figure 2. Isolation of human fetal prostate stroma (hFPS) for use in prostate tissue regeneration assays. A. Gross specimen containing 17-week fetal bladder (FB), prostate (FP), and urethra (U) en block with adjacent panel showing transverse hematoxylin and eosin (H&E) stained histological section. Developing prostate glands budding from the prostatic urethra are surrounded by abundant stroma. B. HFPS cells are cultured in DMEM supplemented with FBS. FACS analysis of cultured hFPS cells using antibodies that target Epcam demonstrates lack of (Epcam+) epithelial cell outgrowth. C. Regenerated graft induced by hFPS after recombination with freshly isolated adult human prostate cells and Matrigel®, followed by subcutaneous injection. H&E staining of paraffin-embedded graft demonstrates tubules with a distinct basal layer, containing cells that express tumor protein 63 (P63+) but lack luminal cell marker expression, including Androgen Receptor (AR), cytokeratin 8 (CK8), and Prostate Specific Antigen (PSA). A luminal layer is identified in the majority of outgrowths and contains cells that are P63−, AR+, CK8+, and PSA+. The bottom panel displays the different types of outgrowths identified in recombinant grafts, including epithelial cords (EC), corpora amylacea (CA), and epithelial cords/buds (EC).
doi:10.1371/journal.pone.0034219.g002

ability for tubule initiation compared to luminal ($Trop2^{+}CD49f^{Lo}$) cells [1,4,6].

In order to investigate the ability of cells fractionated based upon Epcam/CD44 expression to form tubules in vivo, human prostate tissue regeneration was performed. Approximately 1×10^{5} unfractionated cells, $Epcam^{+}CD44^{+}$ cells, or $Epcam^{+}CD44^{-}$cells were combined with 2×10^{5} hFPS and Matrigel®, followed by subcutaneous implantation into SCID-$NOD^{IL2grNULL}$ mice. Approximately twelve weeks following implantation, grafts were harvested and analyzed for tubule induction via histological analysis of paraffin embedded sections (Figure 3A). A table containing the rate of engraftment of unfractionated and fractionated cells is shown in Figure S2. Tubular structures were identified in grafts that developed from unfractionated cells and in $Epcam^{+}CD44^{+}$ recombinant grafts. Surprisingly, the $Epcam^{+}CD44^{-}$ luminal enriched/non-sphere-forming fractions yielded the largest number of tubular structures (Figure 3A and 3C). All grafts demonstrated a range of epithelial cord-like structures and more fully developed tubules with secretion-filled lumens (Figure 3A). Immunohistochemical staining confirmed the presence of basal ($p63^{+}$) and luminal ($CK8^{+}$) cells in regenerated tubules (Figure 3B). Although FACS and cytospin examination of fractionated cells confirmed $CD44^{-}$ status (data not shown), $CD44^{+}$ cord-like structures and tubules containing a distinct $CD44^{+}$ basal layer were identified in mature grafts induced by $Epcam^{+}CD44^{-}$ cell fractions (Figure 3B). This data suggests that $Epcam^{+}CD44^{-}$ cells may be precursors for $Epcam^{+}CD44^{+}$ cells found in regenerated tubular structures.

A functional role for a non-sphere-forming/luminal-enriched fraction appeared to contradict prior published results, in which fractionation of luminal cells based on Trop2/CD49f expression displayed no functional capabilities in vitro and in vivo[6]. To

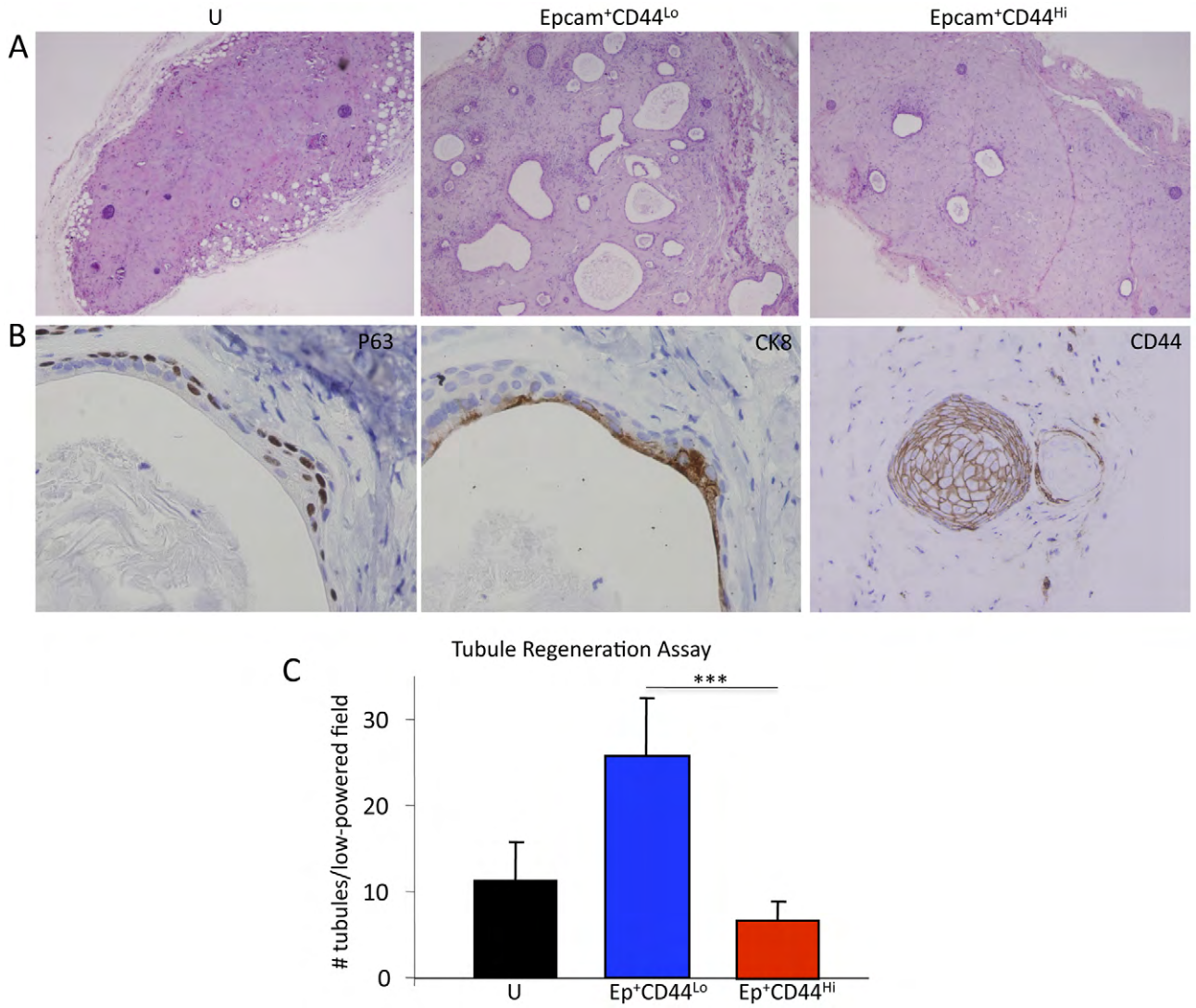

Figure 3. Tubule formation induced by unfractionated and fractionated (Epcam$^+$CD44$^+$ and Epcam$^+$CD44$^-$) prostate cells in human prostate tissue regeneration assays. A. H&E stained sections of paraffin-embedded 12-week grafts harvested from SCID-NOD$^{IL2\gamma rNULL}$ mice. Unfractionated (U) total prostate cells or Epcam$^+$CD44$^+$ and Epcam$^+$CD44$^-$ cell fractions combined with human fetal prostate stromal cells and Matrigel® were implanted subcutaneously into male SCID-NOD$^{IL2\gamma rNULL}$ mice. Testosterone was supplemented via pellets inserted subcutaneously. B. Example of secretion-filled ducts that display basal (p63 positive) and luminal (CK8 positive) cells induced by Epcam$^+$CD44$^-$ prostate cell fractions. Tubules and epithelial developed from cords containing CD44$^+$ cells also developed from the CD44$^-$ cell fraction. C. Comparison of the number of tubular structures identified in unfractionated, Epcam$^+$CD44$^+$, and Epcam$^+$CD44$^-$ grafts. After paraffin embedding, sections were made throughout the grafts. The two representative sections containing the highest number of tubules were identified and all tubules present in the low power (4X magnification) field were quantitated. The average numbers of tubules from total grafts obtained from unfractionated or fractionated cells are complied for the graph. Statistical analysis was performed using standard one-way ANOVA analysis; $P < 0.001$ (***).
doi:10.1371/journal.pone.0034219.g003

investigate this discrepancy, FACS analysis comparing Epcam and Trop2 expression was performed to evaluate co-expression of these surface markers. Indeed, there appeared to be almost complete overlap in expression of Trop2 and Epcam, with virtually all Trop2$^+$ cells co-expressing Epcam (Figure S3A). On the contrary, high expression CD49f did not appear to be confined to the CD44+ population, since a fraction of CD44$^-$ cells were CD49f^{Hi} (Figure S3B). This result suggests that Epcam$^+$CD44$^-$ prostate cells may be further subdivided based upon CD49f expression and may explain differential functional capabilities of basal/luminal cell fractions isolated based on Epcam/CD44 profile compared to Trop2/CD49f.

CD49f enables functional delineation of putative SCs, PCs, and LCs.

As described above, previous studies indicated that Trop2$^+$CD49f^{Hi} basal cells display both sphere forming and tubule regenerating capabilities, compared to the Trop2$^+$CD49f^{Lo} luminal cells, which lack these functional capabilities [4,6]. Given the surprising result that luminal-enriched Epcam$^+$CD44$^-$ cells display predominant tubule-initiation activity, we investigated whether or not CD49f^{Hi} cells present within this subpopulation may be responsible for tubule initiation in vivo. FACS analysis was performed on total prostate cells after incubation with antibodies targeting Epcam, CD44, and CD49f. Both CD49f^{Hi} and CD49f^{Lo} subpopulations were identified in Epcam$^+$CD44$^+$ and Ep-

cam^{+}CD44^{-} fractions (Figure 4A and S4). Cell sorting enabled isolation of prostate cells based upon Epcam/CD44/CD49 status. Prostasphere culture of Epcam^{+}CD44^{+}CD49f^{Hi} cells demonstrated enrichment of sphere-forming capability (10-fold over unfractionated cells and 3-fold over Epcam^{+}CD44^{+} cells) with 40–50% of cells within this fraction capable of forming spheres (Figure 4B). On the other hand, less than 1% of Epcam^{+}CD44^{+}CD49f^{Lo} or Epcam^{+}CD44^{-}CD49f^{Hi} cells were able to form spheres (Figure 4B and data not shown, respectively).

In order to evaluate tubule initiation activity of Epcam^{+}CD44^{-} non-sphere-forming cells subdivided by CD49f, in vivo tissue regeneration with hFPS was employed (Figure 4C). Recombinant grafts were retrieved from Epcam^{+}CD44^{-}CD49f^{Hi} cell fractions containing significantly more tubules than those induced by Epcam^{+}CD44^{-}CD49f^{Lo} cells (Figure 4C). FACS analysis of dissociated grafts induced by Epcam^{+}CD44^{-}CD49f^{Hi} cells demonstrated a similar composition of cells (based on Epcam/CD44/CD49f expression) as the original prostate surgical specimen (Figure 4E), indicating that this minority population could induce an intact prostate tissue profile.

As previously described, bright CD49f expression is associated with a basal cell profile, therefore, Epcam^{+}CD44^{-}CD49f^{Hi} and Epcam^{+}CD44^{-}CD49f^{Lo} cell fractions were evaluated by RT-PCR analysis to determine if the original Epcam^{+}CD44^{-} fraction contained a mix of luminal and basal cells [4,6,11]. RNA expression of p63 in association with a lack of AR and PSA indicated that Epcam^{+}CD44^{-}CD49f^{Hi} cells possessed a basal profile, while Epcam^{+}CD44^{-}CD49f^{Lo} cells exhibited a luminal profile, demonstrated by significant AR and PSA expression (Figure S5). This contrasting expression profile of Epcam^{+}CD44^{-}CD49f^{Hi} cells compared to RT-PCR analysis of Epcam^{+}CD44^{-} cells (in which fractionation with CD49f was not performed), indicates that the

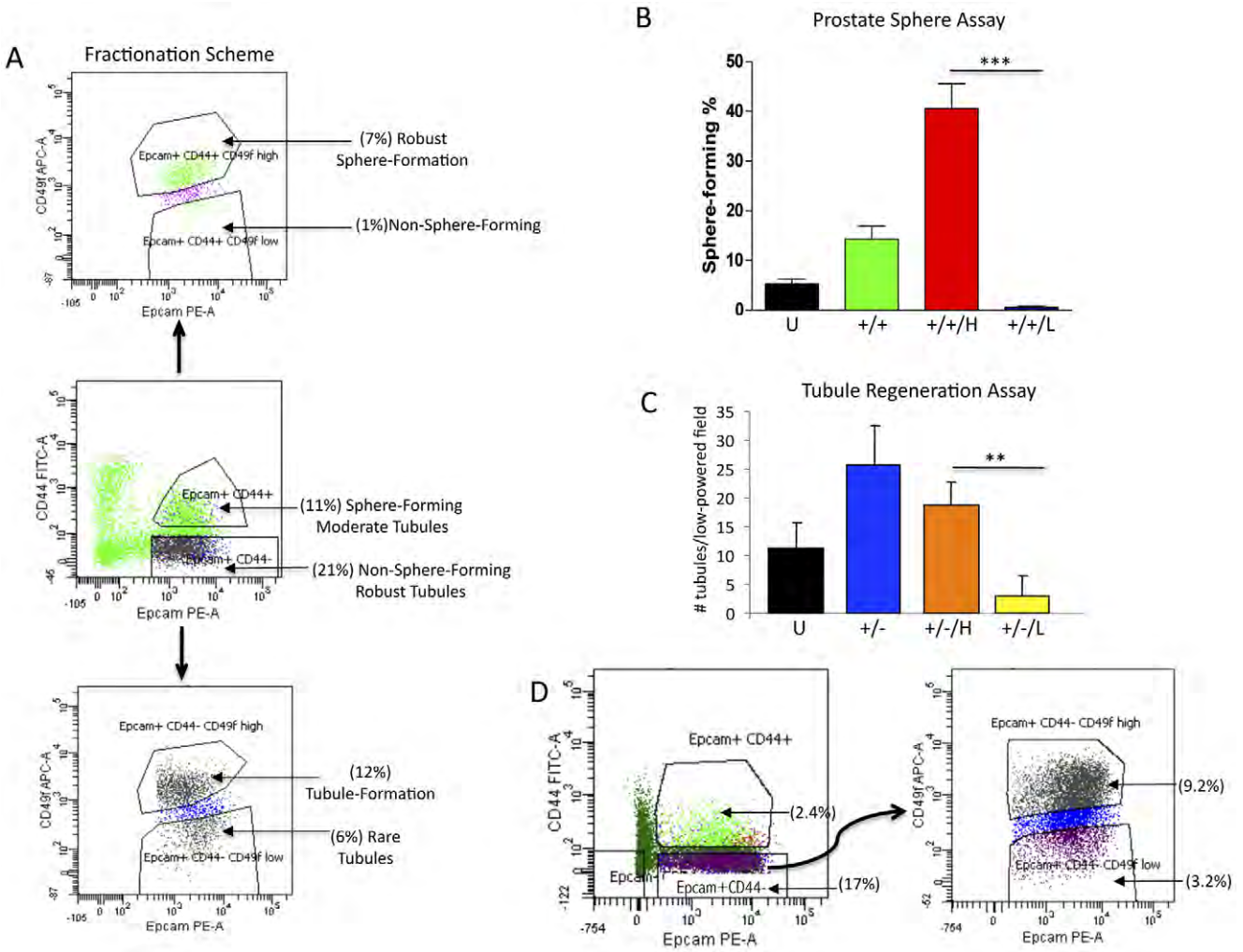

Figure 4. Identification and functional evaluation of CD49f$^{Hi/Lo}$ cells present in Epcam^{+}CD44^{+} and Epcam^{+}CD44^{-} fractions. A. FACS analysis of Epcam^{+}CD44^{+} and Epcam^{+}CD44^{-}for CD49f^{Hi} expression, with functionally distinct populations annotated. B. Sorting of Epcam^{+}CD44^{+} based on CD49f expression followed by sphere analysis in vitro (***P<0.001). Unfractionated (U), Epcam^{+}CD44^{+} (+/+), Epcam^{+}CD4+^{i}CD49f^{Hi} (+/+/H), Epcam^{+}CD44^{+}CD49f^{Lo} (+/+/L). C. Sorting of Epcam^{+}CD44^{-} based on CD49f expression followed by quantification of tubule initiation in vivo. After paraffin embedding, sections were made throughout the grafts. The two representative sections containing the highest number of tubules (4× magnification) were identified and quantitated. The average number of tubules from all the grafts retrieved is represented in the bar graph (**P<0.01). Epcam^{+}CD44−CD49f^{Hi} (+/−/H), Epcam^{+}CD44^{-}CD49f^{Lo} (+/−/L). D. FACS analysis of total cells obtained from three grafts induced by the Epcam^{+}CD44^{-}CD49f^{Hi} cell fraction. Grafts were mechanically and enzymatically digested to retrieve single cells that were pooled for FACS analysis. Although only highly enriched Epcam^{+}CD44^{-}CD49f^{Hi} cell fractions were combined with hFPS and Matrigel prior to injection, all of the cell types identified in the original prostate surgical specimens were found in regenerated tissue grafts.
doi:10.1371/journal.pone.0034219.g004

luminal expression profile observed with $Epcam^{+}CD44^{-}$ cell fractions was likely due to a masking effect by true luminal cells ($Epcam^{+}CD44^{-}CD49f^{Lo}$) that co-segregated with the non-sphere-forming basal subpopulation ($Epcam^{+}CD44^{-}CD49f^{Hi}$). Taken together, these results suggest that the human prostate basal cell population can be divided into populations with enriched sphere-forming activity ($Epcam^{+}CD44^{+}CD49f^{Hi}$) or tubule-initiating activity ($Epcam^{+}CD44^{-}CD49f^{Hi}$).

Discussion

Identifying functionally distinct populations of prostate epithelial cells could provide new insights about the cells of origin for human prostate cancer, by determining which cells within the hierarchy are susceptible to malignant transformation. Additionally, the mechanisms employed by normal prostate SCs that enable interaction with the niche and initiation of tubule development could lead to therapeutic approaches that interfere with similar pathways exploited by cancer cells or contributing to the development of benign prostatic hypertrophy (BPH). revious studies investigating human prostate S/P cells isolated from benign tissues have indicated that both general epithelial and basal antigens (Trop2, CD44, $alpha_2beta_1$-$integrin^{Hi}$, $alpha_6$-$integrin^{Hi}$ (CD49f)) are expressed [1,2,4]. In these studies, the ability to form self-renewing prostaspheres coincides with the potential to induce fully differentiated prostate tubules in vivo. In the current study, subpopulations of prostate basal cells with robust sphere-forming capability are distinguished from those with optimal tubule initiating capability based on specific antigenic profiles. Prostate epithelial cells with an increased potential to induce tubules inclusive of basal and luminal cell layers (putative SCs) are incapable of forming prostaspheres in vitro. On the other hand, highly proliferative sphere-forming cells (putative PCs) appear to have more limited potential for tubule initiation. This study is the first to functionally separate prostate epithelial cells based upon sphere-forming versus tubule initiating capabilities.

Combinations of antigens that subdivide the basal population and functionally distinguish prostate SCs from PCs have not been reported, with the exception of CD133, a rare surface marker found on less than 1% of basal cells [2]. A recent report regarding $\alpha_2\beta_1{}^{Hi}CD133^{+}$ cells indicated that these cells were incapable of forming spheres, but readily formed proliferative monolayer cultures [23]. Additional studies have demonstrated acinar-like outgrowths induced by $\alpha_2\beta_1{}^{Hi}CD133^{+}$ cells, in vivo [2]. This combined data suggests that $CD133^{+}$ cells are non-sphere-forming, but possess SC traits of self-renewal and differentiation capability, similar to the $Epcam^{+}CD44^{-}CD49f^{Hi}$ population reported here. In previous studies, we have also reported that CD133 expression did not enrich for sphere-forming cells [4]. However, given the surprising new finding of increased tubule formation induced by the non sphere-forming, $Epcam^{+}CD44^{-}CD49f^{Hi}$ cell fraction, analyzing concomitant expression of CD133 (and other putative SC markers) within this subset, including further fractionation and functional analysis, should be considered.

In previous studies of prostate S/P cells, Trop2, which has an almost identical pattern of expression as Epcam (Trop1) within prostate epithelial cells, was utilized to separate prostate epithelial from stromal and blood cells [1]. One advantage of using Epcam, as an alternative to Trop2, is stable and/or highly expressed Epcam is detected in most adenocarcinomas, as well as metastases, malignant effusions, and cancer stem cells [24]. Confirming the presence of Epcam within the human prostate S/P population may lead to investigations of therapeutic agents targeting Epcam and evaluation of specific effects on prostate SC and PC activity [24,25].

In the current study, CD44 expression appears to determine whether $Epcam^{+}$ prostate epithelial cells will form robust spheres ($CD44^{+}$) or remain quiescent in vitro, but induce robust tubule formation in vivo ($CD44^{-}$). In the neural system, it is a well-recognized limitation that quiescent neural SCs cannot be isolated using the neurosphere assay [26]. Additionally, it is emphasized that sphere-formation and self-renewal is a trait possessed by both SCs and PCs. In the current study, the antigenic profile of cells with the highest prostate sphere-forming capability is $Epcam^{+}CD44^{-}CD49f^{Hi}$. However, sphere-forming cells marked by $Epcam^{+}CD44^{+}$ expression can form tubules in vivo, but at a statistically significant lower rate than non-sphere-forming $Epcam^{+}CD44^{-}$ cells. Since previous in vivo studies clearly demonstrate that $CD49f^{Hi}$ is required for prostate tubule formation, we hypothesized that the $Epcam^{+}CD44^{-}CD49f^{Hi}$ antigenic profile designates non-sphere-forming cells capable of tubule regeneration in vivo. Indeed, this antigenic profile was confirmed in our study to represent a subpopulation of prostate basal cells with relatively robust tubule-initiating capability (compared to $Epcam^{+}CD44^{-}CD49f^{Hi}$ luminal cells) [6]. In contrast to our sphere results, sub-fractionation of $Epcam^{+}CD44^{-}$ cells with increased tubule initiation capability did not appear to further enrich for this activity. One factor that may have contributed to this observation is the fact that FACS sorting with three markers requires longer sort time, which could impact the long-term viability of these cells that is required for in vivo grafting. Despite enrichment with the more refined cell fraction, our results clearly demonstrate an advantage in tubule formation capability compared to luminal $Epcam^{+}CD44^{-}CD49f^{Lo}$ cells. Consequently, three distinct populations of prostate epithelial cells are revealed, including subdivided basal ($Epcam^{+}CD44^{+}CD49f^{Hi}$ and $Epcam^{+}CD44^{-}CD49f^{Hi}$) and luminal ($Epcam^{+}CD44^{-}CD49f^{Lo}$) fractions.

Bona fide SCs should be capable of residing in the quiescent state and become activated to differentiate and form new tubules as needed. With asymmetric cell division, progenitor daughter cells develop with less potential to induce new tubules. In the current study, although some sphere-forming cells retain the potential to induce new tubules, the proportion is far less than the in vitro quiescent $Epcam^{+}CD44^{-}$population. This result implies that prostaspheres contain both SCs and rapidly proliferating progenitors (possible transit-amplifying cells), resulting in an overall decreased potential to induce tubules compared to non-sphere-forming SCs. Hence, $Epcam^{+}CD44^{Hi}CD49f^{Hi}$ cells may be further along the developmental pathway and suggests a hierarchy of prostate epithelial cells.

Although the sphere-forming assays indicate that our putative SCs are quiescent, further studies are needed to evaluate this trait. It has been suggested that sphere-formation is an indicator of self-renewal, yet we have found that the non-sphere-forming ($Epcam^{+}CD44^{-}CD49f^{Hi}$) cells are capable of inducing differentiated tubules and regenerated grafts that include the full spectrum of prostate cells found in original surgical specimens, including putative SCs. This data indicates that in addition to differentiation and niche interaction capabilities, the putative SCs are self-renewing (despite the inability to form spheres).

Taken together, our results suggest that $Epcam^{+}CD44^{Lo}CD49f^{Hi}$ cells are non-sphere-forming SCs that may be activated to form tubules when exposed to inductive stroma cells in vivo. Lack of CD44 expression distinguishes non-sphere-forming SCs from the more proliferative state of the $CD44^{+}$ population, which may contain an increased proportion of PCs with limited

induction potential, relative to tubule-initiating SCs. Support for CD44 as a proliferative marker exists. The majority of primary prostate epithelial cells (transient amplifying cells) that grow as a monolayer, in vitro, express CD44 [27,28,29]. Examination of human prostate cancer cell lines and xenografts indicate that the $CD44^+$ population is more proliferative, clonogenic, tumorigenic, and metastatic than $CD44^-$ cells[30,31,32].

Future studies that may yield more insight into prostate SC/PC characteristics and function include gene expression array analysis comparing $Epcam^+CD44^-CD49f^{Hi}$ and $Epcam^+CD44^+CD49f^{Hi}$ cells. Such efforts could reveal novel antigens and genetic pathways that are unique to each subpopulation. Additionally, genetic manipulation of benign prostate cell fractions based on Epcam/CD44/CD49f expression, followed by in vivo regeneration may suggest mechanisms of tumorigenesis or benign proliferation (BPH) at different developmental stages.

Methods

Tissue Digestion and Cell Dissociation.

Human prostate tissue was obtained via a research protocol that was approved by the Office for the Protection of Research Subjects at UCLA and the Greater Los Angeles VA Medical Center. Informed written consent was obtained on all participants where identifying information was included. In cases where no identifying information was included and tissue was acquired in an anonymous fashion at UCLA, an approved Institutional Review Board protocol with written consent was not required by Office for the Protection of Research Subjects. Adjacent tissue specimens were snap frozen in liquid nitrogen or fixed in formalin and paraffin-embedded for histological analysis. Frozen sections were immediately examined by a genitourinary pathologist and cancer foci encircled. Fresh tissue specimens were matched with the frozen section slides to enable macrodissection of benign tissue away from tumor nodules. Typically, 2–10 grams of fresh tissue was allocated for research studies. Tissue specimens were then mechanically and enzymatically digested as previously described [16]. Dissociated tissue containing single cells and organoids was sequentially filtered through 100-μm and 40-μm cell strainer, and then passed repeatedly through a 23-gauge needle, in order to generate a single cell suspension. Cells were counted with a hemocytometer and resuspended in RPMI supplemented with 10% FBS prior to cell sorting or plating in prostasphere cultures. Approximately 1–2 million viable cells per gram of fresh tissue were routinely obtained.

Magnetic activated cell sorting(MACS).

Miltenyi auto MACS® was used to separate $Epcam^+CD44^+$ and $Epcam^+CD44^-$ prostate epithelial cells. For $Epcam^+$ cell separation, single cell suspensions obtained from freshly dissociated prostate tissue were stained with anti-human Epcam-PE antibody (Miltenyi Biotech), followed by incubation with anti-PE Multisort Microbeads (Miltenyi Biotech). Stained cells were separated through autoMACS (Miltenyi Biotech) with Mode POSSEL (Positive Selection). Positive fraction was collected as $Epcam^+$ cells and microbeads were removed using Multisort Release Reagents (Miltenyi Biotech). Cells were then stained with CD44 microbeads before separation through auto MACS® separator with POSSEL, with collection of positive ($Epcam^+CD44^+$) and negative ($Epcam^+CD44^-$) fractions. The negative fraction was separated further with Mode DEPLETES (Depletion in sensitive mode. The $Epcam^+CD44^+$ and $Epcam^+CD44^-$ cells were stained with anti-human CD44-PE-Cy-7 (eBioscience) and analyzed by FACS to evaluate the purity of sorted cells.

Fluorescence-activated cell sorting (FACS).

Prostate cells were suspended in PBS, 2 mM EDTA,0.5%BSA and stained with antibody for 15 minutes at 4°C. Fluorescence-activated cell sorting and analysis were performed on a BD Special Order FACS Aria II system and Diva v6.1.1 (BD Biosciences). Live single cells were gated based on scatter properties and analyzed for their surface marker expression. Cells were sorted and collected at 4°C using 100um nozzle and 23psi. Antibodies used for FACS include Epcam-PE (Miltenyi Biotech), CD44-FITC (ebioscience), and CD49f-APC (BioLegend).

In vitro prostasphere assay.

Prostate cells were counted and re-suspended in 50:50 Matrigel: PrEGM with a concentration of 5×10^3 cells/80microliters. This Matrigel/cellular suspension was plated at the edge of the well on 12-well plates and allowed to solidify by incubation at 37°C for 30 minutes. One milliliter of defined sphere media was then added to each well and plates were replaced in 37°C incubator, as previously described [4]. Quantitation of prostaspheres was performed approximately 10–14 days after plating.

Tissue acquisition, isolation and culture of fetal prostate cells.

Human fetal prostate tissue was acquired from 16–17 week specimens in accordance with federal and state guidelines. Adjacent prostate tissue was snap frozen in liquid Nitrogen or fixed in formalin and paraffin-embedded to evaluate anatomy and glandular architecture. The remainder of the tissue was mechanically and enzymatically digested as described (13). Dissociated prostate cell suspensions were sequentially filtered through 100-micron and 40-micron filters, and then passed through a 23-gauge needle. Cells were counted with a hemocytometer and resuspended in RPMI supplemented with 10% fetal bovine serum (FBS), penicillin/streptomycin (Mediatech Inc.), and Methyltrienolone R1881 (Sigma) for culture in vitro. After 3 passages, cells were analyzed via FACS to confirm purity of stromal cells (See below). HFBS is cryopreserved and thawed as needed for use in recombination assays.

In vivo tissue regeneration.

In vivo tissue experiments were performed in male SCID-$NOD^{IL2grNULL}$ mice in accordance with protocol number 2007-189-11A, approved by the Animal Research Committee within the Office for the Protection of Research Subjects at UCLA. Mice (6–8 weeks old) were subjected to subcutaneous injections of prostate epithelial cells. Approximately 1×10^5 epithelial cells were combined with 2×10^5 primary human fetal prostate stroma cells (hFPS). The epithelial and stromal cells were then suspended in 50 microliters 50:50 Matrigel®: PrEGM. Subcutaneous implantation of time-release testosterone pellets (Innovative Research of America) was simultaneously performed at the time of graft implantation. Subcutaneous nodules at the site of injection were removed after approximately 12 weeks of the implantation and frozen/paraffin-embedded sections were generated for immunohistochemical analysis. Fresh hFPS cells were cultured in RPMI supplemented with 10% FBS and R1881 (Sigma) and passaged three times prior to use in tissue regeneration assays.

Immunohistochemistry of tissue sections.

Prostate tissue was paraffin embedded as previously described [33]. Four-micron thick sections of frozen or paraffin embedded tissue were deparaffinized with xylene and rehydrated through a descending series of ethanol washes as described [4]. Antigen

retrieval and standard immunoperoxidase procedures were used in combination with primary antibodies, including CK5, CK8 (Convane), p63, androgen receptor (AR), Prostate Specific Antigen (PSA) (Santa Cruz), and CD44 (Abcam).

Real time RT-PCR Analysis.

RNA was extracted using Qiagen RNAeasy Micro Kit, following the manufacturer's instructions. The concentration and purity of total RNA was assessed spectrophotometrically at 260 and 280 nm. CDNA was generated from total RNA (up to 5 μg) using SuperScript III First-Strand Synthesis Kit (Invitrogen). For quantitative Real-time PCR, a Bio-Rad CFX Multicolor Real-time PCR detection system was employed, using the SYBR®-Green Supermix (Bio-Rad Laboratories). Real-time PCR primer pairs for CK8, PSA, AR and p63 were purchased from SABiosciences Corporation. The PCR reaction conditions included an initial step at 95°C for 3 min, followed by 40 cycles at 95°C for 15 s (Melt) and 60°C for 45 s (Anneal/Extend). Detection of PCR products was accomplished by measuring the emitting fluorescence at the end of each reaction step (reaction cycles). Threshold cycle corresponds with the cycle number required to detect a fluorescence signal above the threshold. Calculations were performed by Bio-Rad IQ5 software provided by the manufacturer. Gene expression analysis was performed using the comparative method.

Supporting Information

Figure S1 Comparison of prostate tissue grafts induced by rUGSM and hFPS. Total adult prostate cells (5×10^5) isolated from fresh benign surgical specimens were combined with either rUGSM or hFPS (1×10^6 cells). Grafts were retrieved approximately 12 weeks following subcutaneous injection into SCID-NOD$^{IL2\gamma rNULL}$ mice. H&E staining of paraffin-embedded sections demonstrated similar composition of tubular structures within grafts, including ductal/acini structures, corpora amylacea, and epithelial cords. Similar to previous studies with rUGSM, grafts that formed from hFPS without additive adult prostate epithelial cells (PCs) did not contain any tubular structures. All grafts with tubules (T) were found to have prominent vasculature (BV) throughout (Right panel).
(TIF)

Figure S2 Table depicting number of patient samples utilized for implants and grafts retrieved. A total of 29 implants yielded 20 grafts with tubules for comparative analysis (69% engraftment rate).
(TIF)

Figure S3 Epcam (Trop1) and Trop2 demonstrate overlapping expression in human prostate cells, while CD49f and CD44 demonstrate disparate expression. A. Total prostate cells were co-stained with antibodies recognizing Epcam and Trop2 and subjected to FACS analysis. The majority of Epcam$^+$ cells co-expressed Trop2. B. Total prostate cells were co-stained with antibodies recognizing CD44 and CD49f. A population of CD49f^{Hi} cells were identified that appear to be CD44$^-$, suggesting that a proportion of Epcam$^+$CD44$^-$cells may co-express CD49f.
(TIF)

Figure S4 FACS analysis of individual patient surgical specimens for Epcam/CD44/CD49f. Four patient specimens (A–D) are shown for comparative analysis of populations retrieved. After mechanical and enzymatic digestion, single cell suspensions are stained with antibodies targeting Epcam, CD44, and CD49f. High and low CD44-expressing populations of Epcam+ cells are gated and analyzed for CD49f expression. High and low CD49f-expressing cells are then isolated for functional analysis.
(TIF)

Figure S5 Quantitative RT-PCR demonstrates Epcam$^+$CD44$^-$CD49f^{Hi} cell fractions have a basal profile (p63$^+$AR^{Lo}PSA$^-$), while Epcam$^+$CD44$^-$CD49f^{Lo} cells display a luminal profile (p63^{Lo}AR^{Hi}PSA$^+$). Primers targeting p63, AR, and PSA were used in fractionated cells to compare expression relative to unfractionated cells (U). Epcam$^+$CD44$^-$CD49f^{Hi} (+/−/H), Epcam$^+$CD44$^-$CD49f^{Lo} (+/−/L). Statistical analysis was performed using standard one-way ANOVA analysis. $P<0.05$(*), $P<0.01$(**).
(TIF)

Acknowledgments

Flow cytometry/FACS was performed in the UCLA Jonsson Comprehensive Cancer Center (JCCC) and Center for AIDS Research Flow Cytometry Core Facility. We gratefully thank Donghui Cheng, who performed additional FACS sorting, Dr. Dong Sun An, who provided fetal prostate samples, and the genitourinary pathologists in the UCLA Tissue Procurement Clinical Laboratory and at the Greater Los Angeles Veterans Hospital for assisting with specimen retrieval and slide review. Additional thanks to Drs. Hong Wu and David Mulholland for manuscript review.

Author Contributions

Conceived and designed the experiments: CG HL IG. Performed the experiments: CG HL BZ RC. Analyzed the data: CG HL BZ AM IG RC. Contributed reagents/materials/analysis tools: AM. Wrote the paper: CG HL IG.

References

1. Goldstein AS, Lawson DA, Cheng D, Sun W, Garraway IP, et al. (2008) Trop2 identifies a subpopulation of murine and human prostate basal cells with stem cell characteristics. Proc Natl Acad Sci U S A 105: 20882–20887.
2. Richardson GD, Robson CN, Lang SH, Neal DE, Maitland NJ, et al. (2004) CD133, a novel marker for human prostatic epithelial stem cells. J Cell Sci 117: 3539–3545.
3. Vander Griend DJ, Karthaus WL, Dalrymple S, Meeker A, DeMarzo AM, et al. (2008) The role of CD133 in normal human prostate stem cells and malignant cancer-initiating cells. Cancer Res 68: 9703–9711.
4. Garraway IP, Sun W, Tran CP, Perner S, Zhang B, et al. (2010) Human prostate sphere-forming cells represent a subset of basal epithelial cells capable of glandular regeneration in vivo. Prostate 70: 491–501.
5. Collins AT, Habib FK, Maitland NJ, Neal DE (2001) Identification and isolation of human prostate epithelial stem cells based on alpha(2)beta(1)-integrin expression. J Cell Sci 114: 3865–3872.
6. Goldstein AS, Huang J, Guo C, Garraway IP, Witte ON (2010) Identification of a cell of origin for human prostate cancer. Science 329: 568–571.
7. Buzhor E, Harari-Steinberg O, Omer D, Metsuyanim S, Jacob-Hirsch J, et al. (2011) Kidney spheroids recapitulate tubular organoids leading to enhanced tubulogenic potency of human kidney-derived cells. Tissue Eng Part A.
8. Deleyrolle LP, Reynolds BA (2009) Identifying and enumerating neural stem cells: application to aging and cancer. Prog Brain Res 175: 43–51.
9. Deleyrolle LP, Reynolds BA (2009) Isolation, expansion, and differentiation of adult Mammalian neural stem and progenitor cells using the neurosphere assay. Methods Mol Biol 549: 91–101.
10. Farnie G, Clarke RB (2006) Breast stem cells and cancer. Ernst Schering Found Symp Proc. pp 141–153.
11. Lawson DA, Xin L, Lukacs RU, Cheng D, Witte ON (2007) Isolation and functional characterization of murine prostate stem cells. Proc Natl Acad Sci U S A 104: 181–186.
12. Xin L, Lukacs RU, Lawson DA, Cheng D, Witte ON (2007) Self-renewal and multilineage differentiation in vitro from murine prostate stem cells. Stem Cells 25: 2760–2769.
13. Went PT, Lugli A, Meier S, Bundi M, Mirlacher M, et al. (2004) Frequent EpCam protein expression in human carcinomas. Hum Pathol 35: 122–128.

14. Zoller M (2011) CD44: can a cancer-initiating cell profit from an abundantly expressed molecule? Nat Rev Cancer 11: 254–267.
15. Palapattu GS, Wu C, Silvers CR, Martin HB, Williams K, et al. (2009) Selective expression of CD44, a putative prostate cancer stem cell marker, in neuroendocrine tumor cells of human prostate cancer. Prostate 69: 787–798.
16. Tran CP, Lin C, Yamashiro J, Reiter RE (2002) Prostate stem cell antigen is a marker of late intermediate prostate epithelial cells. Mol Cancer Res 1: 113–121.
17. Epstein JI (2010) An update of the Gleason grading system. J Urol 183: 433–440.
18. van Leenders G, van Balken B, Aalders T, Hulsbergen-van de Kaa C, Ruiter D, et al. (2002) Intermediate cells in normal and malignant prostate epithelium express c-MET: implications for prostate cancer invasion. Prostate 51: 98–107.
19. van Leenders GJ, Aalders TW, Hulsbergen-van de Kaa CA, Ruiter DJ, Schalken JA (2001) Expression of basal cell keratins in human prostate cancer metastases and cell lines. J Pathol 195: 563–570.
20. Signoretti S, Loda M (2006) Prostate stem cells: From development to cancer. Semin Cancer Biol.
21. Cunha GR, Lung B (1978) The possible influence of temporal factors in androgenic responsiveness of urogenital tissue recombinants from wild-type and androgen-insensitive (Tfm) mice. J Exp Zool 205: 181–193.
22. Xin L, Ide H, Kim Y, Dubey P, Witte ON (2003) In vivo regeneration of murine prostate from dissociated cell populations of postnatal epithelia and urogenital sinus mesenchyme. Proc Natl Acad Sci U S A 100 Suppl 1: 11896–11903.
23. Lang SH, Anderson E, Fordham R, Collins AT (2010) Modeling the prostate stem cell niche: an evaluation of stem cell survival and expansion in vitro. Stem Cells Dev 19: 537–546.
24. Patriarca C, Macchi RM, Marschner AK, Mellstedt H (2011) Epithelial cell adhesion molecule expression (CD326) in cancer: A short review. Cancer Treat Rev.
25. Kurtz JE, Dufour P (2010) Adecatumumab: an anti-EpCAM monoclonal antibody, from the bench to the bedside. Expert Opin Biol Ther 10: 951–958.
26. Pastrana E, Silva-Vargas V, Doetsch F (2011) Eyes wide open: a critical review of sphere-formation as an assay for stem cells. Cell Stem Cell 8: 486–498.
27. Litvinov IV, Vander Griend DJ, Xu Y, Antony L, Dalrymple SL, et al. (2006) Low-calcium serum-free defined medium selects for growth of normal prostatic epithelial stem cells. Cancer Res 66: 8598–8607.
28. Peehl DM (2004) Are primary cultures realistic models of prostate cancer? J Cell Biochem 91: 185–195.
29. Peehl DM (2005) Primary cell cultures as models of prostate cancer development. Endocr Relat Cancer 12: 19–47.
30. Patrawala L, Calhoun T, Schneider-Broussard R, Li H, Bhatia B, et al. (2006) Highly purified CD44+ prostate cancer cells from xenograft human tumors are enriched in tumorigenic and metastatic progenitor cells. Oncogene 25: 1696–1708.
31. Patrawala L, Calhoun-Davis T, Schneider-Broussard R, Tang DG (2007) Hierarchical organization of prostate cancer cells in xenograft tumors: the CD44+alpha2beta1+ cell population is enriched in tumor-initiating cells. Cancer Res 67: 6796–6805.
32. Liu C, Kelnar K, Liu B, Chen X, Calhoun-Davis T, et al. (2011) The microRNA miR-34a inhibits prostate cancer stem cells and metastasis by directly repressing CD44. Nat Med 17: 211–215.
33. Garraway IP, Seligson D, Said J, Horvath S, Reiter RE (2004) Trefoil factor 3 is overexpressed in human prostate cancer. Prostate 61: 209–450.

Published in final edited form as:
Cancer Cell. 2011 June 14; 19(6): 792–804. doi:10.1016/j.ccr.2011.05.006.

Cell Autonomous Role of PTEN in Regulating Castration-Resistant Prostate Cancer Growth

David J Mulholland[1], **Linh M. Tran**[1], **Yunfeng Li**[1], **Houjian Cai**[2], **Ashkan Morim**[1], **Shunyou Wang**[1], **Seema Plaisier**[1], **Isla P. Garraway**[3], **Jiaoti Huang**[4], **Thomas G. Graeber**[1], and **Hong Wu**[1,5,*]

[1]Department of Molecular and Medical Pharmacology and Institute for Molecular Medicine, University of California, Los Angeles

[2]Department of Microbiology, Immunology and Molecular Medicine, University of California, Los Angeles

[3]Department of Urology, University of California, Los Angeles

[4]Department of Pathology, University of California, Los Angeles

[5]Eli and Edythe Broad Center of Regenerative Medicine and Stem Cell Research, University of California, Los Angeles

SUMMARY

Alteration of the PTEN/PI3K pathway is associated with late stage and castrate resistant prostate cancer (CRPC). However, how PTEN loss involves in CRPC development is not clear. Here we show that castration-resistant growth is an intrinsic property of *Pten*-null prostate cancer (CaP) cells, independent of cancer development stage. PTEN loss suppresses androgen-responsive gene expressions by modulating androgen receptor (AR) transcription factor activity. Conditional deletion of *Ar* in the epithelium promotes the proliferation of *Pten*-null cancer cells, at least in part, by down-regulating androgen-responsive gene *Fkbp5* and preventing PHLPP-mediated AKT inhibition. Our findings identify PI3K and AR pathway crosstalk as a mechanism of CRPC development, with potentially important implications for CaP etiology and therapy.

INTRODUCTION

Prostate cancer (CaP) is the most common male malignancy and a leading cause of mortality in western countries (American Cancer Society, 2010). Androgens are critical both for the development and function of the normal prostate gland and for the maintenance of CaP cells that arise from the secretory epithelium of the prostate. Androgens function through their cognitive receptor, the androgen receptor (AR). Therefore, therapies for advanced CaP usually involve either reducing or blocking the production of androgens or antagonizing the AR and its target genes (Chen et al., 2008). However, all men with metastatic disease develop resistance to these therapies and will progress to castration-resistant prostate cancer (CRPC).

AR is expressed in CRPC and that AR signaling may be activated via autocrine or androgen-independent manner such as through cross-talk with other pro-survival and proliferative pathways (Attard et al., 2009a; Montgomery et al., 2008). However, levels of AR are also

*Corresponding author: Hong Wu, M.D, Ph.D. 650 Charles E Young Drive S. Los Angeles, CA 90095, Phone: 310.825.5160, FAX: 310.267.0242, hwu@mednet.ucla.edu.

heterogeneous and in some instances absent from late stage diseases (Roudier et al., 2003). Such clinical observations raise the possibility that loss of AR expression or activity may serve as an alternative means of escaping androgen withdrawal or AR-targeted therapies, possibly through concomitant activation of compensatory signaling pathways. One of the possible survival and proliferative pathways is the PI3K/AKT/mTOR pathway, which is negatively regulated by the PTEN tumor suppressor (Hill and Wu, 2009; Taylor et al., 2010). *PTEN* loss occurs frequently during human CaP progression, with up to 70% of late stage samples exhibiting loss of PTEN function or activation of the PI3K pathway (Taylor et al., 2010). PTEN loss or activation of the PI3K/AKT pathway leads to enhanced cell proliferation, survival and migration (Stiles et al., 2004; Vivanco and Sawyers, 2002) as well as castration-resistant growth (Gao et al., 2006; Jiao et al., 2007; Wang et al., 2003).

Progress in defining the mechanisms of CRPC has been limited due to a paucity of xenograft models and scarcity of matched human clinical specimens representing castration-sensitive and castration-resistant disease. Several well-established transgenic CaP models, i.e. TRAMP (Greenberg et al., 1995) and *hi-Myc* (Ellwood-Yen et al., 2003) have the limitation that the oncogene is driven by an androgen-dependent promoter. Therefore, the effect of androgen ablation on CaP growth is confounded by its effect on transgene expression. Previously, we established the *Pten*-null CaP model by conditional deletion of *Pten* in the murine prostatic epithelium and showed that *Pten* null CaPs progress with defined kinetics that mimic histopathological features of human disease (Wang et al., 2003). We also tested whether the *Pten* null CaP model could be used for studying CRPC by surgically castrating mutant mice at 16 weeks, when invasive adenocarcinoma had already developed. Despite activation of pro-survival AKT signaling, *Pten* null cancer cells are sensitive to androgen withdrawal and the cell death index is higher than that of age- and genetic background-matched WT controls and persists 5–10 weeks after castration. However, the cell proliferation index is not changed in comparison to intact *Pten* null mice. Such androgen-independent growth overrides androgen-dependent cell death and causes castration-resistant growth and invasive adenocarcinoma (Wang et al., 2003). The *Pten* conditional murine CaP model, therefore, provides a unique opportunity to address the mechanism of resistance to androgen ablation therapy in a genetically defined model where the oncogenic event is androgen - independent. Using this defined genetic model, we tested whether CRPC development is cancer stage-dependent and whether CRPC remains dependent on AR signaling in the epithelium in this study.

RESULTS

Early castration cannot prevent *Pten* null CaP initiation and castration-resistant growth

In our previous work (Wang et al., 2003) we castrated *Pten* conditional knockouts after the development of invasive adenocarcinoma. However the androgen-independent proliferative signal could be either intrinsic to Pten loss or due to other molecular/genetic alterations accumulated during cancer progression. To separate these two possibilities, we tested whether CRPC development depends on cancer stage by castrating the mutant mice at time points corresponding to prostatic epithelial *Pten* deletion, hyperplasia, and PIN lesion stages, respectively (Wang et al., 2003) (Figure 1A). Age-and genetic background-matched *Pten* null intact and WT castrated mice were used as controls and all animals were sacrificed at 10 weeks of age. Early castration, particularly when performed at 2 weeks old, significantly reduced the total prostate volume (data not shown). However, E-cadherin-positive PIN lesions and localized invasion, judged by loss of smooth muscle actin (SMA) staining, was clearly evident in the dorsolateral lobes of the mutants (Figure 1B, arrow). Elevated P-AKT (S473) and P-S6 (S240) were also observed, coinciding with Pten loss, in mutant mice castrated at 2 weeks old or 6 week old (Figure 1B and Figure S1). Proliferation index (%Ki67+ cells and Cyclin D1+ cells), was significantly increased in the mutant prostates

although those of mice castrated at 2 weeks old were less proliferative than were those of mice castrated at 6 weeks old (Figure 1C), which suggests that other molecular or genetic events may occur between 2 and 6 weeks after the *Pten* deletion and collaborate with PI3K pathway to promote cell proliferation. Nevertheless, these results suggest that androgen-independent proliferation is intrinsic to Pten loss, which is consistent with previous studies (Jiao et al., 2007) (Gao et al., 2006).

Pten null CaPs are less dependent on AR signaling and Pten loss can suppress androgen-responsive genes expression

That *Pten* null CaP cells can proliferate under castrate conditions suggests that Pten loss may sensitize AR to castrated androgen levels or even obviate the requirement of androgens. To test this, we compared the AR signaling status, defined by the expression of androgen-responsive genes, in age- and genetic background-matched *Pten* null and WT prostates at 0, 3, 6 and 14 days post castration (n=3). To determine the AR-responsive genes in normal, non-cancerous prostate, we analyzed a previously published data set (Wang et al., 2007) with two criteria: gene expressions were up- or down-regulated at least 2-fold post castration (castration/intact) and their expressions are reverted upon hormone replacement (hormone replacement/castration). This led to the selection of 148 androgen-responsive genes, including 47 activated and 101 suppressed genes (Table S1). When compared with published human androgen-responsive gene lists (Chauvin and Griswold, 2004; Nelson et al., 2002), we found many overlaps (data not shown).

Surprisingly, Pten loss in the epithelium does not sensitize AR signaling, and in the contrary, it suppresses androgen-responsive gene expression or AR transcriptional output in the intact mice (Figure 2A, orange brackets). Although the expressions of the androgen-responsive genes are significantly changed in WT mice after castration the expressions of the majority of these genes are similar in *Pten* null prostates before and after castration (Figure 2A, B; Figure S2A). Strikingly, the overall AR transcriptional output of 14-day castrated WT prostates is similar to that of intact *Pten* null prostates (Figure 2C; Figure S2A). Using a rank-rank analysis and a hypergeometric overlap algorithm (Plaisier et al., 2010), we also found the similarity between the global expression profiles of genes altered in *Pten* null CaPs (*Pten* null cancer - WT control) with those enriched after castration (castration - intact or day 0 control, Figure S2B and 2C). Together, these results indicate that PTEN loss not only suppresses AR transcriptional output but also drives the overall gene expression profiles towards a castration-like phenotype.

To test the relevance of our finding to human CaPs, we analyzed two public datasets (Lapointe et al., 2004; Taylor et al., 2010). Human samples were first stratified according to their *PTEN* DNA copy number status (PTEN CN; Figure 2D) and then tested if the murine-derived *Ar* signature genes are differentially expressed according to the *PTEN* CN status. We found 81/148 murine androgen-responsive genes in both human datasets, including 26 activated and 55 suppressed genes (Figure 2D). The two dimensional comparison illustrates the consistency between the two human datasets for the differential expression of the murine derived androgen-responsive genes in *PTEN* CN mutant vs. normal cohorts (p value of the correlation coefficient=2.2e−6), suggesting the overall suppression of AR-output in human CaPs with *PTEN* CN variation, similar to our observation in *Pten*-null mutants. In contrast, cancers with abnormal copy number (CN) of the *MYC* oncogene showed less agreement between the two datasets (p value of the correlation coefficient=1.1e−4) (Figure S2D), indicating that suppression of AR transcriptional output may depend on specific oncogenic events.

PTEN controls AR transcription factor activity by regulating EGR1, c-JUN and EZH2 expression

To determine how PTEN loss leads to repression of AR output, we used an inducible system in which *PTEN* expression is controlled in a doxycycline-dependent manner in *Pten* null, $Pten^{\Delta loxp/\Delta loxp}$ murine cells (Chang et al., 2004). While *Ar* expression is not influenced by *PTEN* re-expression, Egr1 and c-Jun transcription factors expressions are down regulated within 24 hrs upon induced PTEN re-expression, which were confirmed in a PTEN-inducible human CaP line, PC3 (Figure 2E and data not shown). Both EGR1 and c-JUN are up regulated in CaPs, especially CRPC, and can physically interact with AR, leading to down regulated AR targeted gene expression and CaP cell growth in androgen-depleted environment (Gitenay and Baron, 2009; Sato et al., 1997; Yang et al., 2006; Yuan et al., 2010). *Egr1* deletion impairs prostate tumorigenesis (Abdulkadir et al., 2001). We therefore hypothesized that by negatively regulating EGR1 and c-JUN expression, PTEN upregulates AR function. Using Network Component Analysis (NCA) (Tran et al., 2010), we deduced the transcription factor activities (TFAs) from the expressions of their target genes. Both EGR1 and c-JUN TFAs are reduced upon *PTEN* re-expression whereas AR TFA is increased 24 hrs after *PTEN* re-expression and EGR1/c-JUN activity changes (Figure 2E), supporting our hypothesis. The activity of AR was further examined using two murine CaP models, our *Pten* conditional knockout (Wang et al., 2003) and the transgenic mice over expressing *mAKT* (Majumder et al., 2004). The AR TFAs are significantly reduced in both models, which can be reverted by rapamycin treatment (Figure 2E), suggesting that the mTOR pathway is involved in PTEN regulation of AR activity.

Besides EGR1 and c-JUN, AR target gene expression is also inhibited by the ERG transcription factor, a member of ETS family whose gene is frequently translocated to the AR responding TMPRSS2 gene (Yu et al., 2010). ERG activates EZH2 expression, a member of the polycomb complex associated with human CaP (Sellers and Loda, 2002; Varambally et al., 2002), and EZH2-mediated dedifferentiation program (Yu et al., 2010). *Ezh*2 expression is upregulated in *Pten*-null prostate cancer (Figure 2F; Figure S2E) and the expressions of several AR and ERG co-targeted genes, including *Nkx3.1*, *Mme* and *Msmb* (Kunderfranco et al., 2010), are also downregulated in *Pten* null prostate at PIN and Cancer stages (Figure 2F). Our analyses suggest that PTEN loss suppresses androgen-responsive genes by regulating AR activity through multiple co-regulators, thereby renders *Pten* null CaP cells less dependent or completely independent of signaling provided by androgens - promoting CRPC growth.

Epithelial AR is not required for the initiation and progression of prostate cancers caused by Pten loss

Having demonstrated that *Pten* null CaP can proliferate independent of androgens, we considered whether CaP can develop in the absence of AR in the epithelium. We crossed $Pb\text{-}Cre^{+};Pten^{L/L}$ (*Pten*-null) mutants with mice carrying the *AR* conditional allele (Ar^{L}) (De Gendt et al., 2004). *Ar* deletion led to minimal effect on prostatic epithelium (data not shown), similar to previous publications (Simanainen et al., 2007; Simanainen et al., 2009; Wu et al., 2007). The resulting $Pb\text{-}Cre^{+};Pten^{L/L};Ar^{L}/Y$ (*Pten*-null;*Ar*-null) mutants were then analyzed at the age of 4–6, 10–14 and >20 weeks (n=4) and compared to their age- and genetic background-matched $Pb\text{-}Cre^{+};Pten^{L/L}$ mutants. *Pten* and *Ar* deletion promoted robust *in situ* latent adenocarcinoma development in the dorsolateral lobes. Overall cancer progression in the double knockouts is similar to that of *Pten* single knockout, as indicated by localized loss of SMA staining (Figure 3C and Figure S3A).

The anterior and ventral lobes often showed mosaic patterns of conditional deletion (Figure S3A), likely due to lower levels of Cre expression in these lobes (Wu et al., 2001) and less

efficient recombination of the Ar^{loxP} allele. This allowed us to directly compare the effect of *Ar* deletion on *Pten* null CaP cells. In Pten and AR deleted regions, we found enhanced nuclear atypia, cell proliferation (Ki67 staining) and cell death (arrow in the H&E section) in contrast to AR intact regions (comparing areas above and below the red dashed lines in the lower panels of Figure 3A). In $Pb\text{-}Cre^{+};Pten^{L/L};Ar^{L}/Y$ mutants $Pten^{-};AR^{-}$ adenocarcinomas also appeared less differentiated than $Pten^{-};AR^{+}$ regions.

We then examined the content of cells positive for the basal cell markers, p63 and cytokeratin 5 (CK5). We found that $Pten^{-};AR^{-}$ cancers had a significant expansion of $p63^{+}$ cells in the proximal region, known to be enriched for stem/progenitor cells (Figure S3B, bottom, 33.5% versus 15.5% of total cells; *, $p<0.05$), accompanied by increased $CK5^{+};CK8^{+}$ transient amplifying and $p63^{+};Ki67^{+}$ double positive cells (Figure S3B,). Conversely, the distal regions of $Pb\text{-}Cre^{+};Pten^{L/L};Ar^{L}/Y$ mutants, which compose the bulk of the tumor mass, contained low or no $p63^{+}$ cells, similar to human CaP (Figure S3C). Proliferation and apoptotic indexes were also increased in Pten-null;AR-null cancers (*, $p<0.05$), most notably in the proximal regions of the dorsal lateral lobe (Figure 3B). Despite this, AR-independent cell proliferation appeared to override AR-dependent cell death, similar to Pten null cancers under castration conditions (Wang et al 2003), resulting in overall AR-independent tumor growth.

Cell autonomous role of PTEN and PTEN controlled pathway in regulating AR-independent growth

The mosaic patterns of AR deletion in $Pb\text{-}Cre^{+};Pten^{L/L};Ar^{L}/Y$ prostates can potentially complicate our conclusions since AR^{+} epithelium may supply paracrine factors to “feed” the adjacent AR− cells. Thus, we employed prostate tissue regeneration assay. We FACS sorted prostate epithelium from $Pten^{L/L}$ (n=6) and $Pten^{L/L};Ar^{L}/Y$ (n=4) mice then infected them with either Cre lenti virus (Cre-FUCRW) or control lenti virus (FUCRW). Infected prostate epithelium combined with WT urogenital mesenchyme (UGSM) were grafted under the kidney capsule of NOD;SCID;IL2rγ-null mice (Figure 4A). Recombinants were examined for the presence of pathology coinciding with Cre-FUCRW or FUCRW infection, as visualized by the expression of viral-associated RFP reporter gene (Figure S4A). $Pten^{L/L};Ar^{L}/Y$ cells infected with Cre-FUCRW generated neoplastic pathology with high levels of P-AKT and P-S6 (Figure 4B), similar to the $Pten^{L/L}$ Cre virus infection control (Figure S4A and S4B) while $Pten^{L/L};Ar^{L}/Y$ cells infected with control FUCRW virus displayed normal acinar structure (Figure S4C).

One explanation of our observation is that epithelial cells isolated from the $Pten^{L/L};Ar^{L}/Y$ prostate have been “primed” by paracrine factors secreted by AR^{+} stroma cells (Cunha et al., 2002). To further affirm the cell autonomous role of PTEN in CaP initiation in the absence of epithelial AR, we carried out prostate tissue regenerations using prostate epithelium isolated from E16–17 $Pten^{L/L};Tfm$ mutant mice obtained from crossing the $Pten^{L/L}$ conditional line with the *Tfm* mutant mice. *Tfm* mutant mice express a rapidly degraded AR mutant resulting in complete blockage of prostate development (Cunha and Chung, 1981). Prostate epithelium of E16–17 $Pten^{L/L};Tfm$ mice therefore should have never been exposed to the potential paracrine factors. We found that $Pten^{\Delta/\Delta};Tfm$ epithelial cells formed PIN lesions with activated AKT (Figure S4D; n=3). Therefore, using two in vivo tissue recombinant models, our data indicates that AR-independent carcinogenesis is intrinsic to PTEN inactivation.

To further assess whether it is PTEN or the PTEN controlled signaling pathway that renders CaP development without epithelial AR, we orthotopically injected LSL-AKT virus directly to the anterior lobe of $Pb\text{-}Cre^{+};Ar^{L}/Y$ prostates (n=3) (Figure 4B). Using this strategy, only regions expressing Cre and infected by lenti-virus (indicated by GFP^{+} expression in Figure

4B; Figure S4E) will coordinately delete AR and express Myr-AKT. While AR-positive regions did not show AKT hyperactivation and abnormal phenotypes (Figure 4B, arrows in lower panels), AR-deleted neoplastic regions are pan-cytokeratin positive and showed higher levels of P-AKT (Figure 4B; arrowheads in lower panels). These data support our hypothesis that neoplastic transformation of the prostate by activated cell autonomous PI3K/AKT signaling can occur in the absence of epithelial AR.

AR downregulates AKT activity by stimulating FKBP5 and PHLPP-mediated AKT dephosphorylation

Postnatal epithelial AR deletion sensitizes prostate epithelium to paracrine signaling mediated by AR^+ stroma, leading to androgen-induced epithelial hyperproliferation (Cunha, 1994; Cunha et al., 2002; Niu et al., 2008a; Simanainen et al., 2009). To block potential stroma-derived androgen-induced mitogenic signals, we castrated *Pb-Cre*$^+$*;Pten*$^{L/L}$*;Ar*^{L}*/Y* mutants at 6 weeks (n=4) and analyzed their response. Similar to *Pten* null mutants, *Pb-Cre*$^+$*;Pten*$^{L/L}$*;Ar*^{L}*/Y* prostates did respond to castration but developed castration-resistance when analyzed 4 weeks later. Histopathological analysis indicated that castration-resistant cancer outgrowths in the dorsolateral lobes are composed mainly of $Pten^-$;AR^- (data not shown) while anterior and ventral lobes contained both AR^+ and AR^- regions (Figure 5A). Strikingly, in comparison to AR^+ regions (arrowheads), AR^- regions (arrows) contain much higher levels of membranous P-AKT and intracellular P-S6 as well as elevated cell proliferation and cell death, whether assessed at 4 weeks or even 2 days post-castration (Figure 5A, C and D; Figures S5A).

In searching for androgen-responsive genes that are decreased during castration, we found FKBP5, a member of the cis-trans prolyl isomerase family (Ratajczak et al., 2003). *FKBP5* is an established androgen regulated gene in humans (Magee et al., 2006) (Mostaghel et al., 2007) whose expression is immediately suppressed after castration but up-regulated upon hormone replacement in the WT mouse prostate (Figure S5B) and down-regulated in the *Pten* null intact and castrated prostates (Figure S5C), similar to *Mme* and *Msmb* (Figure S5D). We found that FKBP5 expression in *Pb-Cre*$^+$*;Pten*$^{L/L}$*;Ar*^{L}*/Y* prostate correlates with AR expression (Figure 5B). A recent study showed that FKBP5, by serving as a scaffolding protein for AKT and PHLPP, promotes PHLPP dephosphorylation of AKT at amino acid S473 (Brognard et al., 2007; Gao et al., 2005) and thereby suppressing AKT activity (Pei et al., 2009). In castrated *Pb-Cre*$^+$*;Pten*$^{L/L}$*;Ar*^{L}*/Y* prostates, we found that regions with *Pten* and *AR* deletion have hyperphosphorylated AKT (S473) and reduced PHLPP, especially membrane-associated PHLPP (Figure 5C and D arrows), while $Pten^-$;AR^+ regions showed opposite effects (Figure 5C and D, arrow heads). These results suggest that down regulation of FKBP5 either by castration or AR loss could release FKBP5-PHLPP-mediated suppression of AKT activity and promote AKT-dependent but androgen and AR-independent cell proliferation.

Correlations among PTEN, AR, FKBP5 and PHLPP in human CaPs

To assess the relevance of our finding in human CaPs, we took consecutive sections from a whole mounted fresh surgically resected human CaP sample and performed IHC analyses for PTEN, AR, FKBP5, PHLPP, P-AKT, P-S6 and Ki67 levels. We observed considerable heterogeneity of AR expression in PTEN null cancerous regions (Figure 6A; arrow, $PTEN^-$;AR^+; arrow head, $PTEN^-$;AR^- while adjacent non-cancer regions showed uniformed $PTEN^+$ and AR^+ staining (Figure S6A). Importantly, high AR expression regions are associated with higher FKBP5 and PHLPP but lower P-AKT and P-S6, similar to our observations in the murine model (Figure S6B). We then took 40 high power images from benign and PTEN-negative;AR-low/negative cancer regions and scored the expression of PTEN, AR, FKBP5, PHLPP, P-AKT, P-S6 and P-4EBP1 in a range of 0–3, with 3 being the

highest expression level. Similar to the *Pb-Cre*$^{+}$*;Pten*$^{L/L}$*;Ar*^{L}*/Y* mouse model (Figure 6B, left panel), we observed moderate to high levels of PI3K pathway effectors in PTEN-negative;AR-low/negative human cancer regions (Figure 6B, right panel). Moreover, PTEN-negative;AR-low/negative regions maintained elevated cell proliferation in comparison to benign regions (19.2% vs. 1.4%, $p<0.01$) (Figure S6C). We then surveyed CaP tissue microarrays generated by the UCLA Prostate SPORE program. Again, consecutive sections were used for IHC analyses and only cores show >30% epithelium were scored. Among 91 cores we analyzed, we found extensive AR heterogeneous expression levels, ranging from nearly 100% AR+ to complete AR− (Figure S6D). Using unsupervised cluster analysis, we affirmed that PTEN is significantly correlated to PHLPP expression ($p = 1.73e{-}7$, χ^2 test), while AR and FKBP5 are closely clustered together ($p = 1.67e{-}3$, χ^2 test) (Figure 6C, Figure S6E). These data suggest that the AR-FKBP5-PHLPP feedback loop may also function in human PTEN-negative;AR-low/negative CaP.

Combined AR/androgen ablation and mTOR inhibition results in enhanced therapeutic efficacy in *Pten*-null CaP

Since ablation of the AR/androgen signaling axis further activates AKT, we hypothesized that cancers with low levels of AR and PTEN loss would have greater dependency on the PI3K/AKT/mTOR signaling axis. To test this *in vitro*, we used CaP8 cells, a Pten-null;AR+ cell line derived from the *Pb-Cre*$^{+}$*;Pten*$^{L/L}$ CaP model (Jiao et al., 2007), infected with either a scramble or a sh-AR RNAi lenti-virus containing a RFP tag for FACS sorting. Analysis of cell viability at 0, 2, 4 and 6 days indicated a cooperative reduction in cell viability using AR knockdown combined with the mTOR inhibitor rapamycin (1 nM) (Figure 7A, left graph) (n=6). We also treated the PTEN-null;AR+ LNCaP human CaP cell line with rapamycin (1 nM), the 2nd generation anti-AR inhibitor MDV3100 (10 μM) (Scher et al., 2010; Tran et al., 2009), or both. Again, we observed a cooperative inhibition effect when both AR and PI3K/mTOR pathways were co-targeted (Figure 7A, right graph) (n=6).

To test our hypothesis in vivo, we treated intact and castrated *Pb-Cre*$^{+}$*;Pten*$^{L/L}$ and *Pb-Cre*$^{+}$*;Pten*$^{L/L}$*;Ar*^{L}*/Y* mice at cancer stage with rapamycin and evaluated the effects by Ki67 index (Figure 7B) and histopathology (Figure 7C and Figure S7; n=4). Rapamycin treatment (4mg/kg daily for 4 weeks) led to a reduction of Ki67 index in *Pb-Cre*$^{+}$*;Pten*$^{L/L}$ intact mutants from 17% to 11%; castration and castration plus MDV3100 (10mg/kg/d) further reduced the rates of cell proliferation to 8% and 3%, respectively (Figure 7B). Similarly, when *Pb-Cre*$^{+}$*;Pten*$^{L/L}$*;Ar*^{L}*/Y* mutants were castrated and treated with or without rapamycin for 4 weeks, we found a significant reduction of prostate volume in comparison to the placebo cohort (Figure 7C). At the histological level, double mutants with combination of rapamycin treatment showed significant atrophy in most glandular structures, similar to that of WT castrated and *Pten* null castrated mice treated with combination of rapamycin and MDV3100 (Figure S7). A reduction in P-S6 (Ser240) staining and reduced cell proliferation (Figure 7B and D; 33.7% versus 4%; **, $p<0.01$) was also observed. Interestingly, many residual epithelia in rapamycin treated castrated mutants appeared to be AR^{+} (high power insert). Collectively, these data suggest that CaPs with AR loss have greater reliance upon the PI3K/AKT/mTOR signaling pathways and that combined AR/androgen blockage in conjunction with PI3K/AKT/mTOR inhibition is more effective for CaPs initiated by PTEN loss or PI3K/AKT activation.

DISCUSSION

PTEN loss or PI3K pathway activation represents one of the most frequent genetic alterations found in human CaPs (Taylor et al., 2010). Dysregulation of the PTEN/PI3K pathway has also been associated with resistance to conventional anti-androgen therapies (Ham et al., 2009). Despite these clinical observations, the consequence of PTEN loss and

how its loss influence androgen/AR signaling axis and CRPC development are unclear. By genetically deleting *Pten* and *Pten/Ar* in the prostatic epithelium and analyzing human CaP samples, our studies support the hypothesis that PTEN loss or PI3K pathway activation may function in a cell autonomous manner to promote androgen/AR-independent CaP progression and CRPC development. Although *Pten* null epithelial cells remain sensitive to androgen withdrawal or AR ablation, the resulting activated PI3K/AKT pathway is sufficient to compensate androgen/AR signaling blockage, mobilize basal and transient amplifying stem/progenitor cells and promote cell proliferation. Therefore, in CaPs initiated by PTEN loss or PI3K activation, the overall outcome of cancer development, especially CRPC development, depends on the balance of androgen-dependent cell survival/differentiation and androgen-independent cell proliferation. PTEN loss enhances the expressions of EGR1, c-JUN and EZH2, which in turn suppresses AR transcription factor activity and output. Inhibiting FKBP5/PHLPP-mediated negative feedback to AKT activation, as a result of castration or AR inhibition, may further enhance the strength of the PI3K/AKT pathway and tilt the balance toward androgen-independent growth (Figure 8). Importantly, results derived from our genetically engineered mouse models, including PTEN controlled AR transcription output and AR-FKBP5-PHLPP regulatory loop, can also be observed in human CaP samples. Given commonly observed heterogeneous *PTEN* deletion/mutation and AR expression patterns within individual human CaPs, shown in our study and published by others (Attard et al., 2009b; Taylor et al., 2010), we would expect to observe a greater range of phenotypic correlating between PTEN loss, AR expression and CRPC development in human patients.

Using genetically engineered animal models, our findings may provide potential insight to the clinical settings. Although hormone therapy immediately after radical prostatectomy improves survival and reduces the recurrence (Messing et al., 1999), it is not clear whether early androgen deprivation therapy (ADT) will prevent cancer progression and CRPC development. That early castration of the *Pten* null CaP model does not significantly impede carcinoma development and castration-resistant growth suggests that patients with PTEN loss or PI3K pathway activation may not benefit from aggressive early hormone treatment. While neoadjuvant ADT may partially reduce tumor load and PSA levels, it may select for cells with activated compensatory cell survival and proliferating signaling pathways, such as those *PTEN* null or PI3K/AKT-activated, and ultimately facilitate resistance to anti-androgen therapy.

An important finding from our study is that PTEN loss suppresses AR transcription factor activity and androgen-responsive gene expression in both murine models and human prostate samples. Interestingly, AR itself is not down-regulated in *Pten* null CaPs, even after castration (data not shown), similar to human cancers after short-term castration or after 9 months of neoadjuvant ADT (Mostaghel et al., 2007). Previous studies suggest that the PI3K pathway can either activate or suppress AR activity (Kaarbo et al., 2010; Lei et al., 2006; Lin et al., 2004; Lin et al., 2003). Our analyses demonstrate that PTEN, by regulating the expressions and activities of EGR1 and c-JUN transcription factors as well as the level of EZH2, controls AR transcription output, and thereby, render *PTEN* null CaP cells less or completely independent of signaling provided by androgens and epithelial AR, hence promote castration-resistant growth. However, how PTEN/PI3K pathway controls EGR1, c-JUN and EZH2 expression and activities requires further study.

The mosaic pattern of AR deletion observed in our in vivo model also mimic the heterogeneous AR expression observed in our human CaP studies and those reported by others (Attard et al., 2009b). After castration of *Pb-Cre*$^{+}$*;Pten*$^{L/L}$*;Ar*^{L}*/Y* mutants, we observed significant outgrowth of Pten^{-};AR^{-} cancerous regions, accompanied by elevated P-PAKT and cell proliferation. Adjacent to these outgrowth are AR^{+} regions. Therefore, it is

possible that within heterogeneous malignant CaPs, those with low or negative AR expression fail to respond to conventional anti-androgen treatment and continue to proliferate and survive as a consequence of PTEN loss and PI3K/AKT activation. While such cells would not constitute PSA producing cancer cells, they would contribute towards overall tumor load.

An intriguing finding of our study is the elevated P-AKT (S473) levels despite genetic deletion of *Ar* and surgical castration. The recently defined relationship between FKBP5 and the AKT phosphatase, PHLPP (Gao et al., 2005) (Brognard et al., 2007) (Pei et al., 2010), provides a potential mechanism as how PI3K/AKT signaling can be activated upon inhibition of the AR/androgen signaling axis. Specifically, while in normal cells PHLPP levels are high, which keeps P-AKT levels low, down-regulation of FKBP5 in Pten-negative cells that have undergone AR/androgen ablation would lead to a reduction of PHLPP's association with P-AKT and consequently enhance AKT activity. Although it is difficult to assess P-AKT levels in all human CaP samples due to various sample harvesting and preparation procedures used, we did observed statistically significant correlation between the levels of PTEN and PHLPP as well as AR and FKBP5. Importantly, when a fresh resected CaP sample was analyzed, we found that regions with low or no AR expression have lower levels of FKBP5 and PHLPP and enhanced P-AKT and P-S6 staining. Besides the AR-FKBP5-PHLPP feedback loop, we also observed changes in other scaffold proteins and mediators of the PI3K pathway (Table S1). It will be interesting for future studies to ascertain whether other AR/androgen regulated genes, such as FKBP11 and IGFBP3/6, also have the capacity to modulate PI3K/AKT signaling in a manner similar to FKBP5.

Increasing evidence suggests that different cellular compartments may contribute differently towards cancer initiation. For example, the prostate epithelial AR may confer some suppressor function while the stromal AR has been postulated to be mitogenic (Cunha et al., 2002; Simanainen et al., 2009), thus raising the possibility that stromal AR plays a dominant role in Pten null cancer initiation or during the development of CRPC. In fact, using the TRAMP CaP model, a previous report has shown that reduction of stromal AR content may lead to reduced tumor progression (Niu et al., 2008b). However, extrapolating these data to human disease is challenging because neuroendocrine carcinoma observed in the TRAMP model, a phenotype which is rare in human disease (Abbas et al., 1995; Tetu et al., 1987). It is also possible that while AR loss or degradation in differentiated luminal epithelium results in cell death, AR loss in basal or transient amplifying initiating cells is well tolerated. In fact, recent reports have shown that the basal "LSC" stem/progenitor cells either from the Pten null CaP model (Mulholland et al., 2009) or from primary human tissue that has been transformed (Goldstein et al., 2010) are sufficient for tumor reconstitution. Thus, it would be interesting and potentially clinically relevant to ascertain if AR-null stem progenitor cells would be capable of cancer initiation. Interestingly, cells with high N-cadherin expression, a marker associated epithelial-mesenchymal transition and cancer metastasis at late stage disease are also AR-null or low and forced expression of N-cadherin results in reduced AR expression and elevated P-AKT in human CaPs (Tanaka et al., 2010).

Previous studies have shown that mTOR inhibition alone is relatively ineffective at reducing overall tumor load in *Pb-Cre*$^{+}$*;Pten*$^{L/L}$ mutants (Kinkade et al., 2008) (Zhang et al., 2009). To test the hypothesis that combined AR and mTOR targeting may be more effective where single agent use is not, we evaluated the impact of total AR/androgen ablation in conjunction with mTOR inhibition. When comparing *Pb-Cre*$^{+}$*;Pten*$^{L/L}$*;Ar*^{L}*/Y* mutants under castration alone to those with rapamycin, we observed marked inhibition of cell proliferation and reduction of tumor load. Thus, these pre-clinical data suggests that complete abolishment of the AR/androgen signaling axis combined with mTOR inhibition is superior to single agent use, most likely by inhibiting the crosstalk between the two pathways. Thus,

more effective blockade of the androgen/AR axis with new generation inhibitors such as abiraterone and MDV3100 in combination with mTOR or PI3K/mTOR dual inhibitors may prove to be further advantageous in treating CRPC cases initiated by alterations of PTEN/PI3K pathway.

EXPERIMENTAL PROCEDURES

Generation of Pb-Cre^{+};Pten$^{L/L}$;Ar^{L}/Y and Pten$^{L/L}$;Tfm mutant mice

Mice with conditional deletion of *Pten* and AR in the murine prostate were developed by crossing male, *Pb-Cre*$^{+}$*;Pten*$^{L/L}$ mice with *Cre*$^{-}$*;Ar*^{L}*/Ar*^{L} female mice on a mixed background. The AR conditional line (AR$^{loxP\text{-}exon2\text{-}loxP}$) was obtained from and previously described by the laboratory of Dr. Guido Verhoeven (De Gendt et al., 2004) while *Pb-Cre*$^{+}$*;Pten*$^{L/L}$ mutants were described by our laboratory (Wang et al., 2003). *Pten*$^{L/L}$*;Tfm* mutant mice were obtained by crossing *Pten*$^{L/L}$ mutants with Tfm mice (JAX) (Cunha and Chung, 1981). All animal experiments were approved by the UCLA Animal Research committee and conducted according to relevant regulatory standards.

Cell Isolation and Flow Cytometry

The isolation of murine prostate epithelium was carried out by mechanical dissociation (5 min mincing) and enzymatic digestion (collagenase type I digestion at 37 C for 2 hours) of all prostate lobes. Single cell suspension were generated and stained in DMEM 10% FBS for 20 min at 4 oC with anti-CD49f (Biolegend), and with a Lin cocktail comprised of anti-CD45, anti-CD31, and anti-Ter119 (ebiosciences). Cell sorting was performed on the BD FACS Vantage or BD FACS Aria II (BD Biosciences). Lin^{-}CD49f$^{hi/mid}$ cells were collected and subsequently used for FACS analysis and/or tissue regeneration assays (Mulholland et al., 2009)

Prostate regenerations

Donor (Lin^{-}CD49f$^{hi/mid}$) epithelia isolated from Cre^{-}, *Cre*$^{-}$*;Pten*$^{L/L}$ or *Cre*$^{-}$*;Pten*$^{L/L}$*;Ar*^{L}*/Y* or *Pten*$^{L/L}$*;Tfm* mutant mice were infected with high titer (>1×10^{9}) Cre-lenti virus (Cre-FUCRW) by low speed centrifugation over 90 min. Infected epithelium (1–2 × 10^{5}) were recombined with UGSM (2 × 10^{5}) in 15 μl collagen pellets and incubated for 6–10 hours in DMEM (high glucose, 10% FBS; Insulin, 0.005 mg/ml, Bovine pituitary extract; 10.7 μg/ml; EGF/FGF, 3.0 ng/ml). Tissue recombinants were then surgically implanted below the kidney capsule of NOD;SCID;IL2rγ-null mice for 6–10 weeks (Mulholland et al., 2009; Lawson et al., 2010, Goldstein et al., 2010).

Plasmids

The murine *Ar*-specific short hairpin RNAs (shRNA) (Jiao et al., 2007) with a 6 promoter were cloned into the *Bam*HI-*Eco*RI site the lentivector FUCRW. The open reading frame for the human *AR* gene with flag tag was cloned at the XbaI site under the human ubiquitin promoter.

Orthotopic lenti-virus injection

The LSL-Akt (loxP-RFP-loxP-myr-Akt-Ires-EGP) lenti vector and virus generated as previously described (Marumoto et al., 2009). To carry out orthotopic injections, 2–3 μl of high titer lenti virus (> 1×10^{8}) was injected to the base of the anterior prostate lobe (proximal to urethra) of *Pb-Cre*$^{+}$*;Ar*^{L}*/Y* mice aged 2–3 weeks using a cemented, 10 μl microsyringe (Hamilton). Mice were then aged for 6–8 weeks and subsequently evaluated at the histological level.

Collection of Patient Samples

Clinical samples were obtained with informed consent under approval from the University of California at Los Angeles (UCLA) Institutional Review Board. All samples were de-identified to protect patients' confidentiality.

Human whole mount and Tissue Microarrays (TMA)

Pathologic specimens (whole mount specimens) were acquired from the UCLA Tissue Procurement Core Laboratory in a de-identified manner. IHC analysis and scoring was carried out on cores containing >30% epithelial content (Thomas et al., 2004).

Drug Treatment

Pb-Cre^{+}*;Pten*$^{L/L}$ and *Pb-Cre*$^{+}$*;Pten*$^{L/L}$*;Ar*^{L}*/Y* were castrated and immediately treated with either 4 mg/kg/d (I.P.) rapamycin (Selleck Chem.), 10 mg/kg/d MDV3100 or vehicle control (P.O.). Mice were treated for 4 weeks and then evaluated at the histological level.

Accession Numbers

Gene expression microarray data have been deposited in the GEO data base with the accession number GSE29010.

Supplementary Material

Refer to Web version on PubMed Central for supplementary material.

Acknowledgments

We appreciate Drs. Guido Verhoeven and Karel De Gendt for generous supplying the AR conditional knockout line; UCLA Prostate SPORE for whole mount human CaP and TMA sections; Dr. Charles Sawyers for MDV3100 and communicating unpublished results. We thank the helpful comments and suggestions from Drs. Owen Witte, Robert Reiter, Peter Nelson and colleagues in our laboratories; DJM was supported by NIH F32 CA112988-01 and CIRM TG2-01169 and LMT is supported by NIH T32 CA009056; This work has been supported in part by award from the Prostate Cancer Foundation (to HW and IPG), Jean Perkins Foundation and Department of Defense (to IPG) and grant from NIH (R01 CA107166 and RO1 CA121110 to HW).

References

Abbas F, Civantos F, Benedetto P, Soloway MS. Small cell carcinoma of the bladder and prostate. Urology. 1995; 46:617–630. [PubMed: 7495110]

Abdulkadir SA, Qu Z, Garabedian E, Song SK, Peters TJ, Svaren J, Carbone JM, Naughton CK, Catalona WJ, Ackerman JJ, et al. Impaired prostate tumorigenesis in Egr1-deficient mice. Nat Med. 2001; 7:101–107. [PubMed: 11135623]

Attard G, Cooper CS, de Bono JS. Steroid hormone receptors in prostate cancer: a hard habit to break? Cancer Cell. 2009a; 16:458–462. [PubMed: 19962664]

Attard G, Reid AH, Olmos D, de Bono JS. Antitumor activity with CYP17 blockade indicates that castration-resistant prostate cancer frequently remains hormone driven. Cancer Res. 2009b; 69:4937–4940. [PubMed: 19509232]

Brognard J, Sierecki E, Gao T, Newton AC. PHLPP and a second isoform, PHLPP2, differentially attenuate the amplitude of Akt signaling by regulating distinct Akt isoforms. Mol Cell. 2007; 25:917–931. [PubMed: 17386267]

Chang CJ, Freeman DJ, Wu H. PTEN regulates Mdm2 expression through the P1 promoter. J Biol Chem. 2004; 279:29841–29848. [PubMed: 15090541]

Chauvin TR, Griswold MD. Androgen-regulated genes in the murine epididymis. Biol Reprod. 2004; 71:560–569. [PubMed: 15115731]

Chen Y, Sawyers CL, Scher HI. Targeting the androgen receptor pathway in prostate cancer. Curr Opin Pharmacol. 2008; 8:440–448. [PubMed: 18674639]

Cunha GR. Role of mesenchymal-epithelial interactions in normal and abnormal development of the mammary gland and prostate. Cancer. 1994; 74:1030–1044. [PubMed: 8039137]

Cunha GR, Chung LW. Stromal-epithelial interactions--I. Induction of prostatic phenotype in urothelium of testicular feminized (Tfm/y) mice. J Steroid Biochem. 1981; 14:1317–1324. [PubMed: 6460136]

Cunha GR, Hayward SW, Wang YZ. Role of stroma in carcinogenesis of the prostate. Differentiation. 2002; 70:473–485. [PubMed: 12492490]

De Gendt K, Swinnen JV, Saunders PT, Schoonjans L, Dewerchin M, Devos A, Tan K, Atanassova N, Claessens F, Lecureuil C, et al. A Sertoli cell-selective knockout of the androgen receptor causes spermatogenic arrest in meiosis. Proc Natl Acad Sci U S A. 2004; 101:1327–1332. [PubMed: 14745012]

Ellwood-Yen K, Graeber TG, Wongvipat J, Iruela-Arispe ML, Zhang J, Matusik R, Thomas GV, Sawyers CL. Myc-driven murine prostate cancer shares molecular features with human prostate tumors. Cancer Cell. 2003; 4:223–238. [PubMed: 14522256]

Gao H, Ouyang X, Banach-Petrosky WA, Shen MM, Abate-Shen C. Emergence of androgen independence at early stages of prostate cancer progression in Nkx3.1; Pten mice. Cancer Res. 2006; 66:7929–7933. [PubMed: 16912166]

Gao T, Furnari F, Newton AC. PHLPP: a phosphatase that directly dephosphorylates Akt, promotes apoptosis, and suppresses tumor growth. Mol Cell. 2005; 18:13–24. [PubMed: 15808505]

Gitenay D, Baron VT. Is EGR1 a potential target for prostate cancer therapy? Future Oncol. 2009; 5:993–1003. [PubMed: 19792968]

Goldstein AS, Huang J, Guo C, Garraway IP, Witte ON. Identification of a cell of origin for human prostate cancer. Science. 2010; 329:568–571. [PubMed: 20671189]

Greenberg NM, DeMayo F, Finegold MJ, Medina D, Tilley WD, Aspinall JO, Cunha GR, Donjacour AA, Matusik RJ, Rosen JM. Prostate cancer in a transgenic mouse. Proc Natl Acad Sci U S A. 1995; 92:3439–3443. [PubMed: 7724580]

Ham WS, Cho NH, Kim WT, Ju HJ, Lee JS, Choi YD. Pathological effects of prostate cancer correlate with neuroendocrine differentiation and PTEN expression after bicalutamide monotherapy. J Urol. 2009; 182:1378–1384. [PubMed: 19683286]

Hill R, Wu H. PTEN, stem cells, and cancer stem cells. J Biol Chem. 2009; 284:11755–11759. [PubMed: 19117948]

Jiao J, Wang S, Qiao R, Vivanco I, Watson PA, Sawyers CL, Wu H. Murine cell lines derived from Pten null prostate cancer show the critical role of PTEN in hormone refractory prostate cancer development. Cancer Res. 2007; 67:6083–6091. [PubMed: 17616663]

Kaarbo M, Mikkelsen OL, Malerod L, Qu S, Lobert VH, Akgul G, Halvorsen T, Maelandsmo GM, Saatcioglu F. PI3K-AKT-mTOR pathway is dominant over androgen receptor signaling in prostate cancer cells. Cell Oncol. 2010; 32:11–27. [PubMed: 20203370]

Kinkade CW, Castillo-Martin M, Puzio-Kuter A, Yan J, Foster TH, Gao H, Sun Y, Ouyang X, Gerald WL, Cordon-Cardo C, Abate-Shen C. Targeting AKT/mTOR and ERK MAPK signaling inhibits hormone-refractory prostate cancer in a preclinical mouse model. J Clin Invest. 2008; 118:3051–3064. [PubMed: 18725989]

Kunderfranco P, Mello-Grand M, Cangemi R, Pellini S, Mensah A, Albertini V, Malek A, Chiorino G, Catapano CV, Carbone GM. ETS transcription factors control transcription of EZH2 and epigenetic silencing of the tumor suppressor gene Nkx3.1 in prostate cancer. PLoS One. 2010; 5:e10547. [PubMed: 20479932]

Lapointe J, Li C, Higgins JP, van de Rijn M, Bair E, Montgomery K, Ferrari M, Egevad L, Rayford W, Bergerheim U, et al. Gene expression profiling identifies clinically relevant subtypes of prostate cancer. Proc Natl Acad Sci U S A. 2004; 101:811–816. [PubMed: 14711987]

Lei Q, Jiao J, Xin L, Chang CJ, Wang S, Gao J, Gleave ME, Witte ON, Liu X, Wu H. NKX3.1 stabilizes p53, inhibits AKT activation, and blocks prostate cancer initiation caused by PTEN loss. Cancer Cell. 2006; 9:367–378. [PubMed: 16697957]

Lin HK, Hu YC, Lee DK, Chang C. Regulation of androgen receptor signaling by PTEN (phosphatase and tensin homolog deleted on chromosome 10) tumor suppressor through distinct mechanisms in prostate cancer cells. Mol Endocrinol. 2004; 18:2409–2423. [PubMed: 15205473]

Lin HK, Hu YC, Yang L, Altuwaijri S, Chen YT, Kang HY, Chang C. Suppression versus induction of androgen receptor functions by the phosphatidylinositol 3-kinase/Akt pathway in prostate cancer LNCaP cells with different passage numbers. J Biol Chem. 2003; 278:50902–50907. [PubMed: 14555644]

Magee JA, Chang LW, Stormo GD, Milbrandt J. Direct, androgen receptor-mediated regulation of the FKBP5 gene via a distal enhancer element. Endocrinology. 2006; 147:590–598. [PubMed: 16210365]

Majumder PK, Febbo PG, Bikoff R, Berger R, Xue Q, McMahon LM, Manola J, Brugarolas J, McDonnell TJ, Golub TR, et al. mTOR inhibition reverses Akt-dependent prostate intraepithelial neoplasia through regulation of apoptotic and HIF-1-dependent pathways. Nat Med. 2004; 10:594–601. [PubMed: 15156201]

Marumoto T, Tashiro A, Friedmann-Morvinski D, Scadeng M, Soda Y, Gage FH, Verma IM. Development of a novel mouse glioma model using lentiviral vectors. Nat Med. 2009; 15:110–116. [PubMed: 19122659]

Messing EM, Manola J, Sarosdy M, Wilding G, Crawford ED, Trump D. Immediate hormonal therapy compared with observation after radical prostatectomy and pelvic lymphadenectomy in men with node-positive prostate cancer. N Engl J Med. 1999; 341:1781–1788. [PubMed: 10588962]

Montgomery RB, Mostaghel EA, Vessella R, Hess DL, Kalhorn TF, Higano CS, True LD, Nelson PS. Maintenance of intratumoral androgens in metastatic prostate cancer: a mechanism for castration-resistant tumor growth. Cancer Res. 2008; 68:4447–4454. [PubMed: 18519708]

Mostaghel EA, Page ST, Lin DW, Fazli L, Coleman IM, True LD, Knudsen B, Hess DL, Nelson CC, Matsumoto AM, et al. Intraprostatic androgens and androgen-regulated gene expression persist after testosterone suppression: therapeutic implications for castration-resistant prostate cancer. Cancer Res. 2007; 67:5033–5041. [PubMed: 17510436]

Mulholland DJ, Xin L, Morim A, Lawson D, Witte O, Wu H. Lin-Sca-1+CD49fhigh stem/progenitors are tumor-initiating cells in the Pten-null prostate cancer model. Cancer Res. 2009; 69:8555–8562. [PubMed: 19887604]

Nelson PS, Clegg N, Arnold H, Ferguson C, Bonham M, White J, Hood L, Lin B. The program of androgen-responsive genes in neoplastic prostate epithelium. Proc Natl Acad Sci U S A. 2002; 99:11890–11895. [PubMed: 12185249]

Niu Y, Altuwaijri S, Lai KP, Wu CT, Ricke WA, Messing EM, Yao J, Yeh S, Chang C. Androgen receptor is a tumor suppressor and proliferator in prostate cancer. Proc Natl Acad Sci U S A. 2008a; 105:12182–12187. [PubMed: 18723679]

Niu Y, Altuwaijri S, Yeh S, Lai KP, Yu S, Chuang KH, Huang SP, Lardy H, Chang C. Targeting the stromal androgen receptor in primary prostate tumors at earlier stages. Proc Natl Acad Sci U S A. 2008b; 105:12188–12193. [PubMed: 18723670]

Pei H, Li L, Fridley BL, Jenkins GD, Kalari KR, Lingle W, Petersen G, Lou Z, Wang L. FKBP51 affects cancer cell response to chemotherapy by negatively regulating Akt. Cancer Cell. 2009; 16:259–266. [PubMed: 19732725]

Pei H, Lou Z, Wang L. Emerging role of FKBP51 in AKT kinase/protein kinase B signaling. Cell Cycle. 2010; 9:6–7. [PubMed: 20016266]

Plaisier SB, Taschereau R, Wong JA, Graeber TG. Rank-rank hypergeometric overlap: identification of statistically significant overlap between gene-expression signatures. Nucleic Acids Res. 2010; 38:e169. [PubMed: 20660011]

Ratajczak T, Ward BK, Minchin RF. Immunophilin chaperones in steroid receptor signalling. Curr Top Med Chem. 2003; 3:1348–1357. [PubMed: 12871166]

Roudier MP, True LD, Higano CS, Vesselle H, Ellis W, Lange P, Vessella RL. Phenotypic heterogeneity of end-stage prostate carcinoma metastatic to bone. Hum Pathol. 2003; 34:646–653. [PubMed: 12874759]

Sato N, Sadar MD, Bruchovsky N, Saatcioglu F, Rennie PS, Sato S, Lange PH, Gleave ME. Androgenic induction of prostate-specific antigen gene is repressed by protein-protein interaction

between the androgen receptor and AP-1/c-Jun in the human prostate cancer cell line LNCaP. J Biol Chem. 1997; 272:17485–17494. [PubMed: 9211894]

Scher HI, Beer TM, Higano CS, Anand A, Taplin ME, Efstathiou E, Rathkopf D, Shelkey J, Yu EY, Alumkal J, et al. Antitumour activity of MDV3100 in castration-resistant prostate cancer: a phase 1–2 study. Lancet. 2010; 375:1437–1446. [PubMed: 20398925]

Sellers WR, Loda M. The EZH2 polycomb transcriptional repressor--a marker or mover of metastatic prostate cancer? Cancer Cell. 2002; 2:349–350. [PubMed: 12450788]

Simanainen U, Allan CM, Lim P, McPherson S, Jimenez M, Zajac JD, Davey RA, Handelsman DJ. Disruption of prostate epithelial androgen receptor impedes prostate lobe-specific growth and function. Endocrinology. 2007; 148:2264–2272. [PubMed: 17317769]

Simanainen U, McNamara K, Gao YR, Handelsman DJ. Androgen sensitivity of prostate epithelium is enhanced by postnatal androgen receptor inactivation. Am J Physiol Endocrinol Metab. 2009; 296:E1335–1343. [PubMed: 19366880]

Stiles B, Groszer M, Wang S, Jiao J, Wu H. PTENless means more. Dev Biol. 2004; 273:175–184. [PubMed: 15328005]

Tanaka H, Kono E, Tran CP, Miyazaki H, Yamashiro J, Shimomura T, Fazli L, Wada R, Huang J, Vessella RL, et al. Monoclonal antibody targeting of N-cadherin inhibits prostate cancer growth, metastasis and castration resistance. Nat Med. 2010

Taylor BS, Schultz N, Hieronymus H, Gopalan A, Xiao Y, Carver BS, Arora VK, Kaushik P, Cerami E, Reva B, et al. Integrative genomic profiling of human prostate cancer. Cancer Cell. 2010; 18:11–22. [PubMed: 20579941]

Tetu B, Ro JY, Ayala AG, Johnson DE, Logothetis CJ, Ordonez NG. Small cell carcinoma of the prostate. Part I. A clinicopathologic study of 20 cases. Cancer. 1987; 59:1803–1809. [PubMed: 3030528]

Tran C, Ouk S, Clegg NJ, Chen Y, Watson PA, Arora V, Wongvipat J, Smith-Jones PM, Yoo D, Kwon A, et al. Development of a second-generation antiandrogen for treatment of advanced prostate cancer. Science. 2009; 324:787–790. [PubMed: 19359544]

Tran LM, Hyduke DR, Liao JC. Trimming of mammalian transcriptional networks using network component analysis. BMC Bioinformatics. 2010; 11:511. [PubMed: 20942926]

Varambally S, Dhanasekaran SM, Zhou M, Barrette TR, Kumar-Sinha C, Sanda MG, Ghosh D, Pienta KJ, Sewalt RG, Otte AP, et al. The polycomb group protein EZH2 is involved in progression of prostate cancer. Nature. 2002; 419:624–629. [PubMed: 12374981]

Vivanco I, Sawyers CL. The phosphatidylinositol 3-Kinase AKT pathway in human cancer. Nat Rev Cancer. 2002; 2:489–501. [PubMed: 12094235]

Wang S, Gao J, Lei Q, Rozengurt N, Pritchard C, Jiao J, Thomas GV, Li G, Roy-Burman P, Nelson PS, et al. Prostate-specific deletion of the murine Pten tumor suppressor gene leads to metastatic prostate cancer. Cancer Cell. 2003; 4:209–221. [PubMed: 14522255]

Wang XD, Wang BE, Soriano R, Zha J, Zhang Z, Modrusan Z, Cunha GR, Gao WQ. Expression profiling of the mouse prostate after castration and hormone replacement: implication of H-cadherin in prostate tumorigenesis. Differentiation. 2007; 75:219–234. [PubMed: 17288544]

Wu CT, Altuwaijri S, Ricke WA, Huang SP, Yeh S, Zhang C, Niu Y, Tsai MY, Chang C. Increased prostate cell proliferation and loss of cell differentiation in mice lacking prostate epithelial androgen receptor. Proc Natl Acad Sci U S A. 2007; 104:12679–12684. [PubMed: 17652515]

Wu X, Wu J, Huang J, Powell WC, Zhang J, Matusik RJ, Sangiorgi FO, Maxson RE, Sucov HM, Roy-Burman P. Generation of a prostate epithelial cell-specific Cre transgenic mouse model for tissue-specific gene ablation. Mech Dev. 2001; 101:61–69. [PubMed: 11231059]

Yang SZ, Eltoum IA, Abdulkadir SA. Enhanced EGR1 activity promotes the growth of prostate cancer cells in an androgen-depleted environment. J Cell Biochem. 2006; 97:1292–1299. [PubMed: 16552752]

Yu J, Mani RS, Cao Q, Brenner CJ, Cao X, Wang X, Wu L, Li J, Hu M, Gong Y, et al. An integrated network of androgen receptor, polycomb, and TMPRSS2-ERG gene fusions in prostate cancer progression. Cancer Cell. 2010; 17:443–454. [PubMed: 20478527]

Yuan H, Young CY, Tian Y, Liu Z, Zhang M, Lou H. Suppression of the androgen receptor function by quercetin through protein-protein interactions of Sp1, c-Jun, and the androgen receptor in human prostate cancer cells. Mol Cell Biochem. 2010; 339:253–262. [PubMed: 20148354]

Zhang W, Zhu J, Efferson CL, Ware C, Tammam J, Angagaw M, Laskey J, Bettano KA, Kasibhatla S, Reilly JF, et al. Inhibition of tumor growth progression by antiandrogens and mTOR inhibitor in a Pten-deficient mouse model of prostate cancer. Cancer Res. 2009; 69:7466–7472. [PubMed: 19738074]

SIGNIFICANCE

Resistance to androgen deprivation therapy is the major hurdle for managing patients with advanced CaP. Therefore, understanding the molecular mechanisms underlying CRPC will be helpful for the design of therapeutic strategies to overcome the resistance. We found that CaPs initiated by PTEN loss result in suppression of AR transcription output and can progress to CRPC independent of epithelial AR, providing a mechanism of escaping the requirement of androgen/AR axis for castration-resistant growth. AR loss or inhibition, on the other hand, can further activate AKT activity via down regulation of the FKBP5 scaffold protein and PHLPP phosphatase. Our study suggests that co-targeting both AR and PTEN/PI3K pathways may enhance therapeutic efficacy for CaPs initiated by PI3K pathway alterations.

HIGHLIGHTS

- Castration-resistant proliferation of Pten null prostate cancer cells.
- PTEN loss suppresses AR transcription factor activity promoting AR-independence.
- AR inhibits AKT through FKBP5 scaffold protein and PHLPP phosphatase.
- Co-targeting of AR and AKT/mTOR signaling leads to better therapeutic outcome.

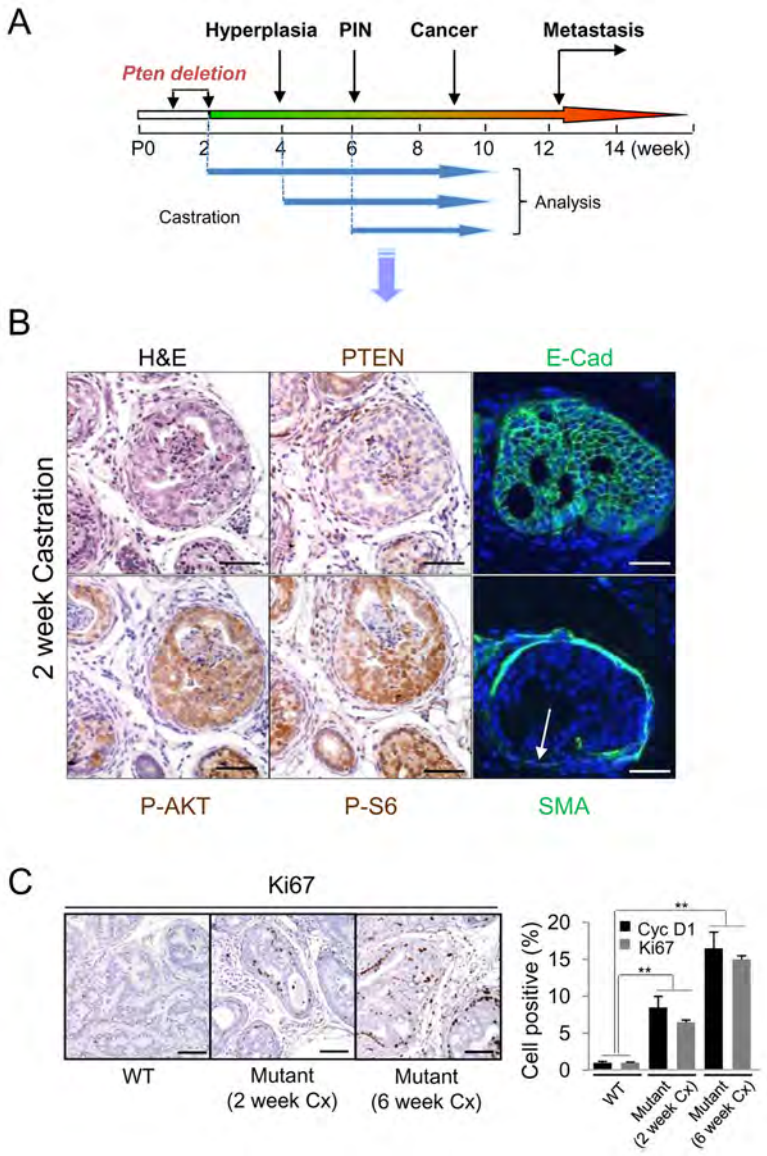

Figure 1. Early castration does not prevent initiation of *Pten*-null CaP

(A) *Pb-Cre*$^{+}$;*Pten*$^{L/L}$ mutants were castrated (Cx) at 2, 4 or 6 weeks and aged to 10 weeks. (B) Mutants Cx at 2 weeks were evaluated for carcinoma, PI3K (P-AKT, P-S6) activation coinciding with PTEN loss and invasiveness based on smooth muscle actin (SMA) loss but maintained E-Cadherin expression (arrow). Bar=100 μm (C) Cell proliferation, Ki67+; Cyclin D1+ (Cyc D1) cells, in 2 and 6 week Cx cohorts in comparison to WT Cx controls (**, $p<0.01$) Bar = 150 μm. Error bars, mean +/− SD. See also Figure S1.

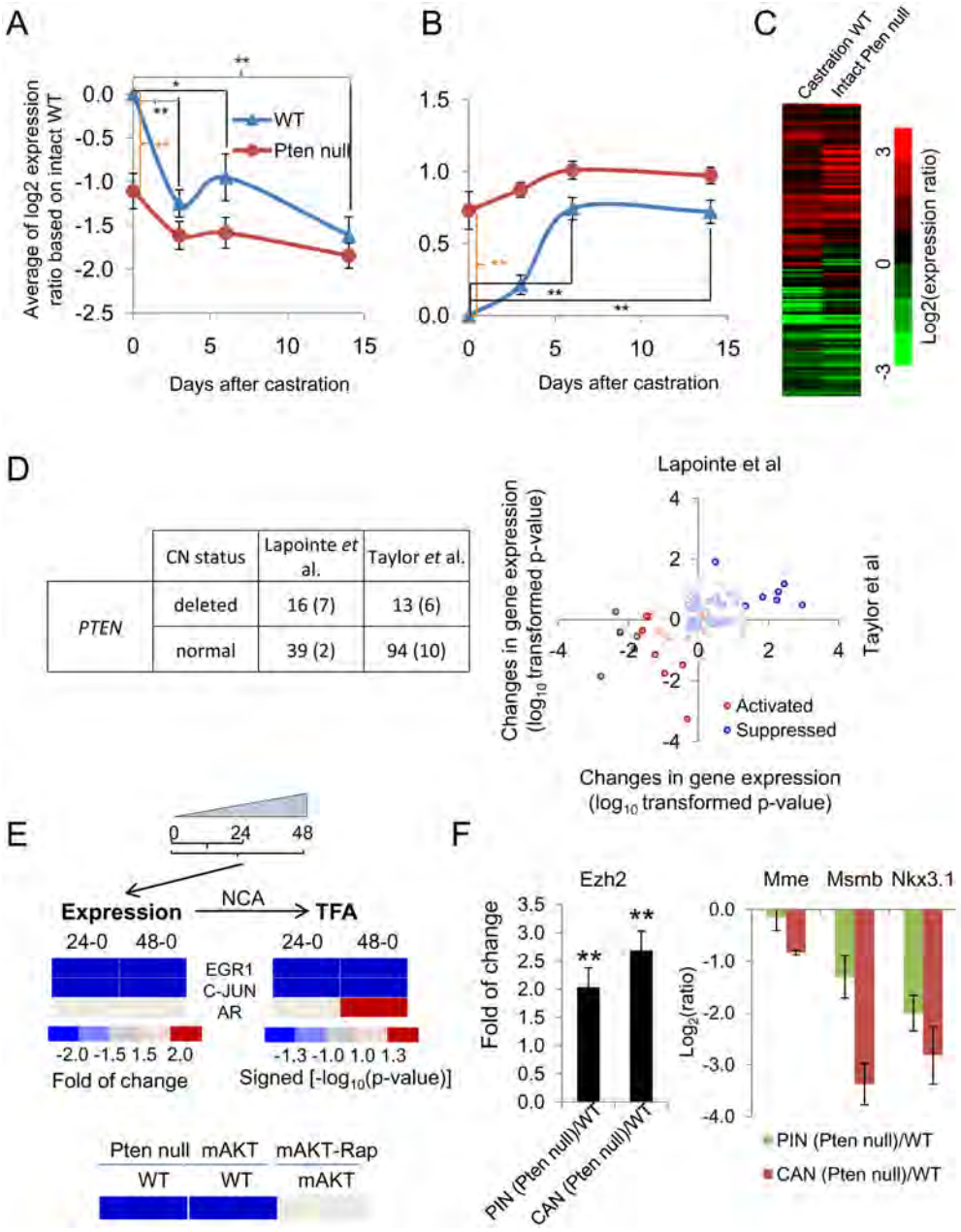

Figure 2. PTEN loss can suppress androgen-responsive gene expression

(A, B) Expression profile (means +/− s.e.m) of AR activated (A) and suppressed (B) genes in WT and *Pten*-null murine prostates after castration. (C) Heat map of expression ratios of androgen responsive genes in WT (14-day post castration) and intact *Pten*-null mutants with respect to intact WT mice. (D) Variation in expression of androgen-responsive genes based on *PTEN* copy number (CN) in human CaP samples. Left, summary of human samples based on *PTEN* CN (the numbers inside parentheses indicates the number of metastatic cases); right, a comparative analysis of AR activated (red circles) and suppressed (blue circles) gene expression values in two human CaP datasets. (E) Top, gene expression and NCA derived activities of EGR1, JUN, and AR transcription factors in induced PTEN expression in *Pten*$^{-/-}$ cells. Bottom, the activity of AR in murine models when PTEN/AKT/mTOR pathway was manipulated genetically or pharmacologically. (F) Expression (means

+/− SD) of *Ezh2* (left), and AR and EZH2 co-target genes (right) in PIN and cancer (CAN) stages of *Pten*-null prostate. *, $p<0.05$; **, $p<0.005$. See also Figure S2 and Table S1.

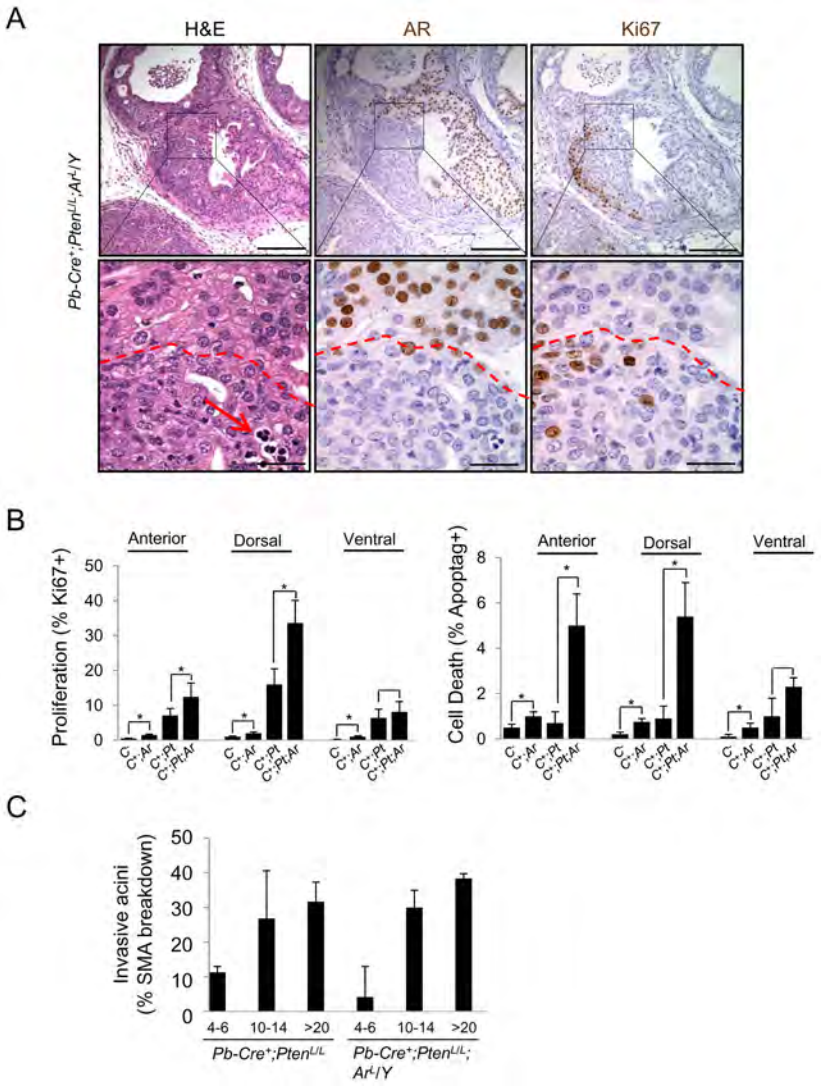

Figure 3. Epithelial AR is not required for the initiation of *Pten*-null CaP

(A) Deletion of epithelial AR in the anterior lobe of *Pten*-null CaP (*Pb-Cre*$^{+}$;*Pten*$^{L/L}$;*Ar*^{L}/*Y*) mutants and the impact on cell proliferation (Ki67+ cells), apoptosis (red arrow) and cancer formation (bar, top = 200 μm; bottom = 50 μm). (B) Cell proliferation (left) and apoptotic indexes (right) in *Cre*$^{-}$ (*C*$^{-}$), *Pb-Cre*$^{+}$;*Ar*^{L}/*Y* (*C*$^{+}$;*Ar*); *Pb-Cre*$^{+}$;*Pten*$^{L/L}$ and (*C*$^{+}$;*Pt*) and *Cre*$^{+}$;*Pten*$^{L/L}$;*Ar*^{L}/*Y* (*C*$^{+}$;*Pt;Ar*) mutants. (C) Frequency of invasiveness based on smooth muscle actin (SMA) break down in *Pb-Cre*$^{+}$;*Pten*$^{L/L}$ and *Cre*$^{+}$;*Pten*$^{L/L}$;*Ar*^{L}/*Y* mutants during progression. Error bars, means +/− SD. See also Figure S3.

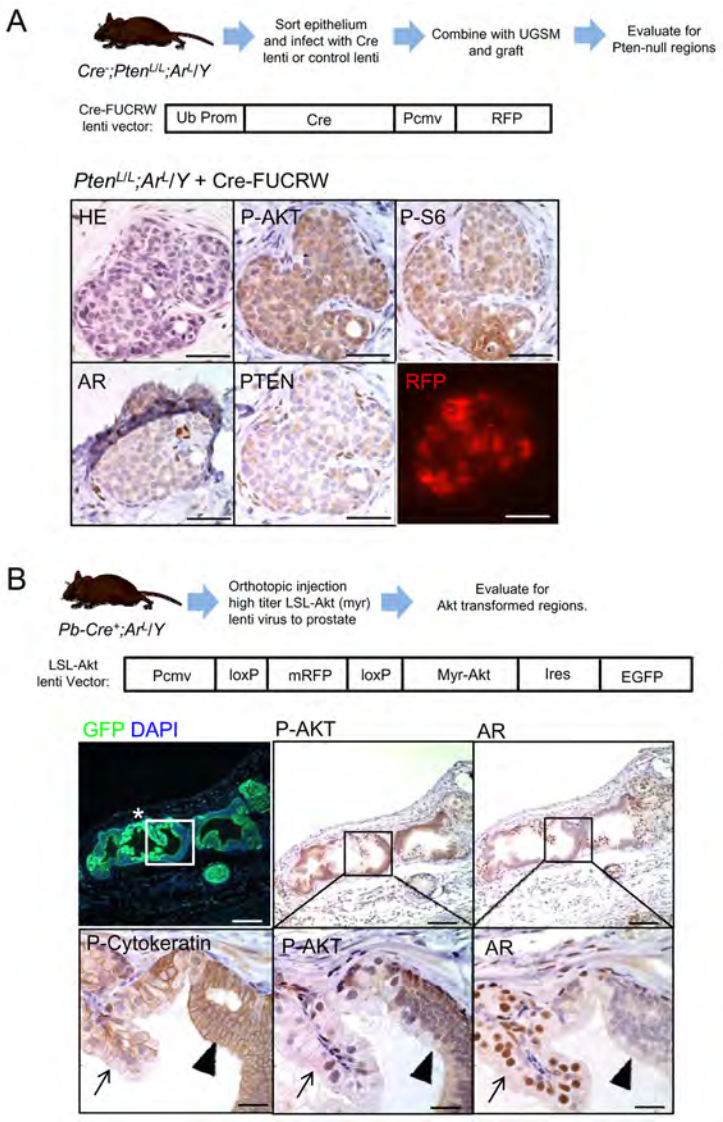

Figure 4. Epithelial AR is not required for transformation by *Pten* deletion or myristoylated Akt in regeneration assays

(A) Evaluating the impact of cre-mediated deletion of *Pten* and *Ar* on histopathology and PI3K signaling. The top panel shows the outline of the experiment and the bottom panels show results of tissues stained as indicated. Bar = 100 μm. (B) Evaluating AR deletion and myristoylated-AKT expression in primary, *Pb-Cre*$^{+}$*;Ar*^{L}*/Y* mutants and the impact on prostate histopathology and PI3K signaling. The top panel shows the outline of the experiment and the bottom panels show results of tissues stained as indicated. Bars, top = 200 μm, bottom = 50 μm. See also Figure S4.

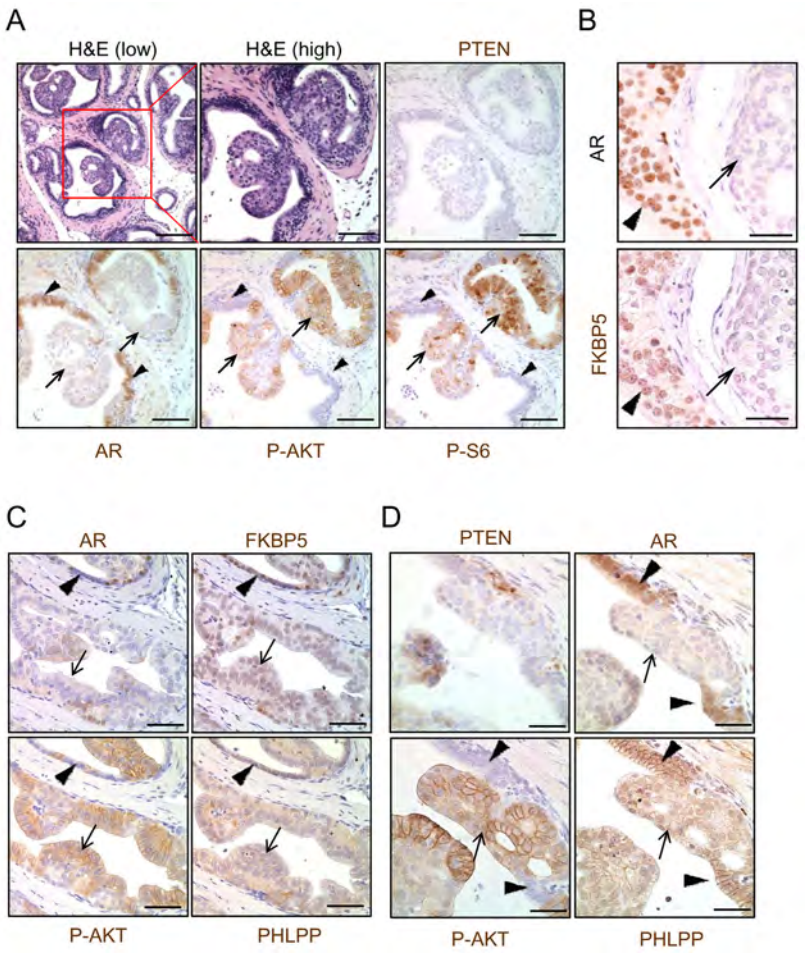

Figure 5. AR down regulates AKT activity by stimulating FKBP5 and PHLPP-mediated, AKT dephosphorylation

(A) PI3K activation (P-AKT, P-S6) in AR+ regions (arrows) versus AR− regions (arrow heads) in castrate, *Pb-Cre*$^{+}$*;Pten*$^{L/L}$*;Ar*^{L}*/Y* mutants. (Bar, low mag = 150 μm, high mag = 75 μm). (B) Effect of AR deletion on FKBP5 expression in *Pb-Cre*$^{+}$*Pten*$^{L/L}$*;Ar*^{L}*/Y* mutants (bar = 50 μm). (C, D) Expression of FKBP5, PHLPP and P-AKT in AR^{+} regions (arrow heads) compared to AR-null regions (arrows) in castrated *Pb-Cre*$^{+}$*;Pten*$^{L/L}$*;Ar*^{L}*/Y* mutants at 2 days (C) and 4 weeks (D) after castration (bar = 75 μm). See also Figure S5.

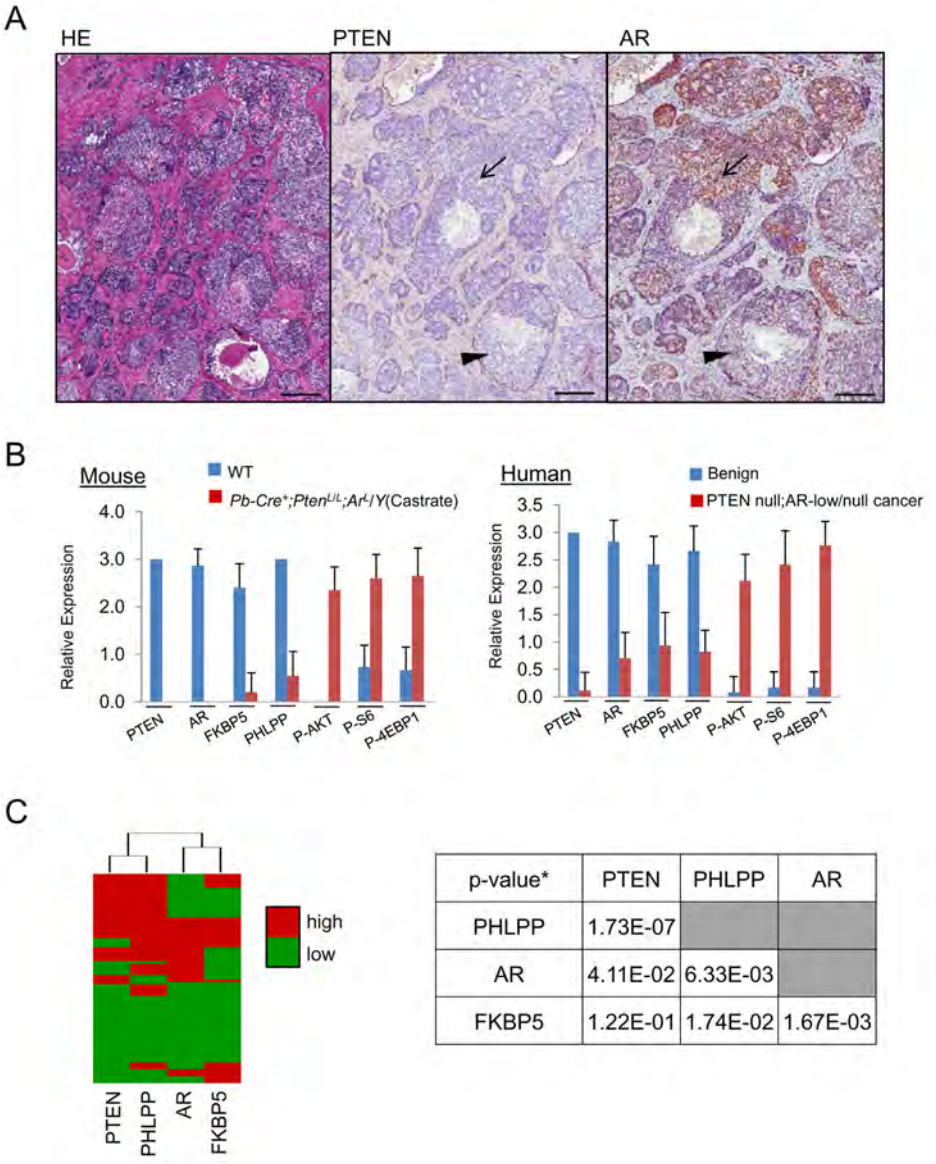

p-value*	PTEN	PHLPP	AR
PHLPP	1.73E-07		
AR	4.11E-02	6.33E-03	
FKBP5	1.22E-01	1.74E-02	1.67E-03

Figure 6. Heterogeneous AR expression in human CaPs correlating with PI3K/AKT signaling and FKBP5 and PHLPP levels

(A) PTEN and AR expression in human CaP (bar = 500 μm). (B) PI3K pathway components (P-AKT, P-S6, P-4EBP1) in Pten^{-};AR^{-} regions of *Pb-Cre*$^{+}$*;Pten*$^{L/L}$*;Ar*^{L}*/Y* mice and in PTEN-negative;AR-low/negative regions of human CaPs. Error bars, means +/− SD. (C) Unsupervised clustering analysis of PTEN, PHLPP, AR, and FKBP5 in human TMA samples (N=91) (left). Chi squared test P-values* (N = 91) were used to quantitate the strength of association between each pair (right, table). Protein level was categorized to high (IHC> 1) and low (< 1) levels). See also Figure S6.

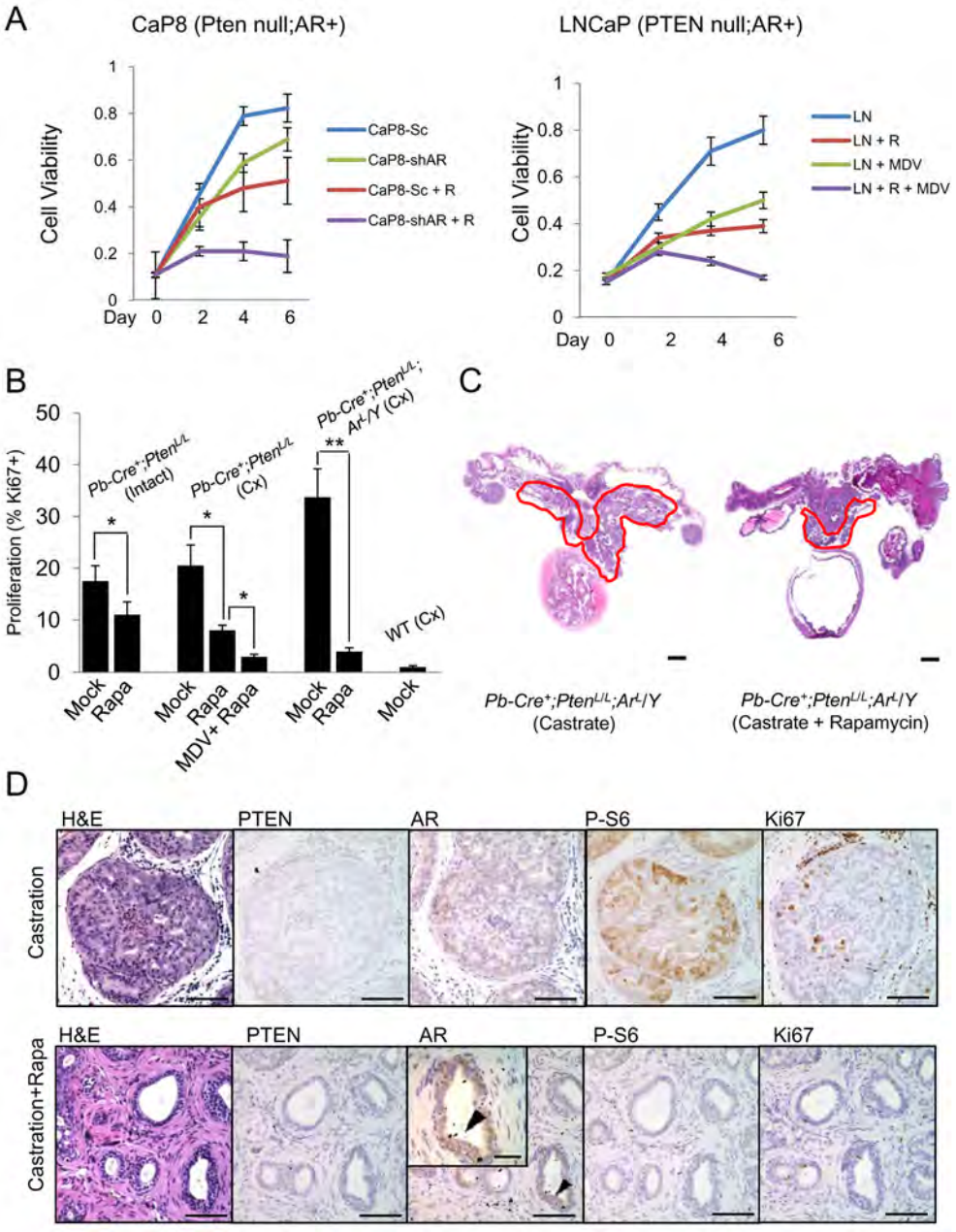

Figure 7. Cooperative effects of AR and mTOR inhibition in vitro and in vivo

(A) In vitro response of *Pten*-null;Ar^{+} mouse (CaP8) and human (LNCaP) CaP cells to AR knockdown (sh-AR) or pharmacological inhibition of AR (MDV3100, 10 μM) with and without rapamycin (R: 1 nM) treatment. (Sc = control sh oligo). (B, D) In vivo response to treatments with castration, MDV3100, rapamycin or their combinations as measured by cell proliferation ($Ki67^{+}$ cells) and (C, D) tumor burden in *Pb-Cre*$^{+}$;*Pten*$^{L/L}$ and *Pb-Cre*$^{+}$;*Pten*$^{L/L}$:*Ar*^{L}/*Y* mutants (C, bar = 2 mm; D, bar = 200 μm; D, inset bar = 75 μm). Error bars = means +/− SD. See also Figure S7.

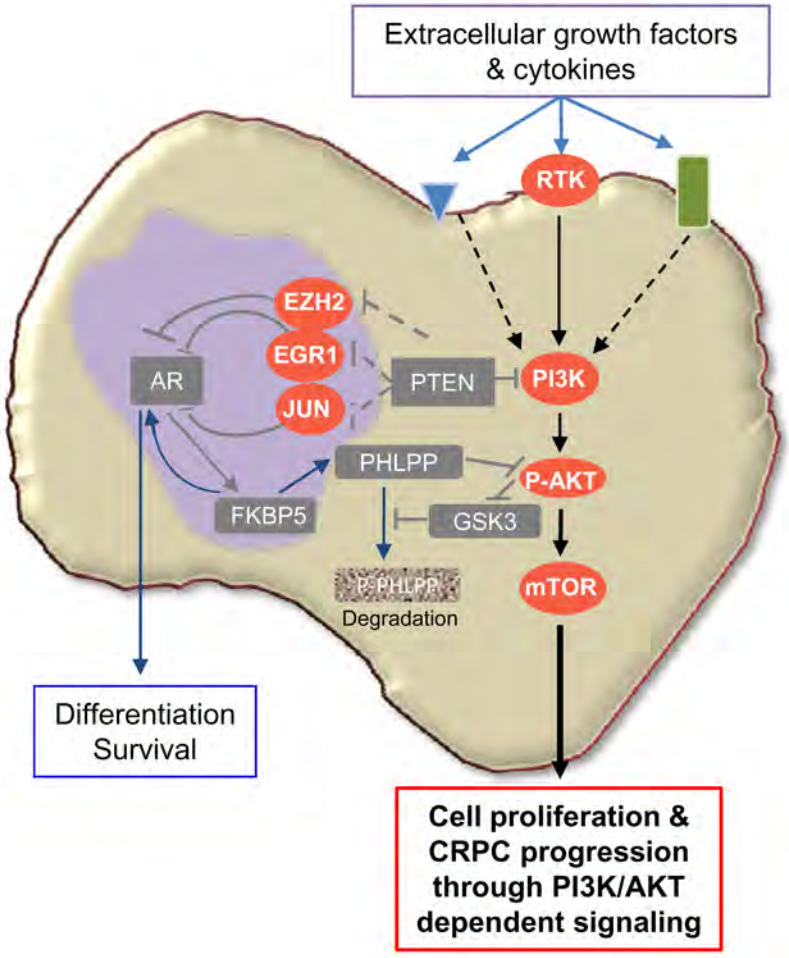

Figure 8. PTEN loss promotes CRPC development by two collaborative mechanisms

By regulating EGR1, c-JUN and EZH2 expression and activities, PTEN loss suppresses AR transcription factor activity and output, leading to reduced prostate epithelial differentiation and survival. Collaboratively, PTEN loss activates the PI3K/AKT signaling pathway and reduces the AR-regulated FKBP5-PHLPP negative feedback loop to AKT activation, further enhances AKT activation, leading to androgen/AR-independent prostate epithelial proliferation.

Identification of CD166 as a marker for enriching prostate tumor initiating cells

Jing Jiao[1,2], Antreas Hindoyan[1,2], Shunyou Wang[1] , Andrew Goldstein[3], Donghui Chen[6], Yunfeng Li[1], Changyong Guo[4], Baohe Zhang[4], Martin Gleave[5], Owen N. Witte[1,2,6,7], Isla P. Garraway[4] , Hong Wu[1,2,7]

[1]Department of Molecular and Medical Pharmacology, [2]Institute for Molecular Medicine, [3]Molecular Biology Institute, [4]Department of Urology, [5]Department of Pathology and Laboratory Medicine, [6]Howard Hughes Medical Institute,[7]Eli and Edythe Broad Center of Regenerative Medicine and Stem Cell Research, UCLA, Los Angeles, CA 90095, USA.

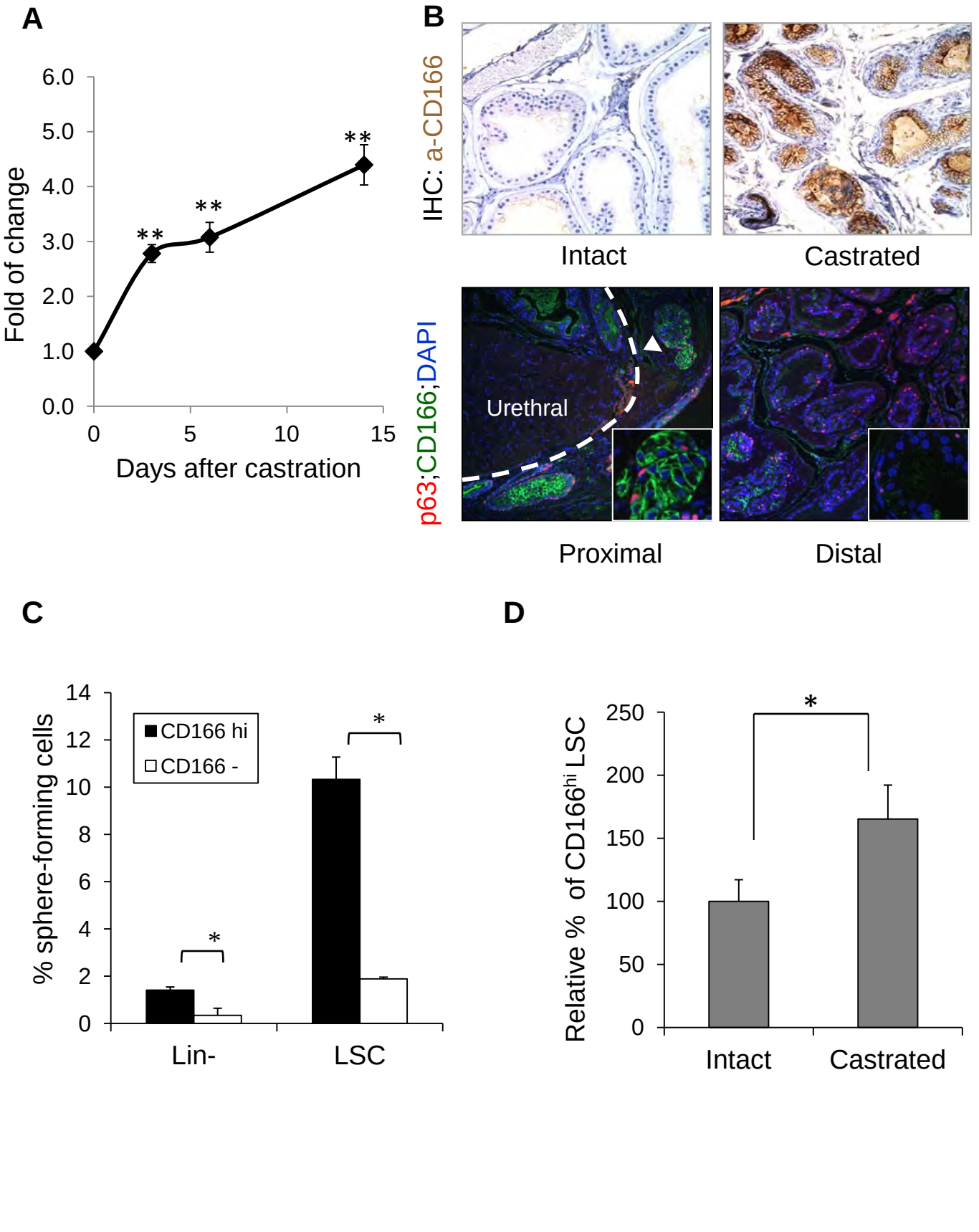
A
Fold of change
6.0
5.0
4.0
3.0
2.0
1.0
0.0
0
5
10
15
Days after castration
**
**
**
B
IHC: a-CD166
Intact
Castrated
p63;CD166;DAPI
Urethral
Proximal
Distal
C
% sphere-forming cells
14
12
10
8
6
4
2
0
CD166 hi
CD166 -
*
*
Lin-
LSC
D
Relative % of CD166hi LSC
250
200
150
100
50
0
*
Intact
Castrated

Fig.2

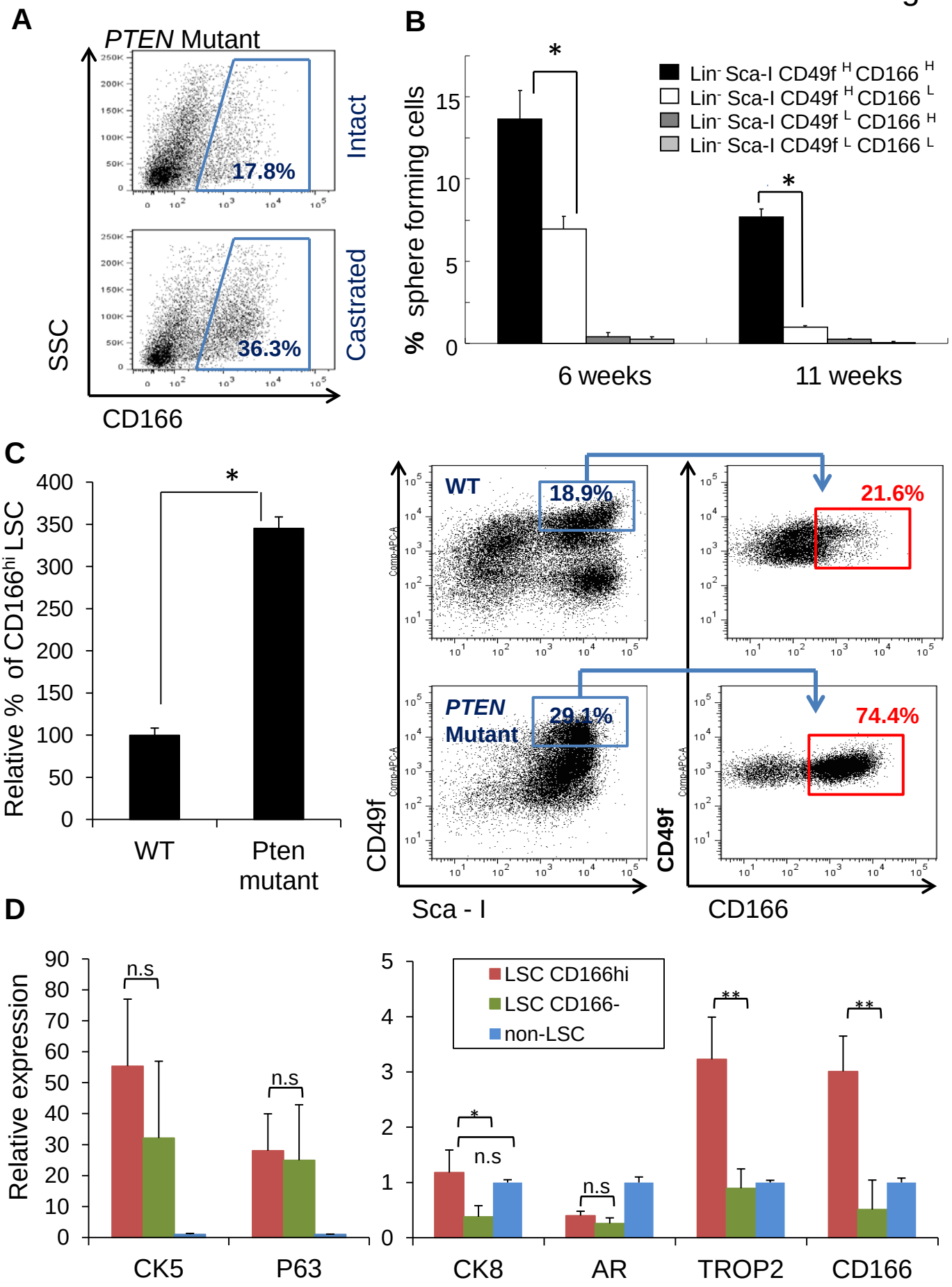
A
PTEN Mutant
17.8%
36.3%
Intact
Castrated
SSC
CD166
B
% sphere forming cells
Lin- Sca-I CD49f H CD166 H
Lin- Sca-I CD49f H CD166 L
Lin- Sca-I CD49f L CD166 H
Lin- Sca-I CD49f L CD166 L
6 weeks
11 weeks
C
Relative % of CD166hi LSC
WT
Pten mutant
WT
18.9%
21.6%
PTEN Mutant
29.1%
74.4%
CD49f
Sca - I
CD166
D
Relative expression
LSC CD166hi
LSC CD166-
non-LSC
n.s
CK5
P63
CK8
AR
TROP2
CD166

Fig.3

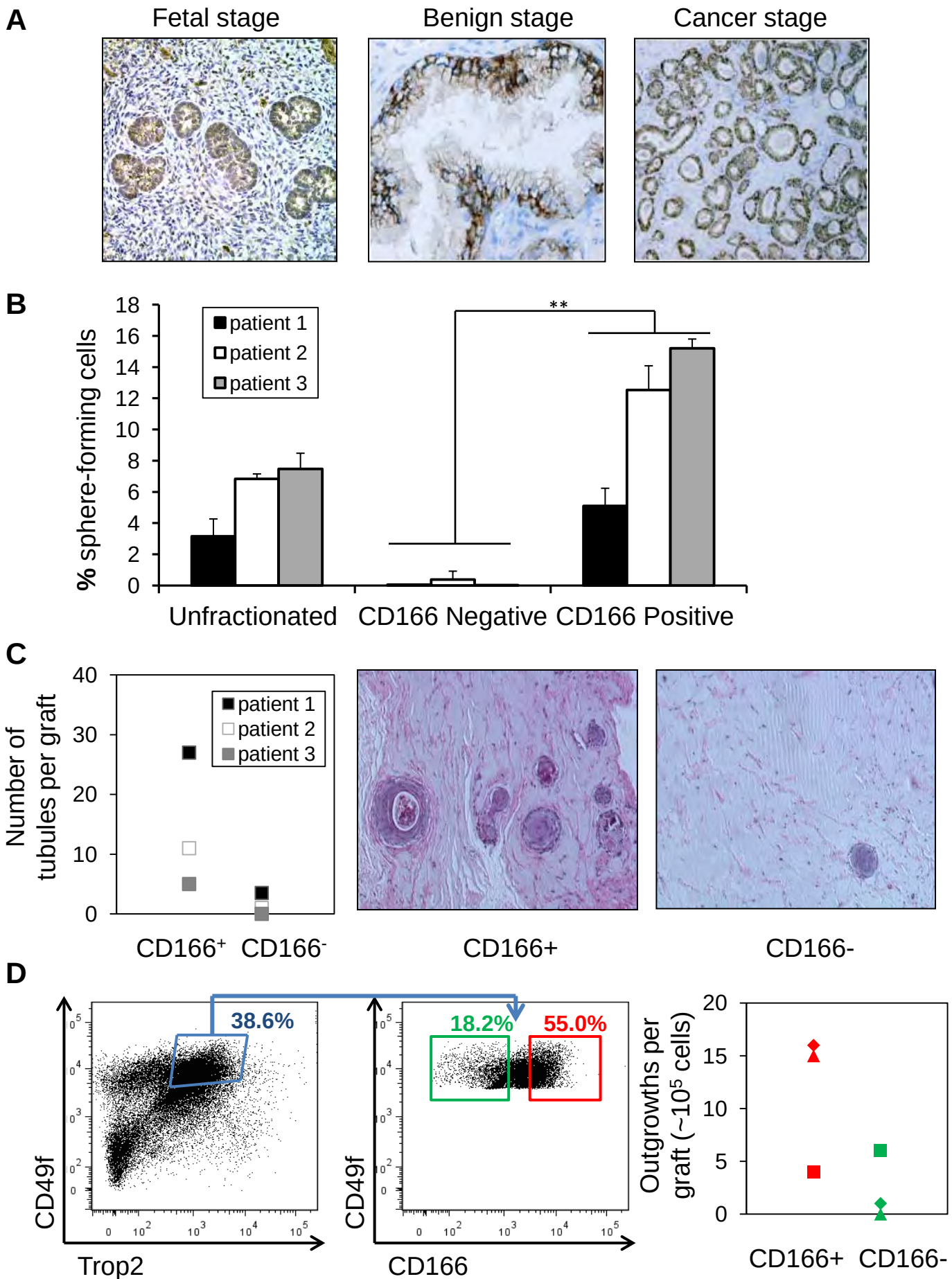
A
Fetal stage
Benign stage
Cancer stage
B
% sphere-forming cells
patient 1
patient 2
patient 3
**
Unfractionated
CD166 Negative
CD166 Positive
C
Number of tubules per graft
CD166+
CD166-
D
CD49f
Trop2
38.6%
CD166
18.2%
55.0%
Outgrowths per graft (~10^5 cells)
CD166+
CD166-

Fig.4

A

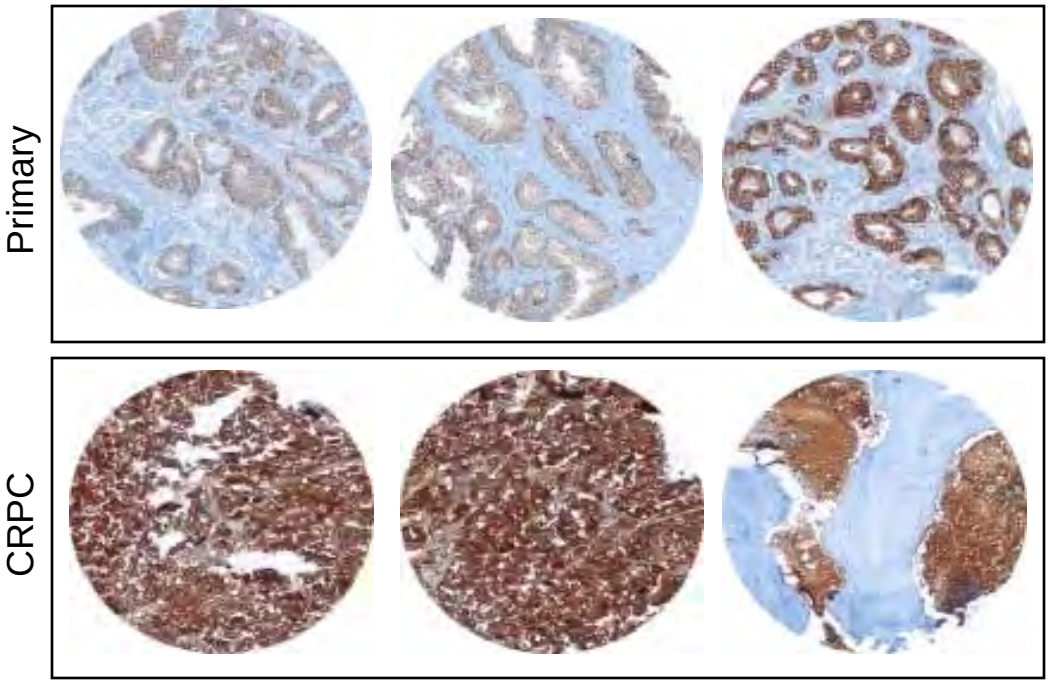
Primary
CRPC

B

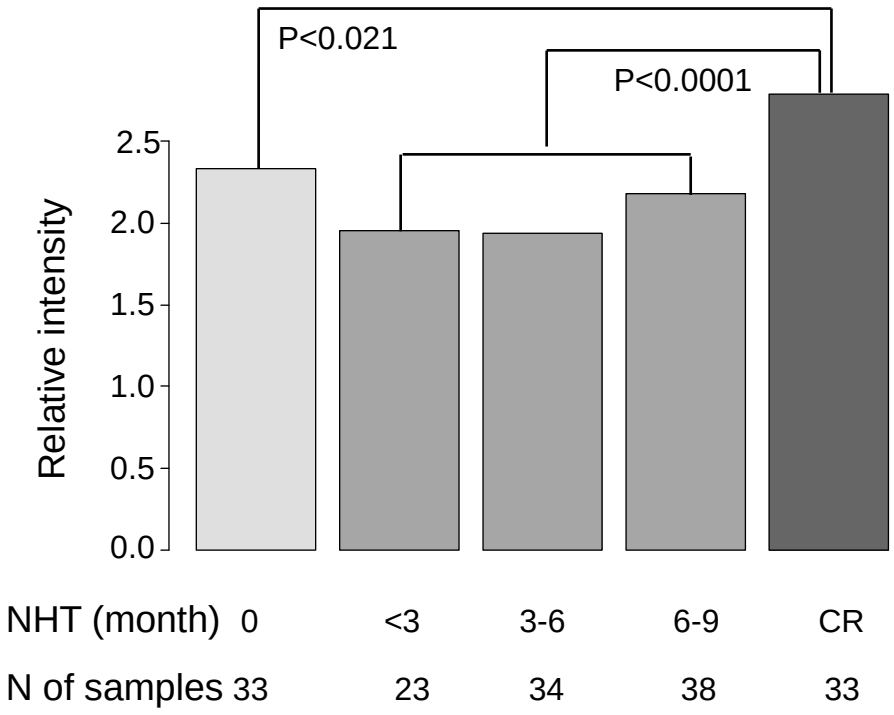
P<0.021
P<0.0001
Relative intensity
2.5
2.0
1.5
1.0
0.5
0.0
NHT (month) 0 <3 3-6 6-9 CR
N of samples 33 23 34 38 33

Fig.5

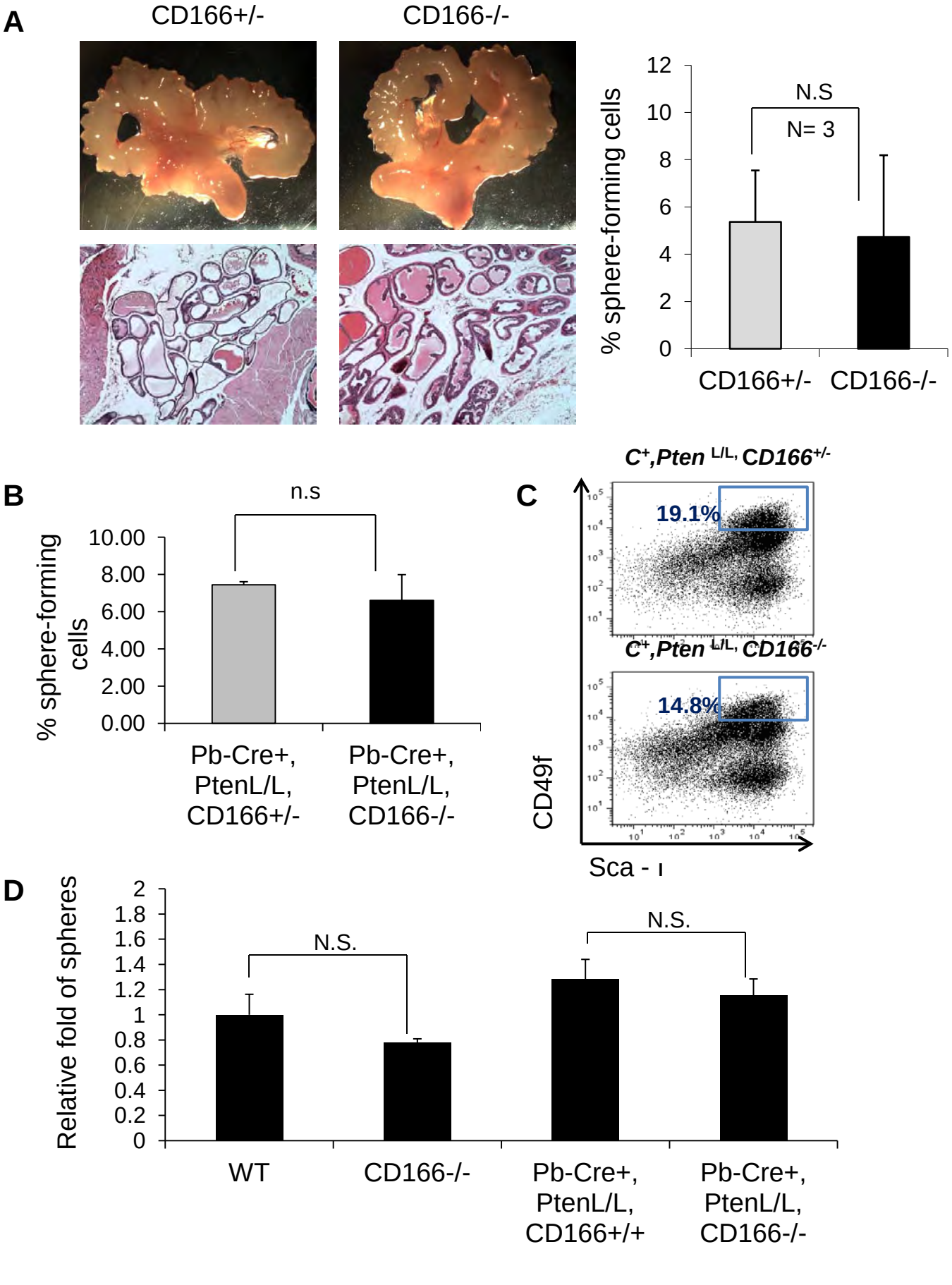
A
CD166+/-
CD166-/-
% sphere-forming cells
12
10
8
6
4
2
0
N.S
N= 3
CD166+/-
CD166-/-
B
n.s
% sphere-forming cells
10.00
8.00
6.00
4.00
2.00
0.00
Pb-Cre+, PtenL/L, CD166+/-
Pb-Cre+, PtenL/L, CD166-/-
C
C+,Pten L/L, CD166+/-
19.1%
C+,Pten L/L, CD166-/-
14.8%
CD49f
Sca - 1
D
Relative fold of spheres
2
1.8
1.6
1.4
1.2
1
0.8
0.6
0.4
0.2
0
N.S.
N.S.
WT
CD166-/-
Pb-Cre+, PtenL/L, CD166+/+
Pb-Cre+, PtenL/L, CD166-/-

Fig.6

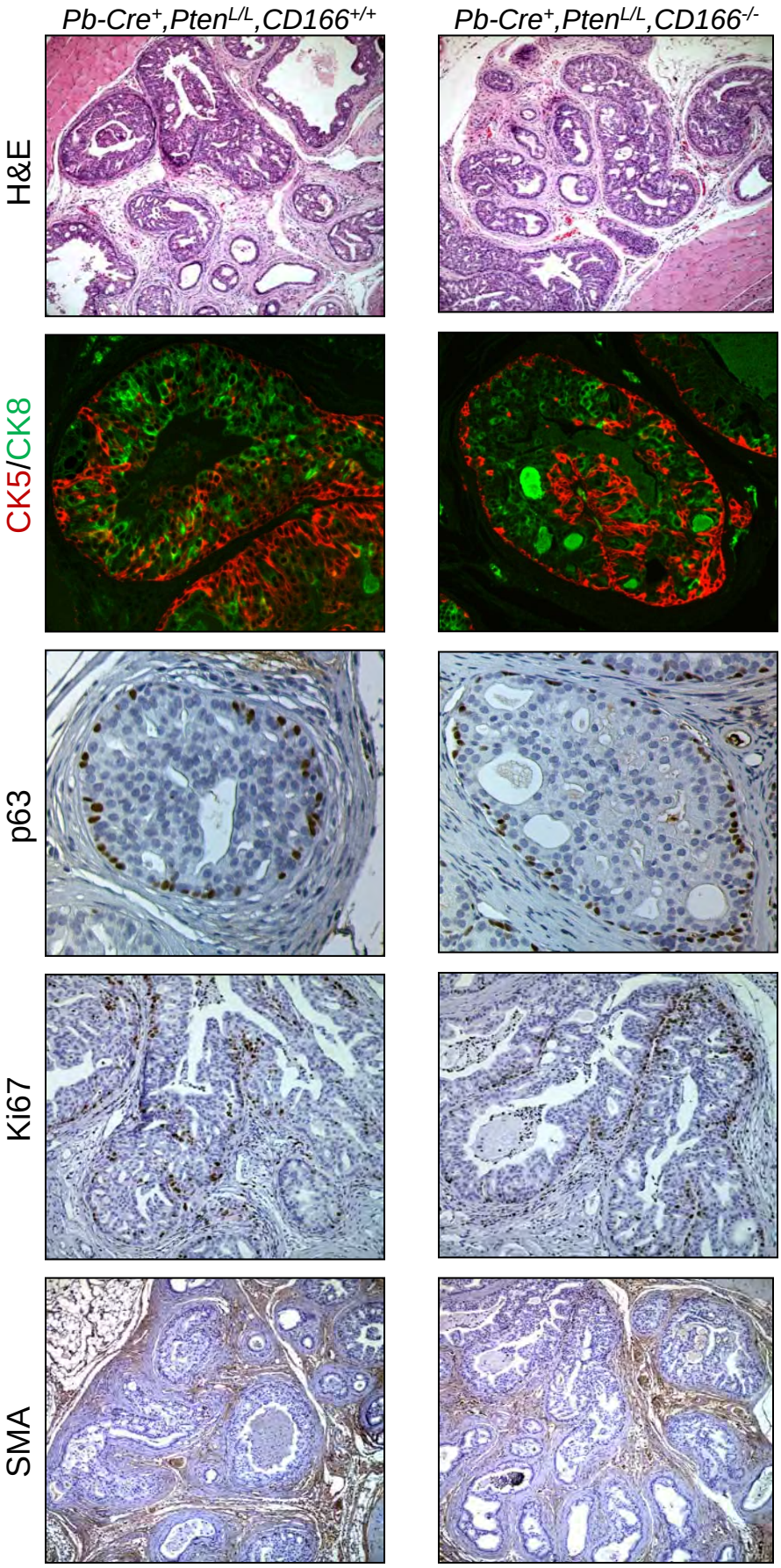
Pb-Cre+,PtenL/L,CD166+/+
Pb-Cre+,PtenL/L,CD166-/-
H&E
CK5/CK8
p63
Ki67
SMA

Fig.S1

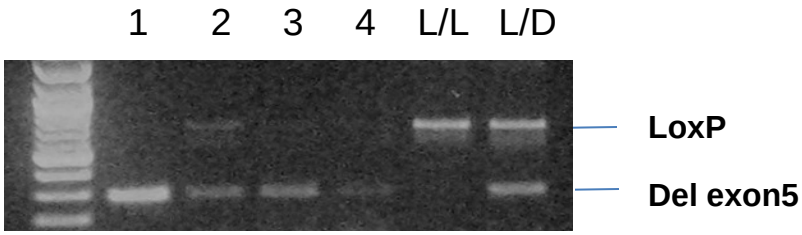

Genotyping of four FACS sorted populations from *Pten L/L, Pb-Cre+* prostate. 1: CD166hi LSC; 2: CD166-LSC; 3: LSC; 4: non-LSC.

Table S1. Antibodies used for FACS, IHC and IF.

application	antibody	company	dilution
IHC/IF	CK5	PRB-160P/Covance	1:1000
	CK8	MMS-162P/Covance	1:1000
	P63	sc-8431/Santa Cruz	1:200
	Ki67	VP-RM04/Vector lab	1:500
	SMA		
	CD166		
	CD166		
	Trop2		
FACS	FITC-CD31	ebioscience	
	FITC-CD45	eBioscience	
	FITC-Ter119	eBioscience	
	APC-CD49F		
	PE-Cy7-SCaII		
	PE-CD166		
	PE-CD31		
	PE-CD45		
	PE-Ter119		

Table S2. Primer sequences for qPCR experiments

CK5	5′-ACCTTCGAAACACCAAGCAC-3′	5′-TTGGCACACTGCTTCTTGAC-3′
CK8	5′-ATCGAGATCACCACCTACCG-3′	5′-TGAAGCCAGGGCTAGTGAGT-3′
p63	5’-CCCACAGACTGCAGCATTG-3’	5’-GAGATGAGGAGGTGAGGAGAAG-3’
AR	5′-AACCAACCAGATTCCTTTGC-3′	5'-ATTAGTGAAGGACCGCCAAC-3′
NKX3.1	5'-CGACTGAACCCGAGTCTGAT-3'	5'-ATGGCTGAACTTCCTCTCCA-3'
CD166	5'-CCTAAGAGAGGAGCGGATTG-3'	5'-CAGCCACTCCCAGAACAAAG-3'
Trop2	5'- AGACCAAAGCCTGCGCTGCG-3'	5'- AGCTGGGGTGCAGCTTGTAG-3'
GADPH	5′-ACTGGCATGGCCTTCCG-3′	5′-CAGGCGGCACGTCAGATC-3′

Fig.S2

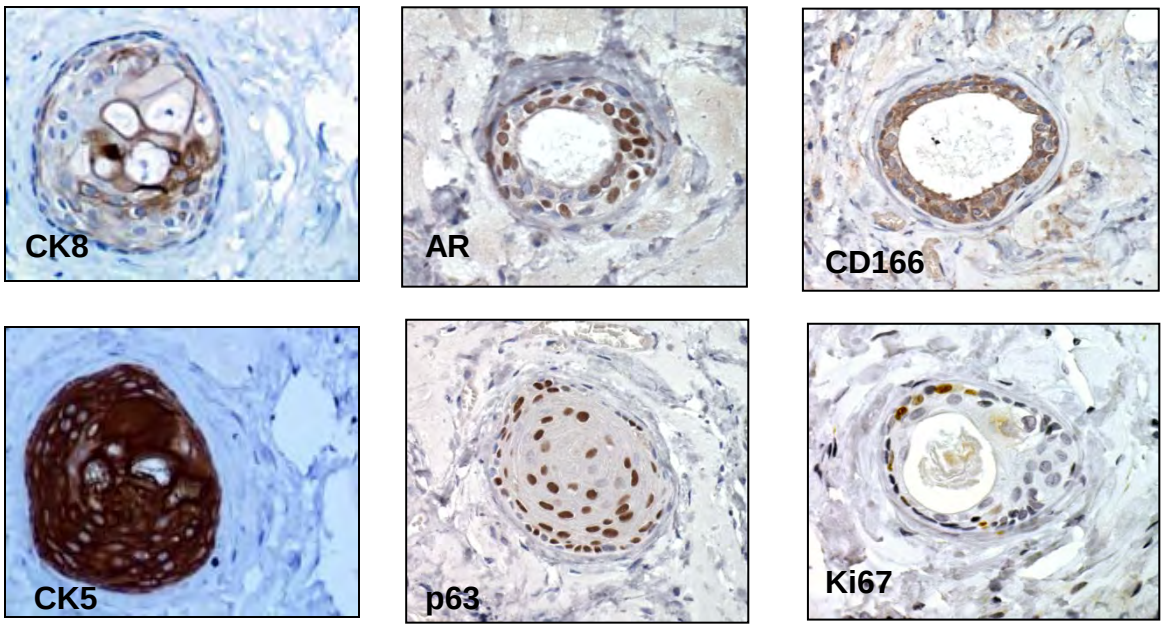

Immunohistochemical analysis of CD166hi-derived graft demonstrates nuclear expression of AR and p63, CK5 and CK8 positive cells and Ki67 positive cells within tubule structure.

Fig.S3

A

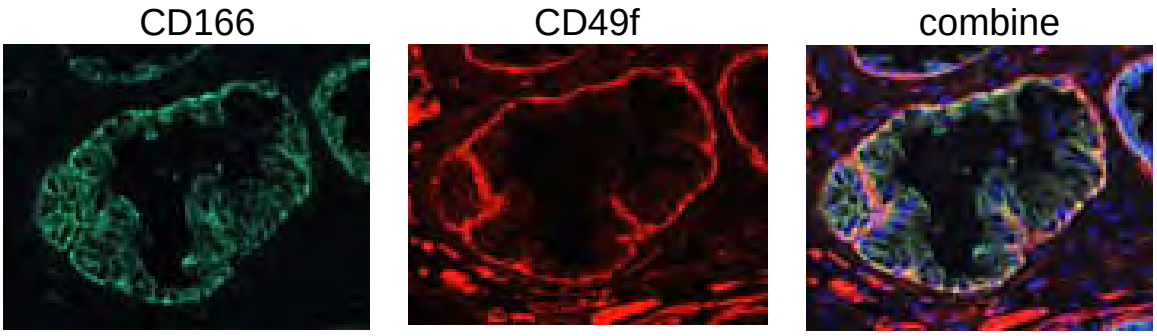

B

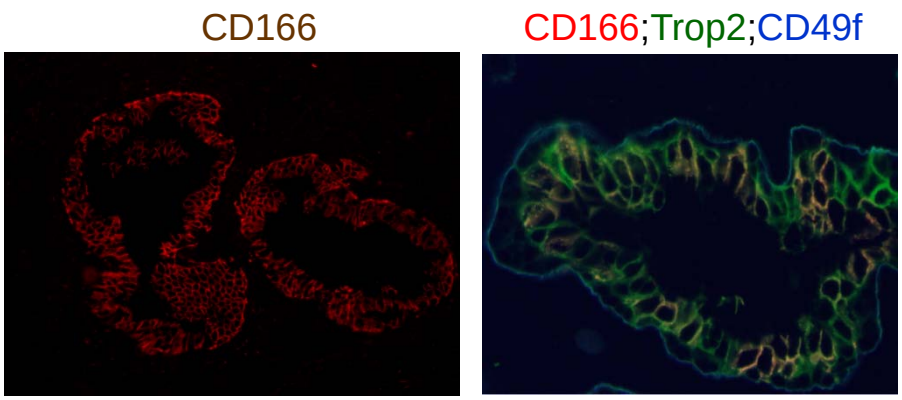

A, Immunofluorescence staining of CD166 and CD49f on WT prostate tissue section.
B, Immunofluorescence staining of CD166, CD49f and Trop2 on human prostate tissues.

Fig.S4

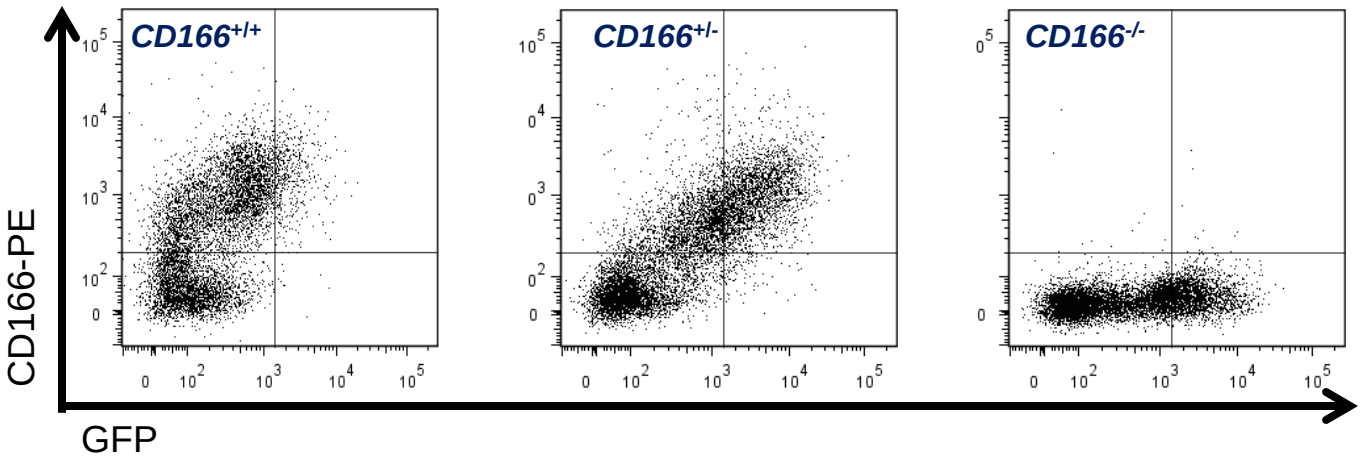

FACS analysis of CD166 expression on CD166+/+, CD166+/-, and CD166-/- prostate by comparing knockin GFP expression and PE-conjugated CD166 antibody staining.

Fig.S5

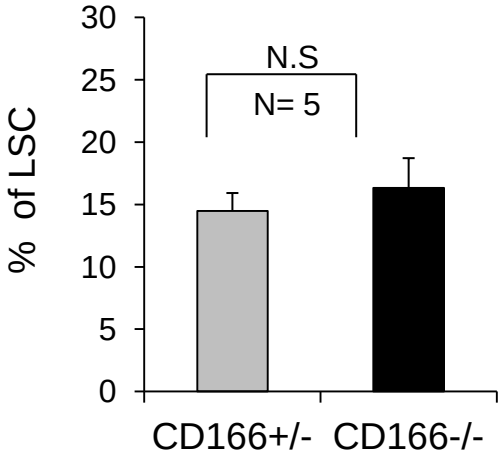

CD166-/- prostate epithelium have similar LSC content as CD166+/- prostate epithelium.

JBC Papers in Press. Published on September 18, 2012 as Manuscript M112.389015
The latest version is at http://www.jbc.org/cgi/doi/10.1074/jbc.M112.389015

Secreted Hsp90 is a novel regulator of the epithelial to mesenchymal transition (EMT) in prostate cancer

Michael W. Hance[1], Krystal Dole[§1], Udhayakumar Gopal[§1], Jessica E. Bohonowych[1], Agnieszka Jezierska-Drutel[1], Carola A. Neumann[1], Haibo Liu[2], Isla P. Garraway[2], and Jennifer S. Isaacs[1*]

From the Departments of [1]Cell and Molecular Pharmacology, Medical University of South Carolina, Charleston, SC 29425 and [2]Urology, David Geffen School of Medicine, University of California, LA, CA 90095

Running Title: eHsp90 is a novel effector of prostate tumor cell EMT.

[*]To whom correspondence should be addressed: Department of Cell and Molecular Pharmacology, Medical University of South Carolina, Hollings Cancer Center, 86 Jonathan Lucas St, Charleston, SC, 29425. Tel: 843-792-8393; Fax: 843-792-3200; email:isaacsj@musc.edu.

Key words: extracellular Hsp90, prostate cancer, epithelial to mesenchymal transition, MMP, ERK, cell motility

Background: EMT correlates with increased metastatic potential and poor prognosis
Results: Secreted eHsp90 induces EMT, MMP activity and cell motility.
Conclusions: EMT inducing activity of eHsp90 provides a mechanistic basis for its tumorigenic and metastatic function.
Significance: The requirement for eHsp90 in supporting tumorigenic events indicates that targeting eHsp90 may represent a therapeutic approach to improve prostate cancer patient survival.

SUMMARY

Prostate cancer (PCa) is the most frequently diagnosed malignancy in men, and the second highest contributor of male cancer related lethality. Disease mortality is due primarily to metastatic spread, highlighting the urgent need to identify factors involved in this progression. Activation of the genetic epithelial to mesenchymal transition (EMT) program is implicated as a major contributor of PCa progression. Initiation of EMT confers invasive and metastatic behavior in preclinical models and is correlated with poor clinical prognosis. Extracellular Hsp90 (eHsp90) promotes cell motility and invasion in cancer cells and metastasis in preclinical models, however the mechanistic basis for its widespread tumorigenic function remains unclear. We have identified a novel and pivotal role for eHsp90 in driving EMT events in PCa. In support of this notion, more metastatic PCa lines exhibited increased eHsp90 expression relative to their lineage related non-metastatic counterparts. We demonstrate that eHsp90 promoted cell motility in an ERK and MMP-2/9-dependent manner, and shifted cellular morphology towards a mesenchymal phenotype. Conversely, inhibition of eHsp90 attenuated pro-motility signaling, blocked PCa migration, and shifted cell morphology towards an epithelial phenotype. Lastly, we report that surface eHsp90 was found in primary PCa tumor specimens, and elevated eHsp90 expression was associated with increased levels of MMP-2/9 transcripts. We conclude that eHsp90 serves as a driver of EMT events, providing a mechanistic basis for its ability to promote cancer progression and metastasis in preclinical models. Further, its newly identified expression in PCa specimens, and potential regulation of pro-metastatic genes, supports a putative clinical role for eHsp90 in PCa progression.

INTRODUCTION

One of the greatest challenges associated with the widespread and early diagnosis of prostate cancer (PCa) in men (1-3) is the inability to accurately distinguish which subset of patients with apparently

localized disease will progress to metastatic disease. The propensity of tumor cells to metastasize to bone, rendering the disease incurable (4), is largely responsible for PCa as the second leading cause of male cancer associated lethality (5). Although rising levels of the serum protein prostate specific antigen (PSA) are indicative of tumor growth, its expression can be nonspecifically modulated by a number of benign conditions (6,7) such that this metric alone risk cannot accurately predict risk for progression. Similarly, Gleason score cannot accurately predict disease progression, relapse, or response to treatment (8,9). These clinical limitations illustrate the pressing need to utilize new and improved molecular indicators of PCa progression.

Activation of the evolutionarily conserved developmental epithelial to mesenchymal transition (EMT) genetic program (10,11) is implicated as a significant contributor to PCa progression. A universal hallmark of EMT is loss of epithelial cell polarity and acquisition of elongated mesenchymal morphology, concomitant with disruption of cell adhesion, increased cell migration, invasion and metastasis (12). The adherens junction protein E-cadherin acts as a gatekeeper in suppressing EMT events, and corresponding cell motility and dissemination, by maintaining the cuboidal phenotype and architecture that defines the morphology of normal epithelium (10,11,13). As such, loss of E-cadherin function is a conserved and fundamental hallmark associated with early EMT events (10,11).

Multiple preclinical models provide strong support for EMT in mediating PCa progression. Pathological EMT events have been shown to potentiate the transition from localized prostate adenocarcinoma to invasive carcinoma and subsequent metastasis (14-19). Conversely, repression of EMT events blocks the metastatic potential of PCa cells (20). In clinical specimens, measures of cancer progression correlate with loss of E-cadherin and upregulation of EMT-inducing transcriptional factors (18,20-23). EMT events are correlated with metastatic recurrence following surgery (18,24), and have recently been observed concurrently following androgen withdrawal therapy (25). Therefore, the ability to identify primary tumor cells with an increased propensity to undergo EMT-like events would improve diagnostic approaches to discriminate patients at risk for progression.

Hsp90 is a well known intracellular chaperone responsible for mediating the ATP dependent folding and signaling function of numerous client proteins, many of which exhibit pro-tumorigenic functions (26-28). In addition to its intracellular localization, Hsp90 is also a secreted and cell surface protein. Extracellular Hsp90 (eHsp90) exhibits distinct function from the intracellular chaperone with its signal transducing activity, in tandem with its receptor low density lipoprotein related protein (LRP1) (29,30). eHsp90 supports cell motility and invasion in several cancer cell lines (31-34), and promotes metastatic spread in preclinical models (35-38). Clinically, eHsp90 was first reported as a tumor antigen (39,40), and more recently found in the serum from patients afflicted with a variety of tumor types (37), including metastatic PCa (41). Although these reports strongly implicate eHsp90 in disease progression, a mechanistic basis for this putative function remains largely unknown.

The present study identifies eHsp90 as a pivotal regulator of E-cadherin function in PCa. Importantly, we demonstrate that modest, physiologically relevant expression of secreted eHsp90 reduces the expression and alters the localization of E-cadherin in phenotypically epithelial cell lines. In addition, eHsp90 modulates numerous genetic events consistent with activation of EMT, as well as promoting diminished cell adhesion, conversion to a more mesenchymal morphology and increased cell motility. In addition to its role in initiating

EMT events, eHsp90 is also essential for sustaining the mesenchymal properties and behavior of more aggressive PCa cell types. Finally, we report that surface eHsp90 is found in primary PCa tumor specimens and is correlated with markedly elevated expression of a subset of pro-tumorigenic eHsp90 regulated transcripts. This newly identified role for eHsp90 as a mediator of EMT events provides a mechanistic basis for its ability to promote cancer progression and metastasis in a variety of preclinical models. Moreover, the newly identified expression of eHsp90 in PCa specimens, coupled with its potential role in modulating gene expression, implicates a clinical role for eHsp90 in PCa progression.

Materials and Methods

Western blot and Antibodies: Cell extracts for Western blot analysis were prepared and performed as described (30) and all blots are representative of a minimum of two independent experiments. Antibodies for N-cadherin (ab12221), Slug (ab27568), Snail (ab63371), and Vimentin (ab8978) were purchased from Abcam. Mouse and rabbit Hsp90 antibodies (ADI-SPA-830, ADI-SPS-771) were from Enzo Lifesciences. E-cadherin (3195), ERK 1/2 (4695), P-ERK 1/2 (4370), MEK1/2 (9122), P-MEK1/2 (9121) and ZO-1(5406) were from Cell Signaling. FAK (AHO0502) and P-FAK (44-624G) were from Invitrogen/Life Technologies. V5 antibody (NB600-381) was from Novus Biologicals. Twist (sc-15393) was from Santa Cruz Biotechnology, and anti-alpha tubulin antibody (T6074) was from Sigma. Mouse monoclonal LRP1 antibody (11H4) was purified from a hybridoma cell line (CRL 1936) purchased from ATCC. The hybridoma supernatant was concentrated with a Vivacell 70 concentrator (Sartorius Biolab products) and purified with an NAb protein G antibody purification kit (Thermo Scientific) according to the manufacturer's instructions, and aliquots were stored at −20°C.

Reagents: Recombinant Hsp90 alpha protein was obtained from Enzo Life Sciences (ADI-SPP-776). Geldanamycin was obtained from the Experimental Therapeutics Branch, National Cancer Institute, DMAG-N-oxide modified geldanamycin, (or non-permeable GA, NPGA used at 1μM) was synthesized by Chris Lindsey and Craig Beeson (Pharmaceutical Sciences, Medical University of South Carolina). MMP inhibitors GM6001 (CC1010 used at 1μM), MMP-2/9 inhibitor IV (444274 used at 1μM) and MMP-3 inhibitor IV (444243 used at 5μM) were obtained from EMD Millipore Chemicals. MEK inhibitor U0126 (V112A used at 10μM) was obtained from Promega.

Cell Culture, Plasmids, and Transfection: The prostate cancer cell lines DU145 and LNCaP were obtained from ATCC, the ARCaP cell pair was purchased from Novicure Biotechnology, and C4-2B was obtained from Viromed. The P69/M12 cell pair was a gift from Joy Ware. The ARCaP pair and P69/M12 cell pair was maintained in T-media supplemented with 5% heat inactivated fetal bovine serum, and the LNCaP and C4-2B pair was maintained in their specified media supplemented with 1% HEPES and 1% penicilin/streptomycin in a 5% CO_2-humidified atmosphere. The plasmid for shLRP1 was as previously described (29,30). The sequence for Hsp90 alpha was cloned in frame to a 5' signal peptide to direct its extracellular localization, and 3' to a V5 tag and 6X His epitope, with each epitope separated by a flexible linker. The product was assembled in a Gateway entry vector and recombined (CRE) into Plenti6.3V5-Dest (Invitrogen). To obtain viral particles for LRP1 suppression and constitutive eHsp90 secretion, 293FT cells (Invitrogen) were co-transfected with the viral packaging plasmids VSVG and PΔR 8.71, along with the corresponding lentiviral vector. All plasmid transfections were performed with Lipofectamine 2000 (Invitrogen) according to the manufacturer's specifications. Following viral plasmid transfection, cell medium was harvested at

48 hr, the lentiviral supernatant was concentrated by ultracentrifugation, titered, and 5×10^4 particles were used to infect the recipient cells in the presence of polybrene (8 µg/ml). Cells transduced with eHsp90 virus were selected in blasticidin (Invivogen), while GFP-shLRP1 transduced cells were selected by flow cytometry to isolate the highest GFP expressing cells. Selection for eHsp90 transduced cells was performed for two weeks, whereupon surviving cells were pooled.

Patient Samples: Human prostate tissue was obtained via an approved research protocol with informed written consent of all participants. Adjacent tissue specimens were snap frozen in liquid nitrogen or fixed in formalin and paraffin-embedded for histological analysis. Tumor tissue specimens were mechanically and enzymatically digested as previously described (42) and dissociated tissue filtered and passed repeatedly through a 23-gauge needle to generate single cell suspensions. Cells were resuspended and incubated (15 min at 4˚C) with either isotype matched control or anti-Hsp90 antibody (SPS-771-PE, 1:50), and subjected to FACS analysis (BD FACS Aria II system). Cell populations corresponding to $eHsp90^{high}$ and $eHsp90^{low}$ subtypes were gated and isolated (minimum signal threshold set at 10e2).

RNA isolation and real time PCR analysis: RNA purification from patient samples was performed according to the manufacturer's recommendations (Qiagen RNeasy Plus Micro kit; 74034). RNA purification from cells was performed following a trizol/chloroform extraction (Qiagen miRNeasy kit; 217004). mRNA from cells and patient material was converted into complimentary DNA (OriGene first strand cDNA synthesis kit; NP100042), and (BioRad iScript advanced cDNA synthesis kit; 170-8842), respectively, and amplified. Array samples were prepared according to the manufacturer's instructions (Qiagen RT^2 first strand kit; 330401), and further analyzed using an EMT profiler array (Qiagen; PAHS-090A). Biological replicates were utilized for the initial array analysis, and select results validated with additional biological replicates. Primers (supplemental table 1) were purchased from IDT.

Cell motility assays: Wounding assays were performed as previously described (30). Briefly, a thin sterile pipette tip was used to create a scratch wound in confluent cell monolayers. Pictures were taken at 0 and 16 -20 hrs with an inverted Nikon eclipse TE 2000-S microscope with 10× magnification, and the extent of migration was calculated by measurement of the gap area using Image J software. For all motility experiments, mitomycin C (5 ug/ml) (Sigma) was added at the time of plating to suppress proliferation.

Gelatin zymography assay: The gelatinolytic activity of MMP-2 and MMP-9 was determined by gelatin zymography in 0.1% gelatin-10% acrylamide gels. Samples were prepared by plating cells at 50% confluency, and conditioned medium (0.25% serum in DMEM) was collected after 36 hr. 1 mM o-phenanthroline monohydrate was added to halt MMP activity. Conditioned medium was incubated with gelatin-sepharose beads (GE Healthcare, 17-0956-01) and eluted samples run in non-reducing conditions. Gels were washed with 2.5% Triton X-100 renaturing buffer, incubated in a Tris-HCL/Brij35 developing buffer (42˚C for 24 hours), and subsequently stained with a 5% Comassie solution.

Hsp90α ELISA: To detect expression of secreted Hsp90α, equivalent cell numbers (7.5×10^5) were plated overnight and replenished with complete media 24 hr prior to harvest. Conditioned medium was collected, debris removed by centrifugation (5 min, 1200 x g) and Hsp90α levels detected by ELISA (Enzo Life Sciences). Values are presented as fold change of Hsp90 per ml of conditioned medium with the standard deviation shown.

Immunofluorescence: To evaluate cellular localization of E-cadherin and ZO-1, equivalent cell numbers (2.5×10^4) were plated overnight and replenished with complete media for 24 hr. Cells were then treated with either NPGA, GM6001, MMP-2/9 and MMP-3 inhibitors for specified times. Cells were fixed with 4% paraformaldehyde and permeabilized with 0.1% Triton X-100 in PBS. Immunofluorescence was performed as described (30).

Statistical analysis: All cell motility and quantitative real time PCR were performed in triplicate. Data shown are presented as means and SD; differences in treatment groups are defined as statistically significant at $P<0.05$ value, as calculated from Student's t test.

RESULTS

An eHsp90-LRP1 signaling pathway initiates prostate cancer cell motility

Although eHsp90 has been implicated in promoting cancer cell motility, invasion and metastasis in several models (30-34,36-38,43), its role in PCa has not yet been explored. To investigate whether eHsp90 supports PCa motility, we examined the effects of eHsp90 inhibition in PC3 cells. To inhibit eHsp90, PC3 cells were treated with two different anti-Hsp90 antibodies, an effective approach to neutralize eHsp90 activity and diminish eHsp90 driven cell motility (30,35-37). As an additional means to inhibit eHsp90 function, cells were treated with NPGA specific for eHsp90 (30,36,44). Exposure of PC3 cells to either NPGA or blocking antibodies to Hsp90α and β isoforms or to Hsp90α similarly suppressed cell migration over 50% (Fig. 1A and S1A). The similar results elicited by these three distinct eHsp90 targeted approaches validate the importance of eHsp90 in PCa motility.

It has been shown that eHsp90 elicits autocrine signaling through LRP1 (29,30). We reasoned that if eHsp90 was eliciting its pro-motility effects through LRP1, then treatment of cells with either NPGA or suppression of LRP1 would similarly impair cell migration. In support of this notion, treatment of DU145 PCa cells with either NPGA or shLRP1 comparably blocked cell motility (Fig 1B and Fig. S1B). NPGA did not further block cell motility in LRP1 suppressed cells, indicating impairment of a similar pathway.

LRP1 has been shown to be required for activation of the pro-motility proteins extracellular-signal-regulated kinase (ERK) and focal adhesion kinase (FAK) (45-47). Treatment of DU145 with NPGA inhibited phosphorylation of both FAK and ERK (Fig. 1C). To provide further evidence for an eHsp90-LRP1 signaling pathway, the activation status of FAK and ERK was evaluated in LRP1 suppressed cells. As shown, LRP1 suppression in DU145 cells dramatically diminished both FAK and ERK phosphorylation, with no further effect elicited by NPGA treatment (Fig. 1D). These data indicate that eHsp90-LRP1 plays an essential role in regulating the activation status of pro-motility effectors and supporting the migratory potential of PCa cells.

eHsp90 is elevated in more aggressive PCa cell types and is essential for cell motility

Increased cell motility is commonly associated with cells adopting a mesenchymal morphology (11,48). We therefore next investigated whether increased eHsp90 expression was associated with more highly motile mesenchymal cell types. To examine this, we analyzed 3 sets of lineage related prostate cancer cell pairs, with the mesenchymal derivative of each pair representing a more tumorigenic and metastatic derivative of its epithelial counterpart. The ARCaP model, consisting of ARCaPE and ARCaPM subtypes, recapitulates many of the pathological

features of PCa (49), and is one of the best characterized cell pairs for investigating EMT events (14,15,50). The epithelial ARCaPE disseminates at low frequency, while its mesenchymal counterpart ARCaPM is highly aggressive and metastatic (14,15,17). EMT events in ARCaPE can be initiated following exposure to a variety of soluble growth factors (22,51,52), and sustained EMT activation increases its metastatic potential (19,52). The cell pair represented by P69 and M12 is another useful model for monitoring EMT events. P69 is a normal nontumorigenic immortalized prostate epithelial cell line, whereas M12 a highly tumorigenic and metastatic subline (53). P69 expresses E-cadherin and is responsive to EMT inducing stimuli that confer tumorigenic properties (54), while M12 expresses mesenchymal markers such as vimentin (17,54). We confirmed the epithelial and mesenchymal nature of these two cell pairs (Supplemental Fig. S2A). We included LNCaP and C4-2B as an additional lineage related model with differential metastatic potential. LNCaP is weakly tumorigenic (55,56), while C4-2B is an osteogenic derivative that is highly metastatic and efficiently forms bone metastases (57). Strikingly, we demonstrate that each of the three metastatic derivatives express several fold higher expression of eHsp90 relative to their less metastatic epithelial counterparts (Fig. 2A).

We next evaluated whether the secretion of eHsp90 in these cell pairs influenced tumor cell motility. To assess this, exogenous Hsp90 protein (to mimic eHsp90 secretion) was added to ARCaPE, while eHsp90 in ARCaPM was targeted by NPGA. Addition of eHsp90 elicited a greater than threefold increase in ARCaPE cell motility, while inhibition of eHsp90 function in ARCaPM resulted in a fivefold reduction of cell motility (Fig. 2B and Fig. S2B). Similar trends were noted in the P69/M12 pair (Fig. 2C and Fig. S2C). These findings solidify a causal relationship between eHsp90 expression and cell motility.

To establish whether eHsp90 elicited its effects via autocrine signaling through LRP1, we evaluated the impact of LRP1 suppression upon eHsp90 driven cell motility in ARCaPE. We show that downregulation of LRP1 suppressed ARCaPE basal migration, and completely blocked eHsp90 mediated cell motility (Fig. 2D and Fig. S2D). To provide further support for eHsp90 initiated pro-motility signaling events, we evaluated the ability of eHsp90 to stimulate the MEK-ERK axis, a critical component of cell motility (58). Our results indicate that eHsp90 elicits a rapid activation of MEK-ERK signaling (Fig. S2E), supporting an autocrine eHsp90 directed signaling pathway in promoting cell motility.

eHsp90 induces molecular and morphological changes consistent with an epithelial to mesenchymal transition

Our data are consistent with the premise that increased eHsp90 expression is associated with migratory potential and mesenchymal morphology. Given this correlation, we next examined whether eHsp90 functionally regulated molecular and morphologic events consistent with activation of an epithelial to mesenchymal transition (EMT). We utilized ARCaPE cells as an EMT responsive model representative of early disease. Our data indicate that eHsp90 suppressed E-cadherin, while increasing the mesenchymal proteins N-cadherin and Twist (Fig. 3A). Strikingly, addition of eHsp90 also induced morphological changes consistent with a mesenchymal phenotype, such as an elongated fibroblastic morphology, and conversion from a tightly packed epithelial cobblestone pattern to a loosely packed scattered phenotype. To assess the possible role of eHsp90 in supporting the mesenchymal phenotype of ARCaPM, eHsp90 was pharmacologically targeted by NPGA. This treatment reduced the mesenchymal marker N-cadherin, concomitantly reduced the extent of cell elongation and increased cell cohesiveness (Fig. 3B). E-cadherin is repressed in

ARCaPM (51) and NPGA treatment was unable to restore this expression.

To solidify these trends, we next examined the role of eHsp90 in the P69/M12 cell pair. Addition of eHsp90 to P69 recapitulated a similar transition toward mesenchymal-like characteristics, with a modest reduction of E-cadherin and increased expression N-cadherin and Twist (Fig. 3C). Addition of eHsp90 elicited similar EMT-like morphological changes, such as cell elongation and increased cell scattering. Targeting eHsp90 in the mesenchymal counterpart M12 resulted in decreased N-cadherin and a less dispersive phenotype, resulting in tight cellular clusters resembling epithelial cell types. These data indicate that targeting eHsp90 in mesenchymal cell types facilitates a reversal of a subset of EMT events, resulting in at least a partial mesenchymal to epithelial (MET) conversion.

Modest elevation of eHsp90 is sufficient to suppress E-cadherin function and promote cell motility.

Although treatment of cells with eHsp90 consistently elicited EMT-like events, use of bacterially produced protein is a less than ideal system, due to confounding factors such as batch variation, protein instability, the potential presence of endotoxin, or additional minor protein species in the preparations. To address these concerns and to create a more physiologically relevant and reproducible model, we designed a genetic approach for eHsp90 secretion by fusing a signal peptide to the N-terminus of Hsp90α. This approach has been shown to direct the extracellular localization of proteins (59), including the chaperone protein Hsp70 (60). Expression of Hsp90α was chosen due to the relative lack of activity of the Hsp90β isoform in our model (data not shown). Lentivirus expressing V5 tagged Hsp90 (V5-eHsp90) was used to infect ARCaPE cells, while ARCaPE cells transduced with V5-lacZ served as the control. Stably transduced ARCaPE (ARCaPE-eHsp90) exhibited a 3-fold increase in eHsp90 secretion, as determined by ELISA analysis for Hsp90α protein (Fig. 4A). The increased secretion was further confirmed by immunoblot analysis of conditioned media for Hsp90α, and by V5 detection, the latter of which is specific for exogenous V5-eHsp90 (Fig. 4A). Intracellular Hsp90 protein levels were not appreciably elevated in ARCaPE-eHsp90 (Fig. 4B). This model replicated the molecular effects of exogenously added protein, and was able to elicit the characteristic cadherin switch associated with EMT events (Fig. 4B). Furthermore, relative to control (ARCaPE-Lacz) cells, ARCaPE-eHsp90 demonstrated a sustained activation of the pro-motility kinase ERK, demonstrated a more mesenchymal morphology, and an approximately 2.5 fold increase in cell motility, the latter of which was suppressed by NPGA (Fig. 4C). Consistent with a pro-EMT role, blockade of eHsp90 reduced E-cadherin to control levels (Fig. 4D).

We next investigated whether eHsp90 affected the integrity of cellular junctional complexes. Loss of membrane localization of the gap junction protein ZO-1 frequently accompanies the disruption of cell polarity during EMT (51,61,62). As clearly demonstrated, diminished expression and protein mislocalization of both E-cadherin and ZO-1 was observed in ARCaPE-eHsp90 compared to control cells (Figs. 4E and 4F). A similar mislocalization of E-cadherin and ZO-1 was observed in a parallel genetic model of eHsp90 transduced P69 cells (P69-eHsp90) (Fig. S3A). To confirm the specific role of eHsp90 in modulating junctional complexes, we evaluated the ability of NPGA to normalize these structures in the ARCaPE model. As shown, both E-cadherin and ZO-1 protein localization was restored to regions of cell-cell contact, corresponding with the restoration of tightly packed cells with epithelial morphology (Figs. 4E and F).

To explore the possible therapeutic implications of eHsp90 treatment, we next examined whether eHsp90 inhibition in more aggressive mesenchymal cell lines might restore junctional complex integrity. Although NPGA did not elicit a re-expression of E-cadherin in ARCaPM, it partially restored membrane localization of ZO-1 (Fig. S3B). Pharmacologic targeting of eHsp90 in M12 cells dramatically restored the junctional localization of E-cadherin and elicited a modest effect upon ZO-1 (Fig. S3B). Taken together, our results indicate that eHsp90 is a pivotal regulator of the junctional complexes that influence epithelial and mesenchymal morphology.

eHsp90 modulates the expression of multiple genes associated with EMT activation

To further strengthen the EMT-initiating role of eHsp90, we evaluated its ability to modulate additional EMT-associated transcripts. To monitor the temporal effects of eHsp90 action, RNA was harvested from ARCaPE cells following exposure to eHsp90 protein for the indicated times. The resultant heat map from a qRT-PCR array demonstrates that eHsp90 regulates a large number of EMT transcripts (Fig. 5A), including N-cadherin, as supported by our protein expression data. Longer eHsp90 protein treatments most effectively increased the core EMT mediators Snail, Slug, Zeb1 and Zeb2. Changes were also observed in cytoskeletal, integrin/ECM proteins, and proteolytic proteins.

To confirm these results, and to more carefully interrogate temporal effects, a subset of these targets was validated in ARCaPE in response to protein exposure for 1, 3, or 5 days. As shown, E-cadherin was progressively suppressed in a time dependent manner (Fig. 5B). Transcriptional upregulation of the key EMT mediators Snail, Slug, Zeb1, and Zeb2 was also validated by qRT-PCR. Our findings indicate that Slug and Zeb1 are early responders to eHsp90, whereas Snail and especially Zeb2 exhibit a delayed response. We next evaluated expression of these transcripts in our ARCaPE-eHsp90 genetic model. Whereas the suppression of E-cadherin was consistent, there was a less dramatic, but statistically significant increase in both Snail and Zeb1. Transcripts for Slug were decreased, implicating this effector as eliciting an early and possibly transient role. A robust increase in Zeb2 suggests that this EMT factor may be required for later events, a finding in accordance with the later elevation of this transcript following protein exposure. In addition to these core EMT transcripts, we also evaluated expression of matrix metalloproteinases (MMPs), zinc-dependent endopeptidases that degrade components of the basement membrane, promote EMT events and support metastatic spread (63,64). We found that MMP-9 transcript expression was upregulated greater than three-fold in both protein treated ARCaPE and ARCaPE-eHsp90 cells (Fig. 5C). In contrast, MMP-3, which also plays an important role in EMT events (65), was preferentially elevated at earlier time points in the protein treated model, whereas MMP-2 was only upregulated in the ARCaPE-eHsp90 genetic model.

MMP and ERK activity are required for eHsp90 mediated motility and EMT events

It has been demonstrated that eHsp90 directly interacts with MMP-2/9 to modulate proteolytic activity and subsequent cell motility (35,66-68). We therefore utilized a standard zymogen gelatinase assay to determine whether the elevated levels of eHsp90 in ARCaPE-eHsp90 would be sufficient to increase MMP activity. As shown, MMP-2 and MMP-9 activity was increased in ARCaPE-eHsp90 cells relative to ARCaPE-LacZ control (Fig. 6A). As expected, this increase was abrogated by NPGA, demonstrating that eHsp90 is the initiating stimulus for increased MMP-2/9 activity. Given that eHsp90 activates ERK in ARCaPE-eHsp90, and the demonstrated

ability of ERK to regulate MMP-2/9 activity (69,70), we evaluated the effects of ERK upon MMP-2/9. ERK inhibition most effectively blocked this activity, supporting the premise that eHsp90 mediated ERK activation is an initiating event for MMP-2/9 activation.

We next evaluated the effect of MMP-2/9, MMP-3 and ERK upon E-cadherin transcript levels in ARCaPE-eHsp90. As indicated, broad spectrum targeting with GM60001 or MMP-2/9 inhibition robustly increased (approximately 10-fold) E-cadherin message levels, comparably to NPGA (Fig. 6B). MMP-3 inhibition weakly induced transcript expression, while UO126 elicited a potent (approximately 35-fold) increase. We further investigated whether these trends correlated with changes in E-cadherin protein expression. Inhibition of either MMP-2/9 or MMP-3 comparably restored E-cadherin protein expression by 3 days, whereas UO126 promoted the most dramatic restoration, in accordance with its effects upon message levels (Fig. 6C). It is unclear why MMP inhibition diminished E-cadherin at 5 days, as this trend was not supported via immunofluorescence microscopy (Fig 6D). It has been shown that E-cadherin may be found in an insoluble membrane fraction (71,72) when associated with the cytoskeletal matrix at apical junctions, offering a potential explanation. Interestingly, inhibition of either MMP-2/9 or MMP-3 attenuated ERK activity, with a more dramatic effect elicited by the former, indicating that these MMPs collaborate with eHsp90-ERK mediated suppression of E-cadherin.

Given that inhibition of MMP-2/9, MMP-3 and ERK increased E-cadherin expression, we assessed whether this effect trended with the restoration of E-cadherin at cellular junctions, a hallmark of its EMT suppressive epithelial function. As shown (Fig. 6D), pan MMP inhibition, or targeted inhibition of MMP-3, MMP-2/9, or ERK, comparably re-established E-cadherin expression at the cell membrane in ARCaPE-eHsp90. Functional restoration of junctional complexes was further confirmed by the membrane expression ZO-1. These findings demonstrate that eHsp90 mediated activation of ERK and MMPs is required for the loss in cell polarity that accompanies the transition to a mesenchymal morphology.

We next evaluated whether MMP and ERK activity were important for eHsp90 directed pro-motility function. As shown, pan MMP inhibition with GM6001 blocked eHsp90 mediated cell motility (Fig. 6E). Interestingly, specific targeting of MMP-2/9 or MMP-3 elicited a similar inhibition, highlighting a prominent role for MMP signaling in eHsp90 directed pro-motility function. ERK inhibition comparably diminished cell migration. Therefore, MMP and ERK are critical regulators of eHsp90's coordinate effects upon junctional integrity and cell motility.

Detection of eHsp90 protein and regulated transcripts in human prostatectomy tumor specimens

The ability of eHsp90 to initiate EMT events has important clinical ramifications. We therefore investigated the potential translational relevance of our results and determined whether eHsp90 was found in primary PCa tumors. We reasoned that tumor cells with autocrine eHsp90 function would be represented by a subpopulation exhibiting higher cell surface eHsp90. Therefore, prostatectomy specimens from high risk, locally advanced patients were subjected to FACS sorting, and tumor cell populations isolated by either high or low surface eHsp90α expression. Interestingly, this approach reproducibly detected a subpopulation of eHsp90^{high} cells corresponding to approximately 5% of the total cell number (Fig. 7A). We next investigated whether surface eHsp90 could be utilized as a marker to define a genetically distinct subpopulation of tumor cells. A modest increase in MMP-2 and a marked induction of MMP-9 was evident in these specimens, when comparing the

eHsp90^{high} population of tumor cells, relative to each tumor matched eHsp90^{low} population (Fig. 7B). No increases were observed in MMP-3 transcript expression. Intriguingly, these data parallel the trends observed in our constitutively expressing ARCaPE-eHsp90 genetic model (Fig. 5C). Importantly, these findings validate the clinical presence of eHsp90 in primary patient tumors, and further support the notion that eHsp90 may drive genetic events associated with increased risk for tumor progression. A working model for eHsp90 mediated EMT events and tumor promotion is depicted in Fig. 7C.

DISCUSSION

Although reports demonstrate the ability of eHsp90 to promote cell motility (30-34) and facilitate metastatic spread in preclinical models (36-38,43), a unifying mechanistic basis for eHsp90 tumorigenic function has not yet been clearly defined. To our knowledge, we are the first to identify eHsp90 as a pivotal initiator of EMT-like events. We demonstrate that eHsp90 increases the cell motility of epithelial ARCaPE and P69 several fold. This pro-motility function of eHsp90 is dependent upon its impairment of E-cadherin, manifest as diminished protein expression and aberrant cellular localization. Strikingly, eHsp90 elicited dramatic changes in cell morphology, converting cells from an epithelial cuboidal clustered morphology to an elongated mesenchymal morphology with loss of cell-cell contacts. Thus, eHsp90 coordinates a multitude of key events associated with cancer progression, including impaired E-cadherin function, loss of junctional integrity, initiation of EMT, and increased cell motility. Importantly, these events were achieved with relatively modest increases in eHsp90 expression comparable to levels observed in metastatic PCa tumor cells and patient sera, further underscoring that eHsp90 is a potent driver of these processes.

The EMT initiating activity of eHsp90 was further supported by its ability to modulate a wide array of genetic events consistent with this program, including upregulation of the EMT effectors Snail, Twist, Zeb, and Slug. Not surprisingly, these factors also serve as transcriptional repressors of E-cadherin (74-77), in accordance with diminished E-cadherin message observed in ARCaPE-eHsp90. The finding that eHsp90 increases transcript expression of the proteolytic enzymes MMP-2, MMP-3 and MMP-9 is relevant given that sustained MMP-2/9 activity increases the tumorigenic and metastatic properties of ARCaPE (19), and initiates EMT events and tumor progression in preclinical models of PCa (19,78). While a causal role for MMPs in tumor progression is well known, the relation between eHsp90 and MMPs is still unfolding. Reports demonstrate that eHsp90 increases the proteolytic activity of MMP-2/9 via direct protein-protein interactions (35,66-68). Our results indicate that eHsp90 plays a dual role in upregulating MMP-2/9 transcript expression, as well as increasing proteolytic function. Given that the eHsp90 regulated EMT transcriptional effectors additionally contribute to MMP expression (79-81), MMP proteolytic activity may be further influenced by these factors, as well as by direct eHsp90-chaperone mediated mechanisms (82).

Collectively, our data support a model (Fig. 7C) whereby an eHsp90-LRP1 signaling axis activates ERK and MMP activity to promote increased cell motility, impairment of E-cadherin function, and initiation of EMT events. The ability of eHsp90 to sustain ERK activation is significant, given the reported role of ERK as a potent effector of EMT, motility, malignant invasion, and metastasis (58,83-86). Our data indicate that the relationships among ERK, MMPs, and EMT are complex. eHsp90 rapidly initiates ERK activation, which is required for increased MMP-2/9 activity, supporting ERK as an upstream regulator of MMP function. In addition, it

was shown that ERK may be activated by MMP-2/9 in ARCaPE and other cancer models (19). Our data also indicate that ERK may additionally function downstream of MMP-2/9. We therefore propose that eHsp90 mediated MMP-2/9 activity is required to potentiate and sustain ERK activity, implicating a feed-forward mechanism. Our data support a contributory role for MMP-3, and MMP-3 has been implicated in promoting cell motility (65), at least in part via activation of MMP-9 (87).

Further work is required to clarify the precise contribution of these proteins to eHsp90 mediated ERK activation and E-cadherin suppression. Additional functions for MMP-2/9 may be considered (Fig 7C). First, MMP-2/9 signaling may induce ERK activation via growth factor initiated receptor activation (19). Although we cannot exclude this possibility, LRP1 silencing precludes ERK activation, indicating that LRP1 plays a dominant role in this process. Second, MMP-2/9 may cleave E-cadherin, thereby attenuating its tumor suppressive function (88). Although this is possible, we did not observe cleavage products (unpublished), and MMP suppressive activity is at least partially due to its modulation of E-cadherin transcript expression. Third, MMP-9 is a ligand for LRP1 (89) and may signal through LRP1 in a non-proteolytic manner to regulate ERK activity (90). Nonetheless, our data conclusively establish that MMP-2/9 and ERK are critical regulators of eHsp90's coordinate effects upon junctional integrity and cell motility.

Hsp90 has been detected from patient serum and ascites fluid in a number of cancer types (37,41,91,92), yet the source of this protein remains unclear. In support of a regulated secretory pathway, surface eHsp90 is detected from patients with metastatic melanoma tumors (93). Our discovery that Hsp90α is found on the surface of a subpopulation of primary tumor cells further reinforces a regulated pathway for Hsp90 secretion. A striking finding is the increased expression of MMP-2 and MMP-9 transcripts associated with the eHsp90^{high} population of tumor cells, which supports trends from our cell based models. Although it is possible that non-tumorigenic and/or stromal cells may be present in these preparations, this does not change the interpretation of our results that eHsp90 appears to mark a distinct (presumably tumor) population of cells exhibiting transcripts associated with protumorigenic properties. Our finding that a relatively small subpopulation of eHsp90 expressing tumor cells may contribute to PCa progression also highlights the challenges in identifying a unifying genetic signature indicative of EMT events clinical samples.

Despite its EMT inducing activity, eHsp90 was unable to enforce a permanent EMT, demonstrated by the ability of NPGA to reverse EMT like events in ARCaPE-eHsp90. Within this context, it was remarkable that continued eHsp90 expression was also required to sustain the aggressive properties of metastatic PCa cell types, including cell motility, expression of N-cadherin, and mesenchymal morphology. This constitutive reliance upon eHsp90 may be widespread, supported by the reported ability of eHsp90 targeting to suppress the metastatic potential of breast and other tumor types (35-38). Although the eHsp90 mediated induction of MMP-2/9 has been implicated in several of these models, (35,37), the precise eHsp90 directed molecular events driving metastatic potential remain unresolved. A recent report has also implicated a role for N-cadherin in the invasion and metastasis of PCa (94). In light of these reports, the ability of eHsp90 targeting to attenuate a subset of EMT events may have clinical utility in blocking or delaying cancer progression. Although more mechanistic details need to be elucidated, our data conclusively position eHsp90 as a novel and pivotal effector of tumor cell EMT plasticity.

REFERENCES

1. Arya, M., Bott, S. R., Shergill, I. S., Ahmed, H. U., Williamson, M., and Patel, H. R. (2006) *Surg Oncol* **15**, 117-128
2. Crawford, E. D. (2009) *Urology* **73**, S4-10
3. Jemal, A., Siegel, R., Ward, E., Hao, Y., Xu, J., and Thun, M. J. (2009) *CA Cancer J Clin* **59**, 225-249
4. Efstathiou, E., and Logothetis, C. J. (2010) *Clin Cancer Res* **16**, 1100-1107
5. Siegel, R., Naishadham, D., and Jemal, A. (2012) *CA Cancer J Clin* **62**, 10-29
6. Culp, S., and Porter, M. (2009) *BJU Int* **104**, 1457-1461
7. Strope, S. A., and Andriole, G. L. (2010) *Nat Rev Urol* **7**, 487-493
8. Andriole, G. L. (2009) *Nat Rev Urol* **6**, 188-189
9. Markert, E. K., Mizuno, H., Vazquez, A., and Levine, A. J. (2011) *Proc Natl Acad Sci U S A* **108**, 21276-21281
10. Polyak, K., and Weinberg, R. A. (2009) *Nat Rev Cancer* **9**, 265-273
11. Thiery, J. P., Acloque, H., Huang, R. Y., and Nieto, M. A. (2009) *Cell* **139**, 871-890
12. Hanahan, D., and Weinberg, R. A. (2011) *Cell* **144**, 646-674
13. Onder, T. T., Gupta, P. B., Mani, S. A., Yang, J., Lander, E. S., and Weinberg, R. A. (2008) *Cancer Res* **68**, 3645-3654
14. Zhau, H. E., Li, C. L., and Chung, L. W. (2000) *Cancer* **88**, 2995-3001
15. Xu, J., Wang, R., Xie, Z. H., Odero-Marah, V., Pathak, S., Multani, A., Chung, L. W., and Zhau, H. E. (2006) *Prostate* **66**, 1664-1673
16. Acevedo, V. D., Gangula, R. D., Freeman, K. W., Li, R., Zhang, Y., Wang, F., Ayala, G. E., Peterson, L. E., Ittmann, M., and Spencer, D. M. (2007) *Cancer Cell* **12**, 559-571
17. Zhang, X., Fournier, M. V., Ware, J. L., Bissell, M. J., Yacoub, A., and Zehner, Z. E. (2009) *Mol Cancer Ther* **8**, 499-508
18. Mak, P., Leav, I., Pursell, B., Bae, D., Yang, X., Taglienti, C. A., Gouvin, L. M., Sharma, V. M., and Mercurio, A. M. (2010) *Cancer Cell* **17**, 319-332
19. Lue, H. W., Yang, X., Wang, R., Qian, W., Xu, R. Z., Lyles, R., Osunkoya, A. O., Zhou, B. P., Vessella, R. L., Zayzafoon, M., Liu, Z. R., Zhau, H. E., and Chung, L. W. (2011) *PLoS One* **6**, e27720
20. Xie, D., Gore, C., Liu, J., Pong, R. C., Mason, R., Hao, G., Long, M., Kabbani, W., Yu, L., Zhang, H., Chen, H., Sun, X., Boothman, D. A., Min, W., and Hsieh, J. T. (2010) *Proc Natl Acad Sci U S A* **107**, 2485-2490
21. Kwok, W. K., Ling, M. T., Lee, T. W., Lau, T. C., Zhou, C., Zhang, X., Chua, C. W., Chan, K. W., Chan, F. L., Glackin, C., Wong, Y. C., and Wang, X. (2005) *Cancer Res* **65**, 5153-5162
22. Graham, T. R., Zhau, H. E., Odero-Marah, V. A., Osunkoya, A. O., Kimbro, K. S., Tighiouart, M., Liu, T., Simons, J. W., and O'Regan, R. M. (2008) *Cancer Res* **68**, 2479-2488
23. Contreras, H. R., Ledezma, R. A., Vergara, J., Cifuentes, F., Barra, C., Cabello, P., Gallegos, I., Morales, B., Huidobro, C., and Castellon, E. A. (2010) *Urol Oncol* **28**, 534-540
24. Zhang, Q., Helfand, B. T., Jang, T. L., Zhu, L. J., Chen, L., Yang, X. J., Kozlowski, J., Smith, N., Kundu, S. D., Yang, G., Raji, A. A., Javonovic, B., Pins, M., Lindholm, P., Guo, Y., Catalona, W. J., and Lee, C. (2009) *Clin Cancer Res* **15**, 3557-3567
25. Sun, Y., Wang, B. E., Leong, K. G., Yue, P., Li, L., Jhunjhunwala, S., Chen, D., Seo, K., Modrusan, Z., Gao, W. Q., Settleman, J., and Johnson, L. (2012) *Cancer Res* **72**, 527-536
26. Isaacs, J. S., Xu, W., and Neckers, L. (2003) *Cancer Cell* **3**, 213-217
27. Whitesell, L., and Lindquist, S. L. (2005) *Nat Rev Cancer* **5**, 761-772

28. Bohonowych, J. E., Gopal, U., and Isaacs, J. S. (2010) *J Oncol* **2010**, 412985
29. Cheng, C. F., Fan, J., Fedesco, M., Guan, S., Li, Y., Bandyopadhyay, B., Bright, A. M., Yerushalmi, D., Liang, M., Chen, M., Han, Y. P., Woodley, D. T., and Li, W. (2008) *Molecular and cellular biology* **28**, 3344-3358
30. Gopal, U., Bohonowych, J. E., Lema-Tome, C., Liu, A., Garrett-Mayer, E., Wang, B., and Isaacs, J. S. (2011) *PLoS One* **6**, e17649
31. Becker, B., Multhoff, G., Farkas, B., Wild, P. J., Landthaler, M., Stolz, W., and Vogt, T. (2004) *Exp Dermatol* **13**, 27-32
32. Eustace, B. K., Sakurai, T., Stewart, J. K., Yimlamai, D., Unger, C., Zehetmeier, C., Lain, B., Torella, C., Henning, S. W., Beste, G., Scroggins, B. T., Neckers, L., Ilag, L. L., and Jay, D. G. (2004) *Nat Cell Biol* **6**, 507-514
33. Sidera, K., Gaitanou, M., Stellas, D., Matsas, R., and Patsavoudi, E. (2008) *J Biol Chem* **283**, 2031-2041
34. Yang, Y., Rao, R., Shen, J., Tang, Y., Fiskus, W., Nechtman, J., Atadja, P., and Bhalla, K. (2008) *Cancer Res* **68**, 4833-4842
35. Stellas, D., El Hamidieh, A., and Patsavoudi, E. (2010) *BMC Cell Biol* **11**, 51
36. Tsutsumi, S., Scroggins, B., Koga, F., Lee, M. J., Trepel, J., Felts, S., Carreras, C., and Neckers, L. (2008) *Oncogene* **27**, 2478-2487
37. Wang, X., Song, X., Zhuo, W., Fu, Y., Shi, H., Liang, Y., Tong, M., Chang, G., and Luo, Y. (2009) *Proc Natl Acad Sci U S A* **106**, 21288-21293
38. Sahu, D., Zhao, Z., Tsen, F., Cheng, C. F., Park, R., Situ, A. J., Dai, J., Eginli, A., Shams, S., Chen, M., Ulmer, T. S., Conti, P., Woodley, D. T., and Li, W. (2012) *Mol Biol Cell* **23**, 602-613
39. Ullrich, S. J., Robinson, E. A., Law, L. W., Willingham, M., and Appella, E. (1986) *Proc Natl Acad Sci U S A* **83**, 3121-3125
40. Luo, L. Y., Herrera, I., Soosaipillai, A., and Diamandis, E. P. (2002) *Br J Cancer* **87**, 339-343
41. Burgess, E. F., Ham, A. J., Tabb, D. L., Billheimer, D., Roth, B. J., Chang, S. S., Cookson, M. S., Hinton, T. J., Cheek, K. L., Hill, S., and Pietenpol, J. A. (2008) *Proteomics Clin Appl* **2**, 1223-1233
42. Garraway, I. P., Sun, W., Tran, C. P., Perner, S., Zhang, B., Goldstein, A. S., Hahm, S. A., Haider, M., Head, C. S., Reiter, R. E., Rubin, M. A., and Witte, O. N. (2010) *Prostate* **70**, 491-501
43. Stellas, D., El Hamidieh, A., and Patsavoudi, E. (2010) *BMC Cell Biol* **11**, 51
44. Qin, Z., DeFee, M., Isaacs, J. S., and Parsons, C. (2010) *Virology* **403**, 92-102
45. Orr, A. W., Pedraza, C. E., Pallero, M. A., Elzie, C. A., Goicoechea, S., Strickland, D. K., and Murphy-Ullrich, J. E. (2003) *J Cell Biol* **161**, 1179-1189
46. Shi, Y., Mantuano, E., Inoue, G., Campana, W. M., and Gonias, S. L. (2009) *Sci Signal* **2**, ra18
47. Langlois, B., Perrot, G., Schneider, C., Henriet, P., Emonard, H., Martiny, L., and Dedieu, S. (2010) *PLoS One* **5**, e11584
48. Polyak, K., and Weinberg, R. A. (2009) *Nat Rev Cancer* **9**, 265-273
49. Zhau, H. Y., Chang, S. M., Chen, B. Q., Wang, Y., Zhang, H., Kao, C., Sang, Q. A., Pathak, S. J., and Chung, L. W. (1996) *Proc Natl Acad Sci U S A* **93**, 15152-15157
50. He, H., Yang, X., Davidson, A. J., Wu, D., Marshall, F. F., Chung, L. W., Zhau, H. E., and Wang, R. (2010) *Prostate* **70**, 518-528
51. Zhau, H. E., Odero-Marah, V., Lue, H. W., Nomura, T., Wang, R., Chu, G., Liu, Z. R., Zhou, B. P., Huang, W. C., and Chung, L. W. (2008) *Clin Exp Metastasis* **25**, 601-610
52. Josson, S., Nomura, T., Lin, J. T., Huang, W. C., Wu, D., Zhau, H. E., Zayzafoon, M., Weizmann, M. N., Gururajan, M., and Chung, L. W. (2011) *Cancer Res* **71**, 2600-2610

53. Bae, V. L., Jackson-Cook, C. K., Maygarden, S. J., Plymate, S. R., Chen, J., and Ware, J. L. (1998) *Prostate* **34**, 275-282
54. Rojas, A., Liu, G., Coleman, I., Nelson, P. S., Zhang, M., Dash, R., Fisher, P. B., Plymate, S. R., and Wu, J. D. (2011) *Oncogene* **30**, 2345-2355
55. Fu, X., Herrera, H., and Hoffman, R. M. (1992) *Int J Cancer* **52**, 987-990
56. Stephenson, R. A., Dinney, C. P., Gohji, K., Ordonez, N. G., Killion, J. J., and Fidler, I. J. (1992) *J Natl Cancer Inst* **84**, 951-957
57. Thalmann, G. N., Anezinis, P. E., Chang, S. M., Zhau, H. E., Kim, E. E., Hopwood, V. L., Pathak, S., von Eschenbach, A. C., and Chung, L. W. (1994) *Cancer Res* **54**, 2577-2581
58. Smolen, G. A., Zhang, J., Zubrowski, M. J., Edelman, E. J., Luo, B., Yu, M., Ng, L. W., Scherber, C. M., Schott, B. J., Ramaswamy, S., Irimia, D., Root, D. E., and Haber, D. A. (2010) *Genes Dev* **24**, 2654-2665
59. Janda, C. Y., Li, J., Oubridge, C., Hernandez, H., Robinson, C. V., and Nagai, K. (2010) *Nature* **465**, 507-510
60. Figueiredo, C., Wittmann, M., Wang, D., Dressel, R., Seltsam, A., Blasczyk, R., and Eiz-Vesper, B. (2009) *Blood* **113**, 3008-3016
61. Thiery, J. P. (2003) *Curr Opin Cell Biol* **15**, 740-746
62. Polette, M., Gilles, C., Nawrocki-Raby, B., Lohi, J., Hunziker, W., Foidart, J. M., and Birembaut, P. (2005) *Cancer Res* **65**, 7691-7698
63. Chambers, A. F., and Matrisian, L. M. (1997) *J Natl Cancer Inst* **89**, 1260-1270
64. Nistico, P., Bissell, M. J., and Radisky, D. C. (2012) *Cold Spring Harb Perspect Biol* **4**
65. Radisky, D. C., Levy, D. D., Littlepage, L. E., Liu, H., Nelson, C. M., Fata, J. E., Leake, D., Godden, E. L., Albertson, D. G., Nieto, M. A., Werb, Z., and Bissell, M. J. (2005) *Nature* **436**, 123-127
66. Eustace, B. K., Sakurai, T., Stewart, J. K., Yimlamai, D., Unger, C., Zehetmeier, C., Lain, B., Torella, C., Henning, S. W., Beste, G., Scroggins, B. T., Neckers, L., Ilag, L. L., and Jay, D. G. (2004) *Nat Cell Biol* **6**, 507-514
67. Lagarrigue, F., Dupuis-Coronas, S., Ramel, D., Delsol, G., Tronchere, H., Payrastre, B., and Gaits-Iacovoni, F. (2010) *Cancer Res* **70**, 6978-6987
68. Song, X., Wang, X., Zhuo, W., Shi, H., Feng, D., Sun, Y., Liang, Y., Fu, Y., Zhou, D., and Luo, Y. (2010) *J Biol Chem* **285**, 40039-40049
69. Ito, H., Duxbury, M., Benoit, E., Clancy, T. E., Zinner, M. J., Ashley, S. W., and Whang, E. E. (2004) *Cancer Res* **64**, 7439-7446
70. Yoshida, T., Hisamoto, T., Akiba, J., Koga, H., Nakamura, K., Tokunaga, Y., Hanada, S., Kumemura, H., Maeyama, M., Harada, M., Ogata, H., Yano, H., Kojiro, M., Ueno, T., Yoshimura, A., and Sata, M. (2006) *Oncogene* **25**, 6056-6066
71. Hinck, L., Nathke, I. S., Papkoff, J., and Nelson, W. J. (1994) *J Cell Biol* **125**, 1327-1340
72. Liwosz, A., Lei, T., and Kukuruzinska, M. A. (2006) *J Biol Chem* **281**, 23138-23149
73. McCready, J., Sims, J. D., Chan, D., and Jay, D. G. (2010) *BMC Cancer* **10**, 294
74. Batlle, E., Sancho, E., Franci, C., Dominguez, D., Monfar, M., Baulida, J., and Garcia De Herreros, A. (2000) *Nat Cell Biol* **2**, 84-89
75. Cano, A., Perez-Moreno, M. A., Rodrigo, I., Locascio, A., Blanco, M. J., del Barrio, M. G., Portillo, F., and Nieto, M. A. (2000) *Nat Cell Biol* **2**, 76-83
76. Grooteclaes, M. L., and Frisch, S. M. (2000) *Oncogene* **19**, 3823-3828
77. Yang, J., Mani, S. A., Donaher, J. L., Ramaswamy, S., Itzykson, R. A., Come, C., Savagner, P., Gitelman, I., Richardson, A., and Weinberg, R. A. (2004) *Cell* **117**, 927-939
78. Johnson, T. R., Koul, S., Kumar, B., Khandrika, L., Venezia, S., Maroni, P. D., Meacham, R. B., and Koul, H. K. (2010) *Mol Cancer* **9**, 148
79. Jorda, M., Olmeda, D., Vinyals, A., Valero, E., Cubillo, E., Llorens, A., Cano, A., and Fabra, A. (2005) *J Cell Sci* **118**, 3371-3385

80. Sun, L., Diamond, M. E., Ottaviano, A. J., Joseph, M. J., Ananthanarayan, V., and Munshi, H. G. (2008) *Mol Cancer Res* **6**, 10-20
81. Zhao, X. L., Sun, T., Che, N., Sun, D., Zhao, N., Dong, X. Y., Gu, Q., Yao, Z., and Sun, B. C. (2011) *J Cell Mol Med* **15**, 691-700
82. Sims, J. D., McCready, J., and Jay, D. G. (2011) *PLoS One* **6**, e18848
83. Ellenrieder, V., Hendler, S. F., Boeck, W., Seufferlein, T., Menke, A., Ruhland, C., Adler, G., and Gress, T. M. (2001) *Cancer Res* **61**, 4222-4228
84. Vial, E., Sahai, E., and Marshall, C. J. (2003) *Cancer Cell* **4**, 67-79
85. Doehn, U., Hauge, C., Frank, S. R., Jensen, C. J., Duda, K., Nielsen, J. V., Cohen, M. S., Johansen, J. V., Winther, B. R., Lund, L. R., Winther, O., Taunton, J., Hansen, S. H., and Frodin, M. (2009) *Mol Cell* **35**, 511-522
86. Shin, S., Dimitri, C. A., Yoon, S. O., Dowdle, W., and Blenis, J. (2010) *Mol Cell* **38**, 114-127
87. Johnson, J. L., Dwivedi, A., Somerville, M., George, S. J., and Newby, A. C. (2011) *Arterioscler Thromb Vasc Biol* **31**, e35-44
88. Rajasekaran, A. K., and David, J. M. (2012) *Cancer Res* **72**, 2917-2923
89. Hahn-Dantona, E., Ruiz, J. F., Bornstein, P., and Strickland, D. K. (2001) *J Biol Chem* **276**, 15498-15503
90. Mantuano, E., Inoue, G., Li, X., Takahashi, K., Gaultier, A., Gonias, S. L., and Campana, W. M. (2008) *J Neurosci* **28**, 11571-11582
91. Luo, L. Y., Herrera, I., Soosaipillai, A., and Diamandis, E. P. (2002) *Br J Cancer* **87**, 339-343
92. Vidal, C. I., Mintz, P. J., Lu, K., Ellis, L. M., Manenti, L., Giavazzi, R., Gershenson, D. M., Broaddus, R., Liu, J., Arap, W., and Pasqualini, R. (2004) *Oncogene* **23**, 8859-8867
93. Becker, B., Multhoff, G., Farkas, B., Wild, P. J., Landthaler, M., Stolz, W., and Vogt, T. (2004) *Exp Dermatol* **13**, 27-32
94. Tanaka, H., Kono, E., Tran, C. P., Miyazaki, H., Yamashiro, J., Shimomura, T., Fazli, L., Wada, R., Huang, J., Vessella, R. L., An, J., Horvath, S., Gleave, M., Rettig, M. B., Wainberg, Z. A., and Reiter, R. E. (2010) *Nat Med* **16**, 1414-1420

ACKNOWLEDGEMENTS

We thank Joy Ware for the P69 and M12 cells, Chris Lindsey and Craig Beeson for synthesis of DMAG-N-oxide (NPGA), and Enzo Life Sciences for their generous reagent support. Imaging facilities for this research were supported, in part, by Cancer Center Support Grant P30 CA138313 to the Hollings Cancer Center, Medical University of South Carolina. We also thank Philip Howe and Simon Hayward for their critical comments on this manuscript.

FOOTNOTES

This work was primarily supported by NIH grant R01 CA135297 (to J. S. I.). Additional funding sources include NIH T32 training grant CA119945 (to M.W.H.) and
IRACDA training grant K12 GM081265 (to J. E. B.)
[§]These authors contributed equally

[*]To whom correspondence should be addressed:
Department of Cell and Molecular Pharmacology
Medical University of South Carolina
Hollings Cancer Center
86 Jonathan Lucas St
Charleston, SC, 29425
Tel: 843-792-8393
Fax: 843-792-3200
email:isaacsj@musc.edu

Abbreviations: eHsp90, extracellular Hsp90; ERK, extracellular signal-regulated kinase; PCa, prostate cancer; MMP, matrix metalloprotease, NPGA, nonpermeable GA; EMT, epithelial to mesenchymal transition; PSA, prostate specific antigen; MEK, MAPK kinase; FAK, focal adhesion kinase; LRP1, low density lipoprotein related protein; shRNA, short hairpin RNA; fluorescence-activated cell sorting, FACS

FIGURE LEGENDS

FIGURE 1. An eHsp90-LRP1 signaling pathway initiates prostate cancer cell motility. *A*, Representative results from a scratch wound assay with PC3 prostate cancer cells following treatment with NPGA (1 uM) or either of two eHsp90 targeting antibodies (SPA-830, Ab1; SPS-771, Ab2). *B*, Similar assay with DU145 cells transduced with either scrambled (scr) shRNA or shLRP1. *C*, Pharmacologic targeting of eHsp90 with NPGA (1 uM, 16 hr) and effects upon FAK and ERK activity. *D*, Comparison of shLRP1 and NPGA upon FAK and ERK activity. UT refers to untreated vehicle control. Asterisks (*) indicate significance of $p \leq 0.05$.

FIGURE 2. eHsp90 is elevated in more aggressive PCa cell types and is essential for cell motility. *A*, Detection of secreted eHsp90 alpha from the conditioned media of indicated cell pairs was assessed by ELISA. Each cell pair is lineage related, with the more metastatic derivative in black. *B*, Scratch wound assay assessed the effects of either exogenous eHsp90 protein (3 day pre-treatment, 3 ug/ml) upon ARCaPE cell motility, or treatment of ARCaPM cells with NPGA. *C*, Similar treatment of epithelial P69 cells with eHsp90, and NPGA treatment of the metastatic counterpart M12. *D*, Effect of shLRP1 upon eHsp90 mediated cell motility in ARCaPE. UT refers to untreated vehicle control. Asterisks (*) indicate significance of p-value ≤ 0.05.

FIGURE 3. eHsp90 induces molecular and morphological changes consistent with an epithelial to mesenchymal transition. *A*, ARCaPE cells treated for the indicated times with exogenous Hsp90 protein, and immunoblot analysis of epithelial E-cadherin (E-cad) and mesenchymal proteins N-cadherin (N-Cad) and Twist. Phase contrast images of cell morphology. *B*, Effects of NPGA treatment of ARCaPM upon E- and N-cadherin expression and corresponding cell morphology. *C*, Analysis of eHsp90 treatment of P69 non-tumorigenic cells as in A. *D*, Analysis of NPGA treatment of M12 as in B.

FIGURE 4. Modest elevation of eHsp90 is sufficient to suppress E-cadherin function and promote cell motility. *A*, (Upper panel) ELISA analysis of eHsp90 secretion from conditioned media collected from parental ARCaPE cells stably transduced with control (lacZ) or V5 tagged eHsp90 alpha lentivirus. (Lower panel) Immunoblot detection of total (endogenous and exogenous) eHsp90 alpha, or V5 detection of transduced eHsp90 protein. *B*, Immunoblot analysis of cell lysates from ARCaPE-LacZ or ARCaPE-eHsp90 confirmed consistent levels of intracellular eHsp90 alpha (IC Hsp90). Indicated analysis of E- and N- cadherin and ERK activity. *C*, Representative morphology of indicated ARCaPE cells. Analysis of cell motility of ARCaPE-eHsp90 either untreated or treated with NPGA. *D*, Effect of NPGA upon E-cadherin expression in ARCaPE-eHsp90. *E*, Analysis of E-cadherin localization in ARCaPE-LacZ and ARCaPE-eHsp90 untreated cells, or treated for the indicated times with NPGA. *F*, Membrane localization of ZO1 in ARCaPE-LacZ and ARCaPE-eHsp90 untreated cells, or treated with NPGA for 3 days. Asterisks (*) indicate significance of p-value ≤ 0.05. Scale bar is 50 um.

FIGURE 5. eHsp90 modulates the expression of multiple genes associated with EMT activation. *A*, A focused EMT qRT-PCR array was utilized to assess EMT regulated genes modulated by eHsp90 in ARCaPE cells. Samples for array data were derived from two identical biological replicate experiments. *B*, Transcript expression of E-cadherin and the indicated EMT transcriptional effectors from the array were validated by qRT-PCR in untreated (UT) ARCaPE or cells treated with eHsp90 protein for 1, 3, or 5 days (upper panel), whereas a similar analysis was performed for control or ARCaPE-eHsp90 genetically modified cells (lower panel). *C*, Increased expression of proteolytic MMP transcripts was also validated from both protein treated (upper panel) and ARCaPE-eHsp90 modified cells (lower panel). Quantitative PCR

levels were normalized to GAPDH expression. UT refers to untreated vehicle control. Asterisks (*) indicate significance of p-value $\leq$ 0.05.

FIGURE 6. MMP and ERK activity are required for eHsp90 mediated motility and EMT events . *A*, A gelatin zymography assay was utilized to assay MMP-2/9 activity in control or ARCaPE-Hsp90 cells. For indicated inhibitors, cells were treated for 2 days prior to media collection. Cells were treated with ERK inhibitor (UO126, 10 uM), MMP-2/9 inhibitor (SB-3CT, 1 uM), or NPGA (1 uM). B, Transcript expression of E-cadherin was evaluated in ARCaPE-eHsp90 following a 3 day treatment with the following: NPGA (1 uM), pan-MMP inhibitor (GM6001, 1 uM), MMP-2/9 inhibitor (SB-3CT, 1 uM), MMP-3 inhibitor (inhibitor IV, 5 uM) or ERK inhibitor (UO126, 10 uM). *C*, Immunoblot analysis of E-cadherin and ERK proteins in ARCaPE-eHsp90 following the time dependent inhibition of the following: MMP-2/9, MMP-3, or ERK. *D*, The effect of 3 days of MMP and ERK inhibition upon E-cadherin and ZO-1 localization in ARCaPE-LacZ and ARCaPE-eHsp90 was assessed by confocal microscopy. Cells were treated as in *A*, with inclusion of the pan-MMP inhibitor (GM6001, 1 uM) and the MMP-3 inhibitor (inhibitor IV, 5 uM). *E*, Evaluation of MMP and ERK in directing eHsp90 cell motility following a scratch wound assay. Scale bar is 50 um. UT refers to untreated vehicle control. Asterisks (*) indicate significance p-value $\leq$ 0.05.

FIGURE 7. Detection of eHsp90 protein and regulated transcripts in human prostatectomy tumor specimens. *A,* Prostate tissue from 2 patients was FACS sorted for $eHsp90^{low}$ and $eHsp90^{high}$ populations using a PE-conjugated antibody specific for Hsp90 alpha. In each instance, the subpopulation of $eHsp90^{high}$ cells represented approximately 5% of the cell population. Patient 1 was identified as Gleason 3+4 (stage T3aNO), while Patient 2 was Gleason 4+5 (stage T3bNO). *B*, RNA was harvested from these subpopulations and transcripts for MMP-2, MMP-3 and MMP-9 were evaluated via qRT-PCR. *C*, Proposed mechanism for eHsp90 mediated regulation of cell motility and EMT events. Tumor secreted eHsp90 functions in an autocrine manner via its receptor LRP1 to transduce ERK phosphorylation. eHsp90-LRP1-ERK signaling subsequently initiates transcription of several pro-EMT transcription factors (Snail/Zeb/Twist), as well as MMPs. MMP activation serves to reinforce sustained ERK activation and E-cadherin suppression through several potential mechanisms (dotted arrows, see text for details). These concurrent processes deregulate junctional complexes (E-cadherin and ZO-1), resulting in a loss of cell polarity, increased migratory potential, and initiation of a subset of EMT events.

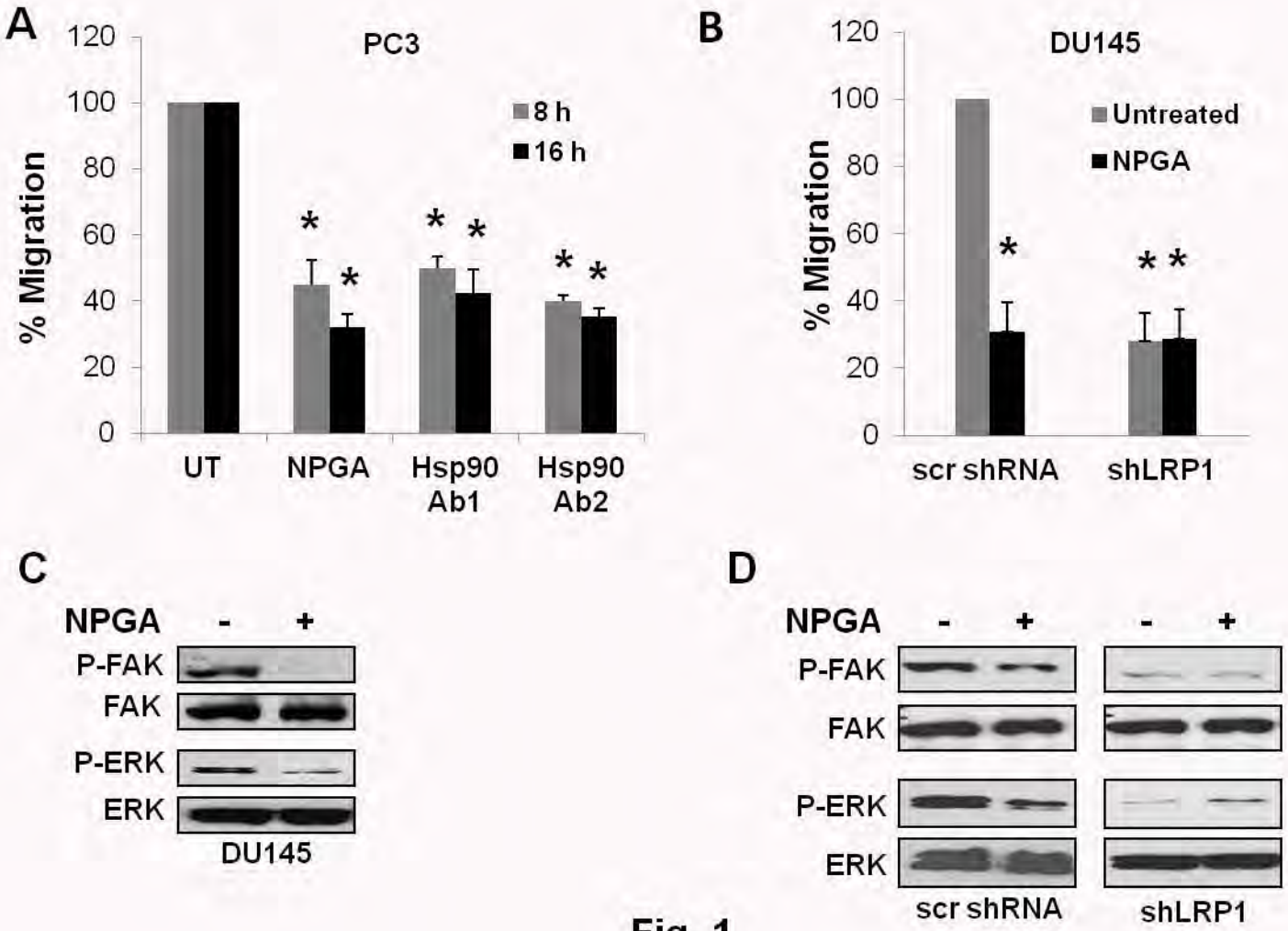

Fig. 1

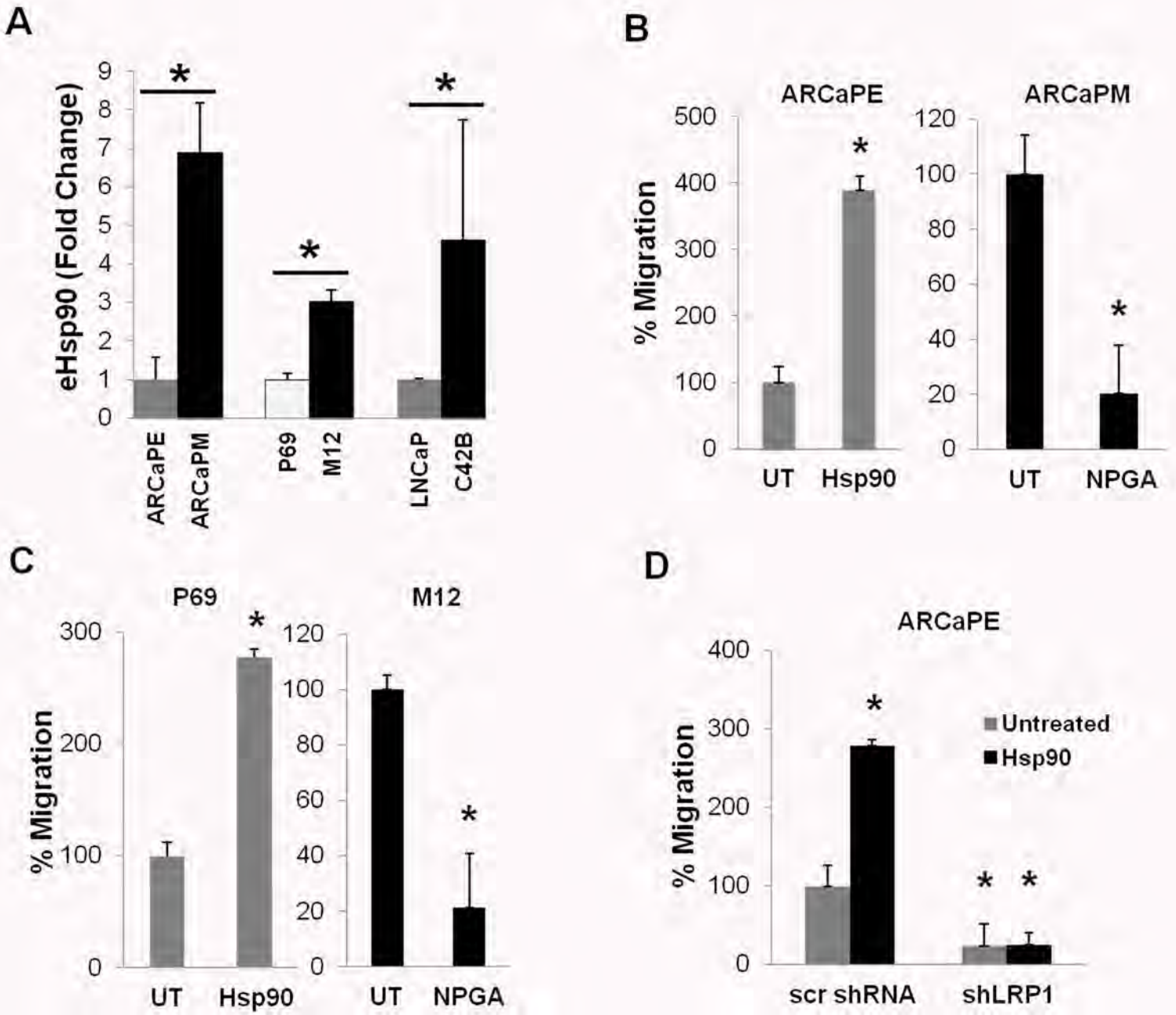

Fig. 2

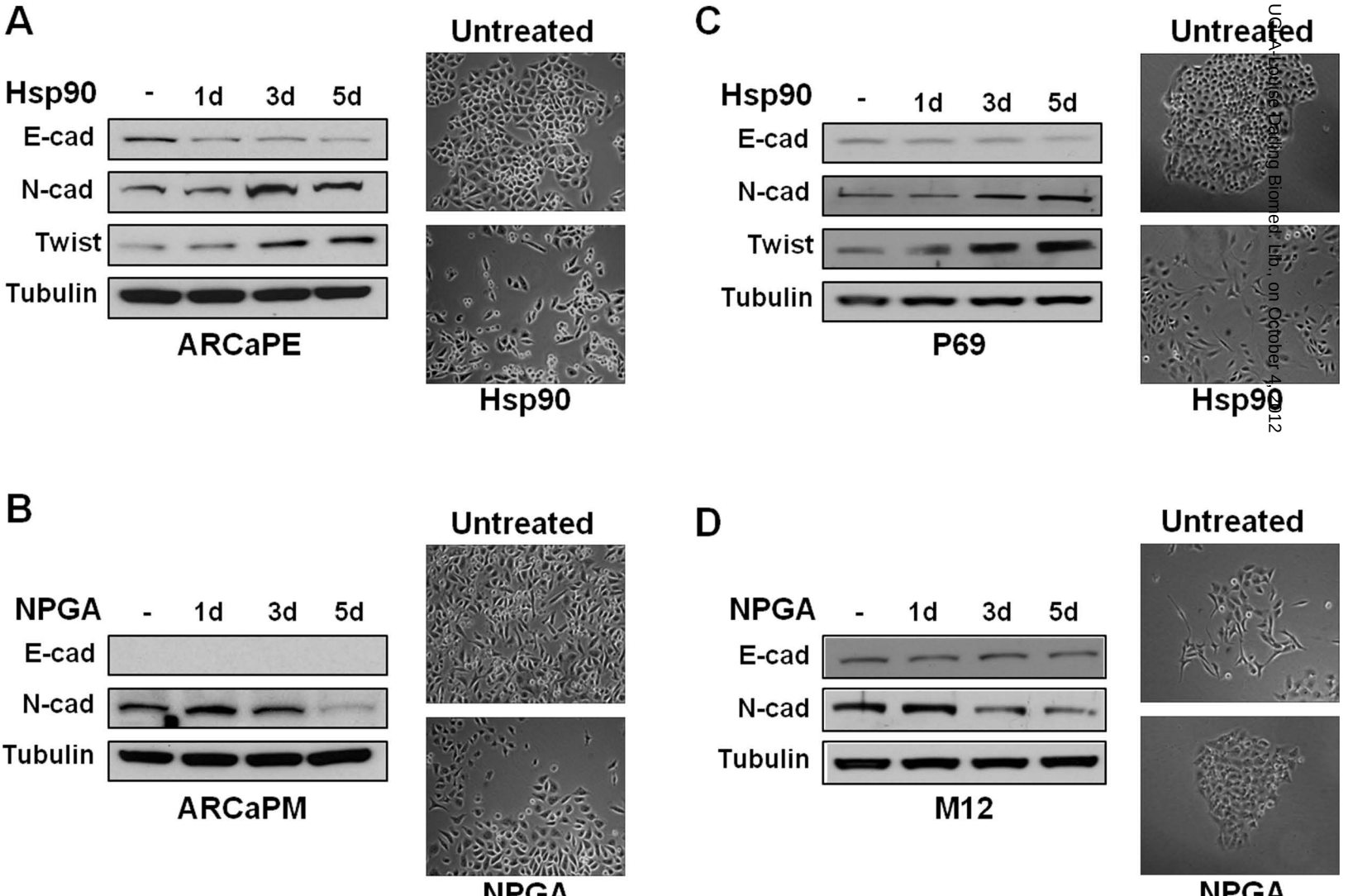

Fig. 3

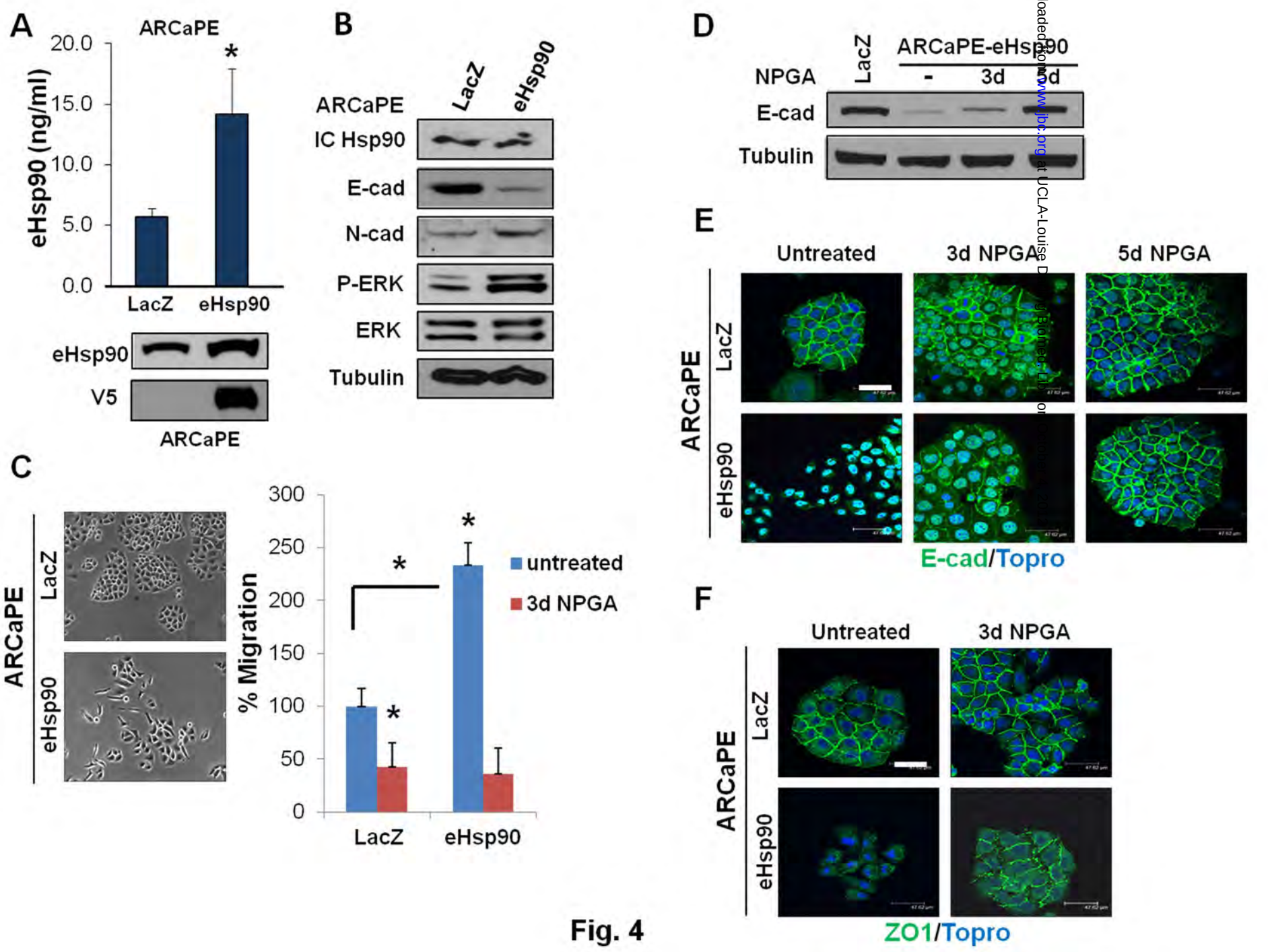

Fig. 4

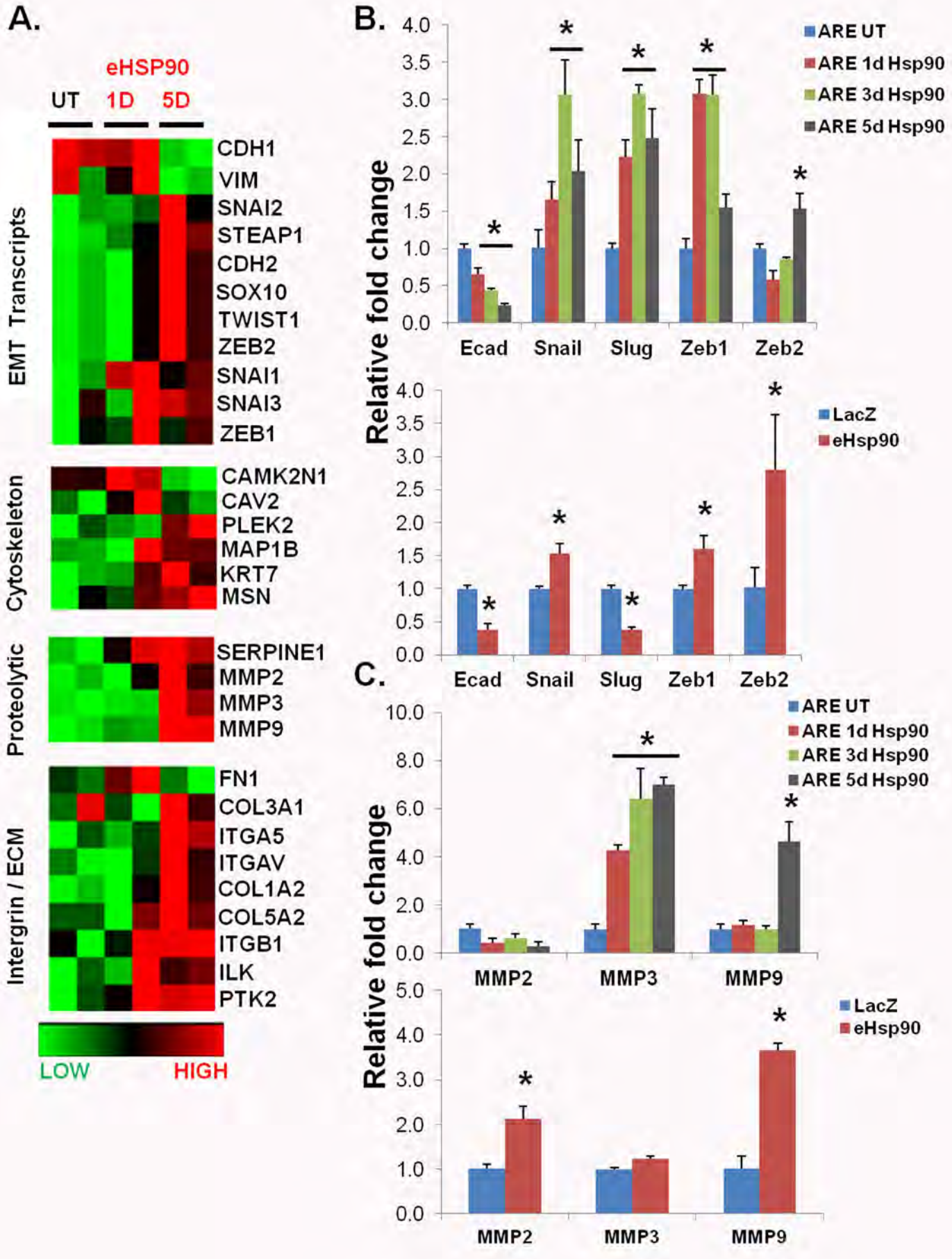
A.
eHSP90
UT
1D
5D
EMT Transcripts
CDH1
VIM
SNAI2
STEAP1
CDH2
SOX10
TWIST1
ZEB2
SNAI1
SNAI3
ZEB1
Cytoskeleton
CAMK2N1
CAV2
PLEK2
MAP1B
KRT7
MSN
Proteolytic
SERPINE1
MMP2
MMP3
MMP9
Intergrin / ECM
FN1
COL3A1
ITGA5
ITGAV
COL1A2
COL5A2
ITGB1
ILK
PTK2
LOW
HIGH
B.
Relative fold change
ARE UT
ARE 1d Hsp90
ARE 3d Hsp90
ARE 5d Hsp90
Ecad
Snail
Slug
Zeb1
Zeb2
LacZ
eHsp90
C.
MMP2
MMP3
MMP9

Fig. 5

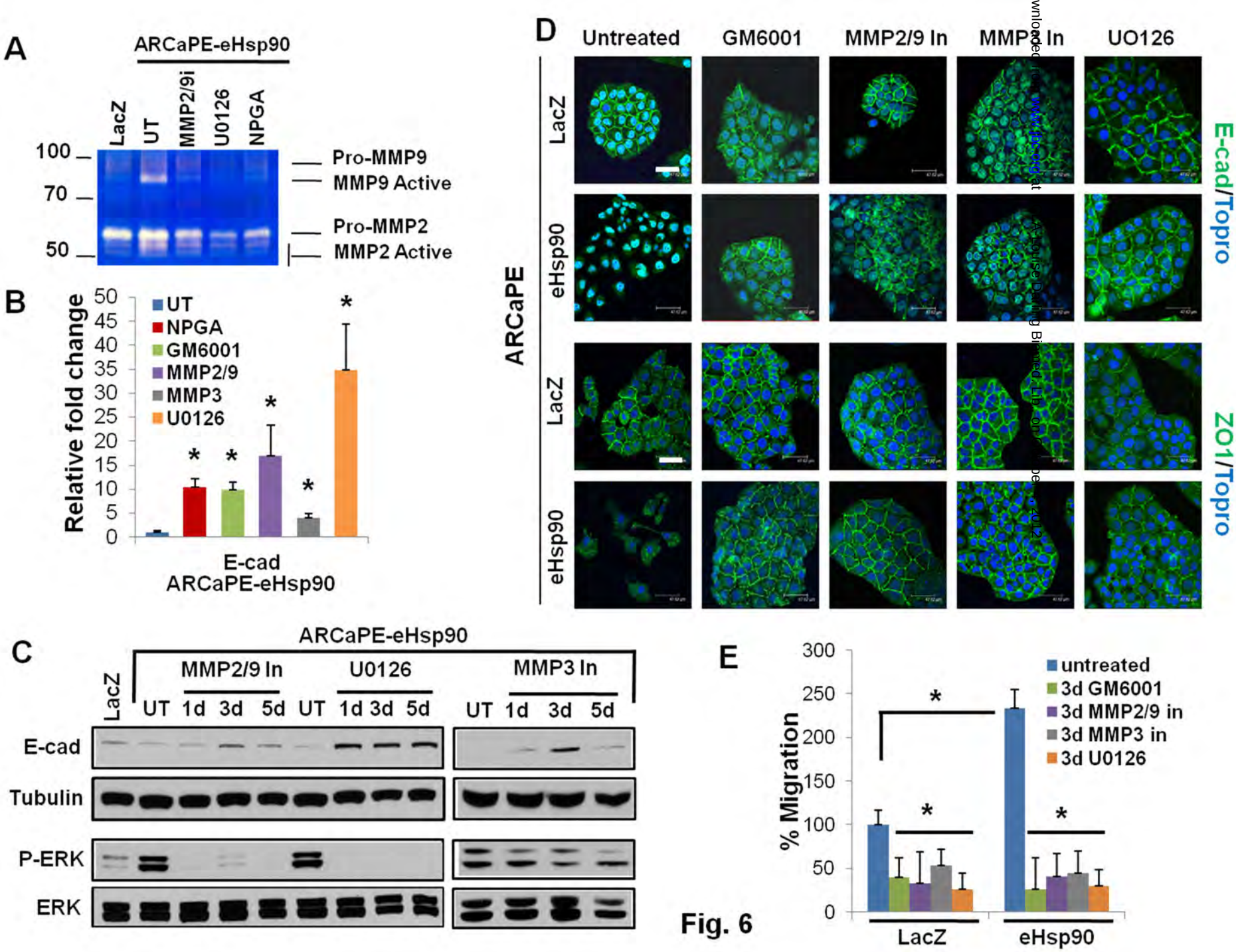
A
ARCaPE-eHsp90
LacZ
UT
MMP2/9i
U0126
NPGA
100
70
50
Pro-MMP9
MMP9 Active
Pro-MMP2
MMP2 Active
B
Relative fold change
UT
NPGA
GM6001
MMP2/9
MMP3
U0126
E-cad
ARCaPE-eHsp90
C
ARCaPE-eHsp90
LacZ
MMP2/9 In
U0126
MMP3 In
UT 1d 3d 5d UT 1d 3d 5d UT 1d 3d 5d
E-cad
Tubulin
P-ERK
ERK
D
Untreated
GM6001
MMP2/9 In
MMP3 In
UO126
ARCaPE
LacZ
eHsp90
E-cad/Topro
ZO1/Topro
E
% Migration
untreated
3d GM6001
3d MMP2/9 in
3d MMP3 in
3d U0126
LacZ
eHsp90

Fig. 6

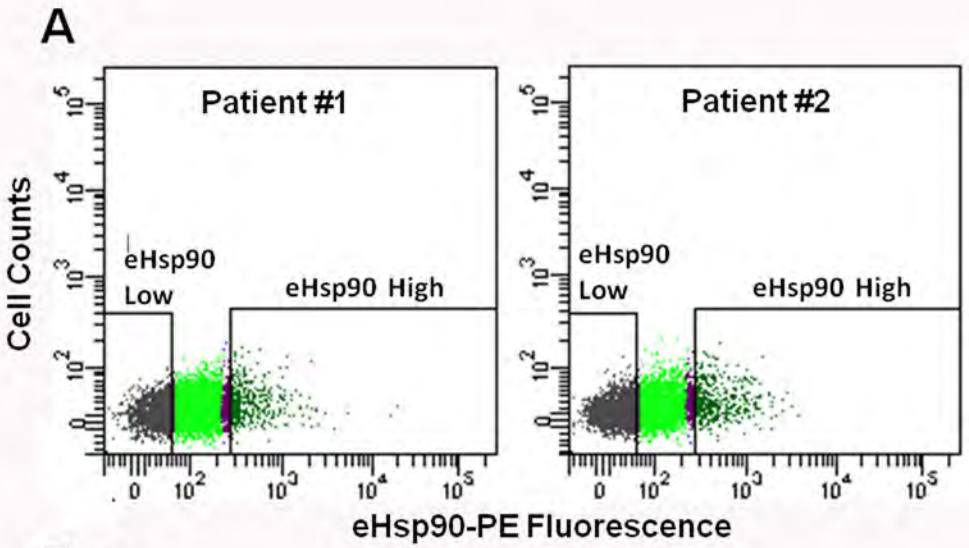

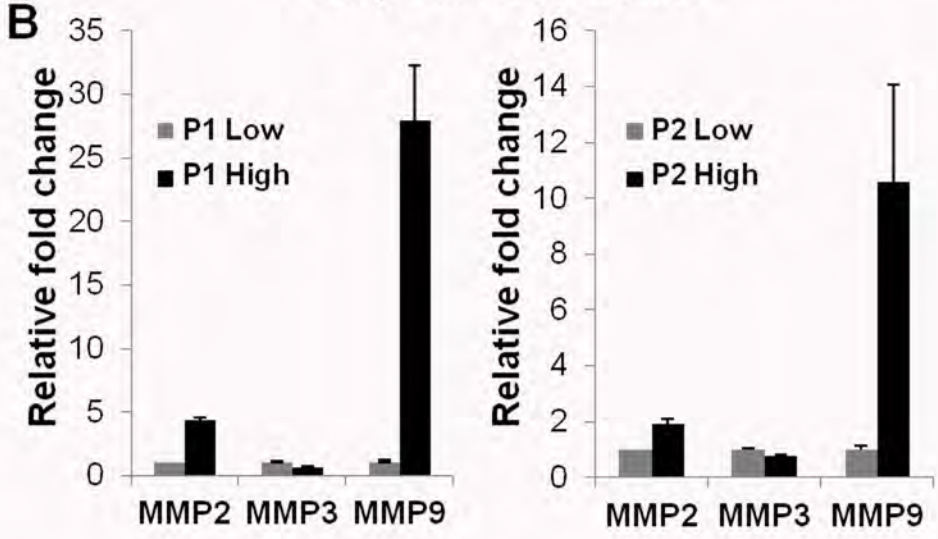

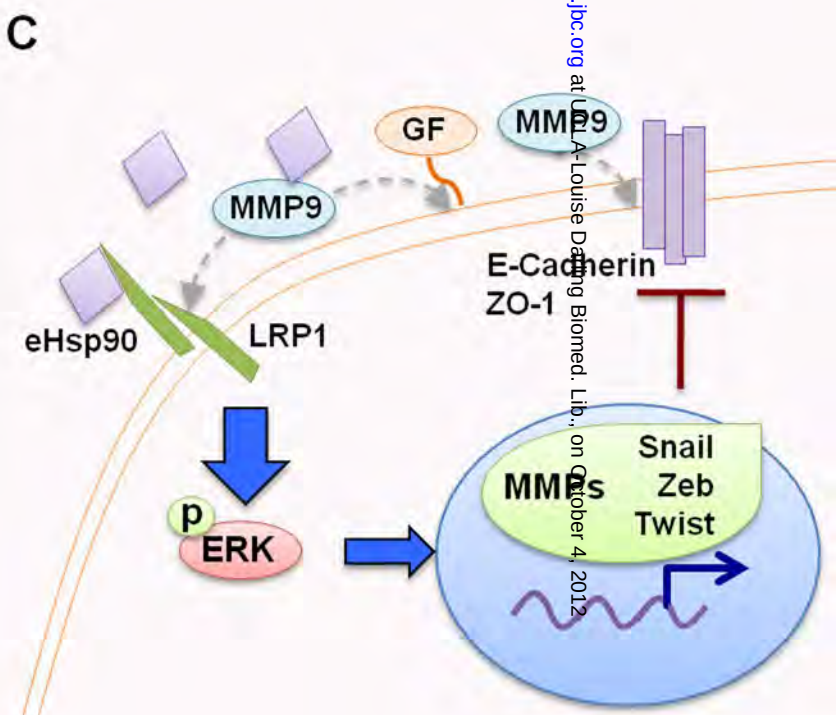

Fig. 7

Am J Cancer Res 2012;2(6):745-751
www.ajcr.us /ISSN:2156-6976/ajcr0000156

Original Article

Stromal modulation of bladder cancer-initiating cells in a subcutaneous tumor model

Elizabeth M Peek[1,2,3*], David R Li[1,2*], Hanwei Zhang[1,2], Hyun Pyo Kim[1,2], Baohui Zhang[1], Isla P Garraway[1,4], Arnold I Chin[1,2,4]

[1]UCLA Department of Urology, Los Angeles, California; [2]Eli & Edythe Broad Center of Regenerative Medicine & Stem Cell Research, UCLA, Los Angeles, California; [3]Molecular Biology Institute at UCLA, Los Angeles, California; [4]Jonsson Comprehensive Cancer Center, UCLA, Los Angeles, California. [*]Elizabeth M Peek and David R Li contributed equally to this work.

Received October 24, 2012; Accepted November 19, 2012; Epub November 20, 2012; Published November 30, 2012

Abstract: The development of new cancer therapeutics would benefit from incorporating efficient tumor models that mimic human disease. We have developed a subcutaneous bladder tumor regeneration system that recapitulates primary human bladder tumor architecture by recombining benign human fetal bladder stromal cells with SW780 bladder carcinoma cells. As a first step, SW780 cells were seeded in ultra low attachment cultures in order to select for sphere-forming cells, the putative cancer stem cell (CSC) phenotype. Spheroids were combined with primary human fetal stromal cells or vehicle control and injected subcutaneously with Matrigel into NSG mice. SW780 bladder tumors that formed in the presence of stroma showed accelerated growth, muscle invasion, epithelial to mesenchymal transition (EMT), decreased differentiation, and greater activation of growth pathways compared to tumors formed in the absence of fetal stroma. Tumors grown with stroma also demonstrated a greater similarity to typical malignant bladder architecture, including the formation of papillary structures. In an effort to determine if cancer cells from primary tumors could form similar structures *in vivo* using this recombinatorial approach, putative CSCs, sorted based on the $CD44^{+}CD49f^{+}$ antigenic profile, were collected and recombined with fetal bladder stromal cells and Matrigel prior to subcutaneous implantation. Retrieved grafts contained tumors that exhibited the same structure as the original primary human tumor. Primary bladder tumor regeneration using human fetal bladder stroma may help elucidate the influences of stroma on tumor growth and development, as well as provide an efficient and accessible system for therapeutic testing.

Keywords: Bladder cancer, cancer stem cell (CSC), subcutaneous tumor model, stroma, sphere

Introduction

Bladder cancer is the second most common genitourinary malignancy, with transitional cell carcinoma representing 90% of the cases [1]. Although BCG immunotherapy is effective in up to 75% of patients [2], treatments for bladder cancer have not significantly advanced in the last 30 years. Advances in therapeutics heavily depend on disease models. Subcutaneous models involving the direct injection of bladder tumor cells suffer from the inability of the tumor to form biologically relevant architecture [3]. Conversely, transgenic models [4-6] lack flexibility and require a longer incubation period. Here, we present a subcutaneous bladder tumor model with the ability to create papillary architecture, a model that may uniquely support the development of therapeutics.

The last few decades of cancer research have focused on the identification of oncogenes and tumor suppressors involved in the emergence of tumors. The effects of the surrounding stromal tissue have been largely ignored until recently. While the quantity of stroma does not appear to correspond with malignancy [7], signaling between tumor and stromal tissue is important for the formation of a complex tumor microenvironment and can influence the phenotype of the tumor [8].

Tumor cells are known to directly influence their surrounding stroma through invasion and angio-

genesis [9]. Growth factors such as VEGF, EGF, FGF, and TGF-β, as well as other cytokines, modulate the tumor microenvironment to promote a more permissive stroma and facilitate tumor growth [10, 11]. We postulated that tumor-adjacent stroma influences both the growth and differentiation of malignant cells.

Recent strides have been made in the identification and characterization of cancer stem cells (CSCs), the cancer-initiating cells within the tumor. By targeting CSCs specifically with new therapies, the risk of tumor recurrence is expected to be greatly reduced [12], justifying the inclusion of and focus on CSCs in any new tumor model. Breast cancer stem cells have been demonstrated to engage in stromal remodeling [13], but a more focused view of the interaction between CSCs and the surrounding stroma is necessary.

Stem cells have been shown to grow in three-dimensional spheroids in culture [14, 15]. This culture system has proven effective at growing cancer stem cells as well [16-18] and allowed for the culture of immortalized cell lines with cancer stem cell properties. For this study, we utilized the SW780 transitional bladder carcinoma cell line, which we found form spheres when grown in serum-free media. These cells exhibit the cancer-initiating cell phenotype, defined as $CD44^{+}CD49f^{+}$. When combined with fetal bladder mesenchymal cells in a novel subcutaneous model, the SW780 spheroids develop tumors that recapitulate primary tumor architecture. Therefore, the addition of stroma to a tumor model may promote both larger and less differentiated tumors.

Materials and methods

Cell lines and tumor samples

The SW780 immortalized human urinary bladder cell line (ATCC #CRL-2169) and the HT-1376 immortalized human urinary bladder cell line (ATCC #CRL-1472) were used in our *in vitro* and *in vivo* models. SW780 monolayer cells were maintained in RPMI 1640 with L-glutamine supplemented with 10% fetal bovine serum (FBS), and 1% penicillin/streptomycin. Sphere cultures for staining and implantation were maintained in floating culture as previously described [19, 20] on uncoated plates in RPMI 1640 with L-glutamine supplemented with 2% B-27 serum-free, 1% Pen/Strep, 2 μg/ml heparin, 20 ng/ml FGF, and 20 ng/ml EGF. When passaged, spheres were gravity-separated for 15-20 minutes before fresh media was added. Fresh bladder tumor samples were surgically resected, immediately suspended in PBS or DMEM, and maintained at 4°C until processed. Tumors were digested in 0.25% collagenase IV-DMEM for 4 hours and plated as above. Experiments were performed under IRB approved protocol #11-001363.

Acquisition, isolation, and culture of fetal bladder stroma

Human fetal bladder tissue was acquired from 16-17 week gestation specimens in accordance with federal and state guidelines. Fetal bladder, prostate, and urethra were removed *en bloc*. A portion of the specimen was fixed in formalin and paraffin-embedded to confirm correct anatomic localization. The remainder of the tissue was mechanically and enzymatically digested as previously described [21]. Dissociated bladder cell suspensions were sequentially filtered through 100-micron and 40-micron filters, and then passed through a 23-gauge needle. Cells were counted with a hemocytometer and resuspended in RPMI supplemented with 10% FBS and 1% Pen/Strep, and Methyltrienolone R1881 (Sigma) for culture in vitro. After 3 passages, cells were cryopreserved and thawed/expanded as needed for use in recombination assays.

Sphere formation efficiency assay

To quantify the percentage of cells that produce spheres, we adapted a previously described MatriGel culture system [22]. SW780 monolayer cells using 0.05% Trypsin-EDTA incubated at 37°C for 5-6 minutes before quenching with RPMI 1640 with L-glutamine supplemented with 10% FBS. Media was replaced with sphere media and cells were resuspended at 2.5×10^4 cells/mL. 40 μL of cell mixture was then mixed with 60 μL ice-cold MatriGel, and well-mixed. 100 μL of MatriGel mixture was then pipetted around the rim of a chilled 12-well plate. Plate was then swirled to evenly distribute the mixture around the edges and incubated at 37°C for 30 minutes to allow the MatriGel to set. 1 mL of sphere media was then gently added to the center of each well. 500 μL of media was aspirated and replaced with fresh

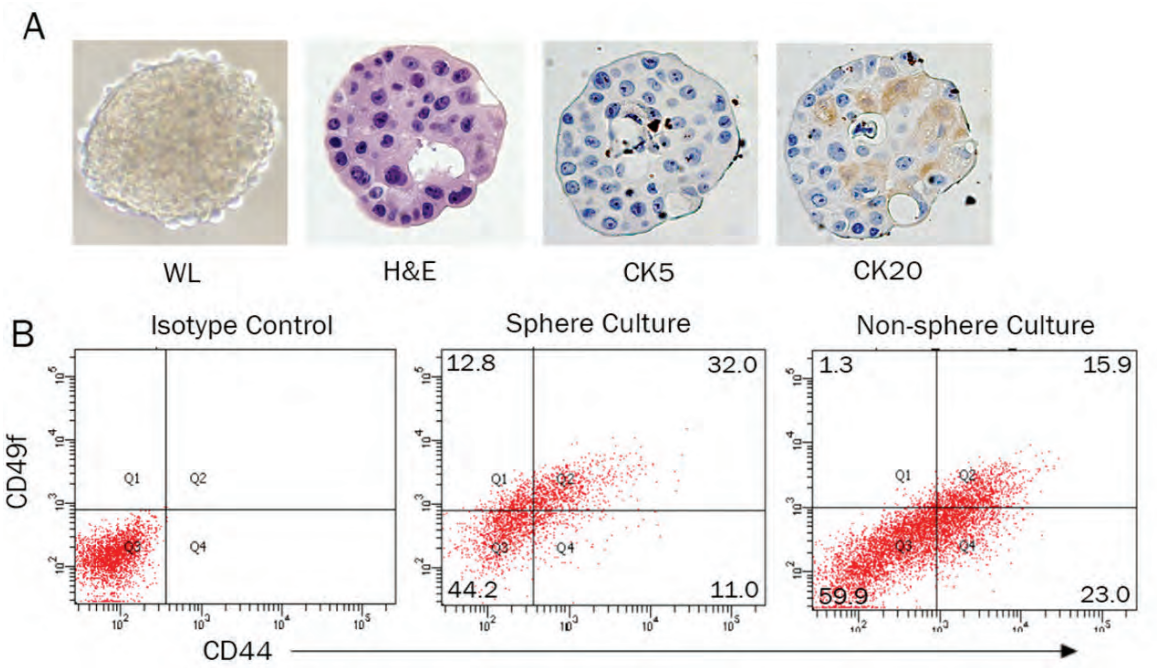

Figure 1. Spherical cultures express both luminal and basal markers. SW780 spheres from serum-free culture were fixed and bisected for IHC (A). Sections were stained with basal (CK5) and luminal (CK20) cell markers, as well as H&E. Representative views are shown, and images were captured at 400X magnification. SW780 spheres were dissociated and compared to SW780 cells grown in monolayer by flow cytometry (B). Cells were stained with anti-CD44-PE and anti-CD49f-FITC antibodies or isotype controls.

sphere media every three days. Spheres were counted at 7 days and 14 days.

Immunohistochemistry

Paraffin-embedded sections were stained with hematoxylin and eosin (H&E) for histological analysis. Immunohistochemistry was performed using antibodies against CK5/6 (Invitrogen), CK20 (DAKO), CD44 (eBioscience), EGFR (BIOCARE), pS6 (Cell Signaling), E-cadherin (BD Biosciences), and N-cadherin (ZYMED). Slides were probed with biotinylated goat anti-rabbit or goat anti-mouse secondary antibodies and with streptavidin conjugated to HRP. Photographs were taken using an Axio Imager 2 (Zeiss).

Flow cytometry

Cell surface marker analysis was performed by flow cytometry using the LSR II (BD Biosciences). Cells were incubated with antibodies against CD44 conjugated to PE (BD Biosciences) and against CD49f conjugated to FITC (BD Biosciences). Mouse IgG antibodies conjugated with each fluorochrome were used as isotype controls.

Subcutaneous tumor model

Non-obese diabetic severe combined immunodeficient gamma (NSG) mice between 6 and 8 weeks old were used for *in vivo* subcutaneous tumor growth experiments. Approximately 10^5 monolayer cells were suspended in 0.1 mL of media for inoculation. Cultured SW780 spheres and patient-derived spheres were prepared for xenograft implantation by first gravity-separating spheres for 15-20 minutes. Approximately 500 spheres were suspended in 0.1 mL of media for inoculation, and an equal quantity of Matrigel (BD Biosciences) was added. All mice were inoculated subcutaneously in the lower flank. Mice were monitored daily, and tumor growth was observed. Mice were sacrificed when tumor size reached 1 cm.

Results

Spherical cultures exhibit a cancer stem cell phenotype

To establish the validity of spheres as a cancer stem cell culture method, SW780 cells were grown in a Matrigel suspension and allowed to form spheres. The efficiency of sphere forma-

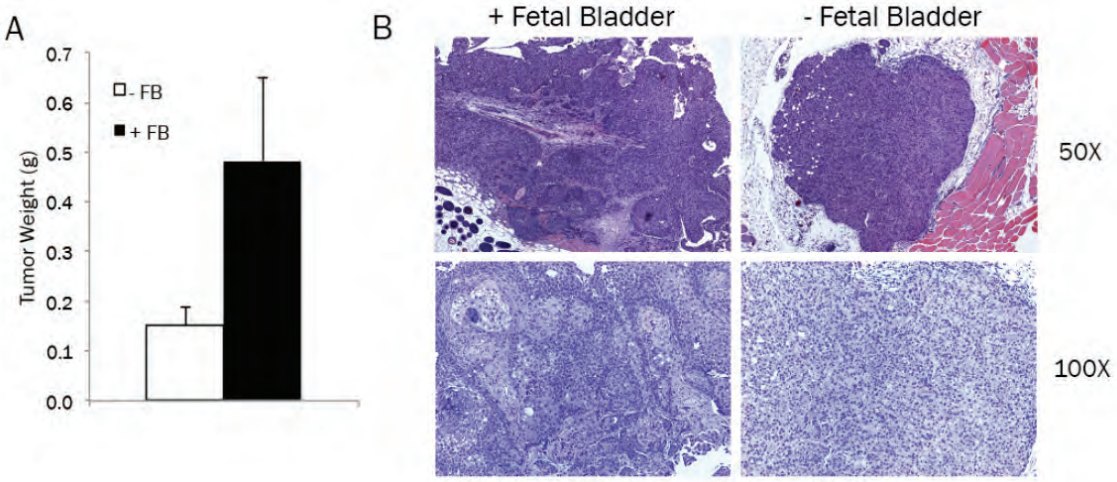

Figure 2. Stromal influence promotes increased tumor growth and invasiveness. NSG mice were implanted subcutaneously with SW780 spheres with and without the presence of fetal bladder stroma. After 4 weeks, tumors were harvested and weighed (A) (n=7 mice/group, $P < 0.001$). Nearby satellite tumors were also included in this weight. Error bars indicate standard deviation from the mean. Tumor sections were stained with H&E for histology. Tissue architecture (B) was compared in representative images captured at 50-100X magnification. Evidence of muscle invasion (C) was noted in images captured at 400X magnification.

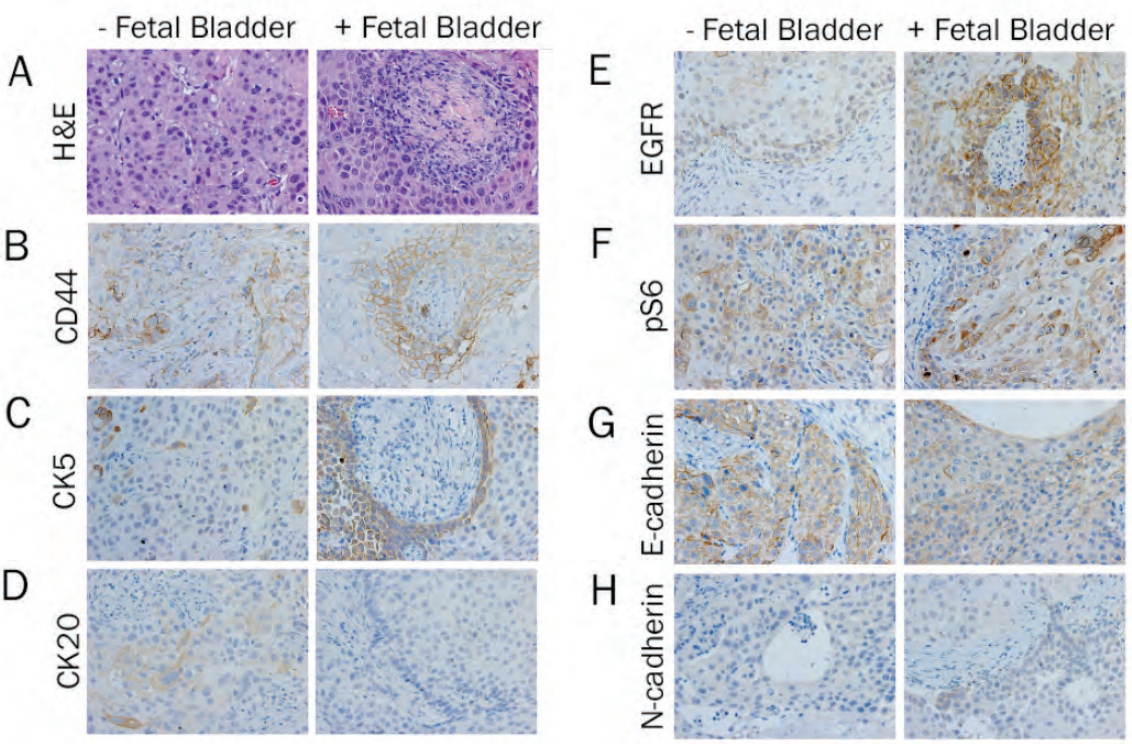

Figure 3. Tumors formed in the presence of stroma are less differentiated and functionally distinct. NSG mice were implanted subcutaneously with SW780 spheres with and without the presence of fetal bladder. After 4 weeks, tumors were harvested and embedded in paraffin for IHC. Slides were stained with H&E (A) for histology, as well as differentiation markers CD44, CK5, and CK20 (B-D). Tumor sections were also stained for functional markers: EGFR, pS6, E-cadherin, and N-cadherin (E-H). Representative views are shown, and images were captured at 400X magnification.

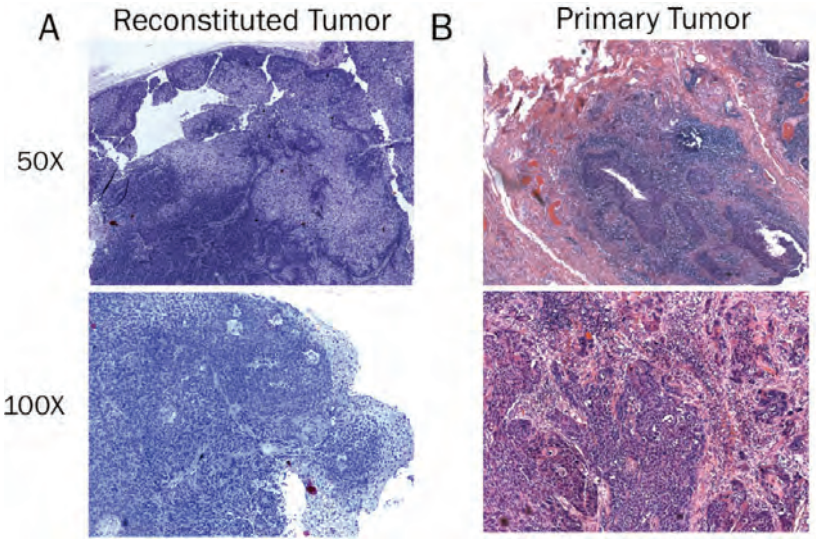

Figure 4. Subcutaneous model using human cells recapitulates both murine and primary tumor architecture. Primary human bladder tumor was sorted to isolate the $CD44^{+}CD49f^{+}$ population. Cells were combined with human fetal bladder and injected subcutaneously into NSG mice. Tumor sections were stained with H&E for histology (A). Pathology slides from the original human bladder tumor were stained with H&E for histology (B). Representative views are shown, captured at 50X and 100X magnification.

tion was measured at 2-4% (data not shown). Spheres from floating culture were fixed and sectioned for staining with basal and luminal markers to determine the cell phenotype (**Figure 1A**). The spheres showed expression of CK20, a luminal marker, towards the center and expression of the basal marker CK5 in the periphery. SW780 spheres were also shown to have a more undifferentiated phenotype than monolayer cells by measuring cell surface levels of the stem cell markers CD44 and CD49f (**Figure 1B**).

Stromal influence on tumor growth and function

To test the influence of stromal cells on tumors in an *in vivo* model, NSG mice were challenged subcutaneously with spheres with or without human fetal bladder stroma. Tumors were harvested, weighed, and stained. Supporting the assertion that the influence of stroma creates a more aggressive tumor, mice challenged with spheres and fetal bladder mesenchyme developed larger tumors than mice challenged with spheres alone (**Figure 2A**). The tumors with stroma present also showed evidence of invasion into the muscle (**Figure 2C**) and surrounding satellite tumors (data not shown), which were not observed in tumors formed without the influence of stroma. Histological analysis (**Figure 2B**, **3A**) showed that tumors formed in the presence of stroma grew papillary architecture, creating a malignant bladder-like structure in the subcutaneous compartment.

The tumors that included fetal bladder also showed higher expression of basal markers CD44 (**Figure 3B**) and CK5 (**Figure 3C**), while conversely, the expression of the luminal marker CK20 is decreased (**Figure 3D**). This indicates the presence of less differentiated malignant cells, which are associated with more advanced tumors [23].

The stromal-influenced tumors expressed more EGFR (**Figure 3E**) and pS6 ribosomal protein (**Figure 3F**), indicating an increase in growth factor signaling. A decrease in E-cadherin (**Figure 3G**), suggested an early stage of epithelial-to-mesenchymal transition (EMT) although we did not observe a corresponding increase in N-cadherin (**Figure 3H**). Both early EMT and activation of growth pathways would be expected in a more advanced tumor.

Primary human bladder tumor was also used to validate this model. A primary tumor was sorted to isolate $CD44^{+}CD49f^{+}$ cells previously described as the cancer stem cell population [24]. NSG mice were challenged with sorted cells combined with fetal bladder. The resulting tumor (**Figure 4A**) not only formed papillary architecture comparative to the murine model (**Figure 2B**), but the architecture recapitulated the structure of the original primary tumor (**Figure 4B**).

Discussion

With this work, we suggest a model for bladder cancer that creates a subcutaneous tumor that

exhibits typical human bladder tumor architecture. It maintains the benefits of subcutaneous implantation while gaining more physiological relevance, allowing comparisons to orthotopic or induced models.

The use of spheres to seed the tumor is validated by their demonstrated expression of the cancer stem cell (CSC) phenotype and their ability to express markers of both basal and luminal cells (**Figure 1**). As CSCs have the ability to differentiate into the heterogeneous malignant cell types found in a tumor [25], they are ideal for implantation. Their use isolates the model from extraneous factors and increases tumor-forming efficiency, as seen in breast cancer with $CD44^{+}CD49^{hi}$ cells [24].

Within the framework of this model, we can also explore the stromal contribution to tumor growth and progression. Fetal bladder induced significantly accelerated tumor growth (**Figure 2A**). The tumors were also less differentiated, showed signs of EMT, and began invading the surrounding muscle (**Figure 2C**, **3**), indicating a more advanced disease. The effects appear to be mediated, at least partially, by stromal activation of growth pathways (**Figure 3E**, **3F**), as has been previously observed [26, 27].

For this tumor model to be physiologically relevant, it should mimic typical bladder tissue architecture. With the addition of the stromal component, the tumors effectively recreated malignant bladder tissue (**Figure 2B**). Similar effects were seen when primary human CSCs were used in place of a cell line (**Figure 4A**). Most significantly, the model recapitulated the architecture seen in the primary tumor (**Figure 4B**).

This novel model of subcutaneous bladder cancer presents a unique opportunity to analyze the influence of the surrounding stroma to tumor growth. The elucidation of the role of stroma represents a significant area of research interest, and a subcutaneous model is particularly well suited to disentangle the contribution of malignant cells and stroma to the tumor microenvironment.

Acknowledgments

The authors thank the UCLA Broad Stem Cell Research Center Flow Cytometry Core Resource and the UCLA Translational Pathology Core Laboratory for providing core support. Funding for this research was provided by American Association of Cancer Research 10-20-14, the Prostate Cancer Foundation, Department of Defense PC073073, and the Jean Perkins Foundation.

Address correspondence to: Dr. Arnold I Chin, Department of Urology, University of California at Los Angeles, 10833 Le Conte Avenue, P.O. Box 951738, Los Angeles, CA 90095-1738. Phone: 310-206-4022; Fax: 310-206-5343; E-mail: aichin@ucla.edu

References

[1] Kim B, Choi HJ, Kim MH and Cho KS. Recurrence patterns of bladder transitional cell carcinoma after radical cystectomy. Acta Radiol 2012; 53: 943-949.

[2] Alexandroff AB, Jackson AM, O'Donnell MA and James K. BCG immunotherapy of bladder cancer: 20 years on. Lancet 1999; 353: 1689-1694.

[3] Chan E, Patel A, Heston W and Larchian W. Mouse orthotopic models for bladder cancer research. BJU Int 2009; 104: 1286-1291.

[4] Zhang ZT, Pak J, Shapiro E, Sun TT and Wu XR. Urothelium-specific expression of an oncogene in transgenic mice induced the formation of carcinoma in situ and invasive transitional cell carcinoma. Cancer Res 1999; 59: 3512-3517.

[5] Grippo PJ and Sandgren EP. Highly invasive transitional cell carcinoma of the bladder in a simian virus 40 T-antigen transgenic mouse model. Am J Pathol 2000; 157: 805-813.

[6] Mo L, Zheng X, Huang HY, Shapiro E, Lepor H, Cordon-Cardo C, Sun TT and Wu XR. Hyperactivation of Ha-ras oncogene, but not Ink4a/Arf deficiency, triggers bladder tumorigenesis. J Clin Invest 2007; 117: 314-325.

[7] Dvorak HF, Senger DR and Dvorak AM. Fibrin as a component of the tumor stroma: origins and biological significance. Cancer Metastasis Rev 1983; 2: 41-73.

[8] Kuperwasser C, Chavarria T, Wu M, Magrane G, Gray JW, Carey L, Richardson A and Weinberg RA. Reconstruction of functionally normal and malignant human breast tissues in mice. Proc Natl Acad Sci U S A 2004; 101: 4966-4971.

[9] Gururajan M, Posadas EM and Chung LW. Future perspectives of prostate cancer therapy. Transl Androl Urol 2012; 1: 19-32.

[10] Mueller MM and Fusenig NE. Friends or foes - bipolar effects of the tumour stroma in cancer. Nat Rev Cancer 2004; 4: 839-849.

[11] Rowley D and Barron DA. The reactive stroma microenvironment and prostate cancer progression. Endocr Relat Cancer 2012 Oct 30; 19: R187-204. doi: 10.1530/ERC-12-0085. Print 2012.
[12] Basile KJ and Aplin AE. Resistance to chemotherapy: short-term drug tolerance and stem cell-like subpopulations. Adv Pharmacol 2012; 65: 315-334.
[13] Parashurama N, Lobo NA, Ito K, Mosley AR, Habte FG, Zabala M, Smith BR, Lam J, Weissman IL, Clarke MF and Gambhir SS. Remodeling of endogenous mammary epithelium by breast cancer stem cells. Stem Cells 2012; 30: 2114-2127.
[14] Reynolds BA and Weiss S. Clonal and population analyses demonstrate that an EGF-responsive mammalian embryonic CNS precursor is a stem cell. Dev Biol 1996; 175: 1-13.
[15] Dontu G, Abdallah WM, Foley JM, Jackson KW, Clarke MF, Kawamura MJ and Wicha MS. In vitro propagation and transcriptional profiling of human mammary stem/progenitor cells. Genes Dev 2003; 17: 1253-1270.
[16] Ponti D, Costa A, Zaffaroni N, Pratesi G, Petrangolini G, Coradini D, Pilotti S, Pierotti MA and Daidone MG. Isolation and in vitro propagation of tumorigenic breast cancer cells with stem/progenitor cell properties. Cancer Res 2005; 65: 5506-5511.
[17] Lang SH, Sharrard RM, Stark M, Villette JM and Maitland NJ. Prostate epithelial cell lines form spheroids with evidence of glandular differentiation in three-dimensional Matrigel cultures. Br J Cancer 2001; 85: 590-599.
[18] Fang D, Nguyen TK, Leishear K, Finko R, Kulp AN, Hotz S, Van Belle PA, Xu X, Elder DE and Herlyn M. A tumorigenic subpopulation with stem cell properties in melanomas. Cancer Res 2005; 65: 9328-9337.
[19] Hemmati HD, Nakano I, Lazareff JA, Masterman-Smith M, Geschwind DH, Bronner-Fraser M and Kornblum HI. Cancerous stem cells can arise from pediatric brain tumors. Proc Natl Acad Sci USA 2003; 100: 15178-15183.
[20] Garraway IP, Sun W, Tran CP, Perner S, Zhang B, Goldstein AS, Hahm SA, Haider M, Head CS, Reiter RE, Rubin MA and Witte ON. Human prostate sphere-forming cells represent a subset of basal epithelial cells capable of glandular regeneration in vivo. Prostate 2010; 70: 491-501.
[21] Jiao J, Hindoyan A, Wang S, Tran LM, Goldstein AS, Lawson D, Chen D, Li Y, Guo C, Zhang B, Fazli L, Gleave M, Witte ON, Garraway IP and Wu H. Identification of CD166 as a surface marker for enriching prostate stem/progenitor and cancer initiating cells. PLoS One 2012; 7: e42564.
[22] Guo C, Zhang B and Garraway IP. Isolation and characterization of human prostate stem/progenitor cells. Methods Mol Biol 2012; 879: 315-326.
[23] Mete O and Asa SL. Pathological definition and clinical significance of vascular invasion in thyroid carcinomas of follicular epithelial derivation. Mod Pathol 2011; 24: 1545-1552.
[24] Meyer MJ, Fleming JM, Lin AF, Hussnain SA, Ginsburg E and Vonderhaar BK. CD44posCD49fhiCD133/2hi defisnes xenograft-initiating cells in estrogen receptor-negative breast cancer. Cancer Res 2010; 70: 4624-4633.
[25] van der Horst G, Bos L and van der Pluijm G. Epithelial plasticity, cancer stem cells, and the tumor-supportive stroma in bladder carcinoma. Mol Cancer Res 2012; 10: 995-1009.
[26] Korc M. Pancreatic cancer-associated stroma production. Am J Surg 2007; 194: S84-86.
[27] Hadari Y and Schlessinger J. FGFR3-targeted mAb therapy for bladder cancer and multiple myeloma. J Clin Invest 2009; 119: 1077-1079.

VOLUME 31 · NUMBER 30 · OCTOBER 20 2013

JOURNAL OF CLINICAL ONCOLOGY

UNDERSTANDING THE PATHWAY

Targeting the RANKL Pathway: Putting the Brakes on Prostate Cancer Progression in Bone

Isla P. Garraway, *Jonsson Comprehensive Cancer Center; David Geffen School of Medicine; Broad Center of Regenerative Medicine and Stem Cell Research, University of California, Los Angeles; and Greater Los Angeles Veterans Affairs Medical Center, Los Angeles, CA*

See accompanying article on page 3800

The spread of prostate cancer (PC) to bone represents a critical turning point in disease progression and occurs in > 90% of lethal cases.[1] In advanced or recurrent nonmetastatic PC, castration-based therapy is often the first line of treatment in an effort to delay metastasis and improve survival.[2] Unfortunately, androgen-deprivation therapy is usually insufficient for durable remission, and serum prostate-specific antigen (PSA) relapse indicates progression to castration-resistant prostate cancer (CRPC).[3] A majority of patients with CRPC develop bone metastases, which may bring a significant risk of skeletal-related events (SREs), including pathologic fractures, spinal cord compression, hypercalcemia, and debilitating pain requiring irradiation or surgical intervention.[1,4,5] Pharmacologic prevention of SREs with zoledronic acid or denosumab is a standard practice in metastatic CRPC; however, the benefit of such agents in metastasis prevention is still under investigation.[6-8]

Bone metastasis–free survival (BMFS) is defined as the time to first bone metastasis or death.[6] In the study reported by Smith et al,[9] accompanying this article, patients with nonmetastatic CRPC were stratified by PSA doubling time (PSADT) and randomly assigned to receive denosumab, a human monoclonal antibody against receptor activator of nuclear factor κB (NF-κB) ligand (RANKL), or placebo. PSADT is directly correlated with risk of progression to bone metastasis or death, and patients with the shortest PSADT (≤ 4 months) displayed the most significant increases in BMFS after treatment with denosumab.[3,10]

RANKL Signaling Pathway

Continuous bone remodeling is essential for skeletal integrity and strength.[11] Bone homeostasis describes the scenario when resorption and rebuilding are appropriately balanced. Osteoclasts and osteoblasts are specialized cells that exist within the bone microenvironment and display a yin-and-yang type of relationship, with osteoclasts breaking down bone while osteoblasts lay new matrix (Fig 1).[12] Osteoclast precursors are derived from the myeloid lineage of hematopoietic cells and express RANK, a type I homotrimeric transmembrane protein related to the tumor necrosis factor (TNF) family of receptors.[13] In response to cytokines and hormones, osteoclast precursors mature, fuse, adhere to bone, and release resorptive enzymes that form pits in bone.[14,15] Osteoclast maturation and function are dependent on RANKL binding through cell-cell interactions with osteoblasts.[16] Derived from mesenchymal stem cells, RANKL-expressing osteoblasts are recruited by osteoclasts to bone resorption sites, where they proliferate, differentiate, and release osteoid to form new bone matrix.[12] Some osteoblasts at the remodeling site develop into osteocytes that are incorporated into the new bone matrix. To achieve physiologic balance, osteoblasts produce osteoprotegerin, a secreted receptor that functions as a RANK decoy and binds to RANKL.[17,18] The ratio of RANKL to osteoprotegerin enables the remodeling process to shift between resorption and rebuilding, as needed.

Signaling pathways activated as a result of RANKL/RANK interaction are currently being elucidated in an effort to fully understand the biology associated with bone disease. A key step in RANKL downstream signaling involves binding of TNF receptor–associated factor (TRAF) adaptor proteins to specific sites within the RANK cystoplasmic domain.[19] RANK interacts with five different TRAF family members; however, its interaction with TRAF6 is particularly important for protein kinase signaling that results in activation of NF-κB and its translocation to the nucleus.[14,20] Osteoclastogenic gene expression ensues after NF-κB induction of c-Fos expression enables complex formation with nuclear factor of activated T cells c1 and transcriptional activation.[21,22] The end results of this signaling pathway are osteoclast formation and activation (Fig 1).

Targeting Osteoclasts via RANKL Inhibition in Prostate Cancer

In the setting of bone metastasis, a vicious cycle of bone destruction and tumor growth emerges as a consequence of tumor-induced dysregulation.[5,23] As PC cells invade the bone, they produce cytokines and growth factors, including parathyroid hormone–related peptide, bone morphogenic protein, transforming growth factor-B, vascular endothelial growth factor, and Wnt. These factors induce RANKL production from bone stromal cells.[23-26] Continuous osteoclast activation via RANK/RANKL interaction allows bone resorption to go unchecked. This results in further tumor-cell invasion and growth in response to the release of additional bone-derived growth factors, including epidermal

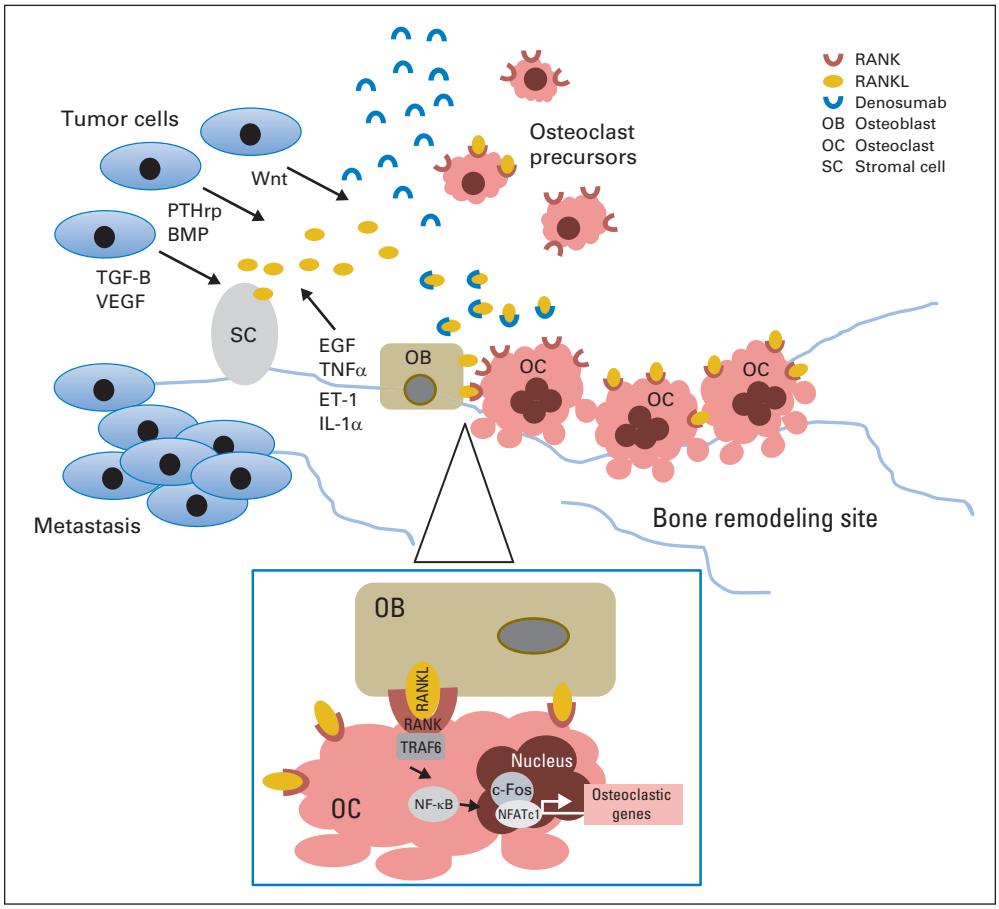

Fig 1. Targeting osteoclasts via the receptor activator of nuclear factor κB (NF-κB) ligand (RANKL) pathway in castration-resistance prostate cancer (CRPC). Bone remodeling is a continuous process in which bone resorption activity mediated by osteoclasts is balanced by production of new bone matrix by osteoblasts. Binding of RANKL (produced by bone stromal cells and expressed on the surface of osteoblasts) to RANK (expressed on the surface of osteoclasts) induces a cascade of events that leads to the maturation and fusion of osteoclast precursors that adhere to the surface of the bone. Osteoblasts appear at remodeling sites and produce osteoid matrix, which eventually mineralizes to form new bone. Protein kinase signaling (inset) induced by RANKL/RANK interaction is mediated by tumor necrosis factor (TNF) receptor–associated factor (TRAF) adaptor proteins. Similar to other TNF-like receptors, RANK lacks a functional domain capable of activating protein kinase signaling. Although several TRAF proteins interact with RANK, TRAF6 seems to be an essential mediator, with downstream effects of NF-κB activation and translocation to nucleus. c-Fos expression is transactivated by NF-κB and forms a complex with nuclear factor of activated T cells c1 (NFATc1), which in turn activates osteoclastogenic genes. In CRPC, dysregulation of bone homeostasis results in continuous osteoclast activation. Tumor cells produce cytokines and growth factors such as parathyroid hormone–related peptide (PTHrp), bone morphogenic protein (BMP), transforming growth factor-B (TGF-B), vascular endothelial growth factor (VEGF), and Wnt, which facilitates their entry into bone via induction of RANKL by osteoblasts and stromal cells. As bone is absorbed, tumor growth and invasion are enhanced by the release of bone-derived growth factors, including epidermal growth factor (EGF), endothelin-1 (ET-1), TNFα, and interleukin-1α (IL-1α). The vicious cycle of tumor growth fueling bone destruction (and vice versa) significantly weakens bone, leading to skeletal-related events. Denosumab is a humanized monoclonal antibody that interferes with this cycle by blocking RANKL binding to RANK. Osteoclast maturation is inhibited by the interference of RANK/RANKL signaling, resulting in reduced bone resorption.

growth factor, endothelin-1, tumor necrosis factor-α, and interleukin-1α.[25] Skeletal deficiencies resulting from the vicious cycle are precursors of frank SREs.

Because excess osteoclast activity is a key mediator of SREs in metastatic cancer, osteoclast inhibition has emerged as a major bone-protective strategy. Bisphosphonates are by far the most widely used bone-targeting agents. These drugs exhibit a high affinity for bone and induce apoptosis in osteoclasts.[27,28] Zoledronic acid is a bisphosphonate approved for use in metastatic CRPC and is considered a standard of care for these patients because of evidence-based reduction in SREs.[8,29,30] The development of denosumab may offer an alternative modality for SRE prevention.[7,31] By blocking RANKL, denosumab suppresses osteoclast differentiation and function.[31] Preclinical models initially demonstrated that denosumab improved bone density and volume by reducing resorption.[31] These findings were affirmed in phase II clinical trials that evaluated denosumab in postmenopausal women with osteoporosis.[32] Phase III clinical trials performed in patients with metastatic CRPC directly compared the safety and efficacy of denosumab with zoledronic acid. Denosumab was found to be superior in lengthening time to SREs and suppressing bone turnover.[7]

Opportunities and Challenges for Preventing Metastasis in Addition to SREs

As evident in the study by Smith et al,[9] denosumab improves BMFS in patients with nonmetastatic CRPC at high risk for developing bone metastasis, especially in those exhibiting short PSADT.

However, the use of denosumab for metastasis prevention has yet to receive US Food and Drug Administration approval, in part because of its equivocal impact on patient survival, pain metrics, and other quality of life measurements.[33] Conceivably, the development of rational therapeutic combinations directed against bone metastasis, together with further molecular and genetic classification of PC, will bring forth greater clarity regarding who should receive treatment and at what point in disease progression. Such knowledge could yield increased quality and perhaps quantity of life for men with CRPC.

AUTHOR'S DISCLOSURES OF POTENTIAL CONFLICTS OF INTEREST

The author(s) indicated no potential conflicts of interest.

REFERENCES

1. Coleman RE: Clinical features of metastatic bone disease and risk of skeletal morbidity. Clin Cancer Res 12:6243s-6249s, 2006

2. Immediate versus deferred treatment for advanced prostatic cancer: Initial results of the Medical Research Council Trial—The Medical Research Council Prostate Cancer Working Party Investigators Group. Br J Urol 79:235-246, 1997

3. Smith MR, Kabbinavar F, Saad F, et al: Natural history of rising serum prostate-specific antigen in men with castrate nonmetastatic prostate cancer. J Clin Oncol 23:2918-2925, 2005

4. Paller CJ, Carducci MA, Philips GK: Management of bone metastases in refractory prostate cancer: Role of denosumab. Clin Interv Aging 7:363-372, 2012

5. Rove KO, Crawford ED: Evolution of treatment options for patients with CRPC and bone metastases: Bone-targeted agents that go beyond palliation of symptoms to improve overall survival. Oncology (Williston Park) 25:1362-1370, 1375-1381, 1387, 2011

6. Smith MR, Saad F, Coleman R, et al: Denosumab and bone-metastasis-free survival in men with castration-resistant prostate cancer: Results of a phase 3, randomised, placebo-controlled trial. Lancet 379:39-46, 2012

7. Fizazi K, Carducci M, Smith M, et al: Denosumab versus zoledronic acid for treatment of bone metastases in men with castration-resistant prostate cancer: A randomised, double-blind study. Lancet 377:813-822, 2011

8. Saad F, Gleason DM, Murray R, et al: Long-term efficacy of zoledronic acid for the prevention of skeletal complications in patients with metastatic hormone-refractory prostate cancer. J Natl Cancer Inst 96:879-882, 2004

9. Smith MR, Saad F, Oudard S, et al: Denosumab and bone metastasis–free survival in men with nonmetastatic castration-resistant prostate cancer: Exploratory analyses by baseline prostate-specific antigen doubling time. J Clin Oncol 31:3800-3806, 2013

10. D'Amico AV, Moul JW, Carroll PR, et al: Surrogate end point for prostate cancer-specific mortality after radical prostatectomy or radiation therapy. J Natl Cancer Inst 95:1376-1383, 2003

11. Reid IR: Anti-resorptive therapies for osteoporosis. Semin Cell Dev Biol 19:473-478, 2008

12. Murthy RK, Morrow PK, Theriault RL: Bone biology and the role of the RANK ligand pathway. Oncology (Williston Park) 23:9-15, 2009 (suppl 5)

13. Anderson DM, Maraskovsky E, Billingsley WL, et al: A homologue of the TNF receptor and its ligand enhance T-cell growth and dendritic-cell function. Nature 390:175-179, 1997

14. Boyce BF, Xing L: Biology of RANK, RANKL, and osteoprotegerin. Arthritis Res Ther 9:S1, 2007 (suppl 1)

15. Teitelbaum SL, Ross FP: Genetic regulation of osteoclast development and function. Nat Rev Genet 4:638-649, 2003

16. Kapur RP, Yao Z, Iida MH, et al: Malignant autosomal recessive osteopetrosis caused by spontaneous mutation of murine Rank. J Bone Miner Res 19:1689-1697, 2004

17. Hofbauer LC, Schoppet M: Clinical implications of the osteoprotegerin/RANKL/RANK system for bone and vascular diseases. JAMA 292:490-495, 2004

18. Simonet WS, Lacey DL, Dunstan CR, et al: Osteoprotegerin: A novel secreted protein involved in the regulation of bone density. Cell 89:309-319, 1997

19. Chung JY, Lu M, Yin Q, et al: All TRAFs are not created equal: Common and distinct molecular mechanisms of TRAF-mediated signal transduction. J Cell Sci 115:679-688, 2002

20. Darnay BG, Besse A, Poblenz AT, et al: TRAFs in RANK signaling. Adv Exp Med Biol 597:152-159, 2007

21. Takayanagi H, Kim S, Koga T, et al: Induction and activation of the transcription factor NFATc1 (NFAT2) integrate RANKL signaling in terminal differentiation of osteoclasts. Dev Cell 3:889-901, 2002

22. Karsenty G, Wagner EF: Reaching a genetic and molecular understanding of skeletal development. Dev Cell 2:389-406, 2002

23. Feller L, Kramer B, Lemmer J: A short account of metastatic bone disease. Cancer Cell Int 11:24, 2011

24. Loberg RD, Gayed BA, Olson KB, et al: A paradigm for the treatment of prostate cancer bone metastases based on an understanding of tumor cell-microenvironment interactions. J Cell Biochem 96:439-446, 2005

25. Loriot Y, Massard C, Fizazi K: Recent developments in treatments targeting castration-resistant prostate cancer bone metastases. Ann Oncol 23:1085-1094, 2012

26. Guise TA, Mohammad KS, Clines G, et al: Basic mechanisms responsible for osteolytic and osteoblastic bone metastases. Clin Cancer Res 12:6213s-6216s, 2006

27. Brown JE, Neville-Webbe H, Coleman RE: The role of bisphosphonates in breast and prostate cancers. Endocr Relat Cancer 11:207-224, 2004

28. Drake MT, Clarke BL, Khosla S: Bisphosphonates: Mechanism of action and role in clinical practice. Mayo Clin Proc 83:1032-1045, 2008

29. Saad F, Eastham J: Zoledronic acid improves clinical outcomes when administered before onset of bone pain in patients with prostate cancer. Urology 76:1175-1181, 2010

30. Saad F, Lipton A: Clinical benefits and considerations of bisphosphonate treatment in metastatic bone disease. Semin Oncol 34:S17-S23, 2007 (suppl 4)

31. Kostenuik PJ, Nguyen HQ, McCabe J, et al: Denosumab, a fully human monoclonal antibody to RANKL, inhibits bone resorption and increases BMD in knock-in mice that express chimeric (murine/human) RANKL. J Bone Miner Res 24:182-195, 2009

32. Seeman E, Delmas PD, Hanley DA, et al: Microarchitectural deterioration of cortical and trabecular bone: Differing effects of denosumab and alendronate. J Bone Miner Res 25:1886-1894, 2010

33. Saylor PJ, Armstrong AJ, Fizazi K, et al: New and emerging therapies for bone metastases in genitourinary cancers. Eur Urol 63:309-320, 2013

DOI: 10.1200/JCO.2013.50.1544; published online ahead of print at www.jco.org on September 16, 2013

UNITED STATES PATENT AND TRADEMARK OFFICE

UNITED STATES DEPARTMENT OF COMMERCE
United States Patent and Trademark Office
Address: COMMISSIONER FOR PATENTS
P.O. Box 1450
Alexandria, Virginia 22313-1450
www.uspto.gov

APPLICATION NUMBER	FILING or 371(c) DATE	GRP ART UNIT	FIL FEE REC'D	ATTY.DOCKET.NO	TOT CLAIMS	IND CLAIMS
61/896,017	10/25/2013		260	UCLA.211-US-P1		

CONFIRMATION NO. 1018

59612
KAREN S. CANADY
CANADY & LORTZ LLP
3701 Wilshire BLV Suite 508
LOS ANGELES, CA 90010

FILING RECEIPT

OC00000065157372

Date Mailed: 11/27/2013

Receipt is acknowledged of this provisional patent application. It will not be examined for patentability and will become abandoned not later than twelve months after its filing date. Any correspondence concerning the application must include the following identification information: the U.S. APPLICATION NUMBER, FILING DATE, NAME OF APPLICANT, and TITLE OF INVENTION. Fees transmitted by check or draft are subject to collection. Please verify the accuracy of the data presented on this receipt. **If an error is noted on this Filing Receipt, please submit a written request for a Filing Receipt Correction. Please provide a copy of this Filing Receipt with the changes noted thereon. If you received a "Notice to File Missing Parts" for this application, please submit any corrections to this Filing Receipt with your reply to the Notice. When the USPTO processes the reply to the Notice, the USPTO will generate another Filing Receipt incorporating the requested corrections**

Inventor(s)

Isla P. Garraway, Manhattan Beach, CA;
Michael S. Lewis, Santa Monica, CA;

Applicant(s)

Isla P. Garraway, Manhattan Beach, CA;
Michael S. Lewis, Santa Monica, CA;

Power of Attorney:
Karen Canady--39927

If Required, Foreign Filing License Granted: 11/22/2013

The country code and number of your priority application, to be used for filing abroad under the Paris Convention, is **US 61/896,017**

Projected Publication Date: None, application is not eligible for pre-grant publication

Non-Publication Request: No

Early Publication Request: No

Title

MARKER TO DETECT AND TARGET METASTATIC PROSTATE CANCER

Statement under 37 CFR 1.55 or 1.78 for AIA (First Inventor to File) Transition Applications: No

PROTECTING YOUR INVENTION OUTSIDE THE UNITED STATES

Since the rights granted by a U.S. patent extend only throughout the territory of the United States and have no effect in a foreign country, an inventor who wishes patent protection in another country must apply for a patent

in a specific country or in regional patent offices. Applicants may wish to consider the filing of an international application under the Patent Cooperation Treaty (PCT). An international (PCT) application generally has the same effect as a regular national patent application in each PCT-member country. The PCT process **simplifies** the filing of patent applications on the same invention in member countries, but **does not result** in a grant of "an international patent" and does not eliminate the need of applicants to file additional documents and fees in countries where patent protection is desired.

Almost every country has its own patent law, and a person desiring a patent in a particular country must make an application for patent in that country in accordance with its particular laws. Since the laws of many countries differ in various respects from the patent law of the United States, applicants are advised to seek guidance from specific foreign countries to ensure that patent rights are not lost prematurely.

Applicants also are advised that in the case of inventions made in the United States, the Director of the USPTO must issue a license before applicants can apply for a patent in a foreign country. The filing of a U.S. patent application serves as a request for a foreign filing license. The application's filing receipt contains further information and guidance as to the status of applicant's license for foreign filing.

Applicants may wish to consult the USPTO booklet, "General Information Concerning Patents" (specifically, the section entitled "Treaties and Foreign Patents") for more information on timeframes and deadlines for filing foreign patent applications. The guide is available either by contacting the USPTO Contact Center at 800-786-9199, or it can be viewed on the USPTO website at http://www.uspto.gov/web/offices/pac/doc/general/index.html.

For information on preventing theft of your intellectual property (patents, trademarks and copyrights), you may wish to consult the U.S. Government website, http://www.stopfakes.gov. Part of a Department of Commerce initiative, this website includes self-help "toolkits" giving innovators guidance on how to protect intellectual property in specific countries such as China, Korea and Mexico. For questions regarding patent enforcement issues, applicants may call the U.S. Government hotline at 1-866-999-HALT (1-866-999-4258).

LICENSE FOR FOREIGN FILING UNDER

Title 35, United States Code, Section 184

Title 37, Code of Federal Regulations, 5.11 & 5.15

GRANTED

The applicant has been granted a license under 35 U.S.C. 184, if the phrase "IF REQUIRED, FOREIGN FILING LICENSE GRANTED" followed by a date appears on this form. Such licenses are issued in all applications where the conditions for issuance of a license have been met, regardless of whether or not a license may be required as set forth in 37 CFR 5.15. The scope and limitations of this license are set forth in 37 CFR 5.15(a) unless an earlier license has been issued under 37 CFR 5.15(b). The license is subject to revocation upon written notification. The date indicated is the effective date of the license, unless an earlier license of similar scope has been granted under 37 CFR 5.13 or 5.14.

This license is to be retained by the licensee and may be used at any time on or after the effective date thereof unless it is revoked. This license is automatically transferred to any related applications(s) filed under 37 CFR 1.53(d). This license is not retroactive.

The grant of a license does not in any way lessen the responsibility of a licensee for the security of the subject matter as imposed by any Government contract or the provisions of existing laws relating to espionage and the national security or the export of technical data. Licensees should apprise themselves of current regulations especially with respect to certain countries, of other agencies, particularly the Office of Defense Trade Controls, Department of State (with respect to Arms, Munitions and Implements of War (22 CFR 121-128)); the Bureau of Industry and Security, Department of Commerce (15 CFR parts 730-774); the Office of Foreign AssetsControl, Department of Treasury (31 CFR Parts 500+) and the Department of Energy.

NOT GRANTED

No license under 35 U.S.C. 184 has been granted at this time, if the phrase "IF REQUIRED, FOREIGN FILING LICENSE GRANTED" DOES NOT appear on this form. Applicant may still petition for a license under 37 CFR 5.12, if a license is desired before the expiration of 6 months from the filing date of the application. If 6 months has lapsed from the filing date of this application and the licensee has not received any indication of a secrecy order under 35 U.S.C. 181, the licensee may foreign file the application pursuant to 37 CFR 5.15(b).

SelectUSA

The United States represents the largest, most dynamic marketplace in the world and is an unparalleled location for business investment, innovation, and commercialization of new technologies. The U.S. offers tremendous resources and advantages for those who invest and manufacture goods here. Through SelectUSA, our nation works to promote and facilitate business investment. SelectUSA provides information assistance to the international investor community; serves as an ombudsman for existing and potential investors; advocates on behalf of U.S. cities, states, and regions competing for global investment; and counsels U.S. economic development organizations on investment attraction best practices. To learn more about why the United States is the best country in the world to develop technology, manufacture products, deliver services, and grow your business, visit http://www.SelectUSA.gov or call +1-202-482-6800.